RESPONSE MECHANISMS OF ATTACHED PREMIXED FLAMES SUBJECTED TO HARMONIC FORCING

A Dissertation
Presented to
The Academic Faculty

By

Shreekrishna

In Partial Fulfillment
Of the Requirements for the Degree
Doctor of Philosophy in Aerospace Engineering

Georgia Institute of Technology

December 2011

RESPONSE MECHANISMS OF ATTACHED PREMIXED FLAMES SUBJECTED TO HARMONIC FORCING

Approved By:

Dr. Tim Lieuwen
Advisor, Professor
School of Aerospace Engineering
Georgia Institute of Technology

Dr. Vigor Yang
William R.T.Oakes Professor and Chair
School of Aerospace Engineering
Georgia Institute of Technology

Dr. Suresh Menon
Professor
School of Aerospace Engineering
Georgia Institute of Technology

Dr. Jerry Seitzman
Professor
School of Aerospace Engineering
Georgia Institute of Technology

Dr. Fei Han
Manager – Combustion and Diagnostics
Laboratory
GE Global Research Center
Niskayuna, NY

Date Approved : 24th August 2011

|| Aum jyOtiH charaNAbhidhAnAt Aum ||[1]

- *BrahmasUtras, 1.1.24*

Prayers to the Almighty for the well-being of the world, to whom the word 'jyOti' (Sanskrit for 'flame') refers to, in the ancient Indian literature, the Vedas.

Dedication

[1]axayam karma yasmin parE svarpitam, praxayam yAnti duHkhAni yannAmataH |
axarO yO ajaraH sarvadEvAmR^itaH, kuxigam yasya vishwam sadAjAdikam ||
preeNayAmO vAsudEvam, dEvatAmaNDala-akhaNDa-maNDanam ......

-   dvAdasha stOtra 8.11

To

The Lord of the universe, the submission of all actions in whom yields infinite results, by the mere utterance of whose name, all sorrows are thwarted, who is without destruction or diminution of power and capacity, who is free from bondage

and

[1]Anandateertha-bhagavad-vadanEndu-bimbam,
vidyA-sudhA-vitata-kAnti sukAnti-kAntam |
yaiH praikShyatAtra bhava-tApa-shamAya bhaktaiH,
tad-dAsadAsyamapi kim na dadAti puMsaH ||

-   madhwavijaya 15.141

That great peerless professor, whose unblemished, unmistaken, clear nectar of knowledge relieves students of all dilemmas, servitude to whose ideologies leaves nothing unachievable!

and

[1]naumi nyAyasudhAdi-kR^it-jayamuneen, SrIpAdarAT sanmaNeen |
vyAsaryAn vividhAgamAbdhi viharAn, SrIvAdirAjAn api
vandE hamsavarAn raghUttama-gurUn, vaidagdhya-vArAn nidheen |
SrIsatyavrata-rAghavEndra-munipAn sadbOdha-saddhyAnapAn ||

To all those great intellectuals who dedicated their life to the pursuit of the most righteous truth, treading on the most righteous of paths,

and

Amma, Appa (my parents) and Vaishnavi (my sister)

---

[1] Uses iTRANS transliteration

Acknowledgements

"A hundred times every day I remind myself that my inner and outer life are based on the labors of other men, living and dead, and that I must exert myself in order to give in the same measure as I have received and am still receiving..." – *Albert Einstein*

In the spirit of the above words of the celebrated scientist, Albert Einstein, I would be ungrateful to the Almighty whose continuous grace this thesis is a manifestation of, if I did not acknowledge the role various people have played in shaping up the last five years that would be culminating in my Ph.D. degree.

My foremost expression of deep gratitude and indebtedness goes out to my doctoral advisor, Prof. Tim Lieuwen, under whose guidance, I have had the opportunity to mature as a student, researcher and a person. His scientific curiosity and inquisitiveness is infectious and has always fueled the flame of inquisitiveness in all his students constantly, and I am no exception. More importantly, I have learned the importance of patience, endurance and tolerance from Tim, values that are of paramount importance for a robust all-round personality. I am extremely grateful to him for all his support, understanding, guidance and affection during these last five years of many ups and downs. I seek the Almighty's bountiful blessings on him and his wonderful family.

In a similar vein, I would like to thank Prof. Satyanarayanan Chakravarthy, who sowed the seeds of interest towards Fluid Mechanics during my undergraduate studies at IIT Madras, as my B.Tech advisor. He was also the first professor under whom I studied Combustion.

I would also like to express my gratitude to my committee members, Prof. Vigor Yang, Prof. Suresh Menon, Prof. Jerry Seitzman and Dr. Fei Han, to agreeing to serve on my committee in spite of their extremely busy schedules, and for offering constructive and valuable critiques regarding my research work.

I am very deeply appreciative of all the assistance that Prof. Jeff Jagoda has provided as the Associate Chair for Graduate Studies and Research, and the help that the ever-smiling Danielle Ramirez, Margaret Ojala and Barbara Gaston have provided over the period of my stay. Thanks also to Prof. Joseph Saleh for introducing me to a whole new way of understanding engineering. My interactions with him have been very memorable, educative and insightful.

I also desire to express my gratitude to Dr. Shivakumar Srinivasan, Dr. Venkateswarlu Narra, Dr. Yongqiang Fu, Dr. Nan Zong, Miss Sarah Crothers and Mr. Willy Ziminsky for providing me with the golden opportunity to gain industrial and practical experience during my stint at GE Energy as a summer intern in 2010. Additionally, the collaborative opportunities that I have had through GE's USA Program, have benefited me largely. I would like to convey my thanks to all members of the USA Program (from GE Global Research Center, GE Energy and Penn State University). In particular, I would like to thank Prof. Domenic Santavicca and Poravee Orawannukkul of Pennsylvania State University for providing me a chance to work with them very closely on some of the exciting problems of combustion dynamics.

The Ben. T. Zinn Combustion Laboratory, where I worked as a graduate research assistant, was my second home for five years, and provided the perfect milieu to thrive

and flourish in intellectually. As a part of this Combustion Lab "family", thanks are due to many people. The intellectual companionship of Prof. Tim Lieuwen's research group has been of great importance in developing my research and academic knowledge. I would like to thank (in no particular order) Bobby Noble, Dong-hyuk 'Tom' Shin, Jacqueline 'Lab-mom' O'Connor, Jack Crawford, Prabhakar 'Chewbacca' Venkateswaran, Andrew Marshall, Vishal 'God' Acharya, Alberto Amato, Ben Emerson, Chris Foley, Jordan Blimbaum, Nick Magina, Ianko Chterev, Qiao Zhang, Tay Akin, Mouna Romani, Mike Aguilar, Michael Melanoski, Dmitriy Plaks and any other current Lieuwenites that I may have missed out. Thanks are in order to Dong-hyuk, Jacqueline and Jack for all the support that I received from them during preparation for my Ph.D. qualifying exams and all through my Ph.D.. Jacqueline made the most awesome eggless cookies for my defense, which certainly is a reason to thank her again!

I would like to also thank the extended family in the combustion lab, including Dr. David Scarborough, Dr. Caleb Cross (who defended a few hours before me!), Brad, Ben, Yash, Karthik, Yogish, Arun, Ravi, Chiluwata and many of my seniors from the lab, Dr. Mohan Bobba, Dr. Priya Gopalakrishnan, Dr. Rajesh Rajaram, Dr. Jayaprakash Natarajan, Dr. Sai Kumar and Dr. Venkata Nori, and any others that I may have inadvertently missed out, who have helped me at various points of time during my Ph.D.

I have been truly inspired by Dr. Santosh Hemchandra, Dr. Preetham and Dr. Santosh Shanbhogue, whose mentorship has been extremely invaluable in grooming me to become a clearer thinker, better researcher, and to strike a 'work-life balance' (a phrase that Preetham has engrained into my mind). Their diligence continues to inspire and influence me! The many hours that Santosh Hemchandra and I have spent discussing life,

politics, Sanskrit, music and mathematics, in addition to Fluid mechanics, as colleagues, are fond memories that I truly cherish. The high-value entertainment derived from the conversations of Preetham, Venkat and Santosh Hemchandra in the theory room at regular intervals in the week are moments that a price cannot be paid for! I should also thank the more recent residents of the theory room, in particular, Vishal Acharya, for putting up with my random ramblings often, and appreciate the patience that Vishal, Tom and Alberto have shown in Mac-vs-Windows-vs-Linux fights between the "mortal and the divine"!

I have also been very lucky to possess a very wonderful circle of family and friends in Atlanta. My roommates over the years, Nagesh Adiga, Manoj Agrawal, Dr. Dhaval Bhandari, Sandeep Kakumanu and Ajay Madhavan, and during the last month of my stay, Kunal Mucchala and Tapan Chaddarwala, have provided me a wonderful and cozy home to return to each evening, and we have lived as a family over the years, and I thank them for everything wholeheartedly. I also thank my other close friends over the years, Deepthi Adiga, Kiruthika Devaraj, Manali Tare, Ashwini Bhagwat and Aarthi Kannan for all the great times that we have spent together. My last year at Georgia Tech was absolutely splendid, all thanks to Balachandra 'Bala' Suri and Ranjini Vaidyanathan, whose company has become addictive. Nights spent at the Atlanta Symphony Orchestra outings with Ranjini and Bala, and afterwards, musing over the many genius gags of Matt Stone and Trey Parker, in addition to regular badminton outings with Bala and the Adigas are times that have made my stay in Atlanta truly memorable.

Right from receiving me at the Atlanta airport when I came to USA, to patiently listening to the proceedings of my thesis defense, my cousin and sister-in-law, Swaroop

and Reena, have given me lots of love and affection that I am indebted to them for. Thanks are due to Vishwa Madhwa Sangha – Atlanta chapter and Nrupathunga Kannada Koota, for providing me with the culture of my country and hometown very close to Georgia Tech, that I would have missed very much otherwise.

Thanks are also due to Prof. Ajit Kumar Kolar, Department of Mechanical Engineering, IIT Madras, for his help and support, especially during my undergraduate days and for offering valuable advice whenever I needed.

The unconditional love and support that I have received from Sai Prasad Viswanathan and Aishwarya Chandhiramouli is wholeheartedly acknowledged. I would be failing in my duties if I did not thank Aishwarya Vidhya Raghunath for all the fun times, support, affection and encouragement she has given me over the last three years.

Lastly, I would like to thank a special set of people who make me what I am.

The 'Gurunath Beat Gumbal' from IIT Madras, comprising of Dr. Supradeepa, Dr. Auditya Sharma, Chinmay Hegde, Sundeep Balaji, Baladitya Suri and Hari Bharadwaj, have been motivating me from my high school days (the former four) and undergrad days (the latter two) at IIT Madras. They continue to inspire me by being the multifaceted achievers that they are, and I wish to express my deepest gratitude to this elite group, which has influenced me immensely for the last decade or so and is very largely responsible for what I am today.

The discipline and conscientiousness that The Home School, Bangalore, India, engrained in me ever since I began my kindergarten schooling, has helped me many times in life, and I am indebted forever to the institution, and in particular, to Late Mr.

Venkatachalam, the principal of the school during my student days there, for his love and encouragement.

I would like to thank my parents Sri Jayakumar Krishna Rao and Dr. Radha Jayakumar for their constant support, unconditional love, and continuous prayers and for always helping me choose the right paths in life. The small successes in my life are tales of their achievements as my parents, rather than anything else. My little sister, Vaishnavi, has been the bundle of joy that I can talk to, to lift my spirits even on the gloomiest of days. I express my indebtedness to my grandparents, Smt. Radha and Late Sri Krishna Rao, and Smt. Manjula and Late Prof. Keshava Rao, and my grandaunt Sumitra Bai, for making me the apple of their eye and for being there to celebrate every moment of my life with me.

I thank my cousin, Ranjani Ramesh, who has always been around for me, showering me with lots of love over the 25 years that we have known each other for. I thank my aunts and uncles, Sudha and Ravi, Parimala and Phaneesh, Vijaya and Ramesh, Sujaya and Sudheendra, and Rohini and Guruprasad, and my cousins Varun, Naina and Sindhu for all their love.

Finally, I prostrate before the lotus feet of my spiritual gurus, Sri Sri Vishwesha Teertha Sripadaru of Pejavara Mutt, Sri Sri Vishwapriya Teertha Sripadaru of Adamaru Mutt, Sri Sri Vidyadheesha Teertha Sripadaru of Palimaru Mutt, Sri Sri Vishwaprasanna Teertha Sripadaru of Pejavara Mutt and Sri Sri Satyatma Teertha Sripadaru of Uttaradi Mutt, for their continuous blessings on me, and for transforming my life in ways that I cannot find words to express.

Table of Contents

List of Tables

List of Figures

Nomenclature

English lower case

c_o = Speed of sound in unburned reactants

f = Frequency of excitation

h_R = Heat of reaction

h_{R1} = Heat of reaction sensitivity to equivalence ratio perturbations

$k_{c,\phi}, k_{c,u}$ = $u_{c,\phi}/u_o, u_{c,u}/u_o$; Dimensionless phase speed of the disturbances in fuel/air ratio and velocity

$p(z,t)$ = Instantaneous acoustic pressure

p_o = Ambient pressure

$q(t)$ = Instantaneous spatially integrated heat release

r = Radial coordinate

s_L = Laminar flame speed

s_{L1} = Laminar flame speed sensitivity to equivalence ratio perturbations

$s_{L1,p}$ = Laminar flame speed sensitivity to acoustic pressure perturbations

u_a' = Acoustic velocity disturbance

$u_{c,\phi}, u_{c,u}$ = Phase speed of the disturbances in fuel/air ratio and velocity

u_o = Mean velocity of the premixed reactants

u_Ω' = Vortical velocity disturbance

z	=	Axial coordinate

English upper case

$A(t)$	=	Instantaneous flame surface area
$\mathscr{D}_F, \mathscr{D}_{Ox}$	=	Fuel and oxidizer mass diffusivities respectively
$\mathscr{D}, \mathscr{D}_T$	=	Average reactant mass and thermal diffusivities respectively
E_a	=	Overall Activation Energy
F	=	Transfer Function
F_p	=	Pressure coupled transfer function
$F_{u,a}$	=	Acoustic velocity coupled transfer function
$F_{u,\Omega}$	=	Vortical velocity coupled transfer function
$F_A, F_{s_L}, F_{h_R}, F_\rho$	=	Transfer function contributions arising due to fluctuations in burning area, laminar flame speed, heat of reaction and reactant density respectively
F_ϕ	=	Equivalence ratio coupled transfer function
Le	=	$\mathscr{D}_T / \mathscr{D}$, Reactant Lewis number
L_f, R	=	Length of flame and duct half-width respectively
M_o	=	Mach number of the unburned reactants, u_o / c_o
M_f	=	Mach number of the laminar flame, s_{Lo} / c_o
Pr	=	Reactant Prandtl number
R_u	=	Gas constant

St	=	Strouhal number based on flame length and mean flow velocity, $\omega L_f / u_o$
St_δ	=	Strouhal based on flame thickness and flame speed, $\omega \delta_f / s_{Lo}$
St_2	=	Reduced Strouhal number $= St \left(\beta^2 + 1 \right) / \beta^2$
T_b	=	Temperature of the burned gases

Greek lower case

α	=	constant $= \beta^2 / \left(1 + \beta^2 \right)$
β	=	Flame aspect ratio $= L_f / R = \cot \psi$
δ_f	=	Thickness of the preheat zone of the laminar flame
δ^*	=	Nondimensionalized flame thickness, δ_f / R
ϕ	=	Equivalence Ratio
γ	=	Ratio of specific heats (c_p/c_v)
λ	=	Wavelength of the pressure disturbances
θ	=	Dimensionless activation energy, $E_a / R_u T_b$
ρ_o	=	Mean density of reactant mixture
ρ	=	Density of reactant mixture
$\hat{\sigma}_c, \hat{\sigma}_s$	=	Markstein lengths for curvature and strain, non-dimensionalized by duct half-width
σ_c^*	=	$\alpha^{1/2} \beta^{-1} \hat{\sigma}_c$
σ_s^*	=	$\alpha^{1/2} \hat{\sigma}_s$

ω	$=$	$2\pi f$, Excitation frequency in *rad s*[-1]
ξ	$=$	Flame front location
ψ	$=$	Half angle of the flame

Greek upper case

Λ_u	$=$	$k_{c,u}St + i\aleph_u$, complex frequency describing diffusion-affected flame response to vortical velocity coupled flame response
Λ_ϕ	$=$	$k_{c,\phi}St + i\aleph_\phi$, complex frequency describing diffusion-affected flame response to equivalence ratio coupled flame response

Hebrew

$\aleph_{c,\phi}, \aleph_{c,u}$	$=$	Spatial diffusion decay rates of the disturbances in fuel/air ratio and velocity

Subscripts and superscripts

$( )_o$	$=$	Steady state variables
$( )'$	$=$	Perturbed variables
$( )^*$	$=$	Non-dimensional variables

Summary

The persistent thrust for a cleaner, greener environment has prompted air pollution regulations to be enforced with increased stringency by environmental protection bodies all over the world. This has prompted gas turbine manufacturers to move from non-premixed combustion to lean, premixed combustion. These lean premixed combustors operate quite fuel-lean compared to the stochiometric, in order to minimize CO and NOx productions, and are very susceptible to oscillations in any of the upstream flow variables. These oscillations cause the heat release rate of the flame to oscillate, which can engage one or more acoustic modes of the combustor or gas turbine components, and under certain conditions, lead to limit cycle oscillations. This phenomenon, called thermoacoustic instabilities, is characterized by very high pressure oscillations and increased heat fluxes at system walls, and can cause significant problems in the routine operability of these combustors, not to mention the occasional hardware damages that could occur, all of which cumulatively cost several millions of dollars.

In a bid towards understanding this flow-flame interaction, this research works studies the heat release response of premixed flames to oscillations in reactant equivalence ratio, reactant velocity and pressure, under conditions where the flame preheat zone is convectively compact to these disturbances, using the G-equation. The heat release response is quantified by means of the flame transfer function and together with combustor acoustics, forms a critical component of the analytical models that can predict combustor dynamics.

To this end, low excitation amplitude (linear) and high excitation amplitude (nonlinear) responses of the flame are studied in this work.

The linear heat release response of lean, premixed flames are seen to be dominated by responses to velocity and equivalence ratio fluctuations at low frequencies, and to pressure fluctuations at high frequencies which are in the vicinity of typical screech frequencies in gas turbine combustors.

The nonlinear response problem is exclusively studied in the case of equivalence ratio coupling. Various nonlinearity mechanisms are identified, amongst which the crossover mechanisms, viz., stoichiometric and flammability crossovers, are seen to be responsible in causing saturation in the overall heat release magnitude of the flame. The response physics remain the same across various preheat temperatures and reactant pressures.

Finally, comparisons between the chemiluminescence transfer function obtained experimentally and the heat release transfer functions obtained from the reduced order model (ROM) are performed for lean, CH_4/Air swirl-stabilized, axisymmetric V-flames. While the comparison between the phases of the experimental and theoretical transfer functions are encouraging, their magnitudes show disagreement at lower Strouhal number gains show disagreement.

Chapter 1 : Introduction

1.1. Motivation

The ever increasing energy demand in the world has led to an increasing amount of usage of fossil fuel based energy sources for production of energy. Significant amongst these is natural gas which is used mostly due to its ready availability and relative safety. However, energy production using natural gas also produces pollutants such as NOx and CO. Over the years, environmental health and safety factors have prompted the permissible emission envelopes of these pollutants to continuously shrink. These emission regulations have compelled manufacturers of land based gas turbines to increasingly migrate from a non-premixed mode towards a premixed mode of combustor operation. The reason for this shift is that combustion and thermal energy production necessarily happens at the stoichiometric ratio in non-premixed mode combustors, hence leading to beyond-acceptable levels of NOx and CO for a specified amount of wattage output. Alternatively, the latter, premixed mode combustion provides the flexibility to use technology such as Dry Low NOx (DLN) to achieve lower levels of NOx and much more efficient combustion.

This operational shift from non-premixed to premixed mode of combustion has brought about the need for a change in design and operation strategies. One of the principal strategies adopted to comply with these emission norms is to carry out the combustion process using premixed and pre-vaporized fuel-air mixtures whose composition is far lean of the stoichiometric. Most gas turbine manufacturers prefer

burning the reactant mixture in a small equivalence ratio window where both the CO and thermal NOx levels are at a combined minimum. However, this emission advantage is not without peril.

A significant drawback of lean, premixed operation is that these combustors are especially prone to self excited oscillations. This dynamic phenomenon generally occurs when the unsteady combustion process couples with the natural acoustic modes of the combustor. This phenomenon, called combustion instabilities, often arises in high performance combustion systems, such as rockets [1-6], afterburners, ramjets, gas turbines [7, 8], industrial devices and residential heaters. These instabilities arise through a self-exciting feedback loop between acoustic and heat release oscillations in the combustor. These oscillations can achieve very high amplitudes and cause structural damage both upstream and downstream of the combustor section (see Figure 1) and/or compromise system performance, emissions or operability [9-12], in addition to reducing combustor lifespan and causing severe maintenance issues.

For example, even a small hardware component that gets liberated in the combustor can cause damage to the hot gas path components such as transition pieces, turbine blades and buckets etc. Alternatively, flame flashback phenomena can cause destruction of components upstream of the combustion chamber. Further, unsteady thermal stresses due to combustion instability can fatigue combustor liners and casings much faster than their design life, leading to degraded performance and premature combustor inoperability. In all of these cases, damages such as these could potentially lead to capital losses running into millions of dollars, both due to actual component damage and operational downtime and maintenance.
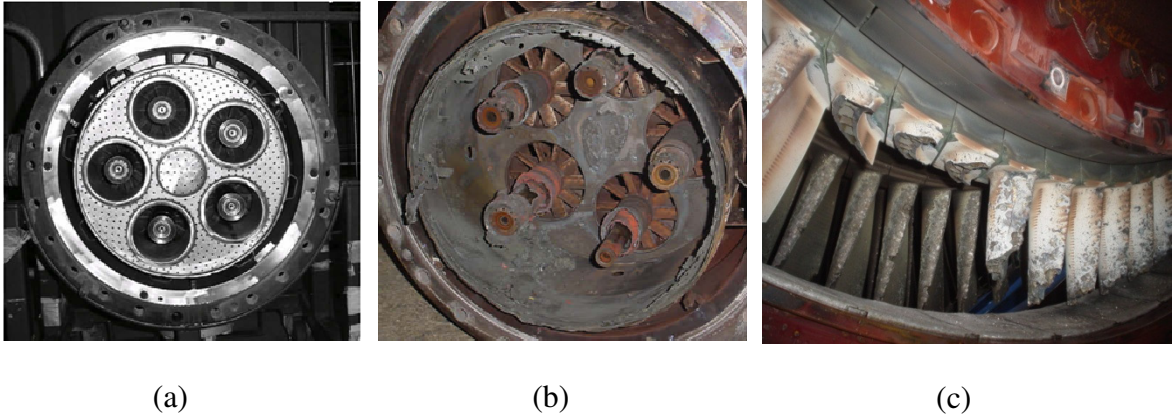
Figure 1 : Illustration of damaged combustor components. Reproduced from [13] – (a) New burner assembly; (b) Destroyed burner assembly; (c) Destroyed turbine blades

An actual example of the damage caused by combustion instabilities is shown in Figure 1. Figure 1(a) shows a new burner assembly while Figure 1(b) shows the destruction of the burner assembly due to flame flashback. Destruction of hardware can also be wrought downstream of the combustor as seen in the destroyed turbine blades in Figure 1(c).

While the majority of the motivation in studying combustion instabilities is derived from lean combustion systems, it is also of value to study combustion instabilities in the context of premixed combustors that run rich. For example, gas turbines that operate in the partial oxidation mode, POGT combustors, have been proposed for the co-production of synthesis gas, starting from a hydrocarbon fuel [14].

Given the complexity of a myriad physical processes occurring during these instabilities, some of which are perhaps, even mathematically intractable, this thesis attempts at a first "slice" of understanding of many of the physical processes, by studying how an established flame responds to various flow field perturbations.

1.2. Background

The flame is subjected to a variety of disturbances in practical combustion devices, leading to oscillations in its position and instantaneous heat release rate. These fluctuations arise through disturbances in flow, mixture composition, and thermodynamic variables (e.g., pressure and temperature) and consist of broadband fluctuations manifested over a continuum of length and time scales, as well as very narrowband oscillations [7, 11]. In fact, the relatively lightly damped nature of the acoustic modes in combustion systems leads to oscillations which are temporally narrowband in spectral space.

Essentially, these upstream flow disturbances in the combustor can perturb the flame and alter the instantaneous heat release rate. The heat release rate disturbances in turn alter the disturbances that caused them in the first place, thereby completing a feedback loop as shown in Figure 2. Given the monopole acoustic nature of the flame [15] the unsteady heat release rate generates sound. These acoustic oscillations could now amplify by virtue of interacting with the unsteady combustion process in accordance with the Rayleigh criterion [16]. The Rayleigh criterion states that these acoustic oscillations are driven when the unsteady combustion process adds energy "in-phase" to the acoustic oscillations. If the rate of this energy addition exceeds the rate of energy loss/absorption in the system, these acoustic oscillations that start off linear grow in amplitude.

Insofar as the perturbations are infinitesimally small, the dynamics of the system can be analyzed using linearized theories. These linear analyses provide useful

information such as frequency and growth rate of these oscillations, as well as about operating conditions which could render the combustor linearly unstable.
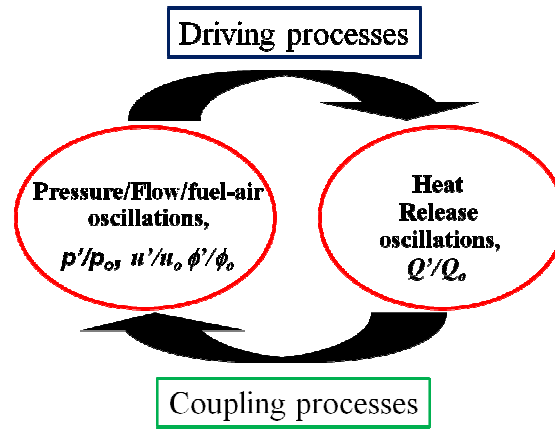
Figure 2 : Feedback loop that leads to combustion instabilities

However, under the influence of nonlinear processes, these linearly growing acoustic oscillations could plateau to a limit cycle. In addition to instability frequencies, the amplitude of these limit cycles are of paramount importance to gas turbine manufacturers. This is owing to the following reason. How safe or unsafe a certain limit cycle amplitude is, is strongly dependent on its instability frequency. For example, an instability whose limit cycle amplitude is 1 psi peak-to-peak might be acceptable at 150 Hz, but could potentially cause detrimental damage at 1.5 kHz.

Limit cycle amplitude prediction is not possible using linear analyses, since it is necessarily determined by nonlinear processes. This point is illustrated in Figure 3, which demonstrates that the amplitude of a disturbance stays the same, increases, or decreases based on whether driving amplitude equals, exceeds or is less than the damping amplitude. The balance between driving and damping processes at low oscillation

5

amplitudes is generally controlled by linear processes, thereby aiding in the determination of the growth rate of inherent disturbances in the combustor. As the amplitude of oscillation increases, nonlinear processes become increasingly important and they control the finite amplitude dynamics of the oscillations. Note that it is absolutely necessary for at least one of the processes to be nonlinear for a limit cycle to be attained. Predicting the limit cycle amplitude of self-excited oscillations hence requires an understanding of the nonlinear characteristics of both the driving and damping processes.

To summarize, while linear analyses are helpful in understanding the growth rate and frequency of the disturbances, modification of these results due to nonlinearities that lead to heat release saturation necessitate nonlinear analyses. Fundamental to either endeavor, however, is the determination of the influence of various driving processes on the heat release rate of combustion.
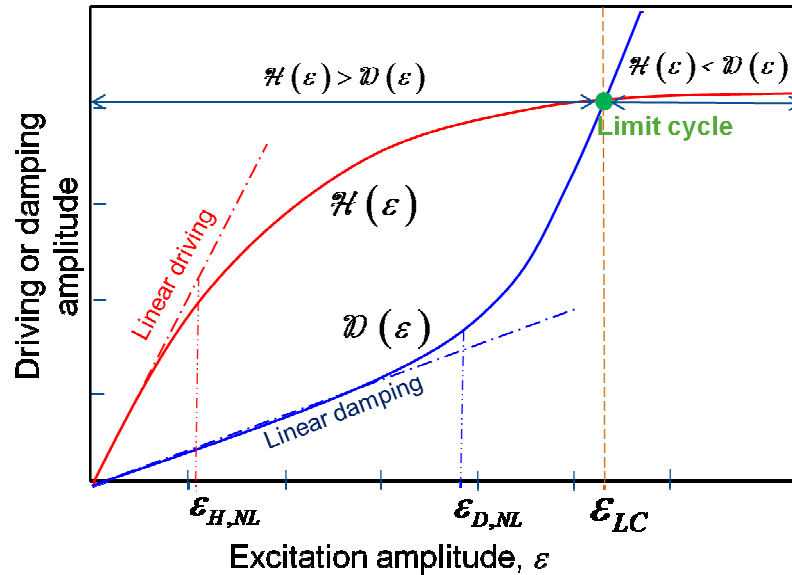
Figure 3 : Cartoon of driving processes, $\mathcal{H}(\varepsilon)$ and damping processes, $\mathcal{D}(\varepsilon)$ and their dependence on perturbation amplitude. Note that initially both processes grow linearly, while at a later stage, nonlinear effects lead to a limit cycle. Note also that nonlinearity can gain importance for either process at different amplitudes.

In typical gas turbine combustors, a variety of processes that complete the flame-acoustic feedback loop exist [11]. Some of these driving processes include equivalence ratio oscillations, acoustic and vortical velocity oscillations, acoustic pressure oscillations, strain rate oscillations, flame extinction and reignition processes, flame-vortex interactions, flame wall interactions etc. (see Figure 4). Typically, one or more of these processes can coexist and drive unsteady combustion, depending on the operating conditions. Each of these "coupling" mechanisms are themselves rich in physics and have been focused upon by various researchers [17-21]. Acknowledging the complexity of the complete problem, the current approach has been to isolate these mechanisms and develop simple experiments/models that enables in better understanding the key physics associated with each of these driving processes [21].
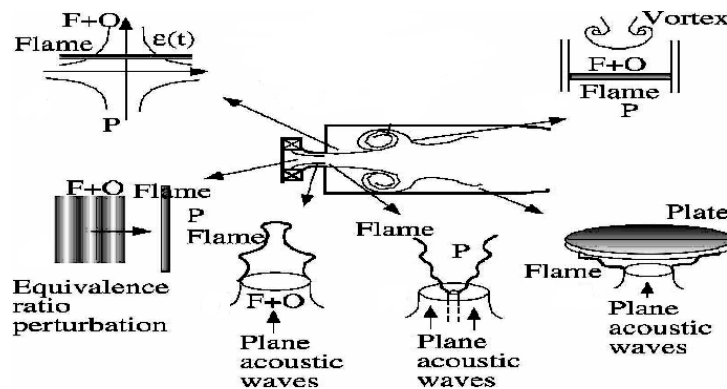
Figure 4 : Various elementary driving processes that lead to combustion instability. Figure reproduced from [11].

This thesis aims at expanding the current understanding on flame response physics and modeling by studying the heat release response of premixed flames to velocity perturbations, equivalence ratio perturbations and pressure perturbations, which are also referred to as velocity coupled flame response, equivalence ratio coupled flame response

7

and pressure coupled flame response respectively. In particular, it is intended to identify, understand and describe the processes by which harmonic disturbances, in particular, those in fuel/air ratio and acoustic pressure, lead to fluctuations in heat release in premixed flames.

The basic problem of interest is depicted in Figure 5. A premixed flame with a characteristic dimension, L_f, stabilized in a high velocity flow. The flame is perturbed by an acoustic, fluid mechanic or fuel/air ratio disturbance with frequency, f, and phase speed, u_c. It is intended to address the following question - For a given disturbance, what is the response of a premixed flame and particularly, the resultant fluctuation in global heat release rate? [21]
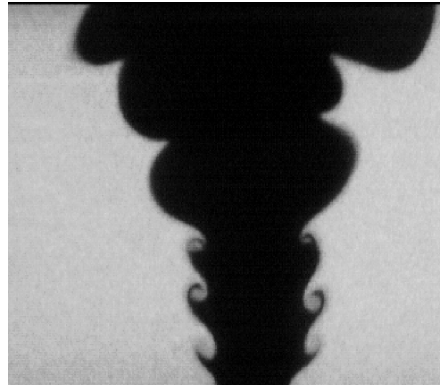
Figure 5 : Interaction of flow disturbances with a premixed flame. Courtesy: Shanbhogue et al. [22].

In wake of the above, it is instructive to look deeper into the physical processes that constitute these coupling mechanisms.

1.3. Overview of Coupling Mechanisms

Modeling combustion instabilities in order to develop rational mitigation approaches requires an understanding of the various mechanisms that cause heat release oscillations in lean premixed combustors [23]. Significant among these are flame burning area fluctuations driven by acoustic velocity oscillations [24, 25] or convected, vortical structures [26-30], flame extinction and re-ignition [31, 32], flame-wall interactions [18] and reactant mixture composition, *i.e.*, equivalence ratio fluctuations [33-37].

To obtain a clearer idea of the different physical mechanisms causing heat release oscillations of a flame subjected to different perturbations, consider the instantaneous global heat release rate of a flame, which is given by

$$q(t) = \int_{flame} \rho_u s_L h_R dA \tag{1.1}$$

Here, the integral is performed over the flame surface area. Equation (1.1) shows four fundamentally different mechanisms generating heat-release disturbances in a premixed flame, *viz.*, fluctuations in reactant density, flame speed, heat of reaction, or flame surface area.

Fluctuation in the mass flow rate of reactive mixture into the flame, corresponding to $\rho_u s_L$ in Eq.(1.1), is a key mechanism for heat release oscillation. Density fluctuations could be due to both acoustic and entropy fluctuations. The burning rate of the flame, s_L, is sensitive to the perturbations in pressure, temperature, strain rate, or mixture composition that accompany the acoustic wave. These pressure and temperature fluctuations are usually generated by acoustic perturbations, while the strain rate fluctuations are associated with acoustic or vortical velocity fluctuations. Flame area

fluctuations are associated with disturbances in the position of the flame and orientation that, in turn, are generated by fluctuations in either the local burning rate or flow velocity. This flame disturbance is convected downstream by the mean flow, so that it varies spatially over a convective wavelength [38]. Finally, fluctuations in heat of reaction, h_R, are driven by variations in reactive mixture composition and, to a lesser extent, reactant pressure and temperature [39].

This thesis focuses on the various perturbations that excite perturbations in density, flame speed (or collectively, mass burning rate), flame area and heat of reaction. These perturbations can arise from acoustic, vortical, or entropy disturbances and, in terms of flow and thermodynamic variables due to pressure, temperature, velocity, fuel/air ratio, acceleration, or density fluctuations. In general, these perturbations are related and co-exist. For example, an acoustic wave is accompanied by pressure, temperature, and flow velocity oscillations. Similarly, a fuel/air ratio fluctuation leads to oscillations in flame speed, heat of reaction, and flame area. In order to provide a framework for appropriately grouping these different mechanisms, the discussion is focused on three important coupling mechanisms: acoustic pressure, flow velocity and fuel/air ratio. It is assumed all through this work that these mechanisms operate independent of one another. Such an assumption is of importance in understanding the influence of each of these disturbances on the dynamics of the flame, which in itself is rich in physics.

From an analytical viewpoint, much insight into the phase response of the flame to such perturbations can be obtained from a simple time delay analysis that treats the flame as a concentrated source of heat release [40-42]. In general, however, flames are

distributed axially over a length scale where the mixture equivalence ratio can significantly vary [33]. In other words, they are *convectively* non-compact, although perhaps being acoustically compact. The flame Strouhal number, defined as

$$St = \frac{\omega L_f}{u_o} \tag{1.2}$$

Chapter 1 which equals the ratio of the length of the stationary, undisturbed flame to the length scale of the imposed upstream excitation, determines whether the flame can be regarded as being a convectively compact or distributed source, and whether the flame response is *geometrically* quasi-steady or non-quasi steady. In the same spirit, as the frequency of forcing increases to satisfy $f \sim s_{Lo}/\delta_f$, additional dynamics associated with diffusion processes in the flame preheat zone needs to be accounted for. This so called "non quasi-steady effect" or more precisely, *structural* non quasi-steady effect may be parameterized by a Strouhal number, St_δ that may be defined as

$$St_\delta = \frac{\omega \delta_f}{s_{Lo}} \tag{1.3}$$

which equals the ratio of the characteristic diffusive time internal to the flame and the time period of oscillation of imposed disturbances. These Strouhal numbers are discussed in more detail in Chapter 2 in the context of the various time scales and length scales that naturally arise from such flame-acoustic interaction problems.

With this background, an overview of some driving mechanisms and the attention they have received in the research community is presented in the following section.

1.3.1. Velocity Coupling Mechanism

The velocity coupled mechanism is considered first, where the flame is perturbed by acoustic [24, 25, 43] and/or vortical [22, 26, 29, 44, 45] perturbations. The figure below illustrates the mechanism by which flow perturbations lead to heat release oscillations.
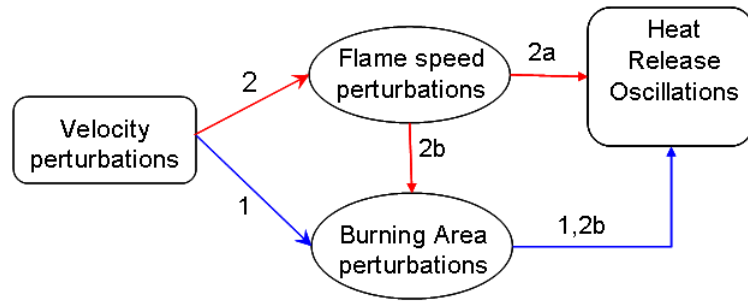
Figure 6 : Fundamental processes controlling the heat release response of premixed flames to velocity fluctuations

At low frequencies, the flame speed remains essentially constant, rendering the heat release oscillations directly proportional to the fluctuating flame area. Route 1 is, hence, the dominating route for heat release oscillations at low frequencies. However, the oscillating stretch along the flame, due to both hydrodynamic straining and curvature, grows in importance with frequency, causing oscillations in flame speed. These flame speed oscillations perturb the heat release both *directly* (route 2a) and *indirectly* (route 2b), by affecting the burning area. As shown in Preetham et al. [46] and Wang et al. [47], route 2b becomes important when $|\sigma_c{}^*|St_2{}^2 \sim 1$, while route 2a becomes important at higher frequencies when $|\sigma_c{}^*|St_2 \sim 1$.

Of the various coupling mechanisms that have been listed earlier, the velocity-coupled flame response is the one that has received widest attention by prior researchers, on both

experimental and theoretical fronts. Bloxisdge et al. [48] investigated the response of confined flames to weak harmonic sound waves experimentally and showed that the unsteady combustion process was driven by velocity fluctuations at an axisymmetric center body that acted as a flame holder, and in whose wake, the flame was stabilized. They provided an empirical relationship for the amount of heat release obtained for specified velocity perturbations (the heat release transfer function, which will be discussed in Chapter 2) and used this to discuss the thermoacoustics of the duct. Other researchers [49, 50] extended this to flows with larger Mach numbers and more complex center body and burner geometries. Durox [51] studied a Bunsen flame that was excited by acoustic waves produced by a loudspeaker placed upstream of the flame and observed distortions of the flame front that convected downstream with the mean flow. Bourehla and Baillot [52] systematically characterized the variety of flame holding behavior and flame shapes experienced by a laminar Bunsen flame excited by low frequency but high amplitude velocity perturbations. The mean flame shape itself was seen to change from being a wrinkled conical flame (as those imaged by Durox et al. [25]) to being hemispherical at higher amplitudes. Similar experiments were carried out by Baillot and other researchers [38, 53, 54], one of which [52] also observed the filtering effect at frequencies of 200 Hz and higher, which Preetham and co-workers [55, 56] theoretically hypothesized, to be due to unsteady flame stretch effects. There has been significant contribution from French researchers [11, 25, 51, 53, 54, 57, 58] in studying this problem experimentally, that has led to better understanding of a variety of physics associated with flame response to velocity perturbations. More recently, Karimi et al. [59] calculated flame transfer functions from the experiments of Bunsen flames perturbed by velocity

13

disturbances. They were seen to be in good agreement with the models of Schuller et al. [17] and in reasonable agreement with the model of Preetham and Lieuwen [60].

On the theoretical front, Boyer and Quinard [43] studied the dynamics of an anchored premixed flame using the G-equation and concluded that the temporal evolution of the flame front was due to the interference of wrinkles convecting along the flame shoulder and wrinkles induced due to the flow. Fleifil et al. [24] studied the response of a premixed flame to velocity disturbances and calculated the transfer function, which revealed that the heat release is related to the inducing velocity disturbances by means of a lag law. Dowling [31] developed a phenomenological model to emphasize the role of flame extinction on heat release saturation and nonlinearity. Dowling [61] also provided the theoretical basis for the empirical observations of Bloxsidge et al. [48]. Candel and co-workers [10, 17, 25, 32, 51, 62, 63] have to the development of flame response models of various fidelities, mostly starting with the G-equation. Assuming a spatially uniform velocity profile that is harmonically varying in time, they evaluate flame response in the form of transfer functions for flames with conical and V-shaped geometries, experimentally and numerically, and demonstrate that V-flame response becomes nonlinear at much lesser amplitudes than that of conical flames at the same excitation frequency. Lieuwen [64] studied the nonlinear kinematic response of flames to velocity perturbations in greater detail and discussed the importance of kinematic restoration as a mechanism for flame area destruction. Preetham and co-workers [55, 56, 65] have advanced the modeling efforts of Dowling, Candel and their respective co-workers, by accounting for a variety of physical phenomena such as non-compactness of the flame geometry to convective vortical disturbances, unsteady flame curvature and

14

hydrodynamic strain effects and gas expansion across the flame. The influence of unsteady stretch has been already described earlier (see Figure 6). Gas expansion was seen to influence the flame response to the extent of having to define an effective Strouhal number, which would then enable to qualitatively use results from the no-density-jump results [55]. More recently, several authors have attempted at using acoustic network models to develop flame response models using a mix of theoretical and experimental work.

1.3.2. Equivalence Ratio Coupling Mechanism

Next, the fuel/air ratio coupling mechanism is considered. Equivalence ratio perturbations cause fluctuations in local flame speed (route 2a) and heat of reaction (route 1) along the flame surface. These fluctuations in flame speed and mixture heat of reaction then cause the local heat release rate to oscillate. This is a direct route of influence. Alternatively, flame speed variations also excite flame wrinkles that propagate along the flame. This leads to an oscillation in the burning area of the flame (route 2b), also causing the net heat release rate to oscillate. This is an indirect route of influence. It is to be noted that the indirect route of influence is also non-local; i.e., the flame area fluctuations at a given time and position are a convolution of the fuel/air ratio oscillations at all upstream locations at earlier times. Due to oscillations caused in the flame shape because of equivalence ratio perturbations, oscillations arise in the curvature of the flame front, which also perturb the flame speed, thereby establishing another route by which flame speed fluctuates (route 2S). These fluctuations in flame speed can then disturb the heat release directly (route 2Sa) or indirectly by altering the burning area fluctuations

(route 2Sb). Note for the problem of interest, that stretch rate oscillations are indirectly caused by equivalence ratio oscillations; i.e., equivalence ratio oscillations perturb the flame speed, which causes flame wrinkles, which lead to oscillations in flame stretch.
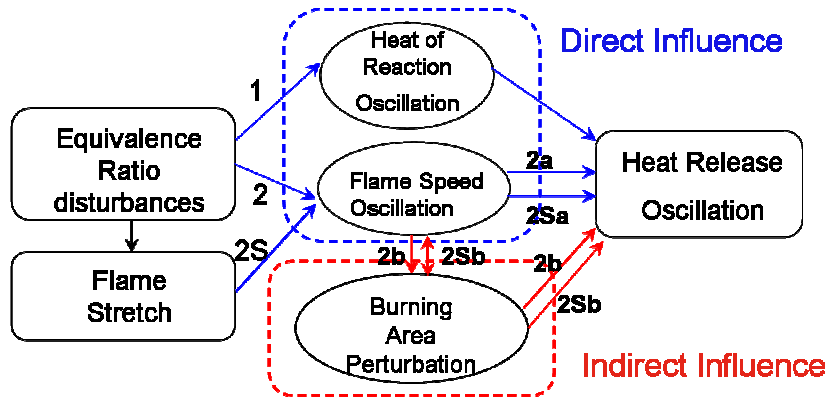
Figure 7 :   Fundamental processes controlling the heat release response of premixed flames to equivalence ratio oscillations. Routes labeled 'S' denote additional routes due to influence of flame stretch.

It is important to note that these routes are intimately influenced by frequency.

Equivalence ratio coupled flame response has also been fairly well-recognized in literature [23, 33-37, 40, 41, 66-72], though complete theoretical modeling efforts are harder to be found in comparison to velocity-coupled flame response. Early discussions on equivalence ratio fluctuations being a potential mechanism for thermoacoustic instabilities have been presented by Keller et al. [71]. Subsequently, several studies have shown strong evidence for the significance of this mechanism in causing heat release oscillations. Some of the experimental efforts have involved conducting direct measurement of equivalence ratio oscillations during instabilities [73-75]. A number of other experimental studies which have characterized operating conditions under which such instabilities occur are also available in the literature [12, 29, 36].

There have also been many early theoretical and modeling studies which have attempted to elucidate the mechanisms that drive the instability and to develop models that can predict their occurrence [20, 33, 66, 70, 76]. Lieuwen et al. [20] demonstrated that the unmixedness of the reactants, i.e., equivalence ratio perturbations, produced large heat release oscillations that could drive combustion instabilities under lean operating conditions, even away from lean blow out. Further, Lieuwen and Zinn [33] developed a preliminary model based on a well stirred reactor framework to study heat release fluctuations due to such perturbations. They predicted the dependence of frequency bands of stability and instability with operating conditions, which, even without accounting for other phenomena such as flame wrinkling, were in decent agreement with the measured experimental data of Richard and Janus [37]. Other studies have demonstrated the importance of this mechanism by comparing the dependence of instability characteristics on geometry and operating conditions with correlations developed from theoretical analyses [34, 36]. These studies hence convincingly suggested that the heat release oscillations excited by the fluctuations in the composition of the reactant mixture entering the combustion zone was a dominant mechanism responsible for the instabilities observed in low NOx gas turbine and aeroengine combustors. However, it has to be noted that these studies only allowed for the heat release to fluctuate due to heat of reaction perturbations, while altogether disregarding the influence of other possible routes, such as flame speed fluctuations and flame area fluctuations. Cho and Lieuwen [72] then accounted for the effects of flame speed and flame area fluctuations, in addition to heat of reaction fluctuations. Their efforts were directed towards understanding the equivalence

ratio coupled linear response of lean flames and comparing it with the velocity response transfer function.

There have also been a few treatments of nonlinear flame response to equivalence ratios, albeit mostly phenomenological. For example, Stow and Dowling [77] modeled to account for nonlinearities in equivalence ratio in the presence of very high velocity fluctuations. The instantaneous equivalence ratio was set to zero whenever a fluid element had crossed the flame, or had crossed the fuel injector more than once owing to flow reversal during the negative velocity disturbance cycle. This model is however only applicable to the mean flame, since on an instantaneous basis, the flow passes through the flame. On the other hand, Perracio and Proscia [76] were perhaps the first to acknowledge the nonlinear relationship between the heat of reaction (defined as the heat of combustion per unit reactant mass) and the equivalence ratio.

On the experimental front, this problem has received much lesser attention. In general, experimental studies have been challenging, because it is not easy to design a system that can generate equivalence ratio fluctuations without generating velocity disturbances. Also, it is difficult to measure the fluctuations in equivalence ratio in the domain of interest. Nevertheless, there have been experimental efforts to study this mechanism in greater detail [75, 76, 78-81]. Most of these are performed on large-scale set ups. Interestingly, studies using laboratory scale burners have almost exclusively involved perturbed jet flames [82, 83].

On the computational front, Flohr and co-authors [42, 84] and Polifke et al. [85] carried out RANS simulations to study the transport of equivalence ratio modulations due to convective processes, their interaction with premixed flames and its consequent

influence on heat release by the flame. Angelberger et al. [86] performed an LES based study to understand the effect of acoustic and chemical forcing in a dump combustor. They identified that acoustic waves also modulate fuel and oxidizer feed entering the combustor, thereby causing fluctuations in the inlet equivalence ratio, while keeping the fuel flow rate constant. They concluded that for small departures from stoichiometry, equivalence ratio fluctuations had a lesser destabilizing effect than the acoustic velocity fluctuations that led to vortex formation, which distorted the flame front and caused heat release fluctuations.

More recently, Birbaud et al. [87] performed a computational study describing nonlinear response of premixed V-flames to equivalence ratio forcing that demonstrated significant influence of this mechanism on flame heat release. They showed that the influence was highly nonlinear, with flame pockets being pinched off the extremities of the flame shoulder due to coalescing of neighboring branches. However, the response of the flame was evaluated at one frequency of forcing alone.

Recent advancements in understanding this problem better have involved developing models that account for the interaction between acoustics, equivalence ratio fluctuations and heat release fluctuations [42, 72, 88, 89]. However, there is still a dearth for work that deals with the frequency response of the flame. While the global (and hence structural) quasi-steady limit has been discussed extensively by Polifke and Lawn [90], who presented a detailed analysis of the general flame response characteristics in the low forcing frequencies ($St \rightarrow 0$) limit starting from simplistic physical principles, the frequencies of practical interest are far from this limit.

The primary contribution of this research work is to expand on the prevalent knowledge that there exists about equivalence ratio coupled flame response [72], by studying rich flames (useful for POGT combustion), high Strouhal number flame response and nonlinear flame response to equivalence ratio perturbations.

1.3.3. Pressure Coupling Mechanism

Finally, the pressure coupling mechanism or, more precisely, *pressure-temperature-density*[2] coupling mechanism is considered. This is shown schematically in Figure 8. This mechanism concerns the sensitivity of the chemical reaction rate, and hence of reactant mass burning rate to local pressure. This mechanism has generally been neglected in prior studies of low frequency flame response, due to the fact that simple scaling arguments show that it is of $O(M_f)$ lower than the velocity coupled mechanism [91]. However, due to the increasing sensitivity of the flame speed to pressure perturbations with frequency, there is some possibility that this mechanism becomes significant at higher frequencies.

Pressure disturbances cause disturbances in the heat of reaction (Route 1), unburned reactant density (Route 2) and flame speed (Route 3), which directly cause the heat release to oscillate. Additionally, flame speed oscillations cause the burning area to oscillate, similar to the velocity and equivalence ratio mechanism (Route 3b) causing heat release oscillations indirectly.

[2] It is assumed that the three are isentropically related in the acoustic perturbation field.
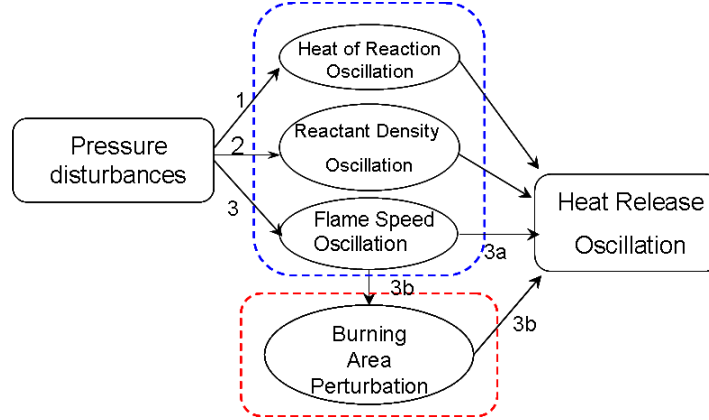
Figure 8 : Fundamental processes controlling the heat release response of premixed flames to fluctuations in pressure

Route 3 (flame speed perturbations) has received considerable theoretical treatment, through analyses of the local mass burning rate response of a flat, freely propagating premixed flame to acoustic pressure perturbations [91-98], all of which employed high activation energy asymptotics [99] with single step chemistry to analyze these interactions. The earliest effort at understanding this problem was undertaken by van Harten et al. [98] who studied the acoustic coupling effects on near-equi-diffusional flames [99] under the structurally quasi-steady, i.e., $St_\delta \to 0$ limit and the non quasi-steady $St_\delta \sim 2\pi$ limit, while operating under the assumption of negligible gas expansion. Following this, McIntosh [100] studied the effects of very low amplitude pressure perturbations, specifically $p'/p_o \sim O(M_f)$ and showed that the only coupling was through velocity perturbations that arose because of acoustic pressure perturbations; temperature perturbations did not result until $p'/p_o \sim O(\theta^{-1})$. All these studies however, operated in the limit of zero heat release by the flame. Clavin et al. [101] and McIntosh [92] independently and simultaneously published the first results which attempted to

21

relax the zero heat release limit of the flame. Linearizing the governing equations slightly differently, both these studies obtained similar results for the mass burning rate response to harmonic acoustic pressure perturbations. McIntosh [92] however provided results for a higher range of frequencies and for general Lewis numbers, while Clavin et al. [101] persisted with near-equi-diffusional flames. Both of these studies show that the flame exhibits a high pass filter character, with a *local* response that increases with as the square root of frequency at high frequencies, up to the point where the reaction zone becomes non quasi-steady.

McIntosh [91] and McIntosh and Wilce [102] then studied the effect of "ultrasound", specifically $St_\delta \sim 2\pi/M_f$ on flat premixed flames and found that even for small amplitudes (of the order of M_f), pressure-temperature coupling was seen. They claimed that nonlinear acoustics needed to be included for higher pressure amplitudes. Thereafter several studies [93-95, 103] have studied acoustic coupling of flames to non-harmonic pressure disturbances such as step disturbances, impulse functions and random disturbances.

Experimental studies of this problem are almost non-existent, save the efforts of Wangher et al. [104] who attempt to validate the models of Clavin et al. [101] and McIntosh [92]. They force a flat, lean premixed flame which is acoustically stabilized in a velocity node of a half open tube, so that the velocity field at the flame front does not oscillate and only the pressure oscillates. They note that while both these Clavin's and McIntosh's models are very similar to each other in the $St_\delta \sim 2\pi$ range of frequencies, disagreement exists between experimental data and either of these models for near-unity Lewis numbers in the range 0.9 to 1.4. They attribute these differences to uncertainties in

interpreting the chemiluminescence signal as a marker of mass burning rate fluctuations, notwithstanding which the acoustic disturbances shows a significant effect on unsteady OH* chemiluminescence, and presumably hence on reaction rate. They also argue that the assumption of single step, infinite chemistry in the models could be the cause of disparity. To investigate into this plausible reason, Schmidt and Jimenez [105] recently performed zero Mach number incompressible simulations and compressible DNS of lean, flat premixed flames using detailed chemistry, reduced chemistry and single-step chemistry. While their results were found to be by and large independent of chemistry, they were unable to reproduce the mass burning rate phase response of Wangher et al. [104], even though the amplitude demonstrated trends similar to experiments and the models of Clavin et al. [101] and McIntosh [92].

It should finally however be noted, that, to date, there are no research initiatives that treat acoustic coupling of flames with a definite geometry, i.e., non-flat flames. This geometry arises in most practical flames, by virtue of their stabilization at flame holders or through fluid mechanic aides (such as recirculation zones, vortex breakdown bubbles etc.) which lead to hydrodynamic scales in the problem. While the efforts of Wu and co-workers have considered flame-vortex interactions [106, 107] and reactant enthalpy fluctuations [108, 109], the implications of flame attachment have not be accounted for.

As may be seen from the discussion above, with multiple mechanisms and multiple routes causing heat release oscillations in premixed flames, the response of such flames to flow field disturbances is rich in physics. The principle objective of this research work, which is detailed in the next section, is to enable a more complete

understanding of some of the hitherto fully unexplored mechanisms and in a sense, filling in more pieces to the jigsaw of thermoacoustics and combustion dynamics.

1.4. Scope of the Current Research Work

1.4.1. Research Objectives

This research work aims at understanding the aforementioned coupling mechanisms and physical processes leading to heat release oscillations in attached flames. While much work has been done in understanding the response of flames to disturbances in the upstream velocity as summarized by Preetham [55], flame response to perturbations in equivalence ratio, and response to perturbations in acoustic pressure have received lesser treatment and shall form the central topics of this thesis. In particular, the equivalence ratio coupled flame response is studied in much greater detail than the pressure coupled flame response, for reasons which shall be discussed later in the thesis.

First, much attention will be focused on thoroughly understanding linear and nonlinear equivalence ratio coupled flame response by means of developing reduced order models by employing the so called G-equation approach [43, 110-113]. Linear flame response will be studied to understand the contributions of the various routes described in Figure 7, with an emphasis on understanding global and structural non quasi-steady heat release responses. The nonlinear problem will be studied using a higher order asymptotic analysis to understand the physical details and using fully nonlinear computation of the G-equation to study the heat release nonlinearity mechanisms and

characteristics. These studies will be conducted at atmospheric and gas turbine conditions in order to ascertain the differences and "scalability" of physical understanding from STP to gas turbine cycle conditions.

Second, this thesis will focus to understand high frequency flame response in greater detail. Given the fact that the velocity and fuel-air ratio coupled flame responses exhibit a low pass response character, and that the gamut of literature on acoustic coupling seems to suggest that flame speed sensitivity rises with frequency of pressure disturbances, these analyses suggest that pressure coupled flame response could grow in significance, or possibly even be dominant at high frequencies. This complex competition between these three mechanisms shall be studied under the assumption of linear acoustics and linear flame response. The practical motivation for this study is that, although high frequency (e.g., kHz frequency range), transverse oscillations have been one of the key instability concerns in rockets for decades [2, 3, 6, 8], in the last few years, a significant number of largely unpublished field occurrences with high frequency, transverse instabilities have similarly plagued low NOx gas turbines. These instabilities are extremely problematic because they can cause major damage within a matter of a few minutes, rather than over hundreds or thousands of hours, as is more typical with lower or mid-range instabilities. These observations motivate a study of high frequency combustion instabilities in premixed systems, in order to understand the potentially unique mechanisms and/or qualitatively different controlling physical processes as compared to lower frequency disturbances.

Third, we catalog and analyze the key parameters influencing the heat release response transfer function that relates various disturbances to heat release oscillations and

to identify parameter space regimes where specific mechanisms are dominant or negligible. This will be of much use in tailoring combustion dynamics models for practical applications.

1.4.2. Thesis Layout

This thesis is divided into four parts. The *first* part, discusses fundamental ideas comprising off Chapter 1 and Chapter 2, which present the 'Introduction' and 'Theoretical Formulation' of the problem of premixed flame response to upstream perturbations.

The *second* part discusses 'Linear Flame Response', and is comprised of Chapter 3 and Chapter 4. Chapter 3 studies linear flame response. The larger focus of this chapter will be on equivalence ratio coupled linear flame response, while pressure coupled flame response and high Strouhal number velocity coupled flame response[3] results are also discussed in decreasing order of detail. Chapter 4 presents a comparative study of flame response phenomena, from both a qualitative and quantitative perspective.

The *third* part of this thesis concerns 'Nonlinear response', specifically of flames responding to equivalence ratio fluctuations. Chapter 5 presents the nonlinear asymptotic analysis and computational formulation used to study nonlinear flame response and presents nonlinear flame response results.

---

[3] The low Strouhal number flame response to velocity perturbations has been comprehensively studied by Preetham [55].

The *fourth* and final part of this thesis puts forth '*Further remarks*' on the problem. Chapter 6 presents comparison of equivalence ratio coupled transfer functions with recent experiments performed at Pennsylvania State University. The implications of an inhomogeneous equivalence ratio field on flame response experimental studies are also discussed. Finally, Chapter 7 discusses problems that need further research.

Chapter 2 : Theoretical Formulation

This chapter discusses the theoretical formulation employed to study the heat release response of premixed flames to upstream perturbations. Considerable time is spent in this chapter in discussing the various time scales and length scales present in the problem. This enables in the identification of key non-dimensional parameters that control the physics of flame-acoustic interactions. This will also put into perspective the domains of applicability of the modeling approach which is used to determine the heat release rate of the flame, which is described in the latter half of this chapter.

2.1. Flame Geometry

To provide clarity to the discussions that follow later in this chapter and thesis, a representative schematic of a premixed flame with coordinate axes and some flame length scales is shown in Figure 9.

(a)   (b)
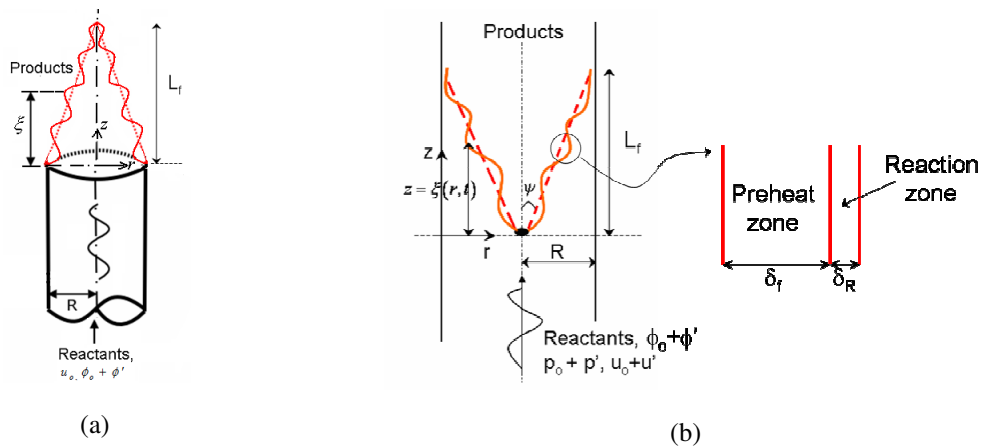
Figure 9 : Schematic of Flame Geometries (a) Axisymmetric Conical Flame (b) Axisymmetric/2D V-flame with an illustration of the flame structure. (The flame structure for the conical flame is similar and not shown)

Figure 9(a) shows a burner-stabilized stationary, conical Bunsen flame (denoted in dashed lines) which is submitted to perturbations in upstream flow velocity, reactant pressure or fuel/air ratio. The flame surface responds to these perturbations by means of wrinkling in order to match the normal component of the incoming mixture velocity, to develop a wrinkled flame shape (denote by solid lines). Figure 9(b) on the other hand, shows a ducted V-shaped flame stabilized on a center body whose dimensions are much smaller than that of the duct. The instantaneous flame position is at a height ξ from the flame holder, as shown in the figure. Suppose that the upstream disturbances occur at a frequency f and possess a phase speed u_c (which need not be equal to the mean flow velocity u_o, in general). The ratio of the mean flow velocity, to the phase speed of the disturbances, defined as

$$k_c = \frac{u_o}{u_c} \qquad (2.1)$$

has been identified in literature [46, 55, 56, 60, 65, 114, 115] as an important non-dimensional parameter in flame dynamics studies.

The orientation of the flame is represented by means of the flame aspect ratio, β, and is related to the flame half angle, ψ by:

$$\beta = \frac{L_f}{R} = \cot \psi \qquad (2.2)$$

A further non-dimensional parameter, $\alpha = \beta^2 / (1 + \beta^2)$ is defined, and is related to the flame geometry as

$$\alpha = \cos^2 \psi \qquad\qquad (2.3)$$

Also presented in Figure 9(b) is a representative sketch of the internal flame structure, which shows the preheat zone and reaction zone of the flame, of thicknesses δ_f and δ_R respectively. The flame structure is similar for a conical flame and is hence not shown.

With this background, the various time scales and length scales that exist inherently in this problem are discussed in the next two sections.

2.2. Flame Time Scales and Length Scales

2.2.1. Time Scales and Non quasi-steadiness

The table below summarizes fundamental time scales that influence the nature of flame-acoustic interactions, either through its "global" (i.e., spatially integrated over the flame surface area) response or the response of its internal structure.

Following Clanet et al. [116], we can distinguish between flame disturbance processes that influence the local internal flame structure (such as the local burning rate) or its global geometry (such as the flame area).

Table 1 : Time scales for flame-acoustic interaction

Time scale	Approximate Scaling
Acoustic disturbances	$\tau_{ac} \sim 1/f$
Mean flow residence time within flame domain	$\tau_{res} \sim L_f/u_o$
Disturbance convective time within flame domain	$\tau_{conv} \sim L_f/u_c$
Wrinkle convection time along flame front	$\tau_w \sim (1/\alpha)(L_f/u_o)$
Relaxation time associated with flame preheat zone [93]	$\tau_D \sim \delta_f/s_{Lo}$
Relaxation time associated with reaction zone [94]	$\tau_R \sim \delta_R/s_{Lo}$

At very low frequencies, the acoustic timescales are much larger than the other timescales. Hence, the convective, diffusive and reactive processes respond essentially instantaneously to harmonic disturbances. However, as frequency increases, the acoustic timescale decreases and leads to non quasi-steadiness in the global flame response.

The Strouhal number, based on frequency instead of angular frequency, defined as

$$St_f = \frac{St}{2\pi} = \frac{\tau_{res}}{\tau_{ac}} = \frac{fL_f}{u_o} \qquad (2.4)$$

arises naturally as a non-dimensional frequency parameter for the problem. However, the "global" flame position is quasi-steady when $\tau_{ac} \gg \tau_{conv}$, or equivalently when

$$\frac{\tau_{conv}}{\tau_{ac}} = \frac{fL_f}{u_c} = k_c St_f \ll 1 \qquad (2.5)$$

This global quasi-steadiness implies that the overall flame shape, length, and position at each instant of time is the same as its steady state position for the same conditions. Non quasi-steadiness in the global position of the flame occurs when the frequency increases such that $\tau_{ac} \sim \tau_{conv}$ or equivalently $k_c St_f \sim O(1)$. This means that different parts of the

flame are responding to the disturbances at different instants of time and at different locations, hence, inherently creating a "time-lag" associated with the problem. Conversely, a chosen location on the flame sees temporally varying upstream flow as it evolves in the domain.

Furthermore, as shall be discussed later, if the flame is constrained to remain attached at a flame holder at all times, a disturbance is generated at the flame holder, which propagates wrinkles generated locally due to flow field inhomogeneities, along the flame front. This means that the flame front dynamics at a chosen location is controlled by fluctuations in the flame surface at the current instant and its interaction with disturbances generated at all locations upstream along the flame front at previous times, that have been convected to the chosen location by the tangential component of the mean velocity. The flame front dynamics is hence controlled by two *fundamental* time scales – (i) the time scale associated with the propagation time of a wrinkle generated at the base along the flame front, τ_w, and, (ii) the time scale associated with the convective time of the disturbance within the flame domain, τ_{conv}. This also hints that flame position dynamics itself might be governed by a time scale that arises due to a 'beating' because of these processes. These, however, are not *fundamental* time scales. Note also, that

$$\frac{\tau_{conv}}{\tau_w} \sim \frac{L_f/u_c}{(1/\alpha)(L_f/u_o)} = k_c \alpha = k_c \cos^2 \psi \qquad (2.6)$$

and

$$\frac{\tau_{conv}}{\tau_{res}} \sim \frac{L_f/u_c}{L_f/u_o} = k_c \qquad (2.7)$$

Equation (2.6) shows that the parameter $\eta = k_c \alpha$ is a very important parameter that controls flame front dynamics for it quantifies the relative values of the disturbance convective timescale and the wrinkle propagation time scale. This point has also been discussed by prior researchers [55, 60, 114]. The role played by the ratio of disturbance phase speed to mean flow speed, k_c shall be discussed later in this chapter, but for now, it suffices to state that for convective disturbances, (i.e., vortical or entropy disturbances), $k_c \sim O(1)$. In fact, Michalke [117] shows that the shear wave convection velocity tends to vary between about 0.7 and 2 as the disturbance frequency changes. The approximation $k_c \sim 1$ attributes to the Strouhal number St_f, a physical significance as the ratio of convective disturbance timescale to excitation timescale, in addition to being a naturally occurring non-dimensional frequency. The dependence of flame front dynamics on α is weaker – in particular, note, that for very steep flames, i.e., $\psi \rightarrow 0$, it is seen that $\alpha \rightarrow 1$, so that $\tau_{conv} \approx k_c \tau_w$.

Next, consider the relative magnitudes of the acoustic time scale and time scales associated with internal flame processes. Note first that the ratio of the diffusive and excitation time scales can be written as:

$$St_{\delta,f} = \frac{St_\delta}{2\pi} = \frac{\tau_{diff}}{\tau_{ac}} = \frac{f \delta_f}{s_{Lo}} \tag{2.8}$$

When the diffusive time scales are much smaller than the disturbance timescales, the flame preheat zone responds instantaneously to imposed disturbances, i.e., the flame response is regarded as *locally* or *structurally* quasi-steady. From Eq.(2.8), the flame response is *structurally* quasi-steady when

$$St_{\delta,f} \ll 1 \qquad (2.9)$$

Hence, structural non quasi-steady response occurs when

$$St_{\delta,f} \sim 1 \qquad (2.10)$$

This time scale is primarily related to the relaxation of the preheat zone of the flame to imposed disturbances.

Note that the structural and global Strouhal numbers are themselves related by

$$\frac{St_\delta}{St} = \frac{\delta_f/s_{Lo}}{L_f/u_o} = \frac{\delta^*}{\alpha^{1/2}} \qquad (2.11)$$

where $\delta^* \triangleq \delta_f/R$ represents the preheat zone thickness non-dimensionalized by the flame holder/duct radius. Equation (2.11) implies now that, in general, $St_\delta \ll St$ for flames with $\beta \gg 1$, so that the following conclusions hold – (i) A globally quasi-steady flame is *necessarily* structurally quasi-steady, and, (ii) A structurally non quasi-steady flame is *necessarily* globally non quasi-steady. Henceforth in this thesis, a "non quasi-steady" flame will mean *structurally* non quasi-steady unless otherwise specified, while a "quasi-steady" flame, will, in general, refer to the $St \rightarrow 0$ limit.

Even when the preheat zone relaxation time is slower than that of the harmonic disturbance, i.e., $St_{\delta,f} \gg 1$, McIntosh [91] notes that the reaction zone can remain essentially quasi-steady, However, at even higher frequencies, the acoustic time scale can become of the order of the much faster reaction zone relaxation time. This would occur when $\tau_{ac} \sim \tau_R$ and can be expressed in terms of $St_{\delta,f}$ as

$$St_{\delta,f} \sim \theta^2 \qquad (2.12)$$

This scaling occurs because the ratio between the reaction and preheat zone thicknesses are related as

$$\frac{\delta_R}{\delta_f} \sim \frac{1}{\theta^2} \qquad (2.13)$$

Flame response modeling studies accounting for global non quasi-steadiness, but internal quasi-steadiness have been carried out in detail by various authors [8, 19, 24, 25, 31, 40, 47, 56, 60, 61, 64, 65, 118], and is fairly well-understood. Extensive research has been carried out on response of freely propagating flames to pressure disturbances in the internally non quasi-steady limit in the context of acoustic coupling of flames [92, 95, 97, 98] and in the context of non quasi-steady flame response to equivalence ratio fluctuations [23, 119]. Also, several analyses of ultrahigh frequency response of a freely propagating flat premixed flame are provided in Refs. [92-94, 120]. All of these analyses assume high activation energies, i.e., that $\theta \gg 1$. Under this assumption, the total flame length

$$\delta_{flame} = \delta_f + \delta_R = \delta_f \left(1 + \theta^{-2}\right) \approx \delta_f \qquad (2.14)$$

To give a feel for typical frequencies at which non quasi-steady processes gain importance, consider a methane-air reactant mixture establishing a flame of $\beta \approx 10$. At 1 atm, a typical estimate of the preheat zone thickness would be 1 mm, while the reaction zone thickness would be about 0.1mm. Thus, for reactants at 1 atm, 300 K, the flame response becomes non quasi-steady at $f\sim$400 Hz. The reaction zone becomes non quasi-

steady at f~40 kHz. For reactants at say, 10 atm, the preheat zone becomes non quasi-steady at f~4 kHz[4], while the reaction zone becomes non quasi-steady at f~400 kHz.

Thus, for typical combustion dynamics applications, we are most concerned with the *locally* non quasi-steady response of the flame, which, for typical flames would occur at frequencies of about f~400 Hz.

2.2.2. Length Scales and Non-compactness

Much in the spirit of the previous section, this section aims to delineate the various length scales that fundamentally occur in the problem. This is summarized in Table 2.

Table 2 : Relevant Length scales for Flame-acoustic interaction

Length Scales	Approximate Scaling
Acoustic wavelength	$\lambda_a = c_o / f$
Disturbance convective wavelength	$\lambda_c = u_c / f$
Wrinkle convective wavelength	$\lambda_w = u_o \cos \psi / f$
Flame length	L_f
Flame preheat zone	δ_f
Flame reaction zone	δ_R

---

[4] The methane-air chemical reaction mechanism is assumed to be estimable with a global reaction of overall order 2.

We define two types of compactness. A region of characteristic length scale l is *acoustically* compact if $l \ll \lambda_a$, i.e., if it is small with respect to the acoustic wavelength. Similarly, it is *convectively* compact if $l \ll \lambda_c$, where λ_c denotes the distance a disturbance propagates over one acoustic period at a phase speed of u_c. Note that the ratio of the acoustic and convective length scales is given by

$$\frac{\lambda_c}{\lambda_a} \sim \frac{M_o}{k_c} \tag{2.15}$$

indicating that $\lambda_c \ll \lambda_a$ at low flow Mach numbers typical of deflagrations. This implies that at low flow Mach numbers, the following hold true – (i) convective compactness implies acoustic compactness, and, (ii) acoustic non-compactness implies convective non-compactness.

With this background, we now discuss various domains of non-compactness. At very low frequencies, the acoustic and convective wavelengths are much larger than the other length scales, and hence, the flame as well as the flame structure is *acoustically* and *convectively compact*.

Consider first the response of the flame to convecting disturbances. The flame length becomes on the order of the convective wavelength (assuming $k_c \sim 1$) when $St_f \sim O(1)$ (or, more precisely, when $St_f \sim 1/k_c$). Thus, *convective compactness implies global quasi-steadiness*, and *global non quasi-steadiness implies convective non-compactness of the global flame*.

Similarly, the internal flame structure for flat flames ($\beta = 0$) becomes non-compact to convecting disturbances when $St_{\delta,f} \sim O(1)$. However, non-compactness and non quasi-steadiness can be directly related only for flat flames. More generally, the preheat zone is convectively non-compact when:

$$St_{\delta,f} \sim \frac{\left(1+\beta^2\right)^{1/2}}{k_c} \qquad (2.16)$$

This may be expressed in terms of St_f as

$$St_f \sim \frac{\beta}{k_c \delta^*} \qquad (2.17)$$

From a modeling perspective, convective non-compactness implies that one has to account for the variation of properties in the preheat zone – it also implies that certain foundational assumptions of the G-equation modeling approach which are detailed in the next section, are suspect and one must carry out a more careful matched asymptotic expansion to couple the flow fields upstream and downstream of the flame [93, 98, 99]. However, for $\beta \gg 1$, the flame structure is convectively non-compact at much higher frequencies, than when the flame response is *locally* non quasi-steady. Finally, the *reaction zone is convectively non-compact* when $\delta_R \sim \lambda_c$, or

$$St_{\delta,f} \sim \theta^2 \left(1+\beta^2\right)^{1/2} \qquad (2.18)$$

We next consider the flame response to acoustic wave disturbances. In these cases, the criteria for non quasi-steadiness and non-compactness are not the same. Rather, for low Mach number flows, the flame response becomes non quasi-steady at

much lower frequencies than when the flame becomes non-compact. For example, the overall flame becomes acoustically compact when

$$St_f \sim 1/M_o \qquad (2.19)$$

The acoustically non-compact limit is an important one because, global heat release transfer functions, such as those that will be considered later in this thesis become less relevant for the combustion instability problem. Rather, as stated by the Rayleigh criterion, one is interested in the spatial integral of the product of the pressure and heat release. Mathematically, the Rayleigh integral may be written as $\int\limits_{flame} p'(x,t)q'(x,t)\,dA$.

For acoustically compact flames, this may be written as $p'(x,t)Q'(t)$. However, non-compact flames with the same global transfer functions can potentially have very different Rayleigh products.

Further, the *preheat zone* becomes *acoustically non-compact* when $\delta_f \sim \lambda_a$, *i.e.,* when

$$St_{\delta,f} \sim 1/M_f \qquad (2.20)$$

Hence, at these frequencies, the flame structure has to be necessarily resolved to be able to understand the physics of flame-acoustic interactions. Finally, the *reaction zone loses acoustic compactness* when $\delta_R \sim \lambda_a$, *i.e.*, when

$$St_{\delta,f} \sim \theta^2/M_f \qquad (2.21)$$

2.2.3. Summary of Flame Non-compactness and Non quasi-steadiness

In order to provide clarity to the discussions of the previous two subsections, this section briefly summarizes observations relating acoustic and convective non-compactness to global and structural/local non quasi-steadiness. The key conclusions are the following.

i.   Global quasi-steadiness implies structural/local quasi-steadiness

ii.   Local non quasi-steadiness implies global non quasi-steadiness

iii. Convective compactness implies acoustic compactness

iv.   Acoustic non-compactness implies convective non-compactness

v.   Convective compactness implies global quasi-steadiness, and hence structural quasi-steadiness

vi.   Global non quasi-steadiness implies convective non-compactness of the global flame. The flame could still be locally quasi-steady, and acoustically compact.
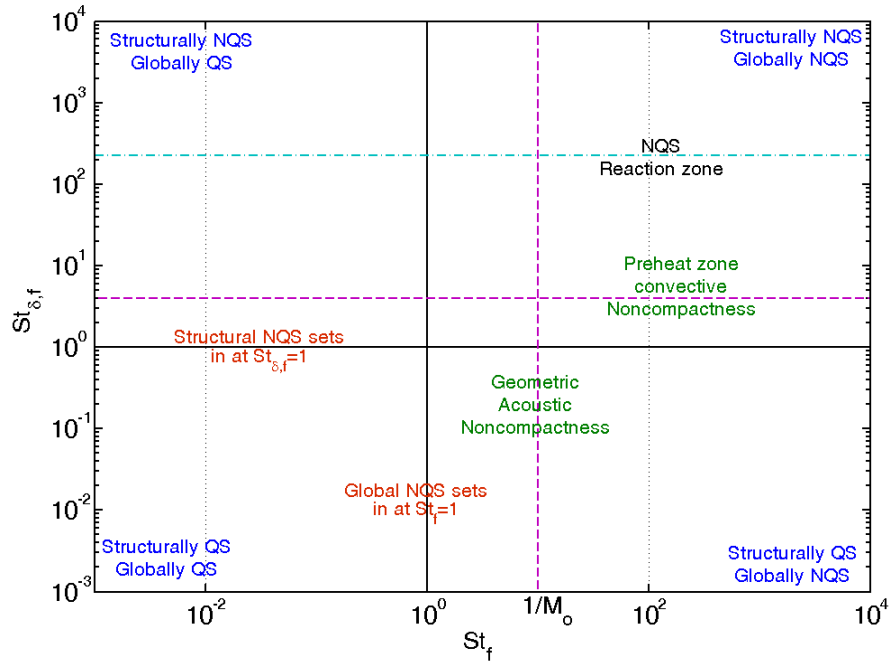
Figure 10 : A preliminary 'Regime diagram' showing various global and structural flame response regimes for $k_c \sim 1$**. The solid lines** $St_f = 1$ **and** $St_{\delta,f} = 1$ **which respectively represent criteria for global and structural non quasi-steady processes to gain importance splits the regime diagram into four quadrants, whose 'properties' are shown in their respective corners.**

The complex relationship between convective/acoustic compactness and local/global quasi-steadiness is elucidated by means of a 'regime diagram' in Figure 10. One of the objectives of this thesis will be to populate this regime diagram using criteria at which various physical processes such as flame stretch and axial diffusion of disturbances etc. influence the global heat release response of the flame, as well as represent the importance of various coupling processes.

2.3. Analytical Formulation

This section discusses the mathematical details of the estimation of the heat release response of the flame. The determination of the instantaneous flame surface location is first discussed, followed by the evaluation of the instantaneous heat release rate and heat release response of the flame. The section concludes with a discussion of the character of the disturbance fields in pressure, velocity and equivalence ratio.

2.3.1. Flame Front Evolution

Central to the determination of the heat release response of the flame are the constituent pieces that form up the heat release rate, as previously discussed in Chapter 1. Fundamentally, flame response is brought about by a change in the flame shape from its stationary flame shape. Further, as noted by Clanet et al. [116], these flame surface disturbances may be effected by processes by either influencing the local internal flame structure, such as flame speed variations, or its global geometry, such as the flame area. Notwithstanding these two possible fundamental routes, the instantaneous flame front location is the first piece of information that is needed to evaluate the flame heat release response.

The analytical framework adopted to model the flame response uses the G-equation, which has received considerable attention in literature for over four decades now, starting with the work of Markstein [110] as far ago as 1970. A number of

researchers, [8, 24, 43, 72, 110, 111, 113][5], for instance, have subsequently used the G-equation in a variety of flame response studies that has involved determination of the flame surface.

As such, the G-equation is a kinematic equation describing the motion of a thin interface, with velocity $\vec{V}_F$ into an incoming velocity field, $\vec{u}(\vec{r},t)$. In the context of premixed flames, as long as the flame structure is *convectively compact* to upstream disturbances, it may be assumed to be a thin gas dynamic surface separating the reactants from the products, which may be represented implicitly by the isocontour of a function, $G(r,z,t)$. In other words,

$$G(r,z,t)\big|_{flame} = G_0 \tag{2.22}$$

The value of G at points that do not lie on the flame may be defined such that $G < G_0$ in the reactants and $G > G_0$ in the products. It has to emphasized here that the choice of G_0 is completely arbitrary and bears no physical reason or value, owing to the generalized scaling symmetry of the G-equation, as discussed by Oberlack et al. [121]. The only requirement, however, is that $G(r,z,t)$ is a monotonically increasing function across the flame surface, and itself differentiable at the flame surface. Since Eq.(2.22) holds good at all instants of time, the Lagrangian derivative of G vanishes at the level-set describing the flame surface, so that

$$\frac{DG}{Dt}\bigg|_{G=G_0} = 0 \tag{2.23}$$

---

[5] This list of references is only representative and, by no means, is an exhaustive list of prior research work that has employed the G-equation.

Expanding Eq.(2.23) in the Eulerian form, with reference to the coordinate system described in Figure 9, yields

$$\frac{\partial G}{\partial t} + \left(\vec{V}_F \cdot \nabla \right) G = 0 \tag{2.24}$$

for all points on the $G = G_0$ iso-surface. The flame front evolution is hence tracked implicitly.

Next, the velocity at which the flame surface advects, $\vec{V}_F$, arises as a resultant of the instantaneous flow velocity just upstream of the flame surface and the motion of the flame surface normal to itself at the local laminar burning velocity, $s_L \vec{n}$, where the normal vector $\vec{n}$ is defined positive into the reactants. Hence

$$\vec{n} = -\frac{\nabla G}{|\nabla G|} \tag{2.25}$$

and

$$\vec{V}_F = \vec{u} + s_L \vec{n} \tag{2.26}$$

This yields the following form of the G-equation [110]:

$$\frac{\partial G}{\partial t} + \vec{u} \cdot \nabla G = s_L |\nabla G| \tag{2.27}$$

To reiterate, the only assumption that has gone into Eq.(2.27) is that the flame structure is convectively compact to disturbances, and is treatable as a thin discontinuity separating reactant and product mixtures. This means that the Eq.(2.27) is, in general, valid even while the flame is wrinkled, insofar as the flame surface is continuous, and there are no local extinction and re-ignition events that lead to flame holes.

As such, the influences of diffusive, reactive and relaxation processes internal to the flame structure are included in Eq.(2.27) through the effect of these processes on the local laminar flame speed, such as the effect of oscillatory stretch rate [122], oscillatory reactant pressure [91-93, 102] etc.

In general, Eq.(2.27), together with a suitable boundary condition, can be solved numerically (implicitly) to capture complex flame front motions, such as cusp and pocket formation [23, 87] or multi-valued flame fronts. This will be discussed later in Chapter 5 in the context of nonlinear flame response to equivalence ratio perturbations.

Alternatively, Eq.(2.27) can also be solved by explicitly specifying a form for the level-set function $G(r,z,t)$. For example, with reference to Figure 9, one may specify

$$G(r,z,t) = z - \xi(r,t) \tag{2.28}$$

so that the flame front evolution may now be explicitly described as

$$\frac{\partial \xi}{\partial t} + s_L \left(1 + \left(\frac{\partial \xi}{\partial r} \right)^2 \right)^{1/2} = u - v \left(\frac{\partial \xi}{\partial r} \right) \tag{2.29}$$

where, $\vec{u}(r,z,t) = u(r,z,t)\vec{e}_z + v(r,z,t)\vec{e}_r$ denotes an axisymmetric field for the velocity of the reactant mixture.

The knowledge of the instantaneous flame front location permits the calculation of instantaneous heat release of the flame, as described next.

2.3.2. Instantaneous Heat Release Calculation

The instantaneous heat release rate of the flame is expressed as the summation of the local mass burning rate times the heat of reaction of the reactant mixture along the entire flame surface area, as expressed in Eq.(1.1), which is reproduced here for convenience:

$$q(t) = \int_{flame} \rho_u s_L h_R dA \qquad (2.30)$$

Equation (2.30) may also be written using G as

$$q(t) = \int_{\mathscr{S}} 2\pi r \rho_u s_L h_R \delta(G) |\nabla G| d\mathscr{S} \qquad (2.31)$$

where the integration is performed locally over a band of grid points $\mathscr{S}$ around the flame and $\delta(G)$ is the Dirac-delta function. This is discussed in greater detail in Chapter 5.

As such, Eq.(2.30) may be utilized to isolate the contributions of various routes that lead to heat release, as discussed in Chapter 1. Perturbing each of the quantities in Eq.(2.30) about their mean values, we obtain

$$\frac{q(t)}{q_o} = \int_{flame} \left(1 + \frac{\rho'}{\rho_o}\right)\left(1 + \frac{s'_L}{s_{Lo}}\right)\left(1 + \frac{h'_R}{h_{Ro}}\right)\frac{dA}{A_o} \qquad (2.32)$$

Expanding Eq.(2.32) yields

$$\frac{q(t)}{q_o} = \begin{cases} \dfrac{A(t)}{A_o} + \\[2mm] + \displaystyle\int_{flame} \frac{\rho'}{\rho_o} \cdot \frac{dA}{A_o} + \int_{flame} \frac{s_L'}{s_{Lo}} \cdot \frac{dA}{A_o} + \int_{flame} \frac{h_R'}{h_{Ro}} \cdot \frac{dA}{A_o} + \\[4mm] + \displaystyle\int_{flame} \frac{\rho'}{\rho_o} \cdot \frac{s_L'}{s_{Lo}} \cdot \frac{dA}{A_o} + \int_{flame} \frac{s_L'}{s_{Lo}} \cdot \frac{h_R'}{h_{Ro}} \cdot \frac{dA}{A_o} + \int_{flame} \frac{\rho'}{\rho_o} \cdot \frac{h_R'}{h_{Ro}} \cdot \frac{dA}{A_o} \\[4mm] + \displaystyle\int_{flame} \frac{\rho'}{\rho_o} \cdot \frac{s_L'}{s_{Lo}} \cdot \frac{h_R'}{h_{Ro}} \cdot \frac{dA}{A_o} \end{cases} \tag{2.33}$$

Equation (2.33) has all possible contributions (due to both *direct* and *indirect* mechanisms) to the unsteady heat release arising due to upstream fluctuations. The terms on the RHS of Eq. (2.33) are grouped linewise in the order of their contributions (i.e. O(perturbation amplitude), O((perturbation amplitude)^2) etc.). The RHS possesses all information regarding the physical processes leading to unsteady heat release. Depending on the actual reactant variable that is being disturbed, some of the contributions on the RHS of Eq. (2.33) may be zero. For example, in the case of an equivalence ratio perturbation that occurs at constant density, all terms with ρ' would be zero. Some of these terms may also be explicitly evaluated in terms of the flame geometry as shall be discussed in Chapter 3.

2.3.3. Heat Release Response of the Flame

The unsteady heat release evaluated in the previous subsection then permits the determination of the flame heat release response, which is quantified by means of a *Transfer Function* written as:

$$\frac{q'(\omega)}{q_o} = F_u \frac{u'(\omega)}{u_o} + F_p \frac{p'(\omega)}{p_o} + F_\phi \frac{\phi'(\omega)}{\phi_o} \qquad (2.34)$$

where these transfer functions F_u, F_p and F_ϕ are defined as :

$$F_p = \frac{\widehat{q'}(\omega)/q_o}{\hat{p}'_{ref}(\omega)/p_o} \qquad (2.35)$$

$$F_u = \frac{\widehat{q'}(\omega)/q_o}{\hat{u}'_{ref}(\omega)/u_o} \qquad (2.36)$$

$$F_\phi = \frac{\widehat{q'}(\omega)/q_o}{\hat{\phi}'_{ref}(\omega)/\phi_o} \qquad (2.37)$$

The numerators in each of the transfer functions of Eqs.(2.35)-(2.37) are the Fourier transforms of the instantaneous heat release evaluated at the forcing frequency, while the denominators are fluctuations in pressure, velocity or fuel/air ratio at a reference location, also evaluated at the forcing frequency. The selection of a suitable reference velocity is a non-trivial question, and for the current research work, fluctuations at the flame base are assumed as reference quantities.

These transfer functions denote the "output" of the flame in terms of the heat release, to a specified "input" strength of the disturbances. These transfer functions are complex quantities, the amplitude of which describes the amplification or attenuation of the input disturbance strength, and the phase (with reference to a suitable reference) describes the time lag in the global flame response to input disturbances. In some sense, this can be treated as an equivalent form of the $n - \tau$ model [9, 31, 40, 41, 61], which may be written generally as

$$\frac{q'(t)}{q_o} = \sum_{\chi=u,p,\phi} n_\chi \frac{\chi'(t-\tau_\chi)}{\chi_o} \qquad (2.38)$$

Before proceeding further, it is important to note that Eq.(2.34) assumes that the heat release response occurs independently to each of the disturbances on the RHS. Each of these disturbances contributes to the heat release rate through various routes, direct and indirect, as discussed in Chapter 1. Hence, the contributions to instantaneous heat release of the flame due to each of these routes can be written as in Eq.(2.33). While nonlinear heat release response due to each of these coupling mechanisms is captured by Eq.(2.34), nonlinear interactions between these coupling mechanisms themselves are disregarded.

In this spirit, the total transfer function arising due to each of these coupling mechanisms, can be estimated by taking the Fourier Transform of all the terms in Eq.(2.33). This may be expressed formally as

$$F = \begin{cases} F_A + \\ F_{\rho-A} + F_{s_L-A} + F_{h_R-A} + \\ F_{\rho-s_L-A} + F_{s_L-h_R-A} + F_{\rho-h_R-A} + \\ F_{\rho-s_L-h_R-A} \end{cases} \qquad (2.39)$$

where the transfer functions on the RHS of Eq.(2.39) arise because of their exact positional counterparts on the RHS of Eq.(2.33). Again, as discussed previously, for a given coupling mechanism, some of these terms may be zero. For example, for pressure coupled flame response, the heat of reaction routes are almost insensitive [39] so that F_{h_R-A}, $F_{s_L-h_R-A}$, $F_{\rho-h_R-A}$ and $F_{\rho-s_L-h_R-A}$ are all zero.

Evaluation of these transfer functions and studying their trends with varying Strouhal numbers provide information on the frequency response characteristics of the heat release of the flame and shall be the central focus of this thesis.

2.4. Disturbance Field Characteristics

The final piece of information needed to estimate the heat release response transfer functions described in the previous subsection is the character of various disturbance fields that perturb the flame and hence, the flame heat release.

An arbitrary, low amplitude disturbance field may be decomposed into three canonical types of disturbances [123, 124] - vortical, entropy, and acoustic. In particular, perturbations in flow vorticity, entropy and pressure may be decomposed as follows:

$$
\begin{aligned}
\vec{\Omega}' &= \vec{\Omega}'_a + \vec{\Omega}'_s + \vec{\Omega}'_\Omega \\
s' &= s'_a + s'_s + s'_\Omega \\
p' &= p'_a + p'_s + p'_\Omega
\end{aligned}
\tag{2.40}
$$

The subscripts a, s and Ω denote fluctuations induced by acoustic, entropy and vorticity mode fluctuations. Following Chu and Kovásznay [123], it may be shown that within the linear approximation (as used in Eq.(2.40)), insofar as the mean quantities are uniform and homogeneous, these three disturbance modes propagate independent of one another, and are completely decoupled. This means that

$$
\begin{aligned}
\vec{\Omega}' &= \vec{\Omega}'_\Omega \\
s' &= s'_s \\
p' &= p'_a
\end{aligned}
\tag{2.41}
$$

Furthermore, this also means that the velocity fluctuations induced by vorticity and acoustic disturbances, $\vec{u}'_\Omega$ and $\vec{u}'_a$ propagate independent of one another and can each influence the flame independently. Also to be noted is the fact that while acoustic disturbances propagate with a characteristic velocity equal to the speed of sound, vorticity and entropy disturbances are convected at a phase speed close to the bulk flow velocity, $\vec{u}_o$. This is what leads to a substantial disparity in the length scales between acoustic and vortical/entropy modes in low Mach number flows.

For the purposes of the discussion in this chapter and use in this thesis, these disturbance fields are assumed to be one-dimensional in nature. As long as the domain is free of sharp edges which induce multidimensional character into these disturbances fields, this assumption is reasonable. Also, wave refraction off the flame, another potential source for disturbance multidimensionality, is also neglected.

The following table summarizes possible coupling mechanisms, their disturbance modes and their governing equations.

Table 3 : Disturbance mode characters, propagation velocities and governing equations for disturbance fields associated with different coupling mechanisms

Coupling mechanism	Disturbance mode character	Propagation velocity	Governing Equation
Velocity	Acoustic	c_o	Acoustic wave/momentum
	Vortical/convective	u_o	Momentum

Table 3 (continued)

Equivalence ratio	Entropy/convective	u_o	Species transport
Pressure	Acoustic	c_o	Wave Equation

Following Table 3, the disturbance fields for acoustic pressure, acoustic velocity, convective velocity and equivalence ratio perturbations can be obtained by solving the respective governing equations, assuming that their respective oscillations at the flame base is harmonic, say,

$$\chi'_{base}(t) = \varepsilon_\chi \chi_o \cos(\omega t) \tag{2.42}$$

With this assumption, the disturbance fields may be obtained as follows:

$$\text{Pressure: } \frac{p'(z,t)}{p_o} = \varepsilon_p \cos\left(\omega\left(t - \frac{z}{c_o}\right)\right) \tag{2.43}$$

$$\text{Acoustic velocity: } \frac{u'_a(z,t)}{u_o} = \varepsilon_{u,a} \cos\left(\omega\left(t - \frac{z}{c_o}\right)\right) \tag{2.44}$$

$$\text{Vortical velocity: } \frac{u'_\Omega(z,t)}{u_o} = \varepsilon_{u,\Omega} \exp\left(-\frac{z}{\mathcal{L}_u(\omega)}\right) \cos\left(\omega\left(t - \frac{z}{u_{c,u}(\omega)}\right)\right) \tag{2.45}$$

$$\text{Equivalence ratio: } \frac{\phi'(z,t)}{\phi_o} = \varepsilon_\phi \exp\left(-\frac{z}{\mathcal{L}_\phi(\omega)}\right) \cos\left(\omega\left(t - \frac{z}{u_{c,\phi}(\omega)}\right)\right) \tag{2.46}$$

Expressions for the decay lengths, $\mathcal{L}_u$ and $\mathcal{L}_\phi$, and the phase speeds $u_{c,u}$ and $u_{c,\phi}$ are provided in Appendix A and Appendix B respectively. Further, from the acoustic Euler equation, it can be seen that

$$\varepsilon_{u,a} = \frac{1}{\gamma M_o} \varepsilon_p \qquad (2.47)$$

Also, following Perrachio and Proscia [76] , it may be shown that

$$\varepsilon_\phi = -\varepsilon_{u,a} \qquad (2.48)$$

Finally, in the low frequency limit, all the disturbances assume the form of travelling waves.

$$\frac{\chi'(z,t)}{\chi_o} = \varepsilon_\chi \cos\left(\omega\left(t - \frac{z}{u_\chi}\right)\right); \quad \chi = p, u_a, u_\Omega, \phi \qquad (2.49)$$

with the disturbance phase speeds

$$u_{c,\chi} = \begin{cases} c_o, & \chi = p, u_a \\ u_o, & \chi = u_\Omega, \phi \end{cases} \qquad (2.50)$$

With the formulation fundamentals presented in this chapter, the subsequent chapters will present results of transfer function calculations and attempt to understand the physics of flame response and the complex competition that exist between various coupling processes.

Chapter 3 : Linear Flame Response

3.1. Synopsis

This chapter presents a discussion of the linear response of the flame to velocity, pressure and equivalence ratio disturbances. As noted previously in Chapter 1 (see Figure 3), for low excitation amplitudes, the driving and damping processes can be approximated to be linear. It is in this $\varepsilon \to 0$ limit that the flame response will be addressed in this chapter. Prior to the actual discussion of the flame transfer function expressions and illustrative results, a generalized theory is developed for linear flame transfer function calculations. The illustrative results account for various phenomena such as flame structural non quasi-steadiness and flame stretch rate oscillations due to burning area oscillations.

Much of the work related to velocity coupled flame response has been extensively treated by Preetham [55] earlier. As such, the contribution of this work to the already existing understanding on this matter will be to explore high frequency flame response more carefully, by accounting for flame stretch and vortical velocity diffusion effects on flame transfer functions. Finally, this work also presents the first comprehensive treatment of equivalence ratio coupled flame response incorporating non quasi-steadiness, flame stretch and disturbance diffusion effects. This will form the bulk of the discussion in this chapter.

From a utilitarian perspective, a linear flame response model is the simplest possible conceptualization of the complex problem of flame-acoustic interaction, as discussed in Chapter 1. Many of these models are used for rapidly being able to predict

growth rates in combustion dynamics analysis tools in the gas turbine industry. Notwithstanding certain inherent assumptions and lacunae, which shall be discussed in Chapter 6, such reduced order modeling approaches are very advantageous to the gas turbine industry, in that, they achieve considerable downsizing in time and cost in comparison to time and capital intensive processes such as reacting flow CFD and/or experimental flame response studies, while accounting for important physical processes that lead to flame response. Of course, a better foundational knowledge of the flow field processes and physics is possible only from CFD/experiments, which ultimately help in improving the fidelity of these reduced order models. In that sense, such modeling approaches have evolved from being mere academic exercises, to one of the central themes in contemporary gas turbine research.

With this background, a generalized theory for linear flame response is presented next.

3.2. Theoretical Considerations

3.2.1. Recap of G-equation and Non-dimensionalization

The starting point for the discussion of linear flame response that follows in this section and the rest of this chapter will be the G-equation, discussed in some detail in Chapter 2, which is reproduced here for convenience.

$$\frac{\partial G}{\partial t} + \vec{u} \cdot \nabla G = s_L \left| \nabla G \right|$$

(3.1)

For very small excitation amplitude, the flame surface can be assumed to wrinkle very slightly, such that the $G = G_0$ isosurface represents a single valued curve. This single-valuedness of the flame surface permits the level-set function $G(r,z,t)$ to be defined explicitly, using a coordinate variable and the flame front location. Choosing $G_0 = 0$, with reference to Figure 9, we let

$$G(r,z,t) = z - \xi(r,t) \tag{3.2}$$

so that the flame front evolution may now be explicitly described as

$$\frac{\partial \xi}{\partial t} + s_L \left(1 + \left(\frac{\partial \xi}{\partial r} \right)^2 \right)^{1/2} = u - v \left(\frac{\partial \xi}{\partial r} \right) \tag{3.3}$$

where, $\vec{u}(r,z,t) = u(r,z,t)\vec{e}_z + v(r,z,t)\vec{e}_r$ denotes an axisymmetric field for the velocity of the reactant mixture.

The following non-dimensionalization is employed. All velocities are normalized by the mean flow velocity u_o, radial length scales by burner duct width R, axial length scales by the stationary flame length L_f. Time is normalized by the disturbance residence time, L_f / u_o. For variables in Eq.(3.3), we have the non-dimensional parameters: $r^* = r/R$, $\xi^* = \xi/L_f$ and $t^* = tu_o/L_f$ with R being chosen to be the duct half-width yields

$$\frac{\partial \xi^*}{\partial t^*} + \left(\frac{s_L}{s_{Lo}} \right) \left(\frac{1 + \beta^2 \left(\partial \xi^* / \partial r^* \right)^2}{1 + \beta^2} \right)^{1/2} = u^* - v^* \beta \frac{\partial \xi^*}{\partial r^*} \tag{3.4}$$

3.2.2. Linear Perturbation Analysis

Equation (3.4) describes the evolution of a single-valued flame front in general. Write $(\ ) = (\ )_o + (\ )'$, where the subscript 'o' denotes undisturbed variables. Then, an equation can be written for the stationary flame position ξ_o^* as:

$$\left(\frac{\beta^2}{1+\beta^2} - \frac{v_o^2}{u_o^2} \beta^2 \right) \left(\frac{\partial \xi_o^*}{\partial r^*} \right)^2 + 2 \frac{v_o}{u_o} \beta \frac{\partial \xi_o^*}{\partial r^*} - \frac{\beta^2}{1+\beta^2} = 0 \tag{3.5}$$

In the case of a homogeneous mean axial flow, continuity equation renders v_o zero. This leads to an equation for flame shape slope as:

$$\frac{\partial \xi_o^*}{\partial r^*} = \pm 1 \tag{3.6}$$

The positive slope for the flame denotes the left branch of the flame, while the negative unity slope represents the right branch. The effect of flame stretch on mean shape is more subtle and discussed later in this chapter. Due to the assumption of axisymmetry, the analyses in the remainder part of the thesis will use the right branch of the flame (negative slope branch). The evolution equation for flame position perturbation may then be derived to be:

$$\frac{\partial \xi'^*}{\partial t^*} + \left(1 + \frac{s_L'}{s_{Lo}} \right) \left(1 - \alpha + \alpha \left(-1 + \frac{\partial \xi'^*}{\partial r^*} \right)^2 \right)^{1/2} = 1 + \frac{u'}{u_o} \tag{3.7}$$

Equation (3.7) may be linearized to yield:

$$\frac{\partial \xi'^*}{\partial t^*} - \alpha \frac{\partial \xi'^*}{\partial r^*} = \frac{u'}{u_o} - \frac{s_L'}{s_{Lo}} \tag{3.8}$$

This may be alternatively cast into the form:

$$\frac{\partial \xi'}{\partial t} - u_{To} \frac{\partial \xi'}{\partial \ell} = u'_n - s'_L \qquad (3.9)$$

The subscripts 'T' and 'n' denote the velocity components tangential and normal to the mean flame front, while $d\ell$ denotes a differential length *along* the flame front. Equation (3.9) sheds light upon the fundamental physical process that causes flame surface fluctuations. The RHS of Eq.(3.9) shows that flame surface fluctuations are generated by perturbations either in the normal component of the reactant flow velocity or flame speed. In the linear flame response regime, it is immaterial whether the velocity perturbations that cause flame front perturbations occur in axial or radial velocity – only the normal component of velocity, which could occur because either of these perturbations is responsible. Further, the fluctuations in flame surface location about its undisturbed position, manifest as 'wrinkles' that are then advected along the flame front at the tangential mean flow velocity.

Hence, the two-tier process that leads to flame response can be envisaged to occur due to (i) local wrinkle generation due to local flow velocity and flame speed fluctuations, and (ii) advection of these wrinkles along the flame surface at the mean tangential flow velocity. Associated respectively with these processes are the time scales $\tau_{conv} = L_f / u_c$ and $\tau_w = \left(L_f / \cos \psi \right) / u_{To}$ identified apriori in Table 1. Furthermore, Eq.(3.9) also puts into perspective the routes that lead to flame response as discussed in Figure 4-6 by means of a mathematical foundation. It also indicates that, to determine flame front fluctuations, in addition to prescription of the velocity disturbance field, it is

required to be able to represent the influence of fuel/air ratio and reactant pressure fluctuations on flame speed fluctuations.

3.2.3. Flame Speed Fluctuations

In the linear framework, for weak curvature, the flame speed perturbation may be expressed in terms of its dependence on various factors, such as flame curvature, hydrodynamic strain, acoustic pressure fluctuations, fuel/air ratio disturbances etc., at the flame front location as follows:

$$\frac{s_L'}{s_{Lo}} = \sum_{j=c,s,p,\phi,\dots} s_{L1,j} \left.\frac{j'}{j_o}\right|_{z=\xi(r,t)} \tag{3.10}$$

where, the coefficients $s_{L1,j}$ are the frequency dependent linear sensitivities to changes in j defined as:

$$s_{L1,j} = \left.\frac{\partial\left(s_L/s_{Lo}\right)}{\partial\left(j/j_o\right)}\right|_{j=j_o} \tag{3.11}$$

3.2.3.1 Effect of Flame Stretch

Consider first, the effect of flame stretch upon the flame speed [125], caused due to curvature and strain rate fluctuations, which are also introduced by acoustic or vortical velocity perturbations. As such, the stretch rate of the flame, defined as the rate of flame surface area change relative to the original area, can be estimated to arise due to flow

strain and flame front curvature, the effects of which can be combined together to obtain [122]:

$$\kappa = -\vec{n} \cdot \nabla \times \left(\vec{u}\big|_{z=\xi(r,t)} \times \vec{n} \right) + \left(\vec{V}_F \cdot \vec{n} \right) \left(\nabla \cdot \vec{n} \right) \tag{3.12}$$

In fact, identities from vector calculus help in rewriting Eq.(3.12) in a more physically insightful as:

$$\kappa = \underbrace{\left(\nabla \cdot \vec{u} - \vec{n} \cdot \left(\vec{n} \cdot \nabla \right) \vec{u} \right)\big|_{z=\xi(r,t)}}_{\kappa_s} + \underbrace{s_L \left(\nabla \cdot \vec{n} \right)}_{\kappa_c} \tag{3.13}$$

The above expression may also be written in tensor notation as:

$$\kappa = \frac{\partial u_i}{\partial x_i} - n_i n_j \frac{\partial u_i}{\partial x_j} + s_L \frac{\partial n_i}{\partial x_i} \tag{3.14}$$

This form of the flame stretch rate aids in isolating the contributions to flame stretch due to curvature and hydrodynamic strain. In fact, either of these contributions can be written explicitly in terms of the flame front location. For example, the curvature of the flame is given by:

$$\nabla \cdot \vec{n} = \frac{\partial^2 \xi / \partial r^2}{\left(1 + \left(\partial \xi / \partial r \right)^2 \right)^{3/2}} + \frac{1}{r} \frac{\partial \xi / \partial r}{\left(1 + \left(\partial \xi / \partial r \right)^2 \right)^{1/2}} \tag{3.15}$$

Here, the two terms on the RHS of Eq.(3.15) account for axial and azimuthal curvature respectively.

In general, for flame thicknesses which are much smaller than the burner duct width or any other characteristic flame geometric length scale, the influence of flame

stretch through curvature and hydrodynamic strain on the flame speed can be expressed as:

$$\frac{s_L}{s_{Lo}} = 1 - \mathscr{L}_c\left(\nabla \cdot \vec{n}\right) + \mathscr{L}_s \frac{1}{s_{Lo}}\left(\nabla \cdot \vec{u} - \vec{n} \cdot \left(\vec{n} \cdot \nabla\right)\vec{u}\right)\bigg|_{z=\xi(r,t)} + O\left(\left(\frac{\delta_f}{R}\right)^2\right) \qquad (3.16)$$

where $\mathscr{L}_c$ and $\mathscr{L}_s$ are the Markstein lengths associated with flame curvature and strain respectively. In fact, in terms of the flame front location, flame slope and convexity, Eq.(3.16) may be rewritten as:

$$\frac{s_L}{s_{Lo}} = 1 - \mathscr{L}_c\left[\frac{\xi_{rr}}{\left(1+\xi_r^2\right)^{3/2}} + \frac{1}{r}\frac{\xi_r}{\left(1+\xi_r^2\right)^{1/2}}\right] + \mathscr{L}_s\left[\frac{1}{s_{Lo}}\frac{\xi_r^2}{1+\xi_r^2}\frac{\partial u'}{\partial z}\bigg|_{z=\xi(r,t)}\right] \qquad (3.17)$$

where the subscripts 'r' and 'rr' denote the first and second partial derivatives with respect to r. When suitably non-dimensionalized, an expression can be written for the flame speed fluctuations arising due to unsteady stretch as:

$$\frac{s_L'}{s_{Lo}} = -\sigma_c\beta\left[\frac{\xi_{r^*r^*}^*}{\left(1+\xi_{r^*}^{*2}\right)^{3/2}} + \frac{1}{r^*}\frac{\xi_{r^*}^*}{\left(1+\xi_{r^*}^{*2}\right)^{1/2}}\right] + \sigma_s\beta\left(1+\beta^2\right)^{1/2}\left[\frac{\xi_{r^*}^{*2}}{1+\xi_{r^*}^{*2}}\frac{\partial u'^*}{\partial z^*}\bigg|_{\xi^*\left(r^*,t^*\right)}\right] (3.18)$$

Here, $\left(\sigma_c, \sigma_s\right) = \left(\mathscr{L}_c/R, \mathscr{L}_s/R\right)$ are the Markstein numbers for curvature and strain. For the general unsteady problem, these Markstein numbers are the linear operators of the curvature and strain integrals with timewise kernels, as discussed by Joulin [126] and Clavin and Joulin [127]. This means that in general, the flame speed response to stretch is a non quasi-steady phenomenon; an equivalent way of stating this, is that the Markstein numbers, $\left(\sigma_c, \sigma_s\right)$ are functions of frequency in the frequency domain representation of Eq.(3.18). Joulin's [126] analysis predicts that the flame speed sensitivity to unsteady

curvature and strain rate have different frequency response characteristics. The unsteady strain effect diminishes with frequency, while the unsteady curvature term is largely independent of frequency. The latter prediction has not been assessed experimentally or computationally, while the former prediction is consistent with the calculations of Im and Chen [128], who show that the flame speed response to strain rate fluctuations attenuates as the frequency increases.

For the case of constant density, Joulin [126] obtains explicit expressions for these Markstein numbers at the excitation Strouhal number as follows [55]:

$$\hat{\sigma}_c = \delta^* \frac{1 + \dfrac{le}{2} \dfrac{h_+}{h^*}}{1 - \dfrac{le}{2} \dfrac{h_-}{h^*}}; \quad \hat{\sigma}_s = \delta^* \frac{1}{h_+} \frac{1 + \dfrac{le}{2} \dfrac{1}{h^*}}{1 - \dfrac{le}{2} \dfrac{h_-}{h^*}} \qquad (3.19)$$

Here,

$$h_{\pm} = \frac{1 \pm \sqrt{h^*}}{2}; \quad h^* = 1 + 4iSt_\delta; \quad le = Ze\left(1 - \frac{1}{Le}\right) \qquad (3.20)$$

It is interesting to note from Eq.(3.20) that the natural non-dimensional frequency that the Markstein numbers in Eq.(3.19) depend on is St_δ, indicating that flame stretch is a phenomenon associated with local non quasi-steady processes. The fact that these Markstein numbers vary differently with frequency imply that as excitation frequency changes, the relative contributions of flame curvature and strain to variations in flame speed and hence to the overall flame transfer function would be different.

To understand this more clearly, consider the asymptotic limits of both these Markstein numbers. It is crucial to note that in the quasi-steady, i.e., $St \to 0$ limit, both the Markstein numbers tend to the same value.

$$\lim_{St \to 0} \hat{\sigma}_c = \lim_{St \to 0} \hat{\sigma}_s = \delta^* \left(1 + \frac{le}{2} \right) \tag{3.21}$$

For *Le=1*, both the quasi-steady Markstein numbers are just equal to the ratio of the flame thickness to burner radius. At very high Strouhal numbers such that $St_\delta \gg 1$, the asymptotic trends of these Markstein numbers are very different, and can be determined to be:

$$\hat{\sigma}_c \sim \delta^*$$
$$\hat{\sigma}_s \sim \frac{e^{-i\pi/4} \delta^*}{St_\delta^{1/2}} = \frac{e^{-i\pi/4} \delta^{*1/2} \alpha^{1/4}}{St^{1/2}} \tag{3.22}$$

Equations (3.21) and (3.22) demonstrate that, while at very low Strouhal numbers, the sensitivities of flame speed to perturbations in flame curvature and flame strain is approximately the same, as Strouhal number increases, flame speed sensitivity to flame curvature dominates over that of flame strain. This is because, the curvature Markstein number varies very weakly with Strouhal number, while owing to the $1/h_+$ dependence, the strain Markstein number rapidly decreases with Strouhal number. Finally at very high Strouhal numbers, flame speed sensitivity to strain is $O\left(St_\delta^{1/2}\right)$ smaller than flame speed sensitivity to curvature, indicating that flame strain effects can perhaps be neglected at very high frequencies.

3.2.3.2 Effect of Equivalence Ratio Perturbations

Simply because the flame speed of a reactant mixture changes with its composition, a fluctuation in fuel mixture composition would lead to fluctuation in flame speed. Writing s_L as a generic function of ϕ as:

$$s_L = s_L(\phi) \tag{3.23}$$

Eq.(3.23) may be expanded in a Taylor series about a nominal value $s_{Lo}(\phi_o)$ for small fluctuations ϕ' about ϕ_o as:

$$s_L(\phi) = s_L(\phi_o) + \frac{\partial s_L}{\partial \phi}\bigg|_{\phi_o} (\phi - \phi_o) + O\left((\phi - \phi_o)^2\right) \tag{3.24}$$

On suitably non-dimensionalizing Eq.(3.24), we may write:

$$\frac{s_L'}{s_{Lo}} = \underbrace{\frac{\partial(s_L/s_{Lo})}{\partial(\phi/\phi_o)}\bigg|_o}_{s_{L1,\phi}} \frac{\phi'}{\phi_o} + O\left(\left(\frac{\phi'}{\phi_o}\right)^2\right) \tag{3.25}$$

The linear flame speed sensitivity to equivalence ratio fluctuations may hence be defined as:

$$s_{L1,\phi} = \frac{\partial(s_L/s_{Lo})}{\partial(\phi/\phi_o)}\bigg|_o \tag{3.26}$$

Where the subscript 'o' denotes evaluation at the mean equivalence ratio ϕ_o. The linear flame speed sensitivity to equivalence ratio fluctuations is hence just the non-dimensionalized slope of the $s_L - \phi$ curve, an example of which is provided in Figure 11.

It is important to bear in mind here, that Eq.(3.26) describes the flame speed sensitivity to fuel/air ratio perturbations in a quasi-steady sense. In general, prior research work [119, 129] has demonstrated that as the frequency (or the Strouhal number) of

excitation increases, the flame speed ceases to respond to equivalence ratio excitation in a quasi-steady manner, which implies, that in general, $s_{L1,\phi} = s_{L1,\phi}(f)$.

Finally, it is important to note that $s_{L1,\phi}$ changes with the reactant temperature, pressure and is different at different equivalence ratios.

3.2.3.3 Effect of Pressure Perturbations:

Much along the lines of the previous section, reactant pressure oscillations bring about oscillations in the flame speed by causing reaction rate oscillations. The linear flame speed sensitivity to pressure fluctuations can be defined quite similarly as that to equivalence ratio fluctuations.

$$\frac{s_L'}{s_{Lo}} = \underbrace{\frac{\partial(s_L/s_{Lo})}{\partial(p/p_o)}\bigg|_o}_{s_{L1,p}} \frac{p'}{p_o} + O\left(\left(\frac{p'}{p_o}\right)^2\right) \tag{3.27}$$

Hence:

$$s_{L1,p} = \frac{\partial(s_L/s_{Lo})}{\partial(p/p_o)}\bigg|_o \tag{3.28}$$

However, it is important to distinguish Eq.(3.28) from Eq.(3.26), in that, though in the quasi-steady limit, $s_{L1,p}$ can be determined by an $s_L - p$ curve, prior research work [92, 95, 98] has shown that the direct effect of pressure disturbance at very low frequencies on flame speed fluctuations is negligible and the flame response in the quasi-steady limit occurs only due to acoustic velocity fluctuations which are caused by acoustic pressure fluctuations. In fact, local flame response to pressure fluctuations has been shown to be

important [92, 95, 98] on in the structurally non quasi-steady regime, i.e., $St_{\delta,f} \sim 1$. Hence, the pressure sensitivity of flame speed is inherently frequency dependent and needs more esoteric methodologies to be determined.

This section poses the evolution equation for the flame front under the influence of upstream disturbances, the so-called ξ-equation. Suitable boundary conditions are prescribed and general expressions are derived for linear flame transfer functions, in terms of the flame front location perturbation, ξ' and its derivatives with respect to *r*.

3.2.4. Boundary Conditions

To obtain the flame front position fluctuations using Eq.(3.8), together with the flame speed model described in the previous subsection and the velocity disturbance field discussed in Section 2.4., boundary conditions need to be prescribed. As such, the influence of flame stretch through the flame curvature term, see Eq.(3.17), makes Eq.(3.8) a second order partial differential equation[6] in the radial coordinate, while being linear in time.

In general, hence, two boundary conditions necessitate in space. The first of the two spatial boundary conditions arise by means of the anchor-fixed boundary condition, which states that the flame base is attached to a flame holder at all times. Referring back to Figure 9, the flame is assumed to be stabilized on a burner tube (axisymmetric/2D

---

[6] Of course, at very low frequencies where stretch is not crucial, Eq.(3.8) would merely be a wave equation with a disturbance source term.

conical flames) or a center-body (axisymmetric/2D V-flames) as the case may be, which provides the following boundary condition for ξ:

$$\xi(t)\big|_{flame-holder} = 0 \qquad (3.29)$$

Furthermore, for a conical flame, the second boundary condition may be used as the symmetry at the centerline, given by

$$\frac{\partial \xi}{\partial r}(0,t) = 0 \qquad (3.30)$$

For an axisymmetric/2D V-flame, following Preetham et al. [115], the flame is assumed to be unconstrained at the tip, yielding a boundary condition at the duct wall as:

$$\frac{\partial^2 \xi}{\partial r^2}(r=0,t) = 0 \qquad (3.31)$$

Physically, this boundary condition prevents "backflow" of information into the flame domain, by prescribing that all characteristics exit the flame domain.

The boundary condition in time is more subtle. Given that the flame is forced by a periodic function, in the linear regime, Eq.(3.8) permits only periodic solutions at the forcing frequency. The need for a time boundary condition can hence be eliminated by rewriting Eq.(3.8) in the frequency domain, as opposed to the current time domain formulation. The above considerations now permit the determination of the flame front fluctuations, which forms the stepping stone for determination of the linear flame transfer functions.

3.2.5. Flame Transfer Functions

To start with, in the linear regime, the expression for the unsteady heat release rate by the flame, Eq.(2.33), reduces to:

$$\frac{q(t)}{q_o} = \frac{A(t)}{A_o} + \int_{flame} \frac{\rho'}{\rho_o} \cdot \frac{dA_o}{A_o} + \int_{flame} \frac{s'_L}{s_{Lo}} \cdot \frac{dA_o}{A_o} + \int_{flame} \frac{h'_R}{h_{Ro}} \cdot \frac{dA_o}{A_o} \tag{3.32}$$

The first term on the RHS denotes the contribution to heat release fluctuation due to oscillations in the area of the flame. These burning area perturbations are associated with fluctuations in flame position, ξ', due to velocity perturbations (*direct mechanism*) and flame speed perturbations (*indirect mechanism*).

The corresponding expression for the flame transfer function, Eq.(2.39), also gets simplified in the linear regime and becomes:

$$F_o = F_{o,A} + F_{o,\rho} + F_{o,s_L} + F_{o,h_R} \tag{3.33}$$

The transfer functions on the RHS of Eq.(3.33) arise from their respective positional counterparts on the RHS of Eq.(3.32). The subscript 'o' is used here just to emphasize that this is the linear transfer function, and hence, by definition, independent of excitation amplitude by virtue of being the $\varepsilon \to 0$ limit of the full, nonlinear transfer function, as defined in Eq.(3.33).

We first focus on evaluating the various expressions on the RHS of Eq.(3.32). In the framework of the ξ-equation, some of these terms can be evaluated in terms of the flame geometry. For example, the global instantaneous flame area may be expressed as:

$$\frac{A(t)}{A_o} = \int_0^1 \frac{W(r^*)}{\sqrt{1+\beta^2}} \sqrt{1+\beta^2 \left(\frac{\partial \xi^*}{\partial r^*}\right)^2} \, dr^* \tag{3.34}$$

where $W(r^*)$ is a weighting factor that depends on the flame geometry, given by:

$$W(r^*) = \begin{cases} 2r^*, \text{ Axisymmetric conical flame} \\ 2(1-r^*), \text{ Axisymmetric 'V' flame} \\ 1, \text{ 2D flames} \end{cases} \tag{3.35}$$

More generally, in the linear limit, we may write

$$\begin{aligned} \frac{dA}{A_o} &= W(r^*)\left[1-\alpha+\alpha\left(\frac{\partial \xi^*}{\partial r^*}\right)^2\right]^{1/2} dr^* \\ &= W(r^*)\left[1-\alpha\frac{\partial \xi'^*}{\partial r^*}+O(\xi'^{*2})\right]dr^* \end{aligned} \tag{3.36}$$

Hence,

$$\begin{aligned} \frac{dA_o}{A_o} &= W(r^*)\,dr^* \\ \frac{dA'}{A_o} &= -W(r^*)\alpha\frac{\partial \xi'^*}{\partial r^*}\,dr^* \end{aligned} \tag{3.37}$$

The integrals on the RHS of Eq.(3.32) can hence be evaluated now as below. Consider, for instance, the third term on the RHS of Eq.(3.32).

$$\int_{flame} \frac{s_L'}{s_{Lo}} \cdot \frac{dA_o}{A_o} = \sum_{j=c,s,p,\phi,\dots} s_{L1,j} \int_{flame} \left.\frac{j'}{j_o}\right|_{z=\xi(r,t)} \frac{dA_o}{A_o} \tag{3.38}$$

The integral on the RHS of the above equation is just the area averaged fluctuations in j, in some sense, the "effective" fluctuation in the quantity j over the flame domain.

Next, note that linear transfer functions may easily be evaluated in terms of the Fourier transformations of the flame position perturbations and the frequency dependent sensitivities. For example, consider

$$F_{A,u} = \frac{\hat{A}'(\omega)/A_o}{\hat{\phi}'_{base}(\omega)/\phi_o} \tag{3.39}$$

The numerator of Eq.(3.39) can be written as:

$$
\begin{aligned}
\frac{\hat{A}'}{A_o} &= -\alpha \int_0^1 W(r^*) \frac{d\hat{\xi}'^*}{dr^*} dr^* = -\alpha \left[W(r^*) \hat{\xi}'^* \right]_{r^*=0}^{r^*=1} + \alpha \int_0^1 \hat{\xi}'^* \frac{dW(r^*)}{dr^*} dr^* = \\
&= \alpha W(0) \hat{\xi}'^*(0) + \alpha \int_0^1 \hat{\xi}'^* \frac{dW(r^*)}{dr^*} dr^*
\end{aligned}
\tag{3.40}
$$

from which the transfer function is evaluable. Note, that the response of the unsteady area fluctuations can be very explicitly written in terms of the flame position response itself, and hence, determination of the flame position fluctuations suffices to determine the flame response. In a similar vein, other transfer functions of Eq.(3.33) arising as responses to different coupling processes may be expressed in terms of the flame position response and evaluated.

In the spirit of Eq.(3.38), the linear transfer functions can be written in a very instructive form, as described below. For example, consider the contribution of flame speed fluctuations to the total linear heat release due to equivalence ratio fluctuations:

$$\frac{q_{s_L}}{q_o} = \int_{flame} \frac{s_L'}{s_{Lo}} \cdot \frac{dA_o}{A_o} \tag{3.41}$$

Furthermore, in the linear regime, we have:

70

$$\frac{s_L'}{s_{Lo}} = s_{L1} \frac{\phi'}{\phi_o} \tag{3.42}$$

Hence:

$$\frac{q_{s_L}}{q_o} = s_{L1} \int_{flame} \frac{\phi'}{\phi_o} \cdot \frac{dA_o}{A_o} \tag{3.43}$$

The above equation demonstrates that flame speed fluctuations contributing to heat release occur because of (i) flame speed sensitivity to equivalence ratio fluctuations, s_{L1}, and (ii) an "effective" area averaged equivalence ratio fluctuation, given by the integral on the RHS of Eq.(3.43), which can be formally written as:

$$\phi_{eff}' = \frac{1}{A_o} \int_{flame} \phi' dA_o \tag{3.44}$$

The contribution of flame speed fluctuations to the transfer function hence becomes:

$$F_{s_L} = s_{L1} \frac{\hat{\phi}_{eff}' / \phi_o}{\hat{\phi}_{base}' / \phi_o} \tag{3.45}$$

The integral in the above equation is in fact, the magnitude of fluctuations in the "effective", i.e., flame area averaged equivalence ratio fluctuations, for an imposed equivalence ratio fluctuation at the flame base. In other words, this is just the "response" of the effective equivalence ratio fluctuations, and hence, a new transfer function may be defined for this response as:

$$F_{\phi_{eff}} = \frac{\left(\hat{\phi}_{eff}' / \phi_o \right)}{\left(\hat{\phi}_{base}' / \phi_o \right)} \tag{3.46}$$

so that:

$$F_{s_L} = s_{L1} F_{\phi_{eff}} \tag{3.47}$$

Similar transfer functions can be defined for effective pressure fluctuations too. This kind of formalism has important implications and is discussed later in Chapter 6.

3.2.6. Heat of Reaction Fluctuations

Before proceeding to actual calculations of the linear flame transfer function, one last point needs to be addressed. The last on the RHS of Eq.(3.32), which represents the contribution of heat of reaction oscillations to flame heat release, needs some attention.

Unlike flame speed fluctuations, heat of reaction fluctuations do not affect the flame position as such, but only influence the overall heat release of the flame. This means that the heat of reaction is not influenced by flame stretch. This point can be appreciated more easily if the definition of heat of reaction is recalled as the amount of heat released by the dissociation and formation of interatomic bonds of the compounds that participate in the combustion reaction, per unit mass of the reactant mixture. The heat of reaction is hence an equilibrium thermochemical property of the reactant system.

However, this now means that the heat of reaction can oscillate when reactant mixture composition or pressure oscillate. Hence, the heat of reaction is sensitive to equivalence ratio and pressure fluctuations, and in general, we can write:

$$\frac{h_R{}'}{h_{Ro}} = h_{R1,p}\,\frac{p{}'}{p_o} + h_{R1,\phi}\,\frac{\phi{}'}{\phi_o} \tag{3.48}$$

where $h_{R1,p}$ and $h_{R1,\phi}$ are the sensitivities of heat of reaction to pressure and equivalence ratio respectively, defined as:

$$h_{R1,p} = \left. \frac{\partial\left(h_R/h_{Ro}\right)}{\partial\left(p/p_o\right)} \right|_o \;\; ; \;\; h_{R1,\phi} = \left. \frac{\partial\left(h_R/h_{Ro}\right)}{\partial\left(\phi/\phi_o\right)} \right|_o \tag{3.49}$$

The contribution of heat of reaction fluctuations to the total transfer functions can be expressed in a manner similar to Eq.(3.47), i.e.:

$$\begin{aligned} F_{h_R,\phi} &= h_{R1,\phi} F_{\phi_{eff}} \\ F_{h_R,p} &= h_{R1,p} F_{p_{eff}} \end{aligned} \tag{3.50}$$

With these ideas, transfer function calculations are performed to understand the underlying physics and relative roles of different coupling mechanisms incorporating different physical processes (such as flame structural non quasi-steadiness and flame stretch).

3.3. Linear Flame Response Calculations

This section presents detailed calculations of equivalence ratio coupled, velocity coupled and pressure coupled linear flame transfer function calculations. Much of the thrust in this section is going to be on understanding equivalence ratio coupled flame response, which has hitherto received lesser attention that velocity coupled flame response. In that regard, this section first discusses flame response to equivalence ratio fluctuations, followed respectively by flame response to pressure fluctuations, and flame response to velocity fluctuations.

3.3.1. Flame Response to Equivalence Ratio Fluctuations

We begin with a more detailed understanding of the sensitivities of flame speed and heat of reaction to equivalence ratio fluctuations, which are very crucial in understanding and appreciating the richness of the problem. For the case of equivalence ratio coupling, the flame front location equation, Eq.(3.4), becomes:

$$\frac{\partial \xi^*}{\partial t^*} + \frac{s_L}{s_{Lo}} \frac{1}{\left(1+\beta^2\right)^{1/2}} \left(1+\beta^2 \left(\frac{\partial \xi^*}{\partial r^*}\right)^2\right)^{1/2} = 1 \tag{3.51}$$

3.3.1.1 Flame Speed and Heat of Reaction Sensitivities to Equivalence Ratio

Consider the effect of mixture composition (i.e., equivalence ratio) oscillations on the flame speed and heat of reaction. Insight into this sensitivity can be gained from the steady state dependence of flame speed and heat of reaction upon equivalence ratio. To better understand these sensitivities, consider Figure 11, which plots the typical ϕ dependence of the flame speed and heat of reaction.
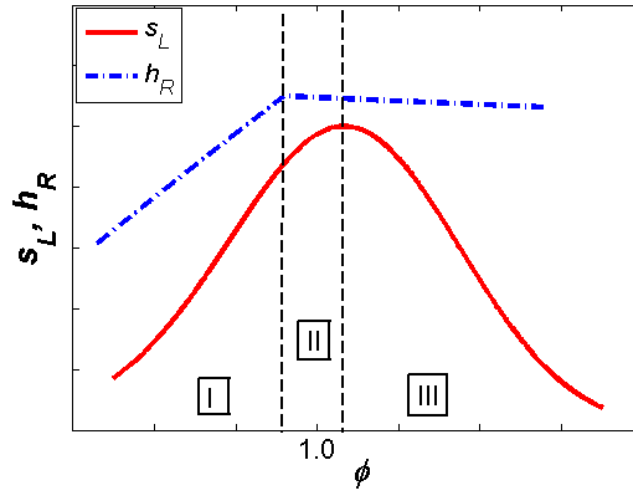
Figure 11: Qualitative plot showing dependence of flame speed, s_L, and heat of reaction, h_R, dependence on fuel/air ratio, ϕ.

The following observations may be made. First, the sensitivities of the flame speed to fuel/air ratio fluctuations of lean and rich flames are opposite in sign; i.e., an increase in fuel/air ratio causes a flame speed increase and decrease on the lean and rich side, respectively. Second, the heat release per unit mass of reactant varies with fuel/air ratio on the lean side, but is nearly constant on the rich side. Hence, there is negligible influence of the heat of reaction (h_R) term on the rich flame response – this term plays an important role in the lean flame response, particularly under low Strouhal number conditions. Furthermore, unlike in the case of flame speed and heat of reaction sensitivities to pressure perturbations or unsteady stretch rate, both these sensitivities are comparable [39]. This leads to an interesting interplay between the flame speed and heat of reaction routes to flame heat release in the context of nonlinear flame response.

Because these s_L and h_R transition regions do not occur at the same ϕ value, the flame response has qualitatively different characteristics in the three stoichiometry

regions, illustrated schematically in Figure 11. Region I is the lean regime which has been explicitly considered in prior studies. Region II is associated with the same s_L sensitivity trend as that of a lean flame, but no h_R sensitivity. Region III is associated with the opposite s_L sensitivity but near-zero h_R sensitivity. Depending upon the specific flame chemistry and reactant composition, the size of Region II in ϕ space can vary; e.g., for fuels like methane with reactants at STP, the nature of both flame speed and heat of reaction change at $\phi \sim 1.0$ leading to a very narrow Region II width of $\Delta\phi \sim 0.07$. On the other hand, the flame speed for 80%H_2/ 20%CO- air synthesis gas mixture peaks at values close to $\phi \sim 1.8$. This leads to a much larger Region II width of about $\Delta\phi \sim 0.8$.

3.3.1.2 Quasi-steady Response

For the quasi-steady flame response, a linear perturbation analysis is performed in the excitation amplitude ε in order to capture the low amplitude flame response characteristics. More specifically, we expand the flame front position $\xi(r,t)$ as:

$$\xi(r,t) = \xi_0(r) + \varepsilon\xi_1(r,t) + O(\varepsilon^2) \qquad (3.52)$$

Some further assumptions need to be made in order to make analytic progress. It is assumed that the fuel/air ratio occurs at constant density. This straight-away renders the density fluctuation contribution to the total transfer function, $F_\rho = 0$. Furthermore, the analysis neglects the density jump across the flame, which changes the character of the approach flow field. This assumption is well understood as a necessary approximation to achieve analytic progress in velocity-coupled analyses [46, 65, 115], but is also required

here for slightly more subtle reasons. Even if there are no velocity perturbations imposed upon the flame, the oscillating fuel/air ratio disturbance generates flame wrinkles. These wrinkles will necessarily excite velocity disturbances in the upstream and downstream flow due to the temperature change across the flame. However, the fuel/air ratio oscillation *per se*, is not affected by gas expansion, and hence, the transfer function of the flame associated *purely* with fuel/air ratio fluctuations still remain valid. This is in contrast to the velocity coupled flame response case, where, gas expansion changes the approach flow field and directly impacts the velocity-coupled flame transfer function. Finally, it is also assumed that the flame thickness is small relative to the burner radius, i.e., $\delta^* \ll 1$.

Under these assumptions, the shape of the mean flame is obtained by solving the mean part of the Eq.(3.51), to be the following:

$$\xi_o\left(r^*\right) = 1 - r^* - O\left(e^{-r^*/\sigma_c^*}\right) \tag{3.53}$$

Here, σ_c^* is a scaled Markstein length non-dimensionalized by the burner radius, defined as

$$\sigma_c^* = \sigma_c \frac{1}{\beta\left(1+\beta^2\right)^{1/2}} \tag{3.54}$$

The mathematical details of the derivation of Eq. (3.53) are presented in detail in Appendix D. Equation (3.53) shows that the correction to the mean flame shape due to flame stretch is exponentially small in σ_c^*. This implies that $\lim_{\sigma_c^* \to 0} \sigma_c^{*n} \exp\left(-r^*/\sigma_c^*\right) = 0$, for all positive integers, *n*. This result is quite helpful for asymptotic analysis in the small

77

σ_c^* limit, since this mean flame shape correction term does not enter the solution when expanded in powers of σ_c^*; i.e., it can be neglected to any order of σ_c^*, except for the very small region where $r^* < \sigma_c^*$ and, thus, the contribution to flame area is negligible.

Furthermore, azimuthal stretch can be neglected at high frequencies where flame stretch is important. The azimuthal curvature term is smaller than the axial term by a factor of the Strouhal number (see Appendix C[7]) and, as such, is negligible at higher Strouhal numbers where stretch effects are significant. For a conical flame, for example, the one exception to this occurs in the vicinity of the flame tip, $r=0$ where, however, the contribution to the flame area is negligible. Hence, only axial curvature effects are considered in the subsequent stretched flame analysis[8]. Under these assumptions, the evolution equation for ξ_1^* may be written as follows:

$$\frac{\partial \xi_1^*}{\partial t^*} - \alpha \frac{\partial \xi_1^*}{\partial r^*} - \alpha \sigma_c^* \frac{\partial^2 \xi_1^*}{\partial r^{*2}} + s_{L1} \cos(St\,(1 - r^* - t^*)) = 0 \qquad (3.55)$$

This equation can be solved to yield expressions for $\xi_1^*\left(r^*, t^*\right)$. For the sake of illustration, consider the solution for $\xi_1^*\left(r^*, t^*\right)$ in the absence of stretch ($\sigma_c^* = 0$).

$$\xi_1^*(r^*, t^*) = \frac{s_{L1}}{(1 - \alpha)\,St}\left[\sin\left\{St\left(1 - r^* - t^*\right)\right\} - \sin\left\{(St/\alpha)\left(1 - r^* - \alpha t^*\right)\right\}\right] \qquad (3.56)$$

---

[7] Though Appendix C presents analyses for a conical flame, the conclusion for a V-flame is similar.

[8] Azimuthal curvature effects on flame position are negligible compared to axial curvature effects for flames subjected to velocity disturbances too [55].

Equation (3.56) is very helpful in understanding the physics of flame front dynamics. This solution explicitly contains two contributions to the linear dynamics of the flame surface evolution. The first term within the brackets represents the effect of local non-uniformities in the burning velocity due to the spatial and temporal oscillations in equivalence ratio. The second term arises because of the fixed-anchor boundary condition, i.e., Eq.(3.29), that the flame does not move at the burner lip, even though the flame speed is oscillating. In physical terms, Eq.(3.56) shows that the flame front position is controlled by two sets of waves that travel along the front – (i) waves generated at each point along the flame due to spatial variations in flame speed and (ii) waves generated at the flame attachment point due to the boundary condition, Eq.(3.29). Notice that the propagation velocities of these two waves along the flame surface are different. The former travels with the mean flow velocity (unity in the non-dimensional case) and the latter with a non-dimensional velocity $1/\alpha$ along the axis of the flame. This characteristic of the flame front position solution is expected from the discussion that followed Eq.(3.9). Thus, these two waves interfere constructively at some flame surface locations and destructively at others. This has a significant influence on the characteristics of the heat release transfer function of the flame. This is similar to the result obtained by Preetham and Lieuwen [65] who emphasized these superposition effects upon the dynamics of flames subjected to excitation in flow velocity.

The quasi-steady, unstretched, heat release transfer function is considered next. To first order in excitation amplitude, the transfer function for a stretch insensitive flame, F_o can be written as a sum of three contributions arising from burning velocity

oscillations, heat of reaction oscillations and flame area oscillations. Equation (3.33) may hence be written as:

$$F_o = F_A + F_{s_L} + F_{h_R} \tag{3.57}$$

or alternatively as:

$$F_o = F_A + \left(s_{L1,\phi} + h_{R1,\phi} \right) F_{\phi_{eff}} \tag{3.58}$$

following Eq.(3.47) and Eq.(3.50)[9]. For an axisymmetric conical flame, for example, these contributions may be evaluated as:

$$F_{\phi_{eff}} = \frac{2}{St^2} \left(1 + iSt - \exp(iSt) \right) \tag{3.59}$$

$$F_A = s_{L_1} \left\{ \frac{2\alpha}{1-\alpha} \left(\frac{1 - \alpha - \exp(iSt) + \alpha\exp(iSt/\alpha)}{St^2} \right) \right\} \tag{3.60}$$

Note that Eq.(3.58) arises from Eq.(3.57) using Eq.(3.47) and Eq.(3.50), since:

$$\begin{aligned} F_{s_L} &= s_{L1} F_{\phi_{eff}} \\ F_{h_R} &= h_{R1} F_{\phi_{eff}} \end{aligned} \tag{3.61}$$

Finally, the low Strouhal number ($St \to 0$) limit of the transfer function can be evaluated for conical and V-flames to be:

$$\lim_{St \to 0} F_A = -s_{L1} \tag{3.62}$$

$$\lim_{St \to 0} F_{\phi_{eff}} = 1 \tag{3.63}$$

---

[9] The subscript ϕ will be dropped for the sensitivities for notational convenience. All through the section on equivalence ratio coupling, s_{L1}, h_{R1}, unless otherwise mentioned, shall denote the flame speed and heat of reaction sensitivities to equivalence ratio.

so that:

$$\lim_{St \to 0} F_{s_L} = s_{L1}$$
$$\lim_{St \to 0} F_{h_R} = h_{R1}$$

(3.64)

Hence, the total linear transfer function, in the limit $St \to 0$ becomes:

$$\lim_{St \to 0} F_o = h_{R1}$$

(3.65)

showing that the low Strouhal number dynamics is completely governed by the heat of

reaction fluctuations.

3.3.1.3 Effect of Flame Stretch

Next, consider the effects of flame stretch, which provides an additional route of flame

relaxation to high frequency disturbances. As described in Figure 7, flame stretch affects

flame response by altering the flame speed directly and the flame burning area indirectly.

Its inclusion leads to the following expressions valid for quasi-steady flames and weak

flame stretch ($\sigma_c^* St \to 0$) to leading order in σ_c^*:

$$F_{sL,c} = F_{o,sL} + \sigma_c^* \left[\frac{2s_{L1}}{(1-\alpha)St} \left(i\alpha \left(e^{iSt} - e^{iSt/\alpha} \right) - (1-\alpha)St \right) \right] + O\left(\sigma_c^{*2}\right) \quad (3.66)$$

$$F_{A,c} = F_{o,A} + \sigma_c^* \left[\frac{2i\alpha s_{L1}}{(1-\alpha)^2 St} \left((1-\alpha)^2 + \alpha e^{iSt} - (1-\alpha+\alpha^2) e^{iSt/\alpha} \right) \right] + O\left(\sigma_c^{*2}\right) \quad (3.67)$$

Some care must be exercised in analyzing the asymptotic dependencies of these

expressions at simultaneously low σ_c^* and high Strouhal numbers. Analysis of the exact

solution of Eq. (3.55) shows that stretch influences the flame burning area term, F_A, when

81

$$\sigma_c^* St^2 \sim 1 \qquad (3.68)$$

At such Strouhal numbers, the flame speed contribution to the stretch correction, F_{sL}, is $O\left(\sigma_c^{*1/2}\right)$ smaller than the burning area contribution, F_A. However, as the Strouhal number further increases to satisfy

$$\sigma_c^* St \sim 1 \qquad (3.69)$$

both the burning area and flame speed terms become comparable in their contributions to the total flame response. It is interesting to note that similar criteria were developed for the effects of stretch on the velocity coupled flame response, see Preetham et. al.[115] and Wang et. al.[47]. Equations (3.68) and (3.69) may respectively also be rewritten in terms of St_δ, for tall flames $(\beta \gg 1)$ as

$$St_\delta \sim \frac{\beta \delta^{*1/2}}{\sigma_c^{1/2}} \qquad (3.70)$$

and

$$St_\delta \sim \frac{\beta^2}{\sigma_c} \qquad (3.71)$$

Next, it is important to note that, in the linear regime (in excitation amplitude, ε), flame stretch does not affect the heat of reaction route to heat release oscillations. Hence, the total response of the flame under the influence of stretch may simply be expressed as

$$F = F_{o,h_R} + F_{sL,c} + F_{A,c} \qquad (3.72)$$

82

Finally, the low Strouhal number, i.e., $St \to 0$ limit of the stretched flame transfer function is, as is to be expected, the same as that of the unstretched flame, Eqs.(3.62)-(3.65). This is because flame stretch effects are negligible in the $St \to 0$ limit.

3.3.1.4 Effect of Non quasi-steadiness

We next account for non quasi-steady effects related to the delayed response of the internal flame structure to equivalence ratio disturbances. Following the modeling approach detailed by Lauvergne and Egolfopoulos [119], it can be shown that in the linear approximation, for an instantaneous equivalence ratio oscillation given by Eq.(2.49), the flame heat of reaction (h_R) and burning rate (s_L) respond to an equivalent equivalence ratio whose instantaneous value in dimensionless form is:

$$\tilde{\phi}\left(z^*,t^*\right) = \phi_o \left[1 + \varepsilon \operatorname{sinc}\left(\frac{St_\delta}{2}\right) \cos\left(\frac{St_\delta}{2} + St\left(z^* - t^*\right)\right)\right] \qquad (3.73)$$

where $sinc(x) = sin(x)/x$. On accounting for non quasi-steady effects in such a manner, the flame speed and heat of reaction sensitivities are diminished and phase shifted by a non quasi-steady scaling factor and may be expressed as [39]

$$s_{L1}{}^{nqs} = s_{L1} \operatorname{sinc}\left(St_\delta/2\right) \exp\left(-i\,St_\delta/2\right) \qquad (3.74)$$

$$h_{R1}{}^{nqs} = h_{R1} \operatorname{sinc}\left(St_\delta/2\right) \exp\left(-i\,St_\delta/2\right) \qquad (3.75)$$

The non quasi-steady transfer function, F^{nqs}, is a relatively simple modification of the quasi-steady transfer function, which may be expressed as

$$F^{nqs} = g\left(St_\delta\right) F^{qs}\left(St\right) \qquad (3.76)$$

where the correction factor accounting for non quasi-steady phenomena is given by

$$g\left(St_\delta\right) = \mathrm{sinc}\left(St_\delta/2\right)\exp\left(-iSt_\delta/2\right) \tag{3.77}$$

By definition, non quasi-steady effects become important when $\tau_{diff} \sim \tau_{eq}$, which may be written in terms of St_δ as

$$St_\delta \sim 2\pi \tag{3.78}$$

Comparing this with Eq.(3.70), it may be seen that for tall flames satisfying $\beta\sigma_c^{-1/2}\delta^{*1/2} \gg 2\pi$, non quasi-steady effects becomes important at smaller frequencies than those due to flame stretch. Conversely, stretch effects are important when non quasi-steady effects are negligible if $\sigma_c^{-1}\beta^2 \ll 2\pi$. Outside of these two inequalities, however, the two are of comparable importance.

It is important to note that the manner of influence of non quasi-steadiness and flame stretch effects on the global heat release response of the flame is different. While non quasi-steadiness seems to affect all the three routes, *viz.*, heat of reaction oscillations, flame speed oscillations and burning area oscillations *identically*, flame stretch affects only the latter two routes; in fact, these two routes are affected differently due to flame stretch. Further, non quasi-steadiness *scales* the transfer function by the scaling factor, *g*, while flame stretch *corrects* the unstretched quasi-steady transfer function.

In addition, it may be seen that the asymptotic high frequency dependence of the stretched, quasi-steady and unstretched non quasi-steady flame response gains differ by an order of Strouhal number; i.e.:

$$\left| F_{o,c} \right| \sim \frac{1}{St}$$

$$\left| F_{o,nqs} \right| \sim \frac{1}{St^2} \tag{3.79}$$

3.3.1.5 Effect of Axial Diffusion

From Eq. (G.24), the equivalence ratio profile may be expressed as:

$$\frac{\phi\left(z^*, t^*\right)}{\phi_o} = 1 + \varepsilon e^{-\aleph_\phi z^*} \cos\left(St\left(t^* - k_{c,\phi} z^*\right)\right) \tag{3.80}$$

where $\aleph_\phi$ and $k_{c,\phi}$ are given by Eq.(G.25) and Eq.(G.23) respectively. The evolution

equation for $\xi_1^*\left(r^*, t^*\right)$ may then be written as

$$\frac{\partial \xi_1^*}{\partial t^*} - \alpha \frac{\partial \xi_1^*}{\partial r^*} + e^{-\aleph_\phi\left(1-r^*\right)} \cos\left(St\left(t^* - k_{c,\phi}\left(1-r^*\right)\right)\right) = 0 \tag{3.81}$$

Using the fixed anchor boundary condition, Eq.(3.29), this yields, in the Fourier domain

$$\hat{\xi}_1\left(r^*\right) = \frac{1}{\alpha\left(\aleph_\phi - iSt_2\left(\eta_\phi - 1\right)\right)}\left[e^{-\aleph_\phi\left(1-r^*\right)} e^{i\eta_\phi St_2\left(1-r^*\right)} - e^{iSt_2\left(1-r^*\right)}\right]$$

$$= i\left(\frac{s_{L1}}{\alpha}\right)\left(\frac{e^{i\Lambda_\phi\left(1-r^*\right)} - e^{iSt_2\left(1-r^*\right)}}{\Lambda_\phi - St_2}\right) \tag{3.82}$$

and the complex frequency Λ_ϕ is given by

$$\Lambda_\phi = k_{c,\phi} St + i\aleph_\phi = \eta_\phi St_2 + i\aleph_\phi \tag{3.83}$$

The flame front position may be rewritten in the time domain by taking an inverse

Fourier transform of Eq.(3.82), which yields

$$\xi_1^*\left(r^*,t^*\right)=\frac{S_{L1}}{\alpha}\cdot\frac{1}{\Lambda_\phi-St_2}\left[\sin\left(St\left(\frac{1-r^*}{\alpha}-t^*\right)\right)-\sin\left(St\left(\frac{\Lambda_\phi}{St}\left(1-r^*\right)-t^*\right)\right)\right] \quad (3.84)$$

This shows that the effect of axial diffusion is seen only in the particular solution, i.e., the flow term. The contribution from the boundary condition is the same as in the case with no diffusion. Furthermore, comparing Eq.(3.84) and Eq.(3.56), it is interesting to note that the effect of axial diffusion can be captured merely using the complex frequency Λ_ϕ in place of St in Eq.(3.56). This just means that the results from the quasi-steady stretched and unstretched analyses neglecting diffusion can be easily extended to account for diffusion by this substitution (and vice-versa).

Also, while diffusion effects are unimportant as long as $\mathcal{L}_\phi=1/\aleph_\phi\gg L_f$, i.e., $\aleph\ll1$, they become important as the characteristic length scale for diffusion becomes comparable to the flame length. A closed form may be evaluated for this frequency as:

$$St_\delta\sim Le\left(1+\beta^2\right)\Gamma'^{1/2}\left(1+2\Gamma'\right)\left(1+\Gamma'\right)^{1/2}; \quad \Gamma'=\frac{\delta^{*1/2}}{\beta Le} \quad (3.85)$$

This expression can be simplified by noting that typical values of $\Gamma'\sim0.1$, so that, diffusion effects are seen to become important when:

$$St_\delta\sim Le\left(1+\beta^2\right)\left(\Gamma'^{1/2}+\frac{5}{2}\Gamma'^{3/2}\right); \quad \Gamma'=\frac{\delta^{*1/2}}{\beta Le} \quad (3.86)$$

For a flame with $\beta=4$, $Le=0.9$, $\Gamma'\sim0.1$, the above expressions yield diffusion effects to become important at $St_\delta\sim6$, while for say, $\beta=2$, diffusion effects become important at $St_\delta\sim1.8$. This indicates that though there could perhaps exist a small region in the St_δ-space where diffusion and non quasi-steady effects can be treated separately,

this region is probably very narrow, and hence both effects need to be considered together to present the complete physics of the problem.

Finally, transfer function expressions may be calculated using Eq.(3.82). For example, for an axisymmetric conical flame, we obtain:

$$F_A = \frac{2s_{L1}}{\Lambda_\phi - St_2}\left(\frac{e^{i\Lambda_\phi}-1}{\Lambda_\phi} - \frac{e^{iSt_2}-1}{St_2}\right) \tag{3.87}$$

$$F_{\phi,eff} = \frac{2}{\Lambda_\phi}\left(i - \frac{e^{i\Lambda_\phi}-1}{\Lambda_\phi}\right) \tag{3.88}$$

In view of the discussion presented in this section, some illustrative results considering these effects are discussed in the following section.

3.3.1.6 Illustrative Results

This section presents explicit results for axisymmetric conical and V-flames with aspect ratio, β=4.0. The investigated geometry is shown schematically in Figure 9. The following correlations for the burning velocity magnitude and heat of reaction for a methane-air flame at STP were assumed [72].

$$s_L(\phi) = A\phi^B \exp\left(-C(\phi-D)^2\right); \quad A = 0.6079,\ B = -2.554,\ C = 7.31,\ D = 1.230 \tag{3.89}$$

$$h_R(\phi) = \frac{2.9125\times10^6 \min(1,\phi)}{1+0.05825\phi} \tag{3.90}$$

3.3.1.6.1 Linear, Quasi-steady Dynamics of Stretch-insensitive Flames

We begin with a brief discussion of the characteristics of the quasi-steady linear transfer function for an unstretched flame. While Cho and Lieuwen [72] provide a discussion of some of the aspect of these linear dynamics, the focus of the discussion here will be primarily on the manner in which the rich flame results are different from those of lean flames. In order to make this comparison, results are presented for two mean equivalence ratios, ϕ_o=0.85 and ϕ_o=1.28, which correspond to conditions where the flame speeds are identical, s_L~ 33 cm/s.

We begin by intending to understand how different the responses of conical flames and V-flames to equivalence ratio disturbances are. Figure 12 plots the contributions of response of flame surface area fluctuations and effective equivalence ratio fluctuations to the total transfer function, F_o for a V-flame and conical flame. It can be clearly seen that the two processes contribute very differently to conical flames as compared to V-flames. In the case of V-flames, F_A dominates over $F_{\phi_{eff}}$ over most of the Strouhal number range.
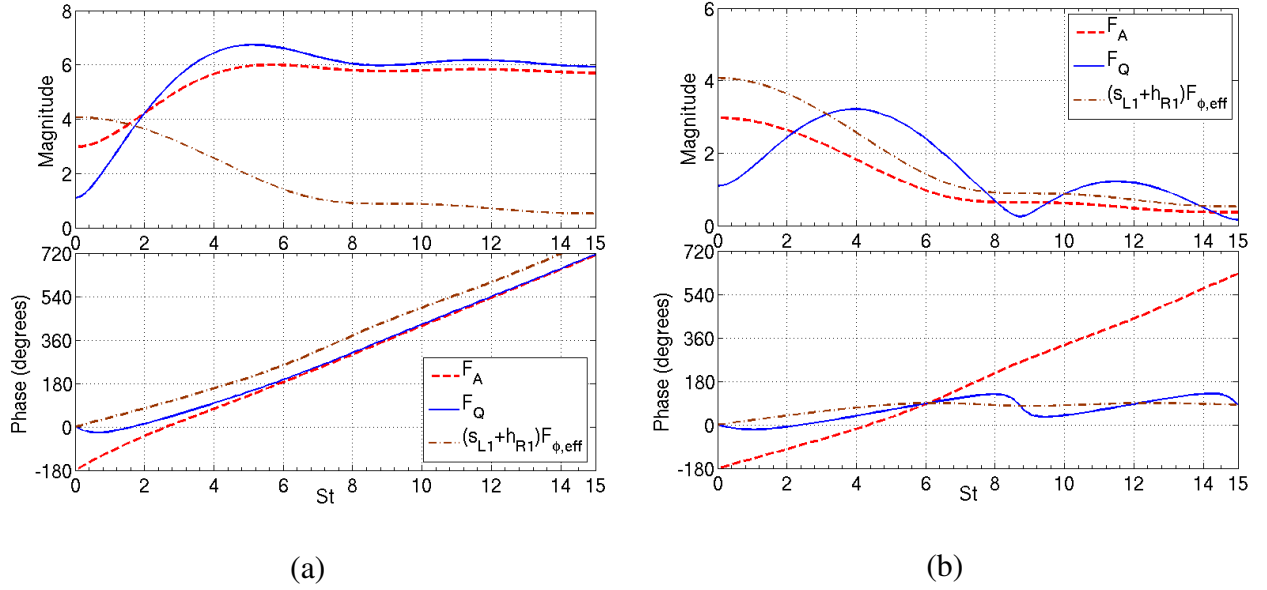
Figure 12 : Contributions to F_o by area and effective equivalence ratio fluctuations for (a) V-flame (b) conical flame at 1 atm, 300 K, ϕ_o=0.6, β=4.

Hence, the heat release response of the flame is primarily due to F_A. However, at lower Strouhal numbers, these effects are comparable. This is seen in the phase too, where the heat release response phase and burning area response phase are noticeably different in the quasi-steady limit and are identical at larger Strouhal numbers.

However, in the case of conical flames, these two effects contribute comparably over the entire Strouhal number range. This noticeable difference in the response characteristics is merely because of the fact that a V-flame has maximum surface area at the flame tip, while the conical flame has maximum surface area at the flame base. Hence, the maximum area in the V-flame is free to move and leads to higher response, while it is constrained at the flame attachment point for conical flames.

The import of the above discussion is the following. The equivalence ratio coupled flame response of V-flames can almost exclusively be understood by studying the burning area contribution. Although very important from a practical perspective, the effect of the flame speed and heat of reaction routes on the total flame response is better understood and studied by considering a conical flame. With this intention in mind, the subsequent discussion of equivalence ratio coupled flame response will focus on conical flame response. We shall however return to the V-flame in the context of flame stretch and axial diffusion effects.

We next consider the response of rich and lean conical flames to equivalence ratio disturbances.

(a)   (b)
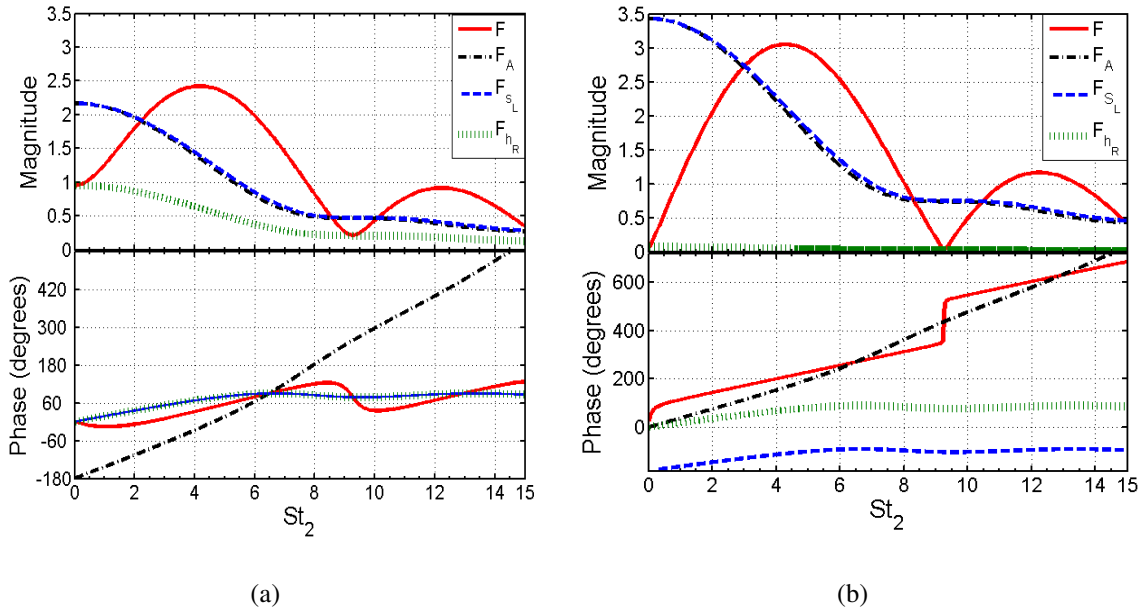
Figure 13: Linear conical flame transfer function for (a) $\phi_o = 0.85$ (lean) (b) $\phi_o = 1.28$ (rich), $\beta = 4$.

Figure 13 shows the variation of the phase and magnitude of the linear transfer function with $St_2 = St/\alpha$ for the two equivalence ratios. Also shown are the phase and magnitude of the individual contributions to the total transfer function. First, note that

both the phase and the magnitude do not monotonically vary with St_2. This is due to the fact that the linear flame response is determined by the net superposition of a boundary generated "wave" and a local disturbance, as discussed in the previous section. Therefore the net flame response depends on exactly how these waves superpose at different Strouhal numbers. It must also be noted from Eq.(3.61) that the phase of the flame speed and the heat of reaction contributions are identical in the linear limit. The linear transfer function for the rich case is shown in Figure 13(b). Notice that the transfer function goes to a near zero value, given by the heat of reaction sensitivity (h_{R1}), at low values of St_2 (see Eq.(3.65)). This is in striking contrast to the corresponding lean case and is due to the fact that the heat of reaction is a nearly constant function of equivalence ratio in the rich regime. This means that in the linear regime, the heat release of a rich flame is relatively insensitive to perturbations in equivalence ratio at low values of St_2.

Another difference between the two transfer functions is the presence of a zero response in the rich case, e.g. at $St_2 \sim 8.7$. At this point, the oscillating flame speed and area oscillation response exactly cancel each other. In the lean case, however, the node is not present. This is due to the fact that the lean case has an additional contribution to the total transfer function, *viz.*, the heat of reaction oscillations. The zero response does not occur in the lean flame response because it consists of a superposition of three terms, whereas the rich flame has only two major contributors. However, it must be noted that these characteristics are strong functions of the sensitivities of flame speed and heat of reaction to equivalence ratio. To understand this, consider flame responses at different equivalence ratio as plotted in Figure 14.
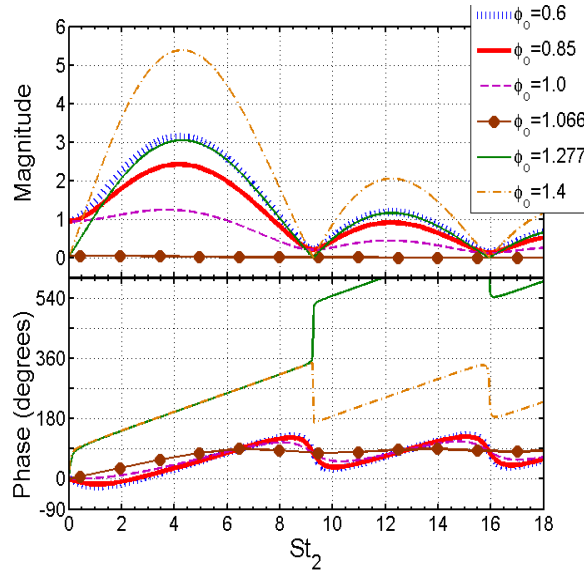
Figure 14: Variation of the linear transfer function with St_2 for different values of equivalence ratio. β=4.

Figure 14 overlays the flame response over a range of fuel/air ratios. Note, first, that the lean cases all start with a gain of nearly unity and the rich cases with a gain of nearly zero at low Strouhal numbers. This is due to the fact that the flame response is entirely controlled by the heat of reaction sensitivity h_{R1} in the quasi-steady case. All transfer functions then initially grow with increasing Strouhal number, because the burning area and the fluctuating flame speed terms progressively come into phase with each other.

As the mean equivalence ratio is increased from an initial lean value, e.g. ϕ=0.6, the s_L and h_R sensitivities progressively decrease and stay nearly constant, respectively, until ϕ~1.06 where the s_L and h_R sensitivities vanish. Hence, the magnitude of the flame response drops to a nearly zero response at ϕ~1.06. This is due to the occurrence of the flame speed maximum at this equivalence ratio. The heat of reaction is a very weak

92

function of equivalence ratio for ϕ_o>1.0. Hence, the magnitude increases from a nearly zero value with increasing St_2 for rich mean equivalence ratios.

Even though the flame speeds at ϕ_o=0.85 and ϕ_o=1.28 are identical, the magnitude of the maximum gain is higher in the rich case due to the higher s_L sensitivity at ϕ_o=1.28. Also to be noted is that the heat release response lags the excitation in the lean case, and leads it in the rich case. This again is due to the fact that the linear s_L sensitivity, $s_{L1,}$ changes sign from positive to negative when ϕ_o>1.06. This may be understood physically from the fact that the burning area response is due to s_L fluctuations that, in turn, are induced by equivalence ratio oscillations. The change in sign of s_{L1} implies that an instantaneous increase in equivalence ratio results in an increase and decrease in the instantaneous value of s_L on the lean and rich side, respectively. Therefore, given the same instantaneous equivalence ratio increase, the corresponding instantaneous burning area decreases for a lean mean equivalence ratio and increases for a rich mean equivalence ratio.

3.3.1.6.2 Linear, Non quasi-steady Dynamics of Stretch-insensitive Flames

This section presents typical results for the non quasi-steady response of the flame. These effects are presented separate from stretch effects in order to illustrate their different influences on the flame response.
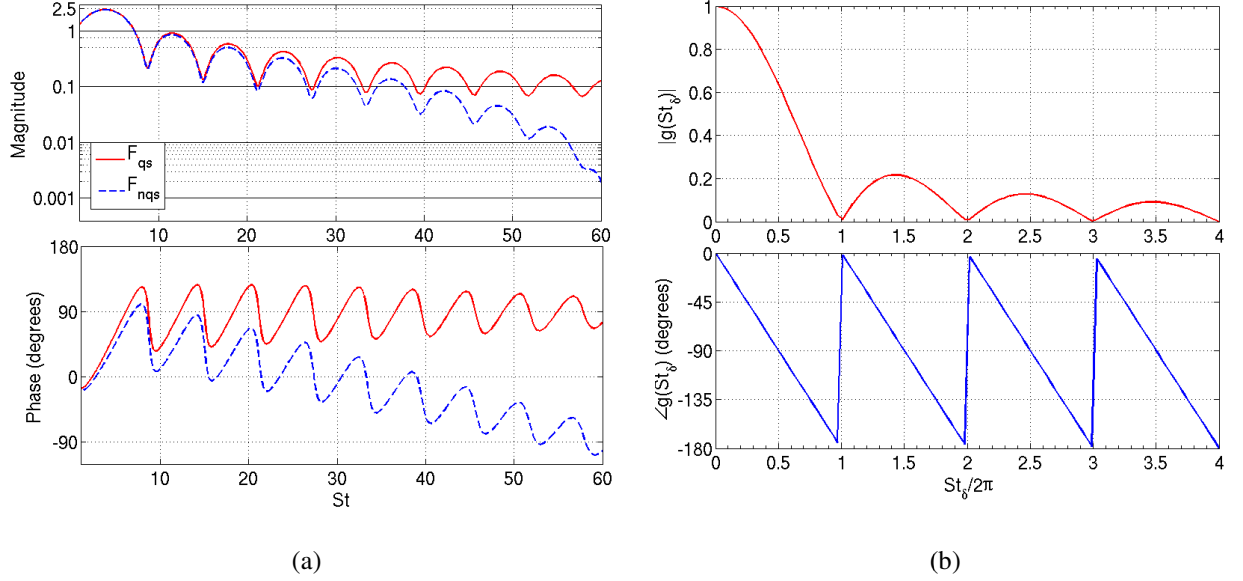
Figure 15 : (a) Non quasi-steady versus quasi-steady flame response for $\phi_o = 0.85$, $\beta = 4$, $\delta^* = 0.1$ (b) Non quasi-steady correction factor

Figure 15(a) compares the magnitude and phase of the linear total transfer function for quasi-steady and non quasi-steady flame response. It may be seen that, as Strouhal number increases, there is a marked departure of the non quasi-steady response from the quasi-steady result. At higher frequencies, corresponding to $St \sim 60$, the response is significantly attenuated, while the quasi-steady response is non-zero. In fact, it may be observed from Figure 15(b), that at $St_\delta \sim \pi$, there is already about 40% attenuation in the gain, and 90 degrees difference in phase with respect to the quasi-steady response.

3.3.1.6.3 Linear, Quasi-steady Dynamics of Stretch-affected Flames

We next present results that quantify the effects of flame stretch on the quasi-steady flame response. We begin by investigating the effect of flame stretch on the contributions

due to flame speed and burning area perturbations to the overall heat release for a lean

flame *(ϕ_o=0.85)*. Similar trends are seen in rich flames.

(a)   (b)
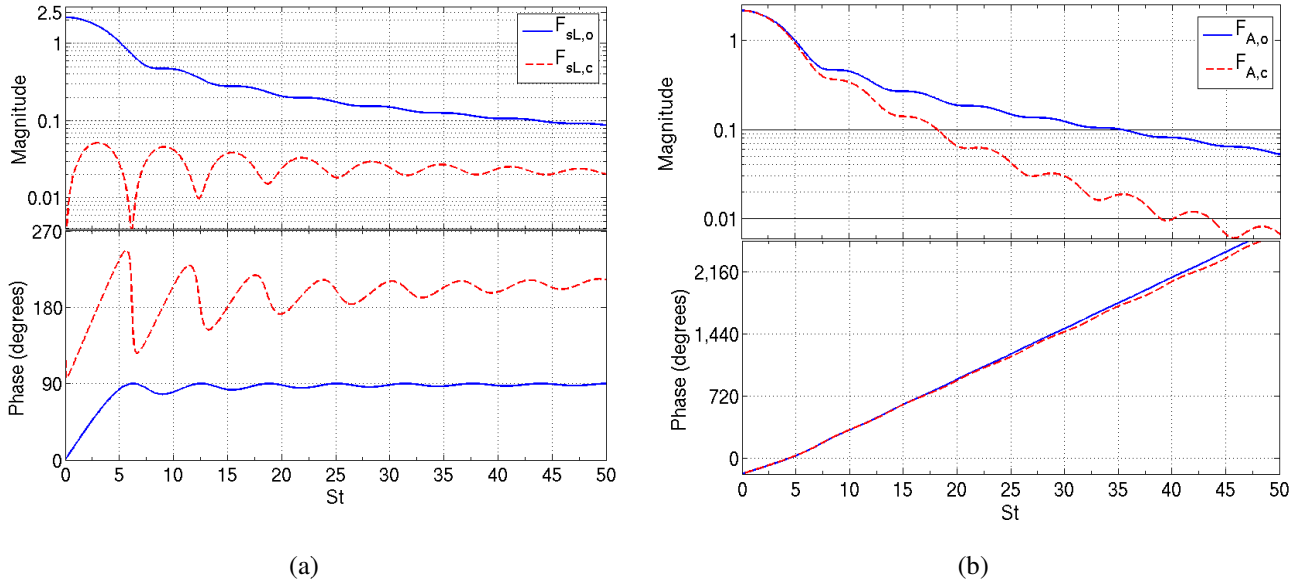
Figure 16 : Effect of flame stretch on (a) flame speed contribution and (b) burning area contribution to unsteady heat release for a lean CH$_4$/air flame, ϕ_o=0.85, β=4, δ^* = 0.1.

Figure 16(a) plots the flame speed contribution of the overall flame response for

an unstretched flame (solid curve) and the stretch correction to this contribution (dashed

curve). To understand the roles played by flame stretch effects and non quasi-steady

effects, Figure 17 plots the total linear response of the flame with and without stretch and

with non quasi-steadiness.
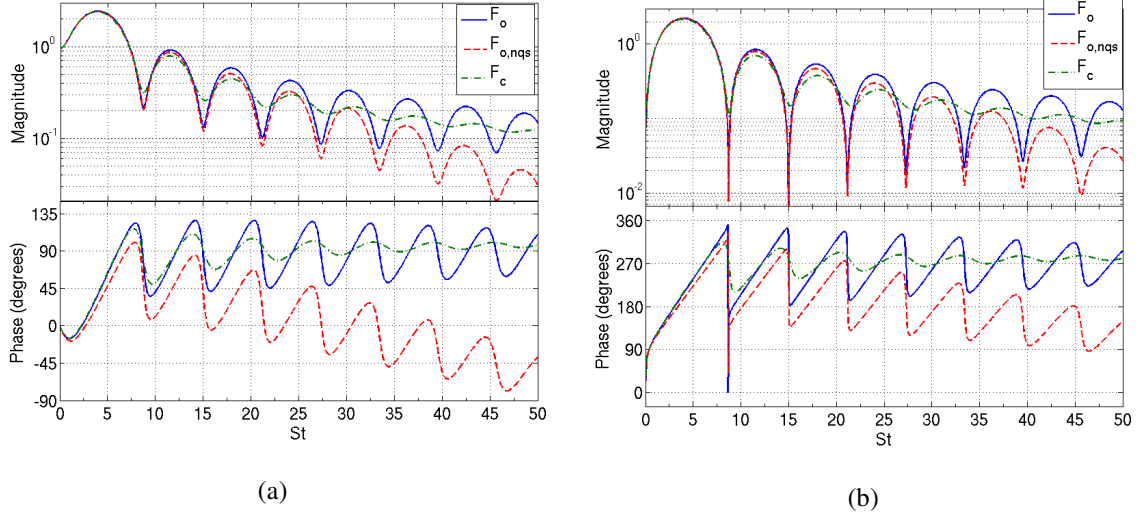
Figure 17 : Comparison between unstretched, quasi-steady (solid blue), stretched, quasi-steady (solid green) and unstretched, non quasi-steady (solid red) global heat release responses of a conical CH$_4$/air flame, β=4.0, δ^* = 0.1: (a) ϕ_o=0.85, (b) ϕ_o=1.28.

These plots show that the effect of stretch is primarily to smooth the undulations in the unstretched gain results, while that of non quasi-steadiness is to rescale the gain.

3.3.1.6.4 Linear, Quasi-steady, Diffusion Influenced Dynamics

Consider next the effect of axial decay in the equivalence ratio disturbance due to mass diffusion effects. Figure 18 compares the diffusion affected flame response with the baseline flame response. As may be seen, diffusion effects become important even at moderate Strouhal numbers of $St \sim 10$. For the conical flame, it is interesting to note that, the flame response accounting for diffusion exceeds the baseline flame response, where as for the V-flame, the diffusion affected flame response is lesser than the baseline flame response. The latter observation is easier to explain, since the V-flame response is controlled mostly by flame area fluctuations. Since diffusion affects the particular

96

solution, i.e., the local burning velocity fluctuations beyond a certain decay length scale, the region of the flame farther away from the flame base is controlled by the homogeneous solution contribution to the area response to a larger extent than the particular solution. Due to this reason, the interference between the two solutions attains maximum amplitudes lesser than the baseline case.

(a)

(b)
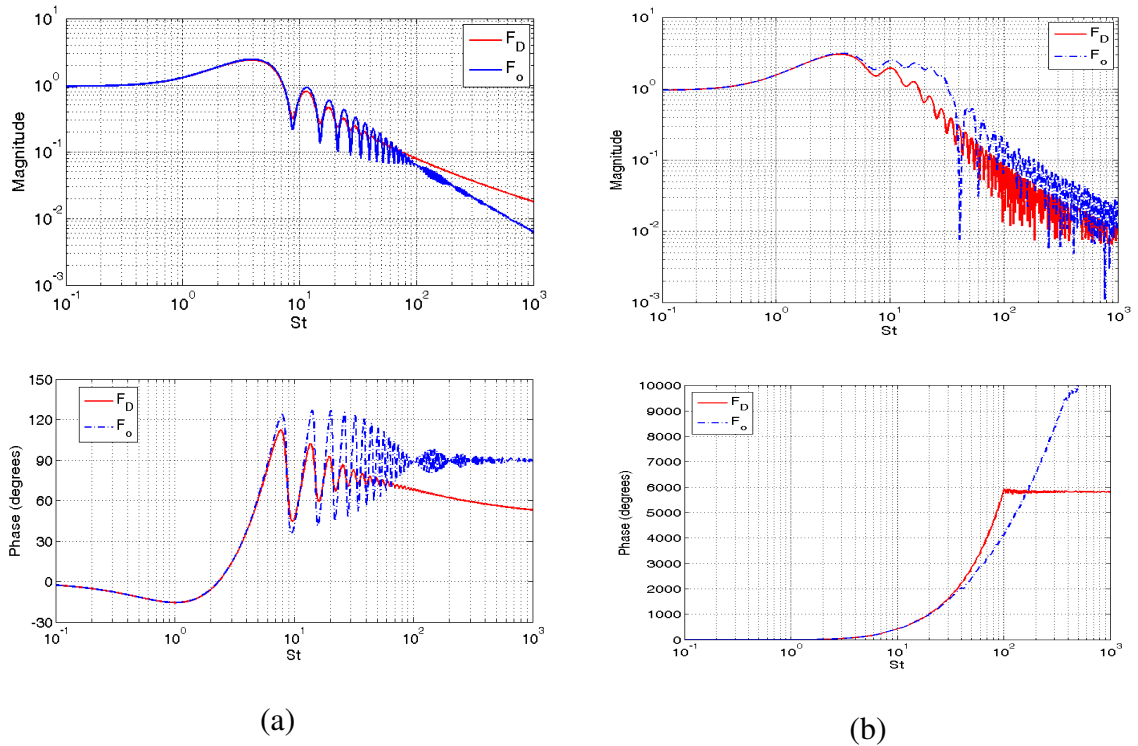
Figure 18 : Effect of decaying equivalence ratio on unstretched flame transfer function for a lean ($\phi_o = 0.85$ **) (a) axisymmetric conical flame (b) 2D V-flame.**

The case in a conical flame is different. The total transfer function is no longer governed merely by flame area fluctuations, but is a complex interplay of effective equivalence ratio fluctuations and the flame area fluctuations. The contribution of the effective equivalence ratio fluctuations, see Eq.(3.88), is on the whole, affected by diffusion

effects. However, there is a constant, non-oscillatory contribution , $(2/\Lambda_\phi)(i+1/\Lambda_\phi)$, about which a decaying oscillatory contribution arises. This constant contribution becomes stronger as Strouhal number increases, leading to the diffusion affected transfer function to exceed the baseline response.

Note finally though, that because of an axially decaying equivalence ratio profile, the oscillations in the baseline transfer function are smoothened. This is similar to what is seen in the velocity coupling counterpart of the problem, to be discussed in greater detail later.

We next consider the effect of diffusion on stretch-affected equivalence ratio coupled flame response in Figure 19.

(a)   (b)
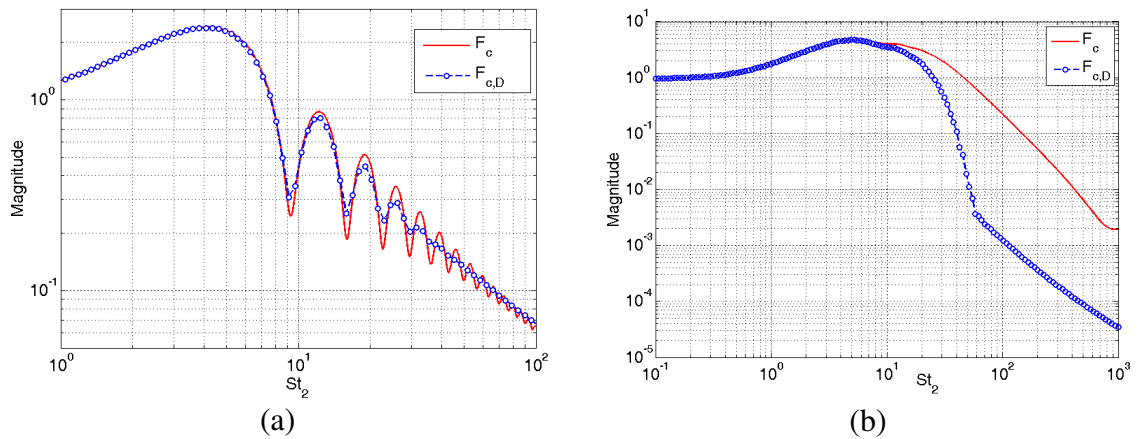
Figure 19 : Effect of equivalence ratio decay on stretch-affected flame response, $\phi_o = 0.85$, $\beta = 4$, $Le = 0.9$, (a) Axisymmetric conical flame (b) Axisymmetric V-flame.

It can be seen from Figure 19(a), that the main influence of an axially decaying equivalence ratio field, is that it further smoothens the undulations that exist in the transfer function magnitude of for stretch affected conical flames. It must be recalled

here, that it was found that, flame curvature effects, as such, were found to smoothen out oscillations in the transfer functions. Hence, equivalence ratio decay further smoothens out the already-smoothened transfer function. Next, consider Figure 19(b), where even the stretch affected flame response magnitude did not seem to possess any undulations. This is because of the reason that, as discussed in the context of Figure 12, V-flame response is dominated completely by burning area fluctuations, thereby nullifying any possibilities of constructive or destructive interference. The role that flame curvature plays in such a scenario, is that it augments burning area destruction and reduces flame response magnitude. The axially decaying equivalence ratio affects the flame at a more fundamental level, by causing flame wrinkle amplitude at a particular location to be much smaller than the baseline case, owing to the flame at that particular location being excited by fuel/air ratio whose amplitude is diminished due to diffusion effects, with respect to the baseline scenario.

(a)   (b)
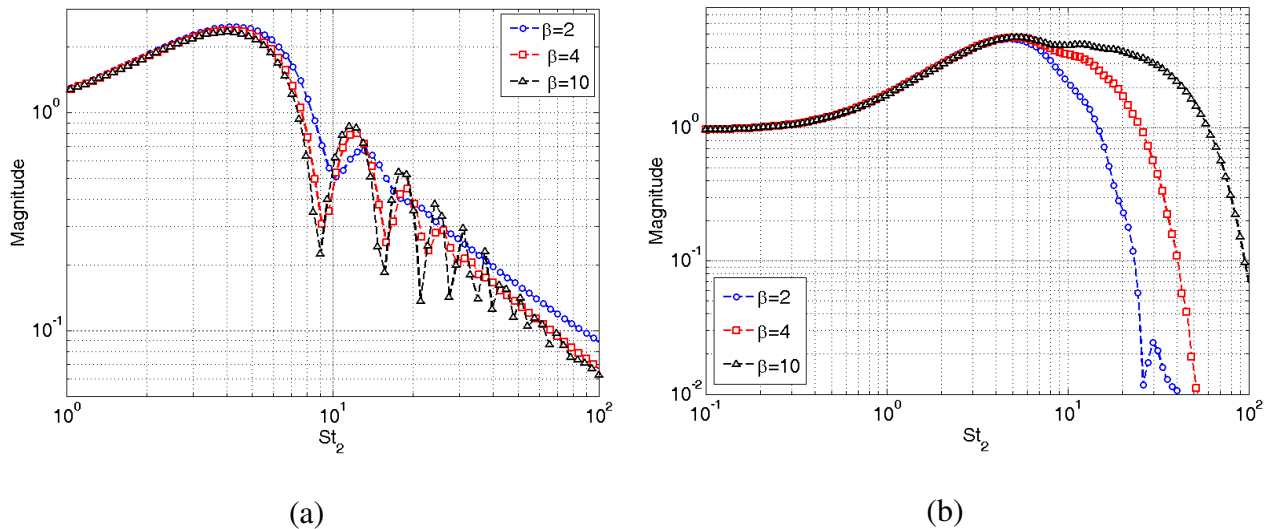
Figure 20 : Influence of axial decay of fuel/air ratio disturbances on flames with different aspect ratios, for (a) axisymmetric conical flame and (b) axisymmetric V-flame.

We finally discuss how axial decay of fuel/air ratio disturbances can affect flames of different flame lengths (and hence flame aspect ratios).

For V-flames, a higher aspect ratio seems to correspond to larger response magnitude. This is attributable to the fact that as flame length increases, the fraction of the flame front over which diffusion effects are important (and where the particular solution contributes lesser than the baseline case) increases. Hence, taller flames have larger burning area fluctuations due to the homogeneous solution than shorter flames.

For conical flames however, the transfer function magnitudes seem comparable even when the flame length changes by a factor of 5. This is again because of the reason that most of the contribution to the flame heat release in conical flames arise from locations where diffusion effects are not as important, say, closer to the flame base.

Finally, though not reported here, the phase characteristics of the flame transfer function seemed largely invariant across the range of flame aspect ratios considered here.

3.3.2. Flame Response to Velocity Fluctuations

We next consider the well-researched topic of velocity coupled flame response. Preetham [55] discusses various physical phenomena of importance that influence velocity coupled flame response including the effects of flame stretch. As discussed apriori, flames can be disturbed by velocity fluctuations arising either due to acoustic pressure fluctuations or vorticity fluctuations, and while either response has been accounted by Preetham [55] through the phase speed ratio $k_c = u_o / u_c$, a very important distinction arises between

acoustic and vortical velocity fluctuations at higher Strouhal numbers. While vorticity fluctuations can diffuse due to momentum transport, viscous diffusion of acoustic velocity is unimportant but in situations like shock waves which are characterized by extreme gradients in properties. This means that vortical velocity fluctuations can diffuse and potentially alter the high Strouhal number response of the flame, an effect not considered in earlier studies of high frequency velocity coupled flame response [47, 55, 56, 115]. The relevance of velocity coupled flame response studies to this thesis hence arises out of two points, *viz.*, (i) include vortical velocity diffusion effects to be able to study high frequency flame response with more physics built in into the response model, and (ii) assess the importance of velocity coupling with equivalence ratio and pressure coupling phenomena over a wide range of Strouhal numbers.

3.3.2.1 **Effect of Flame Stretch**

The effect of flame stretch has been discussed at length by Preetham and co-workers [55, 56] and only the key observations are presented here, for the sake of completeness. Neglecting diffusion, the influence of flame stretch may be worked out similar to the influence of flame stretch on equivalence ratio coupling. However, the significant difference between stretch affected flames responding to velocity fluctuations and equivalence ratio fluctuations is that, in the latter case, since there is assumed to be no velocity disturbances, there is no contribution from the hydrodynamic strain to flame stretch – the first term on the RHS of Eq.(3.13) is rendered zero, thus leading to a pure curvature effect. In the case of velocity coupling, there will be a contribution to stretched flame response from tangential velocity gradient at the flame.

We start by perturbing the mean flame, as earlier:

$$\xi(r,t) = \xi_o(r) + \varepsilon \xi_1(r,t) + O(\varepsilon^2)$$ (3.91)

where, analyses similar to equivalence ratio coupling analyses yield:

$$\xi_o(r^*) = 1 - r^* - O\left(e^{-r^*/\sigma_c^*}\right)$$ (3.92)

as the steady state flame location, and the perturbation $\hat{\xi}_1(r^*)$ is presented in 0. These

expressions for flame front perturbation locations can be used to calculate actual transfer

function expressions as described earlier. As discussed in Figure 6, at moderately high

frequencies, flame stretch effects materially influence the velocity-coupled flame

response and provide additional pathways which influence heat release fluctuations. The

flame transfer function hence consists of contributions from fluctuations of both the

flame surface area and flame speed. For 2D V-flames, unsteady stretch has an O(1)

contribution to the flame surface area fluctuations (route 2b in Figure 6) when

$$\left|\sigma_c^*\right| St_2^2 \sim 1$$ (3.93)

Fluctuations in flame speed (route 2a in Figure 6) become important at higher Strouhal

numbers, when

$$\left|\sigma_c^*\right| St_2 \sim 1$$ (3.94)

The effects of hydrodynamic strain become important at much larger Strouhal numbers,

when

$$\left|\sigma_s^*\right| St_2 = \alpha^{1/2} \left|\hat{\sigma}_s\right| St_2 \sim 1$$ (3.95)

The dimensionless stretch sensitivities are themselves frequency dependent as detailed in Joulin [126] and as described earlier in this chapter (see Sec.3.3.1.3). Using the asymptotic expressions for $\hat{\sigma}_c, \hat{\sigma}_s$, see Eq.(3.22), at very high Strouhal numbers, the effects of unsteady flame stretch through flame area fluctuations, direct influences on flame speed through curvature, and through hydrodynamic strain, i.e., the criteria in Eq.(3.93), (3.94) and (3.95), reduce respectively to

$$St_2 \sim \beta \delta^{*-1/2} \tag{3.96}$$

$$St_2 \sim \beta^2 \delta^{*-1} \tag{3.97}$$

$$St_2 \sim \alpha^{1/2} \delta^{*-1} \tag{3.98}$$

We may also express Eqs.(3.96), (3.97) and (3.98) in terms of St and St_δ as

$$St \cdot St_\delta \sim \beta^4 \tag{3.99}$$

$$St_\delta \sim \beta^2 \tag{3.100}$$

$$St_\delta \sim \alpha \tag{3.101}$$

In a similar vein, high St_2 limits may be evaluated for the transfer functions as well. For example, for a 2D V-flame, The high St_2 limit[10] for these transfer functions can be written as:

$$F_{sL,str} \sim -\frac{\beta}{\eta St_2} \tag{3.102}$$

$$F_{A,str} \approx \frac{\sigma_s^*}{\sigma_c^*} \frac{e^{i\eta St_2}}{\eta St_2} \approx e^{-3i\pi/4} \frac{\beta}{\alpha^{1/4} \delta^{*1/2}} \cdot \frac{e^{i\eta St_2}}{\eta St_2^{3/2}} \tag{3.103}$$

---

[10] The complete expressions for the transfer functions are provided in Appendix F.

It should be recollected that these transfer function limits are valid when the flame thickness is compact to velocity disturbances.

3.3.2.2 Effect of Axial Diffusion

The effect of axial diffusion on velocity coupled flame response is very similar to that on equivalence ratio coupling. For a flame perturbed by a velocity disturbance given by Eq.(2.45), or equivalently represented as:

$$\frac{u_{\Omega}\left(z^{*},t^{*}\right)}{u_{o}}=1+\varepsilon_{u}e^{-\aleph_{u}z^{*}}\cos\left(St\left(t^{*}-k_{c,u}z^{*}\right)\right) \quad (3.104)$$

First consider axial diffusion effects in the absence of flame stretch. This leads to an expression for the flame front perturbation amplitude as:

$$\hat{\xi}_{1}^{*}\left(r^{*}\right)=-\frac{i}{\alpha}\frac{\left(e^{i\Lambda_{u}\left(1-r^{*}\right)}-e^{i\left(1-r^{*}\right)St_{2}}\right)}{\left(\Lambda_{u}-St_{2}\right)} \quad (3.105)$$

where the complex frequency Λ_{u} is given by:

$$\Lambda_{u}=k_{c,u}St+i\aleph_{u}=\eta_{u}St_{2}+i\aleph_{u} \quad (3.106)$$

This is very similar to the complex frequency Λ_{ϕ} that arose in the equivalence ratio coupled counterpart of this problem (i.e., effect of diffusion without flame stretch). Again, it is easy to see that the effect of diffusion enters the velocity coupled problem, by merely modifying the local solution, while the boundary condition term remains unaffected. As earlier, the flame response transfer function for unstretched flames

subjected to a diffusing vortical velocity field can be obtained by merely using the complex frequency given by Eq.(3.106) in place of its real part, i.e., $\eta_u St_2$, in the transfer function expressions derived by Preetham [55]. For example, for a 2D V-flame, the flame transfer function of an unstretched flame subjected to an axially decaying velocity field can be obtained as:

$$F_o = F_A = \frac{e^{i\Lambda_u} - e^{iSt_2}}{i\Lambda_u - iSt_2} \tag{3.107}$$

Furthermore, a criterion similar to Eq.(3.86), at which, effects of axial diffusion become important in the absence of flame stretch, can be derived for the velocity coupling problem as:

$$St_\delta \sim \Pr\left(1+\beta^2\right)\left(\Gamma'^{1/2} + \frac{5}{2}\Gamma'^{3/2}\right); \quad \Gamma' = \frac{\delta^{*1/2}}{\beta\Pr} \tag{3.108}$$

For a flame with $\beta = 4$, $\Pr \approx 0.7$, $\Gamma' \sim 0.1$, the above expressions yield diffusion effects to become important at $St_\delta \sim 4$, while for say, $\beta = 2$, diffusion effects become important at $St_\delta \sim 1.6$. As concluded in the equivalence ratio counterpart of this problem, diffusion effects seem to become important at Strouhal numbers lesser than or around about when flame stretch effects become important. For $\beta = 4$, for example, flame stretch influences through flame area fluctuations become important at $St_\delta \sim 0.9$, while for $\beta = 2$, these effects become important at about $St_\delta \sim 0.5$. This shows that, in general, the domain in St_δ space where flame stretch has to be included, but axial diffusion effects can be neglected is very small, and a complete treatment needs to account for either effect simultaneously.

The evolution equation for the flame front perturbation accounting for both flame stretch and axial decay of velocity disturbances bears a very similar form as the evolution equation without axial diffusion [55, 56]:

$$\frac{\sigma_c \beta}{(1+\beta^2)^{3/2}}\frac{d^2\hat{\xi}_1^*}{dr^{*2}}+\alpha\frac{d\hat{\xi}_1^*}{dr^*}+iSt\hat{\xi}_1^*+\left(1-\frac{i\sigma_s\beta\aleph_u}{\sqrt{1+\beta^2}}\right)e^{i\aleph_u(1-r^*)}=0 \qquad (3.109)$$

The solutions of Eq.(3.109) for conical and V-flame geometries is provided in Appendix F, using which transfer functions may be derived (also provided in Appendix F). In the limit of weak curvature and strain, such that $\max\left(|\sigma_c|,|\sigma_s|\right)St_2 \to 0$, simplified expressions may be derived for the transfer functions to understand the nature of influence on flame response as follows:

$$\hat{\xi}_1\left(r^*\right) \approx C_1 e^{iSt_2\left(1-r^*\right)} + K_1 \qquad (3.110)$$

Where:

$$C_1 = -\frac{1}{\alpha\left(\Lambda_u - St_2\right)}\left(-i+\sigma_c^*\Lambda_u - \sigma_s^*\Lambda_u\right)+O\left(\sigma_c^{*2},\sigma_s^{*2},\sigma_c^*\sigma_s^*\right) \qquad (3.111)$$

$$K_1 = i\Lambda_u e^{i\Lambda_u}C_1$$

Using Eq.(3.110) and Eq.(3.111), expressions may be written for the transfer function contributions in the limit $|\sigma_c|St_2 \to 0$, as follows:

$$F_{A,c} = \frac{e^{i\Lambda_u} - e^{iSt_2}}{i\Lambda_u - iSt_2}+i\sigma_c^*\Lambda_u\left(\frac{e^{i\Lambda_u} - e^{iSt_2}}{i\Lambda_u - iSt_2}\right)-i\sigma_s^*\Lambda_u\left(\frac{e^{i\Lambda_u} - e^{iSt_2}}{i\Lambda_u - iSt_2}\right)+O\left(\sigma_c^{*2},\sigma_s^{*2},\sigma_c^*\sigma_s^*\right) \qquad (3.112)$$

$$F_{s_L,c} = -\left(1-e^{i\Lambda_u}\right)\sigma_s^*+\frac{\Lambda_u\left(1-e^{i\Lambda_u}\right)}{\Lambda_u - St_2}\sigma_c^*+O\left(\sigma_c^{*2},\sigma_s^{*2},\sigma_c^*\sigma_s^*\right) \qquad (3.113)$$

It may be seen from Eq.(3.112) and Eq.(3.113), that in the absence of flame stretch effects, i.e., $\sigma_c = 0, \sigma_s = 0$, the unstretched, diffusion-affected flame transfer function, Eq.(3.107) is retrieved. Further, in the $\max(\sigma_c, \sigma_s) \to 0$ limit, flame response occurs only due to flame burning area fluctuations, and the contribution of direct influences on flame speed is an order of Markstein number smaller than that due to flame burning area, and hence As such, though the above expressions can be used to understand the onset of flame stretch effects, caution should be exercised in interpreting results as $\min\left(\left|\sigma_c^*\right|, \left|\sigma_s^*\right|\right) St_2 \to 1$, which will then render the neglected higher order terms in Eq.(3.112) and Eq.(3.113) to contribute comparably with the linear terms in the curvature and strain Markstein numbers.

It needs to be recalled here, that these conclusions are exactly the same as obtained by the analyses of Preetham [55, 56] in a similar limit. In this sense, the effect of axial diffusion on flame transfer functions still seems to be characterized by the complex frequency Λ_u of Eq.(3.106). It hence appears that the impact of axial diffusion on unstretched and stretched flame response depends on the actual dependence of Λ_u on St, through Eq.(G.38), and is discussed in the next section.

3.3.2.3 Illustrative Results

In order to understand the explicit effects due to flame stretch and axial diffusion on unstretched and stretched flames, this section provides illustrative results for conical and V-flames for a reactant mixture with $Pr = 0.7$. In order to assess the importance of flame

length in the axial diffusion problem, two flames with aspect ratios $\beta = 2$ and $\beta = 4$ are considered. The motivation for treating the flame aspect ratio as a parameter is the same as in the equivalence ratio coupling problem – axial diffusion effects could become more important for taller flames whose flame lengths are closer to the disturbance decay length scale.

3.3.2.3.1 Linear Response of Stretch-affected Flames, without Diffusion Effects

We first compare the importance of flame stretch in axisymmetric V-flames and conical flames, with an emphasis on high Strouhal number response, disregarding the effects of disturbance diffusion.
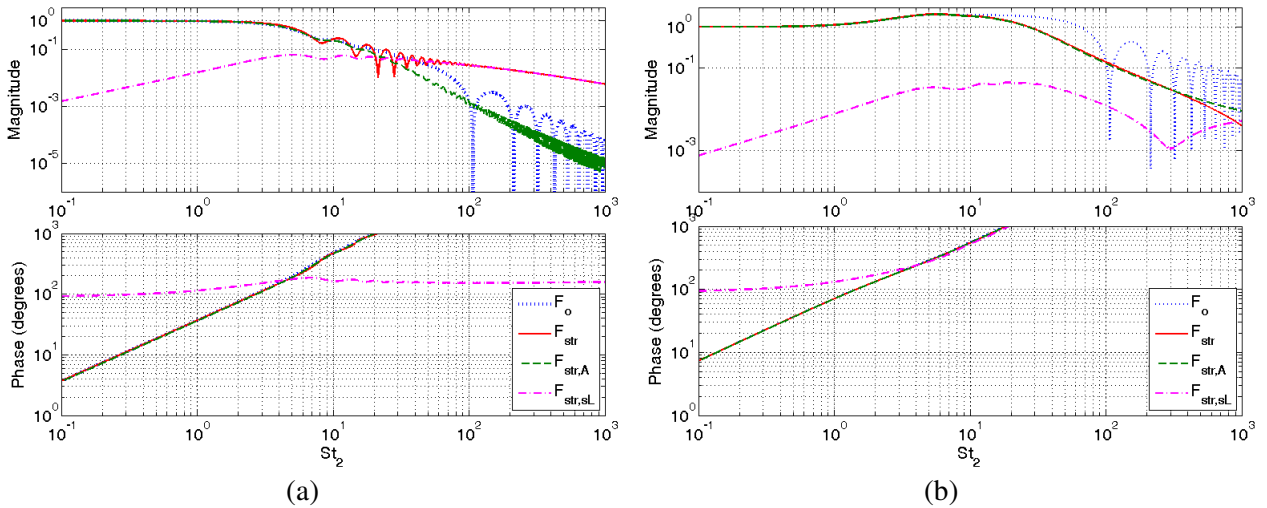
Figure 21: Influence of flame stretch on velocity coupled flame response. $k_{c,u} = 1$, $\beta = 4$, $\delta^* = 0.04$ **flame. (a) Axisymmetric conical flame. (b) Axisymmetric V-flame.**

Figure 21(a) and (b) plot the effect of flame stretch on an axisymmetric conical and V-flame respectively, in the absence of diffusion. The upper graph plots transfer function

magnitudes and the lower graph plots transfer function phase in degrees. Consider, for instance, Figure 21(a). It may be seen from the magnitude plots, that at low Strouhal numbers, $St \to 0$, the effect of flame stretch is almost completely absent – the red and blue curves, denoting the stretched and the unstretched flame response, F_{str} and F_o respectively, coincide. Further, the total flame response is equal to that of the burning area contribution, $F_{str,A}$, denoted by the green curve. The contribution to flame response due to the direct effect of flame speed perturbations, $F_{str,sL}$, is at least two orders of magnitude smaller than $F_{str,A}$. However, as the Strouhal number increases, the magnitude of $F_{str,sL}$ increases. As the Strouhal number increases to about $St_2 \sim 20$, F_{str} begins to diverge from F_o. In fact, at about $St_2 \sim 60$, the stretched flame response F_{str} begins to depart from F_o and $F_{str,A}$ and arises completely due to $F_{str,sL}$. This is in conformity with what has been explained in the previous section. In the case of an axisymmetric V-flame, $F_{str,A}$ begins to gain importance at about $St_2 \sim 20$, as for the case of the axisymmetric conical flame. However, the 'switch' from the burning area route to the s_L route seems to occur at a higher Strouhal number than for the conical flame. This switch is less evident from Figure 21(b), for the range of frequencies considered. Nevertheless, departure of the stretch flame response from the burning area response can be seen at $St_2 \sim 400$. Note that these values for the Strouhal number are in agreement with the theoretical values that can be calculated using Eq.(3.96) and Eq.(3.97) respectively (although Eq.(3.96) and Eq.(3.97) are valid for 2D V-flames).

Next, the reason for the order of magnitude difference between the Strouhal number at which the flame speed route is affected due to flame stretch, for V-flames and conical flames, can be explained using the simplified expression for the flame front perturbation amplitude, Eq.(3.110). As such, flame stretch effects are more dominant closer to the flame holder, than away from it. The fundamental difference between the conical flame and V-flame configurations is that the maximum contribution to flame response in V-flames occurs due to the flame tip, which is the region of maximum flame surface area flapping in an unconstrained manner, where as, for the conical flame, the region of maximum flame surface is the flame base, which is constrained not to move. Hence, in conical flames, regions close to the flame holder, though contributing lesser, are heavily influenced by flame stretch. However, for V-flames, the regions where flame stretch contributes maximum to flame area fluctuations has very little flame surface area, and hence the local response of these regions of the flame is shadowed by the response of the flame tip, where in fact, from Eq.(3.31), the contribution of flame curvature effects to flame response is zero. These reasons cause flame stretch effects to be more important at lower frequencies in conical flames than in V-flames. Also, it is important to note that the maximum transfer function magnitude value of an axisymmetric V-flame can exceed unity, while for a conical flame, the maximum response magnitude is always less than 1.

Consider next, the differences between responses of a 2D V-flame and an axisymmetric V-flame. The fundamental difference between these two configurations, is that, in the former, all flamelets along the flame front contribute equally to the global area response; this leads to the weighting factor $W(r^*) = 1$. On the contrary, for the V-flame,

regions closer to the flame holder contribute lesser than those close to the flame tip, since

$$W\left(r^*\right) = 2\left(1 - r^*\right).$$
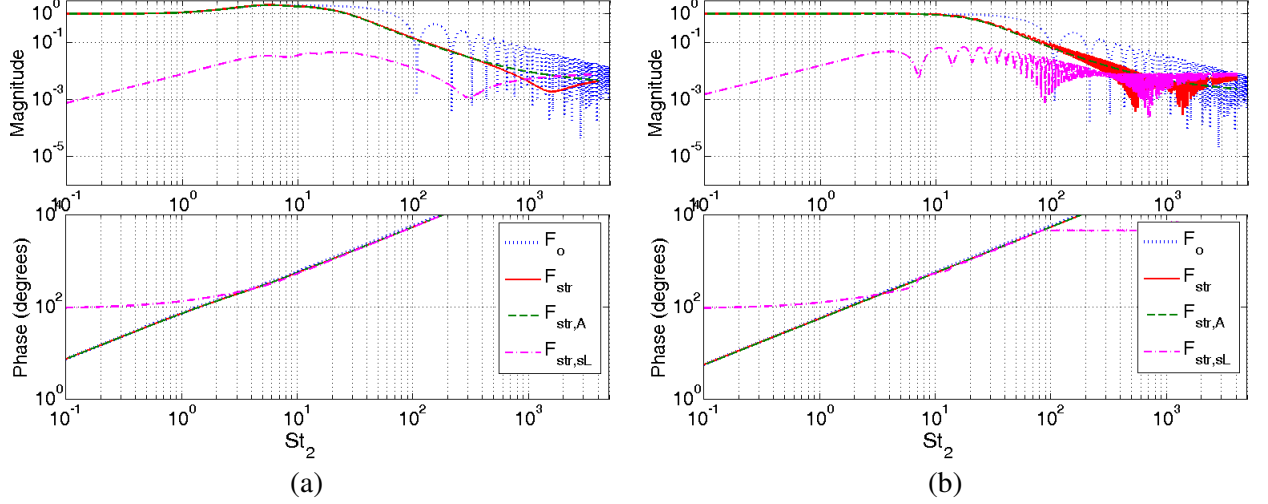
Figure 22: Influence of flame stretch on velocity coupled flame response. $k_{c,u} = 1$, $\beta = 4$, $\delta^* = 0.04$ flame. (a) Axisymmetric V-flame (b) 2D V-flame.

Figure 22 plots the effect of flame stretch on axisymmetric V-flames (left) and 2D V-flames (right) respectively. As may be seen from both the magnitude and phase plots, there seems to be very little qualitative difference between the two configurations. In fact, due to equal contributions of every part of the flame for a 2D V-flame, the contribution of the regions closer to the flame holder is more important than in axisymmetric V-flames. This leads to a more pronounced interference pattern in the transfer function for a 2D V-flame, leading to oscillatory character for the transfer function magnitude. Furthermore, the maximum gain value for a 2D V-flame is always less than 1, much like the conical flame. Note finally that flame stretch effects due to burning area fluctuations seem to become important at almost the same frequency, of about $St_2 \sim 20$ for either case, while

for stretch effects due to flame speed perturbations occur at $St_2 \sim 400$ for either case.

Given the similarity of response between axisymmetric and 2D V-flames, further analyses of velocity coupled flame response will be carried out for the 2D V-flame configuration, as the analytical expressions for the transfer functions are much simpler.

Consider next, the stretched and unstretched flame transfer functions for an axisymmetric conical flame and a 2D V-flame, perturbed by an acoustic disturbance.
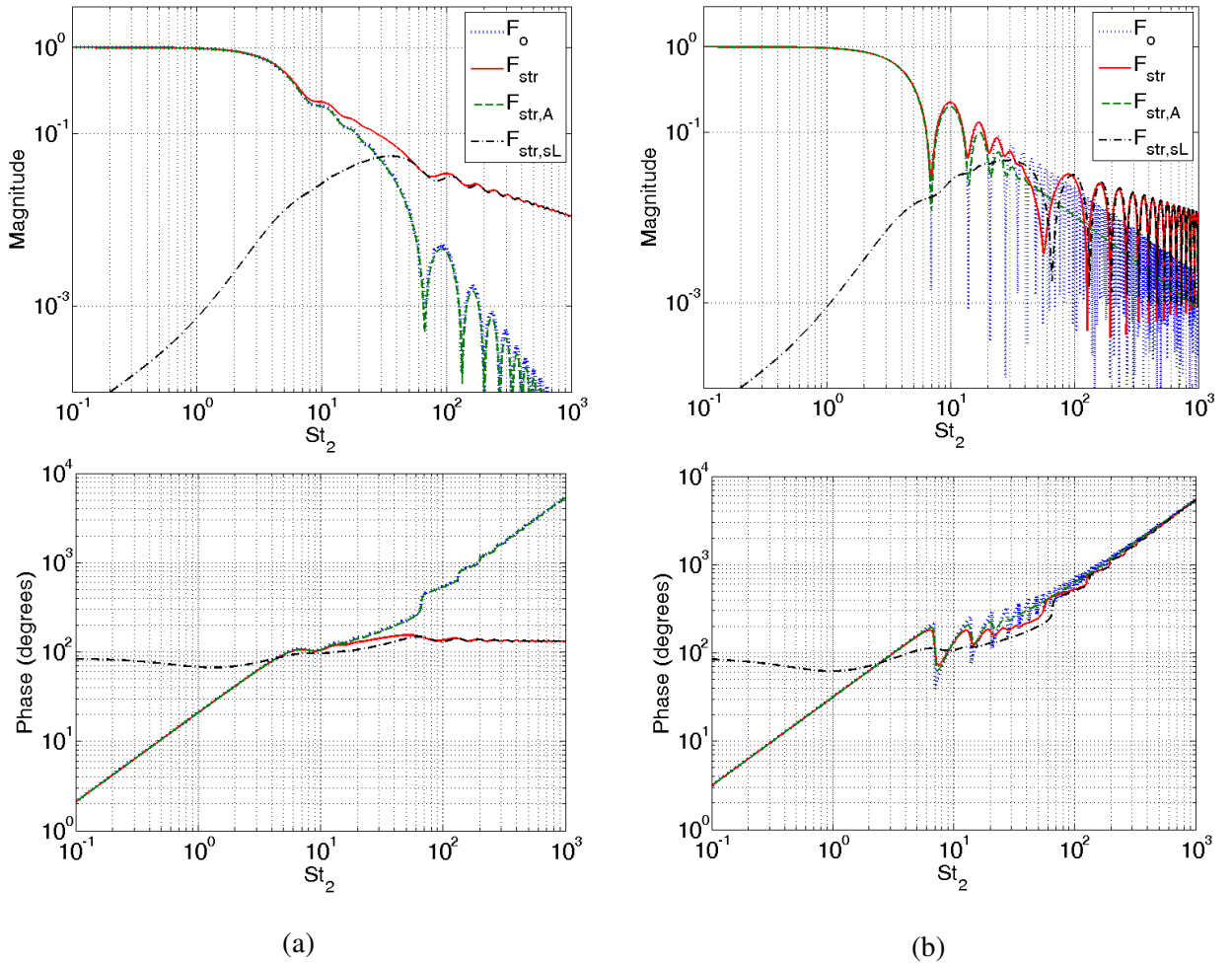
Figure 23: Influence of flame stretch on velocity coupled flame response. $k_{c,u} = M_o = 0.1$, $\beta = 4$, $\delta^* = 0.04$ flame. (a) Axisymmetric conical flame (b) 2D V-flame.

Figure 23 plots the transfer function of a stretch-affected axisymmetric conical flame (left) and a 2D V-flame (right). It may be seen that most of the conclusions that held good for the case of flames being perturbed by vortical disturbances hold good for the response caharacteristics of flames perturbed by acoustic fluctuations. However, $F_{str,A}$ begins to diverge from F_o at a lower Strouhal number, $St_2 \sim 10$ for conical flames, and $St_2 \sim 20$ for the 2D V-flame, while the flame speed route to heat release oscillations becomes important at $St_2 \sim 40$ and $St_2 \sim 80$ for the conical flame and V-flame respectively.

In general, consider the effect of varying $k_{c,u}$ on stretched flame response, for say, a conical flame, as considered in Figure 24.
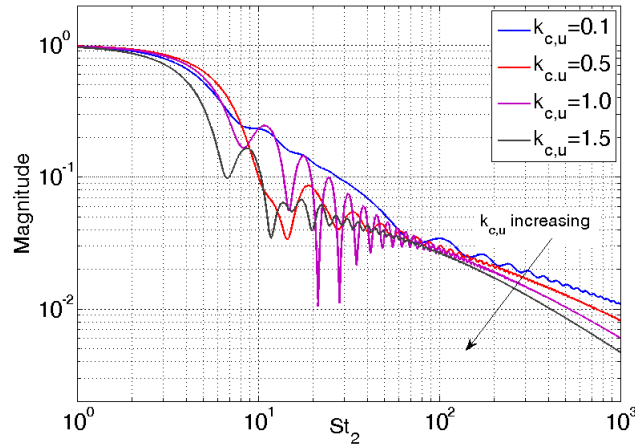
Figure 24 : Variation of stretch-affected flame transfer function magnitude for an axisymmetric conical flame with $k_{c,u}$. $\beta = 4$, $\delta^* = 0.04$.

At very high Strouhal numbers, a monotonic trend is seen for the total transfer function magnitude, and at a given Strouhal number, the transfer function magnitude decreases

with increasing $k_{c,u}$. This can be attributed to the fact that as $k_{c,u}$ increases, the flame transfer function magnitude varies as $1/k_{c,u}$ at a fixed Strouhal number, see Eq.(3.102).

3.3.2.3.2 Effect of Axially Diffusing Velocity Disturbances on Linear Flame Response

We next move on to understand how axial diffusion of velocity disturbances affect the responses of unstretched and stretched axisymmetric conical and V-flame. To begin with, Figure 25 plots the total responses of flames with and without axial diffusion effects.

(a)   (b)
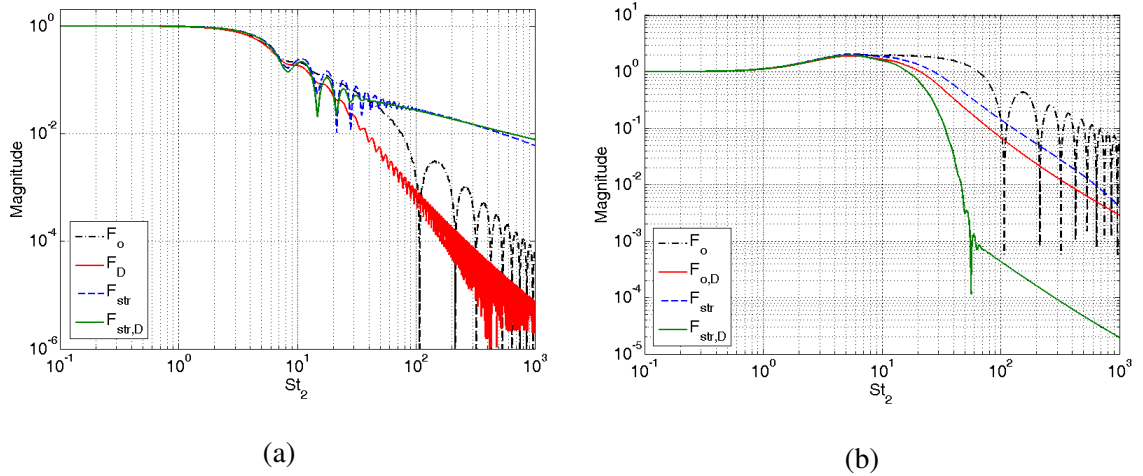
Figure 25 : Velocity coupled flame response characteristics with and without diffusion and stretch effects. (a) Axisymmetric conical flame, (b) Axisymmetric V-flame, $\beta = 4$, $\delta^* = 0.04$.

The graphs of Figure 25 plot the magnitudes of the transfer function for four cases – (i) the baseline flame response, i.e., neglecting axial diffusion or stretch effects, F_o, (ii) diffusion affected flame response of an unstretched flame, F_D, (iii) stretch affected flame response without axial diffusion effects, F_{str}, and (iv) flame response accounting for both

disturbance decay and flame stretch effects, $F_{str,D}$. First consider the former two transfer functions, F_o and F_D. It may be seen from the magnitude plots in Figure 25(a) and (b), that diffusion effects become important at fairly low Strouhal numbers for both conical and V-flames, at $St_2 \sim 10$ for either geometry.

In fact, at higher Strouhal numbers of about 100, the diffusing velocity field leads to two effects – first, the overall magnitude of the flame transfer function is reduced by about an order of magnitude, and second, the undulations in the baseline transfer function response are smoothened out. The second effect may be seen more pronouncedly from Figure 25(b), for a V-flame. The first effect occurs purely due to the fact that as one moves away from the flame base towards the flame tip, the amplitude of the velocity disturbance exponentially decays and hence, the burning area fluctuations also reduce, leading to lesser response. The second effect occurs because, as seen earlier, axial diffusion effects affect the local (particular) solution to the flame front evolution equation, and the waves generated at the flame holder, i.e., the homogeneous solution is unaffected. The amplitude of the particular solution now decays exponentially away from the flame base. Hence, as opposed to the baseline solution, where the particular and homogeneous solutions would have the same amplitude and could constructively interfere to lead to local maxima in the flame response, the veracity of the constructive interference is now reduced due to very small amplitudes for the particular solution at locations close to the flame tip. This is also the reason why this effect is more pronounced in V-flames. These locations where the diffusion-affected solution is now mostly composed of the homogeneous solution are the locations that have larger burning area, and contribute more significantly to the heat release rate, than locations close to the

flame holder, where diffusion effects are less significant. The reverse occurs in conical flames – i.e., locations where diffusion is important are those with lesser burning area and contribute lesser to overall flame response. Finally, though not shown here, these decaying velocity perturbations have very little effect on the transfer function phase, but at very high Strouhal numbers. These conclusions are similar to the equivalence ratio coupling counterpart of the problem.

Consider next the effect of diffusion on stretch affected flame response. It may be seen from Figure 25(a) and (b), that diffusion mainly acts to undulate the oscillations in the transfer function further. This is seen more clearly in Figure 26 which plots the magnitude of the stretch affected transfer functions with and without the additional effects of vortical velocity diffusion.

(a)   (b)
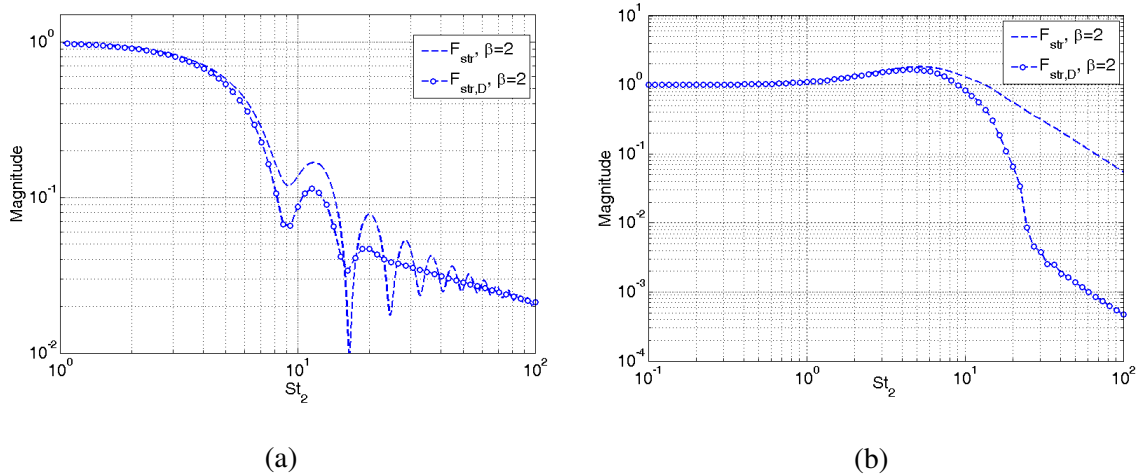
Figure 26 : Effect of axial diffusion of vortical velocity fluctuations on stretch-affected flame response, $\beta = 2$, $\delta^* = 0.04$ (a) Axisymmetric conical flame. (b) Axisymmetric V-flame.

The axial decay of velocity perturbations *naturally* damps out burning area fluctuations by disturbing different locations along flame with progressively lesser amplitudes,

moving from flame base to the flame tip. This is in addition to the flame front relaxation mechanism that flame stretch provides, which also smoothens out oscillations in the transfer function, by undulating flame wrinkles. It is however important to note that while both diffusion effects and stretch effects achieve similar purposes, i.e., smoothening out transfer function oscillations, the former is due to the nature of the flow disturbance, and the latter is due to flame speed response to flame stretch effects, and hence a *flame-related* cause leading to wrinkle modulation.

In the case of a V-flame, the near-absence of the particular solution contribution to flame front fluctuations in the stretch affected case (which in the first place leads to a monotonic decrease in the stretch affected flame transfer function) is augmented by further diminishing of the contribution of the particular solution due to very low amplitudes of the local velocity disturbances, thereby leading to a more rapid decrease in the total response transfer function.

Lastly, the effect of diffusion on flames with different flame lengths (and hence aspect ratios) is studied.
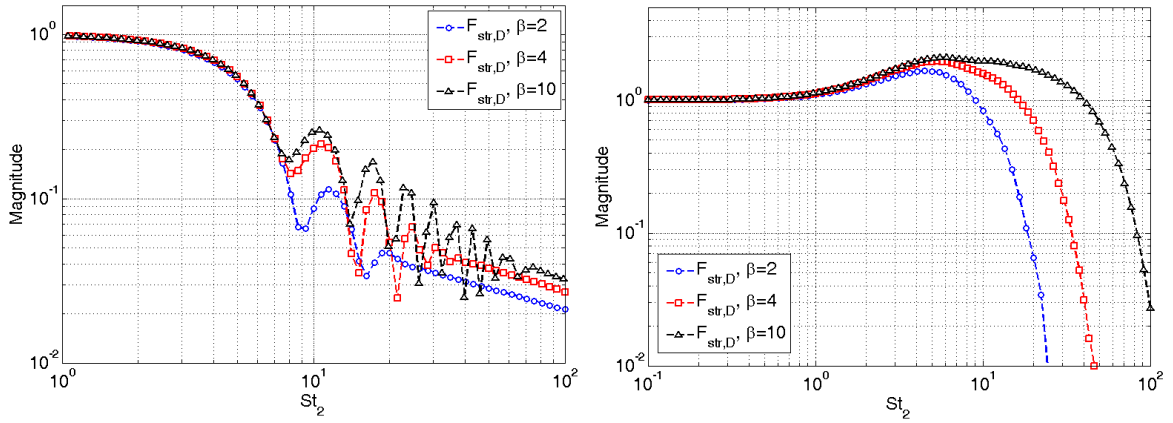
Figure 27 : Dependence of total flame transfer function on flame aspect ratio. $\delta^* = 0.04$ **(a) Axisymmetric Conical flame (b) Axisymmetric V-flame.**

Figure 27 plots the stretch and diffusion affected total transfer function for axisymmetric and conical flames of different aspect ratios. It may be seen that for both conical and V-flames, the low Strouhal number, quasi-steady dynamics is independent of the flame aspect ratio. As the Strouhal number increases, noticeable quantitative differences arise in the transfer function magnitudes for different aspect ratios. However, qualitatively, they are very similar. The characteristics seen in Figure 27 can be explained based exactly on the arguments used to explain the observations of Figure 20.

Finally, though not reported here, the phase characteristics of the flame transfer function seemed largely invariant across the range of flame aspect ratios considered here.

3.3.3. Flame Response to Pressure Perturbations

3.3.3.1 Flame Speed and Heat of Reaction Sensitivity to Pressure Perturbations

Consider first the response of the flame speed to the unsteady pressure and temperature variations in an acoustic wave. A number of publications [92, 95-98] have analyzed the internal structure of a flat flame perturbed by an acoustic wave using high activation energy asymptotics and single step kinetics. Many of these results are summarized by McIntosh [130], who emphasizes the different characteristics of the interaction depending upon the relative magnitudes of the length and time scales of the acoustic wave and flame preheat and reaction zone. Following McIntosh [92], the following expression relating the mass burning rate and the harmonic acoustic pressure perturbation that causes it, can be written for a structurally non quasi-steady flame ($St_\delta \sim 2\pi$) as follows:

$$\frac{\hat{\mu}'/\mu_o}{\hat{p}'/p_o\big|_{z=\xi(r,t)}} = -\frac{iSt_\delta\left(1-\gamma^{-1}\right)\theta\left(2s_1-\left(1-\vartheta^{-1}\right)\right)}{\left(Le\left(s_1-\frac{1}{2}\right)+\left(\frac{1}{2}-s_2\right)\right)\theta\left(1-\vartheta^{-1}\right)-4s_1\left(\frac{1}{2}-s_2\right)} \quad (3.114)$$

Here:

$$s_1 = \frac{1}{2}\left(1-4i\,Le\,St_\delta\right)^{1/2} \;\; ; \;\; s_2 = \frac{1}{2}\left(1-4i\,St_\delta\right)^{1/2} \quad (3.115)$$

From the above, it may be seen that the local mass burning rate response increases roughly with θ, St_δ, and flame temperature jump, $\vartheta = T_u/T_b$. The Lewis number dependence is quite weak for Le values near unity. This result illustrates that the mass burning rate response is substantially larger than its quasi-steady value in the physically

interesting ($St_\delta \sim 2\pi$) case. This also provides reason to believe that the global heat release response of the flame to pressure perturbations could potentially increase with frequency beyond a certain threshold.

For flames with low temperature jump, i.e., $\vartheta \to 1$, Eq.(3.114) can be expanded to leading order in $\left(1 - \vartheta^{-1}\right)$ to yield:

$$\mu_{1,p} = \frac{\hat{\mu}'/\mu_o}{\hat{p}'/p_o\big|_{z=\xi(r,t)}} = \frac{(\gamma-1)\theta}{4\gamma}\left(1+\left(1-4i\,St_\delta\right)^{1/2}\right) \tag{3.116}$$

Further, since:

$$\frac{\mu'}{\mu_o} = \frac{\rho'}{\rho_o} + \frac{s_L'}{s_{Lo}} \tag{3.117}$$

the explicit response of the flame speed to pressure perturbations, i.e., the flame speed sensitivity $s_{L1,p}$ may be obtained from the above, using an isentropic p-ρ relationship. Note further that fluctuations in mass burning rate may be expressed using the sensitivity in Eq.(3.116). More explicitly, we may write:

$$\frac{\mu'}{\mu_o} = \mu_{1,p}\frac{p'}{p_o}; \quad \frac{\rho'}{\rho_o} = \gamma^{-1}\frac{p'}{p_o} \tag{3.118}$$

The flame speed sensitivity to pressure disturbances may now be expressed as follows:

$$s_{L1,p} = \mu_{1,p} - \gamma^{-1} \tag{3.119}$$

In the limit of very high Strouhal numbers, Eq.(3.116) can be used to write:

$$s_{L1,p} \approx \frac{\left(1-\gamma^{-1}\right)\theta}{2}e^{3\pi i/4}St_\delta^{1/2} - \frac{1}{\gamma} \approx \frac{\left(1-\gamma^{-1}\right)\theta}{2}e^{3\pi i/4}St_\delta^{1/2} \tag{3.120}$$

For typical values of the parameters, such as those used in Figure 28, this dimensionless sensitivity is ~2.5 at St_f~100. Also, define the heat of reaction sensitivity to pressure perturbations as

$$h_{R1,p} = \frac{\partial (h_R/h_{Ro})}{\partial (p/p_o)}\bigg|_{p=p_o} + \frac{\partial (h_R/h_{Ro})}{\partial (T/T_o)}\bigg|_{T=T_o} \frac{\gamma-1}{\gamma} \tag{3.121}$$

The heat of reaction sensitivity to pressure perturbations is small in comparison to the other terms contributing to the heat release and is neglected. For example, quasi-steady equilibrium calculations for a methane-air flame with reactants at 300K and $\phi=0.7$ indicate h_{R1p}~3.3 x 10^{-2} and 3.2 x 10^{-2} at 1 and 10 atm, respectively.

3.3.3.2 Heat Release Response Transfer Functions

As earlier, we begin by calculating the flame front perturbation due to acoustic pressure fluctuations. The flame front position function $\xi(r,t)$ may be expanded in terms of the amplitude of pressure perturbations ε_p as:

$$\xi^*(r^*,t^*) = \xi_o^*(r^*) + \varepsilon_p \xi_1^*(r^*,t^*) + O(\varepsilon_p^2) \tag{3.122}$$

This leads to the following evolution equations:

$$\xi_o^*(r^*) = 1 - r^* \tag{3.123}$$

$$\frac{\partial \xi_1^*}{\partial t^*} - \alpha \frac{\partial \xi_1^*}{\partial r^*} + s_{L1,p} \cos(St(1-r^*-t^*)) = 0 \tag{3.124}$$

Together with the anchor-fixed BC, we can solve (3.124) to get

$$\xi_1^*(r^*,t^*) = \frac{s_{L1,p}}{(1-\alpha)St}\left[\sin\left\{St\left(1-r^*-t^*\right)\right\}-\sin\left\{(St/\alpha)\left(1-r^*-\alpha t^*\right)\right\}\right] \quad (3.125)$$

The pressure coupled flame response arises due to density and flame speed fluctuations. As such, the flame speed fluctuations lead to flame response directly and indirectly by causing flame area fluctuations (See Figure 8). Hence, the transfer function may be expressed as:

$$F_p = F_{A,p} + F_{s_L,p} + F_{\rho,p} \quad (3.126)$$

These transfer functions can be calculated by using the solution of the flame front fluctuation, Eq.(3.125), as detailed earlier. For example, for a 2D V-flame, the transfer function contributions can be determined to be the following:

$$F_{\rho,p} = \frac{i}{\gamma}\frac{1-e^{i\eta_1 St_2}}{\eta_1 St_2} \quad (3.127)$$

$$F_{A,p} = -s_{L1,p}\frac{e^{i\eta_1 St_2} - e^{iSt_2}}{(\eta_1-1)iSt_2} \quad (3.128)$$

$$F_{s_L,p} = s_{L1,p}\frac{1-e^{i\eta_1 St_2}}{i\eta_1 St_2} \quad (3.129)$$

where $\eta_1 = \alpha M_o$.

We next study the asymptotic limits of the transfer functions, Eqs.(3.127)-(3.129). First, the low Strouhal number limits might be evaluated as follows:

$$\lim_{St_2\to 0} F_{\rho,p} = \frac{1}{\gamma} \quad (3.130)$$

$$\lim_{St_2\to 0} F_{s_L,p} = -\lim_{St_2\to 0} F_{A,p} = \frac{1}{\gamma}\left(\frac{(\gamma-1)\theta}{2}-1\right) \quad (3.131)$$

122

Hence, in the quasi-steady limit, the contributions to the total transfer function due to flame speed fluctuations and burning area fluctuations cancel each other. It may be noted that this is analogous to the interaction between these two routes in the case of fuel/air ratio coupling. In fact, the role played by density fluctuations here, is somewhat similar to that of heat of reaction fluctuations in the case of fuel/air ratio coupling. This fact can be further appreciated by noting that, in the globally quasi-steady limit, the total pressure-coupled response function attains the value of "density sensitivity" to pressure fluctuations, i.e.:

$$\lim_{St_2 \to 0} F_p = \lim_{St_2 \to 0} F_{\rho,p} = \gamma^{-1} \tag{3.132}$$

Consider next, the asymptotic trends of the transfer functions for very high Strouhal numbers. It follows from Eqs.(3.127)-(3.129), that:

$$\left| F_{\rho,p} \right| \sim \frac{1}{St_2} \; ; \left| F_{s_L,p} \right| \sim \frac{1}{St_2^{1/2}} \tag{3.133}$$

The latter asymptotic trend arises because of the $\sqrt{St}$ dependence of $s_{L1,p}$ at very high Strouhal numbers, see Eq.(3.120). Further, note that the area contribution shows the same $\sqrt{St}$ dependence. This implies that the pressure coupled flame response is dominated by reactant density fluctuations at low frequencies and flame speed fluctuations at high frequencies.

3.3.3.3 Illustrative Results

To get a feel for pressure coupled transfer function characteristics, consider a 2D V-flame with $\beta = 4$. Figure 28 plots the heat release response transfer functions for the pressure coupled flame response problem.
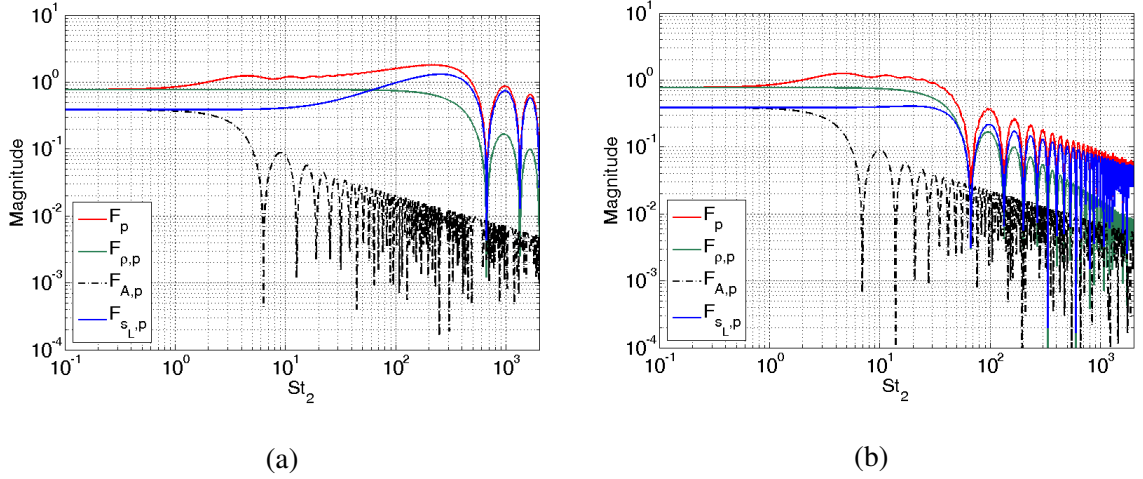
Figure 28 : Pressure coupled flame response transfer function magnitude and its constituents for a 2D V-flame, with $(\gamma - 1)\theta = 3$, $\beta = 4$, for (a) $M_o = 0.01$ (b) $M_o = 0.1$.

At very low Strouhal numbers, the transfer function magnitude is completely dominated by density fluctuations. The contribution to the transfer function due to flame speed and burning area fluctuations is about an order of magnitude smaller than the density fluctuation contribution. However, as Strouhal number increases, the contribution of the flame speed fluctuations begins to grow in significance. In fact, for $M_o = 0.01$, it even grows in absolute magnitude. about $St_2 \sim 1$, there is already significant contribution to F_p due to F_{s_L}. At about $St_2 \sim 10$, the pressure coupled response arises almost exclusively due F_{s_L}. As such, F_{s_L} attains a maximum value and then begins to decrease

slowly, in accordance with the scaling in Eq.(3.133) . The phases of all contributions show a monotonic increase with Strouhal number, with the phase of F_{s_L} being identical to F_p. This occurs because beyond about $St_2 \sim 10$, there is no significant contribution to the flame response from F_ρ.

As such, a rough scaling when the flame speed fluctuation route becomes important in the pressure coupled flame response problem may be determined using:

$$\left| F_\rho \right| \sim \left| F_{s_L} \right| \tag{3.134}$$

This now leads to:

$$St_2 \sim \left(\frac{(\gamma-1)\theta}{2\eta_1} \right)^2 \delta^* \alpha^{1/2} \tag{3.135}$$

Finally, it is important to note that the fact that pressure coupled flame response decrease as $St_2^{-1/2}$ provides sufficient ground to expect that at very high Strouhal numbers, pressure coupling could potentially become of equal significance as velocity coupling and equivalence ratio coupling. An investigation of this claim will be undertaken in Chapter 4, which will discuss the relative importance of these different mechanisms.

Chapter 4 : Relative Importance of Coupling Mechanisms

The previous chapter dealt with a quantitative study of the response of premixed flames to various coupling mechanisms, by means of their transfer function. It was noted that while the sensitivity of the flame speed to equivalence ratio fluctuations or stretch rate fluctuations decreased with increasing Strouhal number, the sensitivity to pressure fluctuations increased as $\sqrt{St}$. This led to a $St_2^{-1/2}$ decay for the magnitude of the pressure coupled flame response transfer function, which was weaker as compared to velocity and fuel/air ratio coupled responses. It was concluded that this could potentially lead to pressure coupling becoming an important phenomenon at high frequencies.

In this chapter, the relative importance of the different coupling mechanisms as a function of frequency is assessed in greater detail by comparing the magnitudes of their transfer functions.

4.1. Transfer Function Comparisons

To start with, the perturbations in equivalence ratio, acoustic pressure and velocity are assumed to be related by:

$$-\frac{\phi'}{\phi_o} = \frac{u'_\Omega}{u_o} = \frac{u'_a}{u_o} = \left(\frac{1}{\gamma M_o}\right)\frac{p'}{p_o} \tag{4.1}$$

Since the ratio of the amplitudes of velocity perturbations and pressure perturbations is $1/\gamma M_o$, we will multiply the pressure coupled transfer function γM_o to

compare them with velocity and equivalence ratio coupled responses. While this chapter considers the comparison for axisymmetric V-flames, comparisons for other geometries may be performed in very similar manner as well. In this spirit, a representative result is presented later for conical and 2D V-flames as well.

We begin by exploring the asymptotic tendencies of F_u, F_ϕ and F_p. Consider first, the flame response at very low St.

$$\lim_{St_2 \to 0} F_u = 1 \tag{4.2}$$

$$\lim_{St_2 \to 0} F_\phi = h_{R1,\phi} \tag{4.3}$$

$$\lim_{St_2 \to 0} \left(\gamma M_o F_p \right) = M_o \tag{4.4}$$

From Eqs.(4.2)-(4.4), it may be seen that in this limit, the pressure coupled response is smaller than the velocity coupled response by $O(M_o)$ and is hence negligible in comparison, since flows in practical gas turbine combustors have $M_o \ll 1$. The equivalence ratio and velocity coupled responses are similar, differing only by factor $h_{R1,\phi}$ which is of $O(1)$ for lean flames. For example, for methane-air flames at 1 atm, 300K and ϕ=0.85, this value is 0.96. However, for rich flames $h_{R1,\phi} \ll 1$. Hence, in the $St \to 0$ limit, for lean flames, velocity coupling and equivalence ratio coupling responses dominate over pressure coupled flame response, while for rich flames, velocity coupling dominates over the other two.

In the high Strouhal number limit, we have, from, Eq.(3.102), Eq.(3.133) and Eq.(3.76) that:

$$\left| F_u \right| \sim \frac{1}{St_2} \tag{4.5}$$

$$\left| F_p \right| \sim \frac{1}{St_2^{1/2}} \tag{4.6}$$

$$\left| F_\phi \right| \sim \frac{1}{St_2^{2}} \tag{4.7}$$

This shows that the pressure coupled flame response transfer function dies the slowest. This could render pressure coupling effects more significant than velocity coupling and equivalence ratio coupling at very high Strouhal numbers.
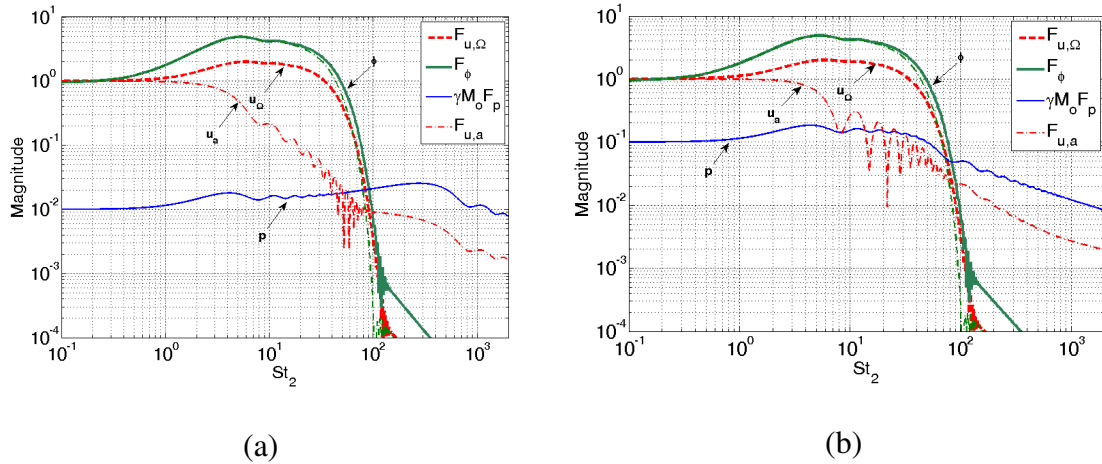
Figure 29: Comparison between vortical and acoustic velocity coupled, equivalence ratio coupled and pressure coupled flame responses, accounting for high frequency effects, for a lean methane/air axisymmetric V-flame with reactants at 300 K, 1 atm, and with $\phi_o = 0.85$, $\beta = 4$, $\delta^* = 0.01$. (a) $M_o = 0.01$, (b) $M_o = 0.1$.

To understand this better, consider Figure 29, which plots[11] the comparison between the magnitudes of equivalence ratio coupled (F_ϕ), acoustic velocity coupled ($F_{u,a}$), vortical velocity coupled ($F_{u,\Omega}$) and pressure coupled ($\gamma M_o F_p$) flame responses.

---

[11] The Strouhal number axes of transfer function plots are truncated approximately where the flame preheat zone becomes convectively non-compact to upstream disturbances.

As discussed earlier, these figures show that at low Strouhal numbers, the pressure coupling gain factor is of $O(M_o)$, while the other mechanisms are of $O(1)$. However, the curves also clearly show the dramatic reduction in flame response for the vortical velocity and fuel/air ratio mechanisms above $St\sim40$. The acoustic velocity gain decays slower, but also rolls off at higher frequencies, so that its gain is comparable to the other two at $St=100$. In contrast, the pressure coupling mechanism stays much flatter with frequency and becomes dominant at Strouhal numbers close to 100. The specific value of this "crossover" Strouhal number, where pressure coupling becomes dominant is discussed further in Sec.4.2. The result in Figure 29 is an important one as it suggests that fundamentally different mechanisms may control screeching instabilities.

The result in Figure 29 is an important one. This reveals that high Strouhal number dynamics not only have to be studied by accounting for additional routes (stretch, diffusion etc.) associated with coupling processes dominant at low Strouhal numbers (viz., fuel/air ratio coupling and velocity coupling), but altogether new physics needs to be incorporated in terms of pressure coupling as a new mechanism for flame response.

Though this problem is of greater relevance to lean premixed systems, a similar analysis performed for rich premixed systems leads to the same qualitative conclusion – i.e., pressure coupling becomes an important mechanism for flame response at high Strouhal numbers. This result is plotted in Figure 30 for a $\phi_o = 0.85$ and a $\phi_o = 1.28$ [12] atmospheric methane/air flame, respectively. It may be seen from Figure 30 that pressure

---

[12] These equivalence ratios were chosen so that the flame speed at 1 atm, 300K is the same, 33 cm/s.

coupling becomes important at about the same Strouhal number for either equivalence ratio.
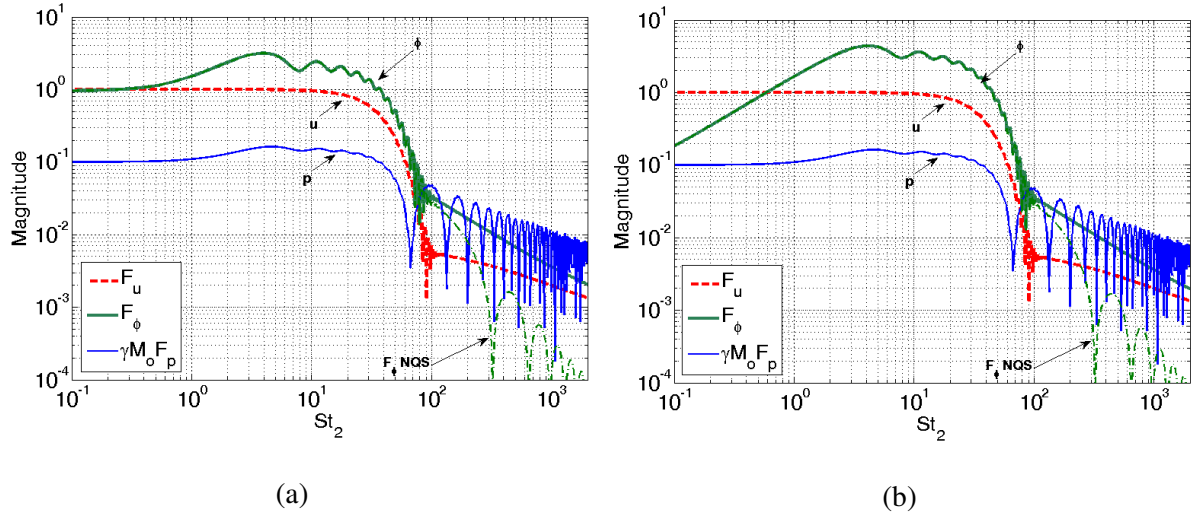
Figure 30: Comparison between lean and rich velocity coupled, equivalence ratio coupled and pressure coupled flame responses, accounting for high Strouhal numbers effects, for a methane/air flame with $M_o = 0.1$, $\beta = 4$, $\delta^* = 0.01$ **- (a) Lean:** $\phi_o = 0.85$ **(b) Rich:** $\phi_o = 1.28$.

In the context of Figure 30, it is important to note that the major difference between Figure 30(a) and Figure 30(b) arises in the low Strouhal number limit, i.e., the $St_2 \to 0$ limit, in which F_ϕ approaches the linear h_R sensitivity, see Eq.(4.3). In this limit, F_ϕ and F_u are comparable for lean flames and hence dominate the low Strouhal number dynamics together. However, for rich flames, $h_{R1,\phi} \sim 10^{-3} \ll 1$, and hence F_u dominates the low Strouhal dynamics exclusively.
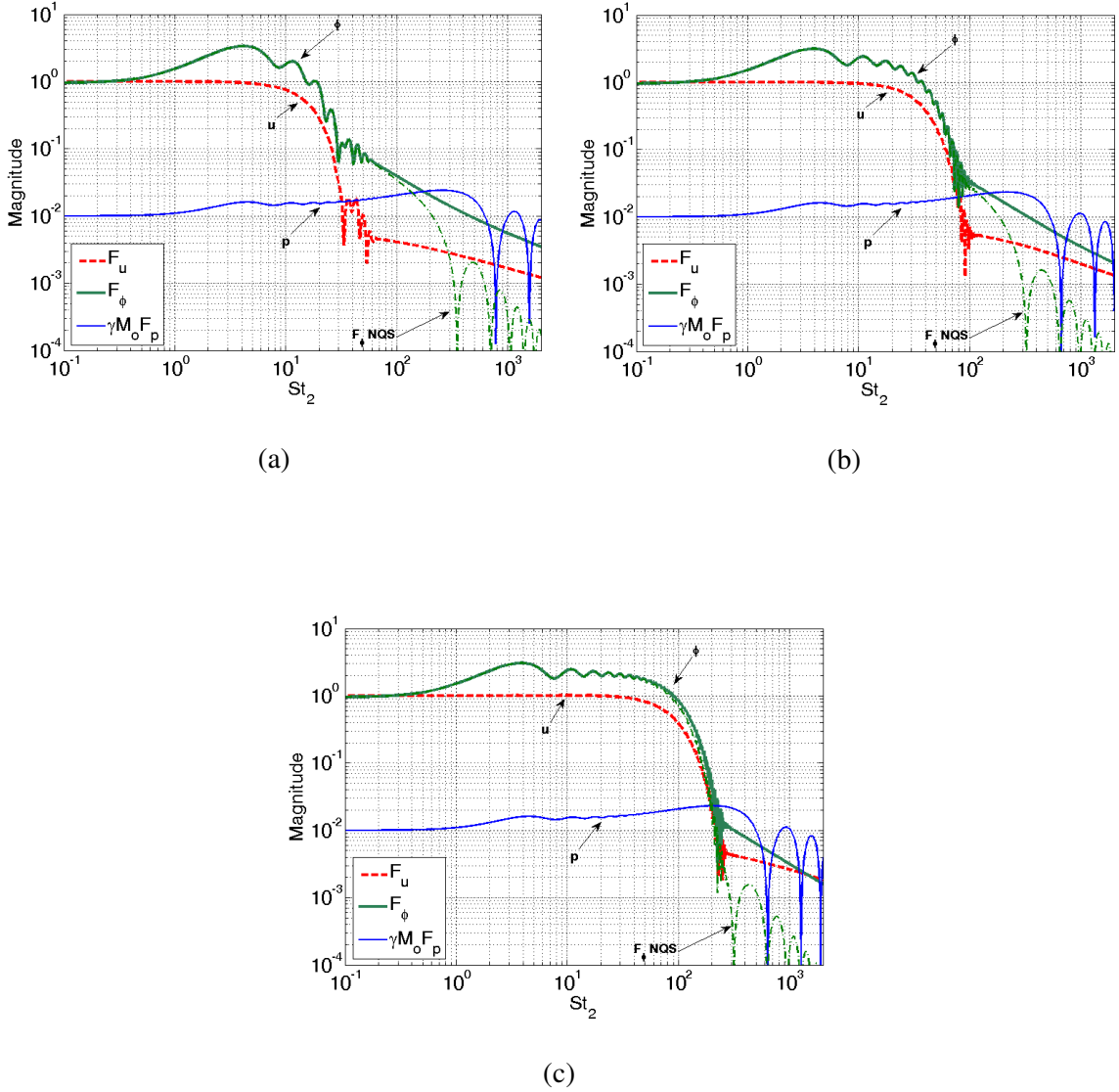
Figure 31 : Comparison between F_u, F_ϕ **and** F_p **for different values of** β **for a methane/air flame with** $\phi_o = 0.85$, $M_o = 0.01$, $\delta^* = 0.01$. **(a)** $\beta = 2$, **(b)** $\beta = 4$, **(c)** $\beta = 10$.

We next consider the effect of flame aspect ratio, β, on this comparison. This is a significant parameter, because, the effect of axial diffusion on fuel/air ratio coupled and

velocity coupled flame responses, depends on β, as discussed in Chapter 3. Figure 31 plots the comparison between F_u, F_ϕ and F_p for different values of β.

It may be seen from Figure 31 that as β increases, the value of the Strouhal number at which pressure coupling becomes dominant increases. For the conditions listed above, for $\beta = 2$, $\beta = 4$, and $\beta = 10$, pressure coupling becomes important at about $St_2 \approx 60$, $St_2 \approx 80$, and $St_2 \approx 200$ respectively, showing monotonic increase with β. This is due to the fact that as β increases, the effect of axial diffusion of velocity and fuel/air ratio disturbances on premixed flame response leads to lesser attenuation of the flame gain in V-flames. This has been discussed earlier in Chapter 3, see Figure 20 and Figure 27.

(a)   (b)
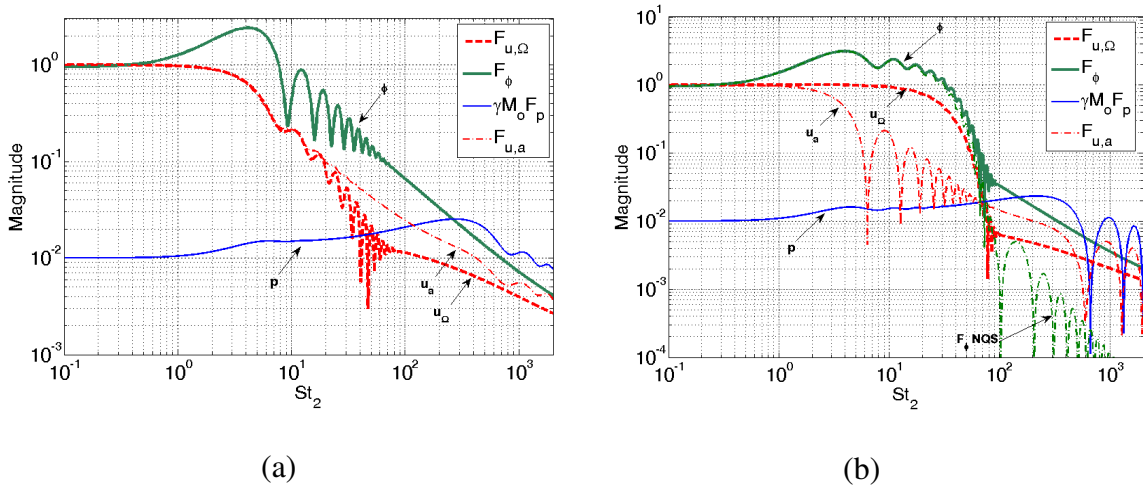
Figure 32: Comparison between velocity coupled, equivalence ratio coupled and pressure coupled flame response magnitudes for a lean methane/air flame with reactants at 300 K, 1 atm, and with $\phi_o = 0.85$, $\beta = 4$, $M_o = 0.01$, $\delta^* = 0.01$. (a) Axisymmetric conical flame, (b) 2D V-flame.

We next consider the effect of flame geometry on the three coupling processes for a lean methane/air axisymmetric conical and 2D V-flame in Figure 32.

Note the difference in frequency where pressure coupling becomes dominant - i.e., it occurs at the lowest Strouhal number with the 2D V-flame and the highest with the conical flame. This difference is related to the distribution of area density, as the V-flame has most of its area farther downstream where the vortical velocity and fuel/air ratio disturbances have decayed most. Also, it is important to also notice the lack of oscillations in the case of the conical flame. This occurs due to comparable contributions to flame position fluctuations from both the local inhomogeneity and the boundary-generated wave. The former, in particular, is not influenced by diffusion effects in the regions that contribute the most to the flame response.

4.2. Crossover Strouhal Number

Next, the Strouhal number at which pressure coupling becomes important is determined. It can be shown that for Strouhal numbers where pressure coupling becomes important, the flame speed routes dominates the pressure coupled flame response, while the burning area fluctuations still dominate the fuel/air ratio and velocity coupled flame responses. In fact, for high Strouhal numbers, pressure coupled flame response may be approximated to be the following:

$$F_p \approx s_{L1,p} \frac{iM_oH_c}{-4i + H_cM_o^2St}\left(e^{iStM_o} - 1\right) \tag{4.8}$$

The Strouhal number at which pressure coupled response becomes dominant, $St_{PC\sim\phi C}$, is not analytically estimable in general. However, if a tall flame is assumed, an

approximate high Strouhal number analysis of the equality $\left|\gamma M_o F_p\right| \approx \left|F_\phi\right|$ yields the following estimate for this Strouhal number.

$$St_{PC\sim\phi C} \approx \frac{\beta^{1/3}}{\delta^*}\left(\frac{Le^2}{4-Le}s_{L1}\frac{1}{2(\gamma-1)\theta}\right)^{2/3} \tag{4.9}$$

Equation (4.9) may be written in terms of St_δ as:

$$St_{\delta,PC\sim\phi C} \approx \beta^{1/3}\left(\frac{Le^2}{4-Le}s_{L1}\frac{1}{2(\gamma-1)\theta}\right)^{1/3} \tag{4.10}$$

Using an analysis similar to obtaining $St_{PC\sim\phi C}$, it can be shown that pressure coupling becomes comparable to velocity coupling at a slightly lesser Strouhal number, given by:

$$St_{PC\sim UC} \approx \frac{\beta^{1/3}}{\delta^*}\left(\frac{Pr^2}{4-Pr}\cdot\frac{1}{2(\gamma-1)\theta}\right)^{2/3} \tag{4.11}$$

It is interesting to notice the $\beta^{1/3}$ dependence of the Strouhal numbers, $St_{PC\sim\phi C}$ and $St_{PC\sim UC}$. This is in tune with the observations from Figure 31 that these increase with β.

For the values used in Figure 29, say, Eqs.(4.11) and (4.9) give values of $St_{PC\sim UC} = 76$ and $St_{PC\sim\phi C} = 130$ respectively, which are in agreement with the figure as well.

To get a feel for what these crossover Strouhal number translate to in terms of actual frequency values and to consider the implication of these results at high pressure and temperature conditions, consider Figure 33, which plots the variation of the crossover

frequency as a function of the mean fuel/air ratio for a laminar methane/air flame, and how it varies with reactant preheat and pressure. In these plots, the flame aspect ratio, β, is held constant and the mean fuel/air ratio is varied, implying that the corresponding flow velocity varies (from 0.5 ms^{-1} to 4 ms^{-1} for reactants at 300 K, 1 atm, and 1.5 ms^{-1} to 7 ms^{-1} for reactants at 700 K, 1 atm) in these calculations as well.

(a)   (b)
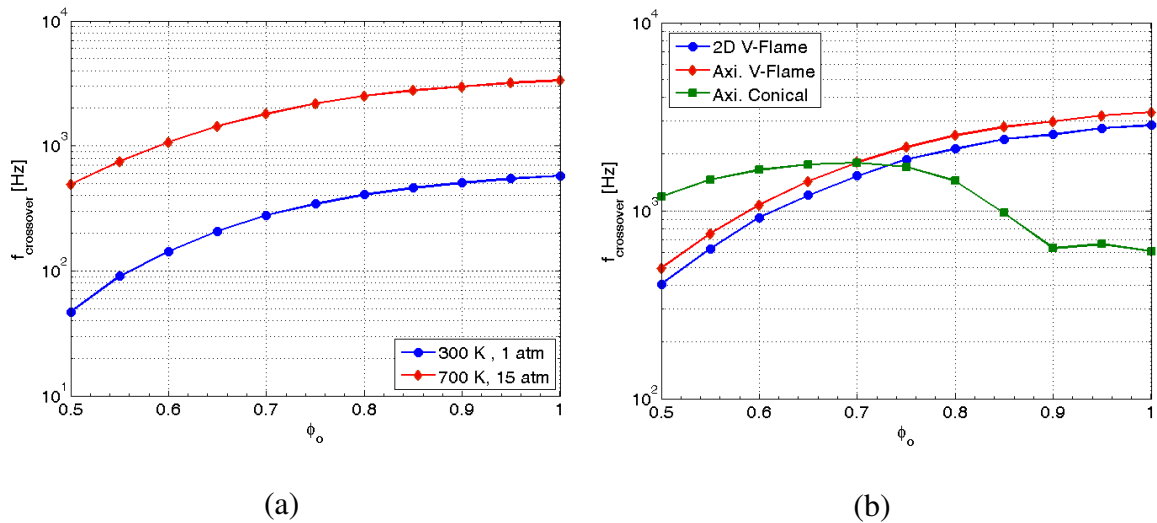
Figure 33 : Typical frequencies in Hz at which pressure coupling begins to dominate over both equivalence ratio coupling and velocity coupling for laminar flames. (a) Effect of preheat and pressure for an axisymmetric methane/air V-flame as a function of equivalence ratio. (b) Effect of flame geometry at 700 K, 15 atm. $\beta = 10$, $(\gamma - 1)\theta = 4.2$, $Le = 0.9, Pr = 0.9$. The burner duct is assumed to be 2 cm in width.

As can be seen from Figure 33(a), the frequency at which pressure coupling becomes dominant increases significantly in going from atmospheric conditions to conditions typical of gas turbine operation. The fact that this crossover frequency varies considerably with pressure illustrates that the dominant mechanisms controlling a 1000 Hz self-excited oscillation in an atmospheric pressure combustor may be totally different than a high pressure engine. Since the flame thermal thickness, flame speed and flame speed sensitivities are all functions of the mean equivalence ratio, the crossover

frequency also considerably changes with operating equivalence ratio and conditions. Note also the relatively "low" frequencies at which pressure coupling can become dominant in these calculations. This is due to the fact that the low velocities used for these laminar flame calculations cause the flame response to become globally non quasi-steady at quite low frequencies; global non quasi-steadiness occurs at frequencies $f \sim u_o / L_f$ which for a $\beta = 10$, $\phi_o = 0.5$ methane/air flame at 300 K, 1 atm occurs at about 5 Hz. In higher velocity flows, the flame position responds much faster, causing the interference related decay in flame response to be shifted to higher frequencies.

However, in the case of practical flames, turbulence augments the mass burning rate, thereby destroying flame wrinkles faster. The pressure coupling crossover frequency for such practical cases is presented in Figure 34. In these plots, to simulate realistic aviation and land based gas turbine combustor conditions, flow velocities and operating conditions typical of such combustors are assumed. Further, the reactant flow velocity is kept constant, as are the flame geometric parameters. Assuming that these turbulent flames fall in the wrinkled flamelet regime of the Borghi diagram, at a flamelet level, they may be approximated to nominally propagate into the reactants in a "laminar" manner to match the local normal reactant velocity. This approximation provides a magnitude for the turbulent displacement speed of the flame, which is used in lieu of the actual laminar flame speed; the latter underestimates the burning rate in realistic scenarios. Varying the equivalence ratio hence varies the dimensionless flame speed sensitivities, which are assumed to be identical for the laminar and turbulent flame speeds.

<table>
<tr><td>(a)</td><td>(b)</td></tr>
</table>
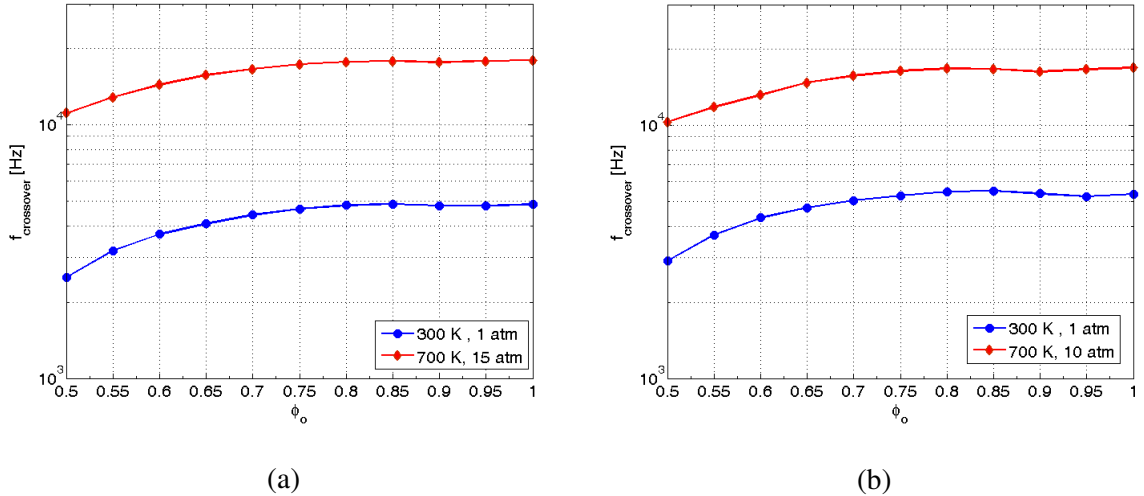
Figure 34 : Typical frequencies in Hz at which pressure coupling begins to dominate over both equivalence ratio coupling and velocity coupling for turbulent flames in practical gas turbine combustors. (a) Land based gas turbines, operating at 700 K, 15 atm, with reactant velocity of 60 m/s. The flame width and length are assumed to be 5 cm and 30 cm respectively. (b) Aviation gas turbines, operating at 700 K, 10 atm, with reactant velocity of 80 m/s. The flame width and length are assumed to be about 8 cm and 20 cm respectively. The following values are also assumed. $(\gamma-1)\theta = 4.2$, $Le = 0.9, Pr = 0.9$.

It may be seen from the above that, as seen earlier, the crossover frequency varies quite significantly between atmospheric conditions and gas turbine operating condition. However, the crossover frequency increases in magnitude as compared to the laminar case by about an order of magnitude. This may be attributed to the turbulent displacement speed which is itself an order of magnitude larger than the laminar flame speed. At gas turbine conditions, both land based and aviation combustors possess pressure coupling crossover frequencies in the range of 10-15 kHz.

Although these frequencies are about an order of magnitude higher than those high frequency tones usually encountered in gas turbine engines, it must be borne in mind that the pressure coupling model implicitly assumes a single step chemical reaction and hence, the results have to be treated with circumspection. Note also, that the model does

not predict transverse instability frequencies, since it is rooted in an axial/longitudinal disturbance perturbing the flame.

Finally, it is important to note that the flame speed sensitivity to pressure begins to decrease beyond a certain critical Strouhal number [91, 93, 102] . However, this would occur at Strouhal numbers characteristic of reaction zone non quasi-steadiness and hence preheat zone convective non-compactness and cannot be studied using the G-equation approach used in prior analyses in this thesis. As such, the next section will summarize various flame response regimes and Strouhal numbers at which various physical processes need to be taken into consideration.

4.3. Summary of Flame Response Regimes

It is useful to summarize the discussions of Chapters 2-4 by means of a flame response regime diagram. Amongst the various physical phenomena discussed in Chapter 2, some high frequency effects, viz., flame stretch effects, axial decay of convective disturbances and non quasi-steady response have been discussed comprehensively in the previous chapters and criteria when these processes become important have been determined. To better understand and appreciate where these different regions lie on a frequency map, these various physical processes are parameterized in terms of the two Strouhal numbers $St_{\delta,f}$ and St_f which characterize local and global non quasi-steadiness respectively. These various physical phenomena become important at different Strouhal numbers and are summarized in Table 4.

Table 4 : Summary of physical processes influencing flame response at different regimes in the $St_{,f}$, $St_{\delta f}$ space

Physical process	Frequency regime
Globally quasi-steady	$St_f \ll 1$
Locally quasi-steady	$St_{\delta,f} \ll 1$
Globally non quasi-steady	$St_f \sim 1$
Locally non quasi-steady	$St_{\delta,f} \sim 1$
Geometric Convective non-compactness	$St_f \sim 1/k_c$
Geometric Acoustic non-compactness	$St_f \sim 1/M_o$
Preheat zone convective non-compactness	$St_{\delta,f} \sim \beta/k_c$
Preheat zone acoustic non-compactness	$St_{\delta,f} \sim 1/M_f$
Reaction zone convective non-compactness	$St_{\delta,f} \sim \theta^2 \beta/k_c$
Reaction zone acoustic non-compactness	$St_{\delta,f} \sim \theta^2/M_f$
Flame curvature affects area fluctuations	$St_f \cdot St_{\delta,f} \sim \beta^2/4\pi^2$
Flame curvature alters flame speed	$St_{\delta,f} \sim \beta^2/2\pi$

Table 4 (continued)

Hydrodynamic strain affects area fluctuations	$St_{\delta,f} \sim 1/2\pi$
Axial diffusion effects affect velocity coupled flame response	$St_{\delta,f} \sim \dfrac{\Pr \beta^2}{2\pi}\left(\Gamma'^{1/2} + \dfrac{5}{2}\Gamma'^{3/2}\right); \quad \Gamma' = \dfrac{\delta^{*1/2}}{\beta \Pr}$
Axial diffusion effects affect fuel/air ratio coupled flame response	$St_{\delta,f} \sim \dfrac{Le\beta^2}{2\pi}\left(\Gamma'^{1/2} + \dfrac{5}{2}\Gamma'^{3/2}\right); \quad \Gamma' = \dfrac{\delta^{*1/2}}{\beta Le}$
Pressure coupling ~ Velocity coupling	$St_{\delta,f} \approx \dfrac{\beta^{1/3}}{2\pi}\left(\dfrac{\Pr^2}{4-\Pr}\cdot\dfrac{1}{2(\gamma-1)\theta}\right)^{2/3}$
Pressure coupling ~ Fuel/air ratio coupling	$St_{\delta,f} \approx \dfrac{\beta^{1/3}}{2\pi}\left(\dfrac{Le^2}{4-Le}s_{L1}\dfrac{1}{2(\gamma-1)\theta}\right)^{1/3}$
Reaction zone non quasi-steadiness	$St_{\delta,f} \sim \theta^2$

Figure 35 plots a regime diagram representation and marks the different areas for the physical processes listed in Table 4. The regimes corresponding to non-compactnesses of the reaction zones have been excluded, since they are ultra-high frequency phenomena, and occur at couple orders of magnitude more than those of interest here.
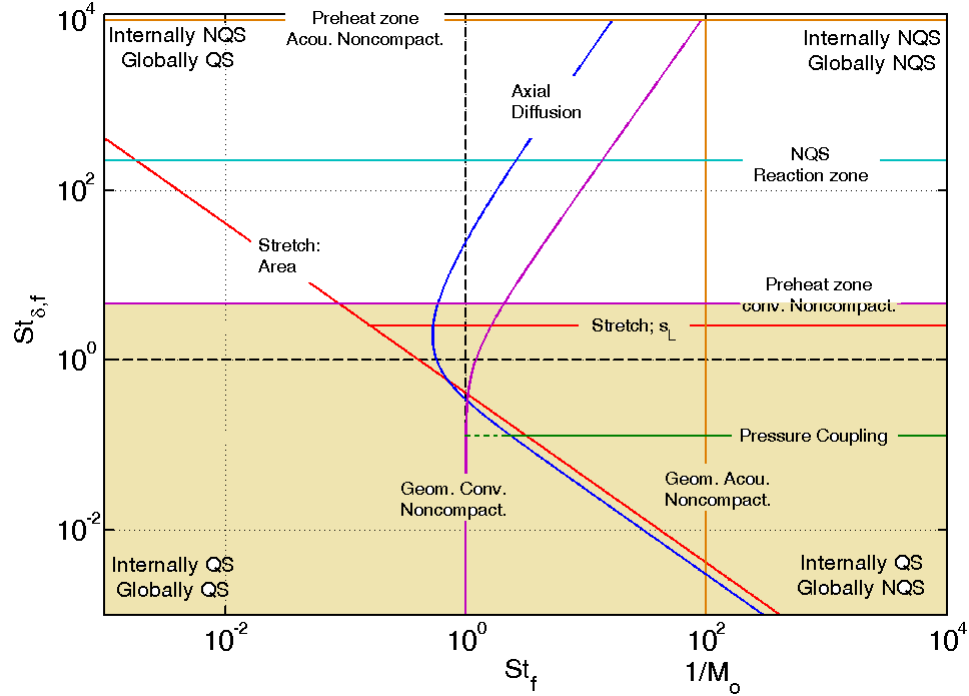
Figure 35 : Summary of heat release response of premixed flames to harmonic disturbances for a premixed methane/air flame with $\phi_o = 0.85$, $\beta = 4$, $M_o = 0.01$, $(\gamma - 1)\theta = 3$.

Although qualitative, the intention is to provide a feel for where these different regimes lie with respect to one another, and what the domain of applicability of the analysis approach in this research work is.

The two dashed lines in Figure 35, $St_{\delta,f} = 1$ and $St_f = 1$ divide the plot into four quadrants, whose "properties" are marked at their respective corners. These four corners show four limits of flame response with respect to global and local/internal non quasi-steadiness. The shaded region in the plot is the extent within which the G-equation approach is valid as-is. This region corresponds to all Strouhal numbers such that the preheat zone of the flame is convectively compact. Even within this limit of preheat zone convective compactness, it may seen that various physical processes assume importance,

141

viz., non quasi-steady processes, flame stretch, axial diffusion effects on convective disturbances and direct influence of the oscillating pressure on flame response. Furthermore, it may be seen that accounting for some of these disturbances would necessarily need accounting for the other. For example, axial diffusion effects and flame stretch effects become significant almost at the same regions in the $St_f - St_{\delta,f}$ space. Similarly, pressure coupled flame response studies need to account for either of these effects simultaneously to be internally consistent.

Finally, it must be noted that although reasonably[13] accurate, the curves representing the onset of various physical phenomena in Figure 35 are sensitive to various parameters such as flame aspect ratio, Mach number, non-dimensional activation energy, etc. The movement of these boundaries with these parameters can be understood with the aid of Figure 35 and Table 4.

---

[13] given the assumptions stated apriori in Chapter 2 and 3, and some assumptions such as tall flames, i.e., $\beta^2 \gg 1$

Chapter 5 : Nonlinear Flame Response to Equivalence Ratio Fluctuations

This chapter considers the nonlinear response of premixed flames to equivalence ratio perturbations. As discussed previously in Chapter 1, while linear flame response models suffice to study the growth rate characteristics of the heat release response characteristics of the flame to upstream disturbances, modification of these characteristics due to nonlinear effects that lead to heat release saturation and limit cycle characteristics necessitate nonlinear analyses.

This chapter studies nonlinear equivalence ratio coupled flame response employing two approaches. *First*, an asymptotic analysis of the single-valued flame front equation, Eq.(3.3), up to third order in the equivalence ratio excitation amplitude, ε, is used to study the lowest order nonlinear correction to the linear flame response calculations performed in Chapter 3. This approach, as shall be described later in this chapter, neglects terms of quartic order and higher in ε. *Second*, fully nonlinear computations of the multi-valued G-equation, Eq.(2.27), are performed. As opposed to the former approach, the latter approach is capable of not only capturing topological changes of the flame front such as multivaluedness, cusp formation and pocket liberation, but also possesses the capability to handle arbitrary excitation amplitudes, and amplitudes at which heat release saturation could possibly occur. However, the former aids in rapidly predicting lower order nonlinear effects, by utilizing analytic expressions, while the latter is more time consuming, although more accurate.

The analyses in this chapter shall focus on the most basic problem of understanding the influence of nonlinearities on a locally quasi-steady, unstretched flame, subjected to equivalence ratio disturbances that do not diffuse axially. In addition to being analytically and numerically tedious, accounting for one or more of the aforementioned neglected effects would also make it difficult to isolate the exclusivity of the influence of nonlinear processes on flame response.

This chapter is structured as follows. Sections 5.1 and 5.2 briefly describe the analytical and numerical formulations specific to the study of nonlinear equivalence ratio coupled flame response respectively. Section 5.3 presents illustrative results for the heat release magnitude and flame transfer functions and its contributions, and also discusses the various physical insights that are specific to the nonlinear response problem that can be obtained from these results. Section 5.5 discusses some additional considerations that have been researched into recently, as an extension of this problem, and their implications on results presented in earlier parts of this thesis and chapter.

5.1. Perturbation Analysis

For the quasi-steady flame, a perturbation analysis is performed to third order in the excitation amplitude ε in order to capture the leading order nonlinear dynamics of the flame analytically. More specifically, we expand the flame front position $\xi(r,t)$ as,

$$\xi(r,t) = \xi_0(r) + \varepsilon \xi_1(r,t) + \varepsilon^2 \xi_2(r,t) + \varepsilon^3 \xi_3(r,t) + O(\varepsilon^4) \quad (5.1)$$

Using the above in Eq.(3.3) and Eq.(3.29) and collecting terms of the same order in ε yields evolution equations for each of the ξ_i's. In order to make analytic progress, we

also assume that the flame thickness is small relative to the burner radius, i.e., $\delta^* \ll 1$.

As discussed in Chapter 3, an equation for the shape of the mean flame may be written as follows.

$$\xi_o\left(r^*\right) = 1 - r^* - O\left(e^{-r^*/\sigma_c^*}\right) \tag{5.2}$$

In the absence of flame stretch effects, the evolution equation for ξ_1 may be written as follows.

$$\frac{\partial \xi_1^*}{\partial t^*} - \alpha \frac{\partial \xi_1^*}{\partial r^*} + s_{L1} \cos(St\,(1 - r^* - t^*)) = 0 \tag{5.3}$$

Here,

$$s_{Lj} = \frac{1}{j!} \frac{\partial^j \left(s_L^{\,d}/s_{Lo}\right)}{\partial \left(\phi/\phi_o\right)^j}\bigg|_{\phi/\phi_o=1} \quad ; \qquad h_{Rj} = \frac{1}{j!} \frac{\partial^j \left(h_R/h_{Ro}\right)}{\partial \left(\phi/\phi_o\right)^j}\bigg|_{\phi/\phi_o=1} \tag{5.4}$$

are respectively the jth order sensitivities of flame speed and heat of reaction of the reactant mixture to fluctuations in equivalence ratio. The evolution equations for the nonlinear corrections to the quasi-steady flame surface location, ξ_2 and ξ_3, in the absence of stretch $(\sigma^*_c=0)$ may be written as:

$$\frac{\partial \xi_2^*}{\partial t^*} - \alpha \frac{\partial \xi_2^*}{\partial r^*} - \alpha s_{L1} \cos(St\,(1 - r^* - t^*))\left(\frac{\partial \xi_1^*}{\partial r^*}\right) + \frac{1}{2}\left(\alpha - \alpha^2\right)\left(\frac{\partial \xi_1^*}{\partial r^*}\right)^2 + s_{L2} \cos^2(St\,(1 - r^* - t^*)) = 0$$

$$\tag{5.5}$$

$$
\left.
\begin{aligned}
&\frac{\partial \xi_3^*}{\partial t^*} - \alpha \frac{\partial \xi_3^*}{\partial r^*} - \alpha \left(s_{L2} \cos^2 \left(St \left(1 - r^* - t^* \right) \right) \frac{\partial \xi_1^*}{\partial r^*} + s_{L1} \cos \left(St \left(1 - r^* - t^* \right) \right) \frac{\partial \xi_2^*}{\partial r^*} \right) \\
&+ \frac{1}{2} \alpha \left(\alpha - \alpha^2 \right) \left(\frac{\partial \xi_1^*}{\partial r^*} \right)^3 + \left(\alpha - \alpha^2 \right) \frac{\partial \xi_1^*}{\partial r^*} \frac{\partial \xi_2^*}{\partial r^*} + \frac{1}{2} s_{L1} \cos \left(St \left(1 - r^* - t^* \right) \right) \left(\alpha - \alpha^2 \right) \left(\frac{\partial \xi_1^*}{\partial r^*} \right)^2 \\
&+ s_{L3} \cos^3 \left(St \left(1 - r^* - t^* \right) \right)
\end{aligned}
\right\} = 0
$$

$$(5.6)$$

The corresponding solutions for ξ_2 and ξ_3 are presented in Appendix G.

The flame surface locations can be used to calculate the instantaneous heat release of the flame, which is given by Eq.(2.30). In the context of flame response to equivalence ratio perturbations, which are assumed to occur at constant density, the heat release can be written as:

$$
\frac{q(t)}{q_o} = \frac{A(t)}{A_o} + \int_{flame} \frac{s_L'}{s_{Lo}} \cdot \frac{dA}{A_o} + \int_{flame} \frac{h_R'}{h_{Ro}} \cdot \frac{dA}{A_o} + \int_{flame} \frac{s_L'}{s_{Lo}} \cdot \frac{h_R'}{h_{Ro}} \cdot \frac{dA}{A_o}
$$

$$(5.7)$$

The corresponding transfer function can now be written as:

$$
F = F_A + F_{s_L - A} + F_{h_R - A} + F_{s_L - h_R - A}
$$

$$(5.8)$$

Note that the last term on the RHS of the above is a contribution that occurs exclusively due to nonlinearities.

5.2. Numerical Formulation

We next discuss the numerical approach adopted to study the nonlinear heat release response of a quasi-steady, unstretched flame. Formally, Eq.(2.27) is a non-conservative Hamilton-Jacobi equation. This equation has the property that the nonlinear term, due to flame propagation normal to itself, results in cusps, or discontinuities in derivative, and

146

possible topological changes (i.e. pocket formation) in the solution. The formation of pockets due to merging of adjacent flame branches was recently emphasized as an important mechanism of nonlinear flame response to fuel/air ratio oscillations by Birbaud et al. [87]. Hence robust numerical schemes that can capture these effects without excessive smearing are required.

The solution domain is discretized using a uniform grid. The initial value for the *G*-field was constructed from the assumed quiescent flame shape. This was done by defining the value of *G* at each grid location to be the signed distance of that location from the quiescent flame surface. The solution at later times was obtained using a low diffusion Courant-Isaacson-Rees scheme with back and forth error compensation and correction (BFECC) [131]. The *G*-field was reset to a distance function after each time step using the re-initialization procedure described by Peng et al. [132].

A considerable reduction in computation time can be obtained by solving Eq.(2.27) in only a narrow band around the actual flame location, rather than in the entire two-dimensional domain. This was achieved by adopting the localization procedure introduced by Peng et al. [132]. This band evolves in time as the flame moves or as pockets form and burnout. These computations were performed using the general purpose level-set program LSGEN2D developed by Shreekrishna et al. [23].

As noted earlier, it is assumed that flame remains attached at the burner lip. This is achieved by setting *G*=0 after every time step of the BFECC scheme at the points corresponding to the burner tube. The velocity of these points is maintained to be identically zero throughout the simulation.

Following Smereka [133], Eq.(2.30) can be written using *G* as:

$$q(t) = \int_\Omega 2\pi r \rho_u s_L h_R \delta(G)|\nabla G| d\Omega \qquad (5.9)$$

where the integration is performed over the whole computational domain described earlier and $\delta(G)$ is the Dirac-delta function. This integral is then evaluated at every sampling time step, using the numerical technique described by Smereka [133]. The grid size ($\Delta r*$) for all the above computations was fixed at 0.001 non-dimensional units in both directions. The non-dimensional time-step was fixed at $0.1\Delta r*$. These were chosen by successive refinement of the grid until the temporal heat release variation changed by less than 5%. Sufficient numbers of grid points were taken along the z-direction to ensure that all pockets formed at the tip of the flame would burn out before being convected out of the grid. The first three contributions to the total heat release on the RHS of Eq.(5.7) were obtained independently using the same techniques described above.

These exact results were used to determine the accuracy of the third order perturbation analysis. The domain in $St_2 - \varepsilon$ space where the magnitude and phase of the transfer function can be determined within specified accuracies E_m and E_ϕ respectively is defined by:

$$St_2(E_m, E_\phi, \varepsilon_0) = \min \left\{ St_2 : \left(\left| \frac{\left| |F_{comp}(St_2)| - |F_{asymp}(St_2)| \right|}{|F_{comp}(St_2)|} \right| \le E_m \right), \left(\left\| \angle F_{comp}(St_2) \right| - \left| \angle F_{asymp}(St_2) \right\| \le E_\phi \right) \right\} \Bigg|_{\varepsilon = \varepsilon_0}$$

$$(5.10)$$
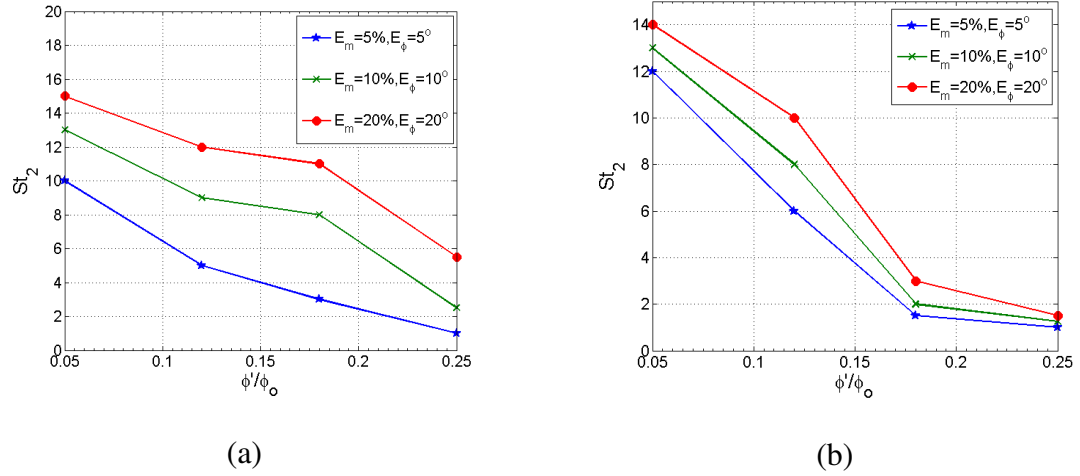
Figure 36 : Domain of applicability of asymptotic analysis (valid to within specified accuracy below line) for a conical flame. (a) ϕ_o= 0.85 (lean) (b) ϕ_o= 1.28 (rich), β = 4.

A similar domain of applicability can plotted for V-flames and is not presented here. The first term within the braces on the RHS gives the value of St_2 for which the error in magnitude prediction from the approximate solution obtained using asymptotics is bounded by E_m. The second term gives the value of St_2 for which the error in phase prediction in the asymptotics solution is bounded by E_ϕ. The sizes of these regions depend on the assumed burning velocity and heat of reaction dependencies on equivalence ratio (e.g., Eqs.(3.89) and (3.90)).

As will be shown later, two mechanisms contribute to nonlinearity in the flame response. The first is due to flame sheet dynamics, as described by the G-equation, see Eq.(2.27). The second is the nonlinearity of the quasi-steady flame speed and heat of reaction dependence upon fuel/air ratio, as plotted qualitatively in Figure 11 and described in the sensitivity derivatives in Eq.(5.4). Figure 36 shows the regions of

specified accuracy of the asymptotic solutions for various values of E_m and E_ϕ for two flames where ϕ_o=0.85 and 1.28. It can be seen that there is an opposing influence of perturbation magnitude and Strouhal number – i.e., the analysis is valid at larger fuel/air perturbation amplitudes at lower Strouhal numbers. This is due to the effects of nonlinearity in the G-equation which grows with amplitude and frequency, see Preetham and Lieuwen [65]. At low Strouhal numbers, the analysis validity is limited by nonlinearities in the quasi-steady flame speed and heat of reaction dependencies upon fuel/air ratio.

5.3. Illustrative Results

5.3.1. Overview of Nonlinearity Mechanisms

As the excitation amplitude/frequency is increased, the higher order contributions to the transfer function become significant. Before presenting explicit results, it is useful to first consider the various mechanisms for nonlinearity. These different mechanisms are summarized in Figure 37, which plots parameter space boundaries where the various physical mechanisms are dominant. These regions were calculated for the lean flame corresponding to ϕ_o=0.85.
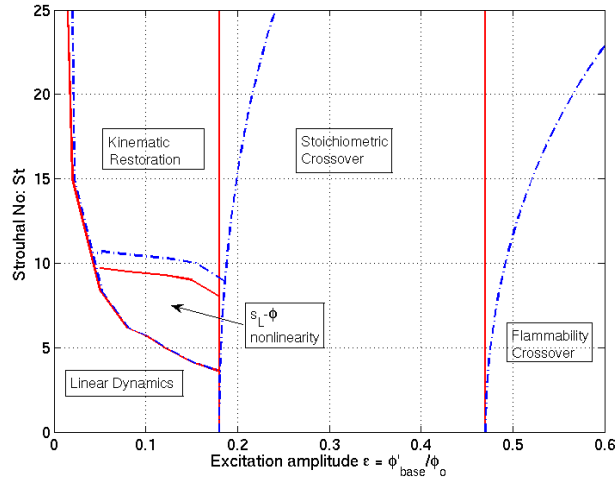
Figure 37: Qualitative map illustrating regimes of dominance of various physical mechanisms at ϕ_o=0.85, St=2π. The solid lines denote quasi-steady boundaries. Dash-dot lines denote approximate non quasi-steady boundaries, obtained by substituting the frequency dependent $\tilde{\phi}$ into the quasi-steady boundary solution.

The region labeled '*Linear dynamics*' in Figure 37 corresponds to the region where nonlinear corrections contribute less than 10% of the transfer function gain, and has the characteristics described in Chapter 3, Sections 3.3.1.6.1 and 3.3.1.6.2.

There are two basic processes causing nonlinearity in the flame response -

(1) nonlinearities in burning area oscillation, due to the nonlinearities in flame kinematics (term 1 in Eq.(5.7)), and

(2) quasi-steady nonlinearities in the s_L-ϕ and h_R-ϕ relationships, as plotted qualitatively in Figure 11 (terms 2-4 in Eq.(5.7)).

There is an additional complication, however, in the fact that the s_L-ϕ nonlinearity has both a direct and indirect influence on the heat release response through term 2 and term 1 in Eq.(5.7), respectively. This indirect mechanism dominates the heat release nonlinearities in the 's_L-ϕ *nonlinearity*' region in Figure 37. Physically, its origin may be explained as follows. Flame surface motion is induced by flame speed fluctuations. The resulting area fluctuations associated with this motion exhibit nonlinearity due to the

intrinsically nonlinear dynamics of flame propagation normal to itself. This latter 's_L-ϕ nonlinearity' dominates in the indicated region of the chart, due to the nonlinear dependence of the local propagation velocity upon fuel/air ratio. This induces nonlinearities in the burning area response.

The propagation of the flame normal to itself, as remarked above is the dominant source of nonlinearity in flame area and overall heat release response in the region labeled '*Kinematic Restoration*' [134, 135] in Figure 37. Larger amplitude fluctuations in flame position slope cause kinematic nonlinearities to correspondingly grow in significance. As *St* is increased, Eq.(3.56) shows that the wavelength of the induced wrinkles on the flame surface is $O(1/St)$. Thus, at high frequencies, propagation of the flame surface normal to itself results in the rapid destruction of these wrinkles [64] causing the fluctuating flame surface area to saturate. Kinematic restoration becomes important at higher frequencies merely because higher frequencies provide short length scale wrinkles which can be destroyed rapidly.

The boundary between these two regions indicated in the figure was determined from the perturbation analysis by artificially setting the higher order flame speed sensitivities (e.g., s_{L2}) to zero. The only source of nonlinearity is then due to kinematic restoration. The indicated boundary was then determined from the points where the nonlinear flame contributions in the cases with and without the higher order s_L sensitivity were within 10% of each other.

We next consider the regime labeled "*Stoichiometric cross-over mechanism*". This nonlinearity is completely due to the second source of nonlinearity noted above, i.e. the s_L-ϕ and h_R-ϕ nonlinearities. However, in this region, this mechanism dominates for

all Strouhal numbers and is due to the drastic change in s_L and h_R characteristics on the lean and rich side of stoichiometric. As described in the introduction section, the equivalence ratio space can be divided into three distinct regions (see Figure 11). For large excitation amplitudes, the local equivalence ratio can instantaneously cross over from region I to region II or region I to region III and vice versa. The trend in the variation of s_L and h_R qualitatively changes when this cross over occurs. For the sake of illustration, consider an instantaneous variation of ϕ over an excitation cycle shown in Figure 38.
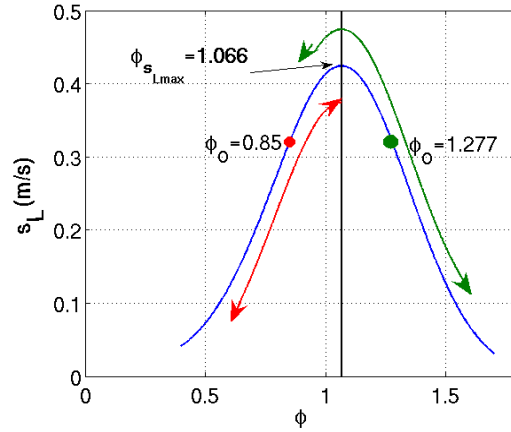
Figure 38: Variation of flame speed with equivalence ratio. The vertical line marks the equivalence ratio for maximum s_L. The arrows show the extent of variation of s_L over one excitation cycle at $\varepsilon =$ 0.25 in each case.

The instantaneous value of s_L falls with decreasing ϕ over a portion of the excitation cycle in the rich case, as opposed to rising further. Hence, if for some instantaneous oscillation amplitude ϕ around some mean equivalence ratio ϕ_o, if $\left| \phi - \phi_o \right| > \left| \phi_{s_L, \max} - \phi_o \right|$, the trend of s_L variation over one excitation cycle changes and causes a very abrupt saturation of the mass burning rate contribution to the total heat release, the second term in Eq.(5.7). Similarly, a sufficiently high excitation amplitude

can result in significant nonlinearities in the heat of reaction contributions in Eq.(5.7) if $|\phi - \phi_o| > |1 - \phi_o|$. The fact that differentiates this mechanism from the kinematic mechanisms is that even if the flame area oscillation is linear, these alone can cause strong nonlinearities in the net heat release. Fortunately, determining the excitation amplitude ε, when this mechanism becomes significant is very straightforward, as it is simply the minimum of the absolute difference in value between the mean equivalence ratio and the stoichiometry where the s_L and h_R characteristics change abruptly; *i.e.*,

$$\varepsilon_{stoich} = \frac{1}{\phi_o} \min\left\{ \left|1 - \phi_o\right|, \left|\phi_{s_{L\,max}} - \phi_o\right| \right\} \qquad (5.11)$$

Henceforth this second non-linearity mechanism will be referred to as the "*cross-over*" mechanism. Note that, in a quasi-steady sense, this mechanism is controlled purely by the oscillation amplitude. Hence the boundary of the crossover region in Figure 37, where this mechanism is dominant has no dependence on St_2. However, the fact that the flame speed sensitivity to fuel/air ratio oscillations at high frequencies progressively diminishes due to non quasi-steady effects, implies that, in reality, this boundary "bends" in St space, as illustrated in the figure.

The final regime, labeled '*Flammability cross-over*", is a special case of the "*cross-over*" mechanism. For sufficiently high amplitudes, the equivalence ratio can instantaneously assume values very close to or beyond the flammability limits of the fuel. This could lead to flame extinction and reignition phenomena over a part of the cycle, and presumably lead to burning area saturation. However, a complete understanding of this region requires solution of the conservation equations with finite rate chemistry, and is not performed as a part of the current work. Moreover, due to spatial variation in the

154

equivalence ratio, "holes" in the flame can advance or retreat with their own associated edge flame dynamics [136]. Recent findings related to this mechanism are summarized later in this chapter.

Define "*cross-over*" amplitude, as the minimum amplitude at which some form of cross-over occurs:

$$\varepsilon_{crossover} = \frac{1}{\phi_o} \min \left(\varepsilon_{stoich}, \underbrace{\phi_o - \phi_{fl,lean}, \phi_{fl,rich} - \phi_o}_{\varepsilon_{fl} = \text{flammability crossover amplitude}} \right) \tag{5.12}$$

where $\phi_{fl,lean}$ and $\phi_{fl,rich}$ denote the dynamic lean and rich flammability limits, see Sankaran and Im [129]. The mean equivalence ratio determines the type of cross-over that is first encountered. For example, a CH_4/Air mixture at a mean equivalence ratio of 0.85 will probably encounter the stoichiometric cross over mechanism prior to the lean flammability limit mechanism ($\varepsilon_{stoich} = 0.18, \varepsilon_{fl} = 0.41$, at STP). However, for a mixture with a mean equivalence ratio of 0.6, flammability cross-over probably occurs first ($\varepsilon_{stoich} = 0.72, \varepsilon_{fl} = 0.09$).

5.3.2. Relative Roles of Different Nonlinearity Mechanisms from Asymptotic Analysis

The transfer function expressions obtained from the asymptotic analysis outlined in the previous section can be used to generate nonlinearity maps such as in Figure 37. Additionally, the relative contribution of these processes to the lowest order nonlinear correction to the flame transfer function can be studied over a range of frequencies. To

see how this can be done, consider, for instance, the expression for the nonlinear

contribution to F_A, which may be expressed generically as follows:

$$F_A = F_{A,o} + \varepsilon^2 F_{A,2} + O(\varepsilon^4) \tag{5.13}$$

where the nonlinear correction $F_{A,2}$ can itself be expressed as:

$$F_{A,2} = \left(f_{A,s_{L1}^3} \right) s_{L1}^3 + \left(f_{A,s_{L1}s_{L2}} \right) s_{L1}s_{L2} + \left(f_{A,s_{L3}} \right) s_{L3} \tag{5.14}$$

The terms in parentheses on the RHS of Eq.(5.14) depend only on flame geometry and

Strouhal number, and are independent of amplitude and flame speed sensitivities. From

the view point of physical understanding, Eq. (5.14) isolates the contributions of two

nonlinear mechanisms discussed earlier, viz., $s_L - \phi$ nonlinearity and kinematic

restoration. In fact, even without the nonlinear $s_L - \phi$ dependence, kinematic restoration

arises due to the normal propagation term in the G-equation, viz., RHS of Eq.(2.27). This

process is captured by the s_{L1}^3 term in Eq. (5.14), which is nonlinearity arising *purely*

because of kinematic restoration. Similarly, the s_{L3} arises *purely* due to the nonlinear

dependence of s_L on ϕ, such that even if the kinematic restoration term was linearized

(which actually means that kinematic restoration is not accounted for at all), this term

would still lead to nonlinearity in flame front fluctuations because of the s_L / s_{Lo} term that

precedes the radical term in Eq.(3.3). Finally, the contribution $s_{L1}s_{L2}$ is a composite term

arising due to $s_L - \phi$ and kinematic restoration nonlinearities. The coefficients of these

sensitivity terms, i.e., the $f_{A,(\ )}$ terms, now weight the contributions from each of these

sensitivity terms (and hence nonlinear processes). Hence, a study of the Strouhal number

variation of the $f_{A,(\ )}$ terms provides insight into the Strouhal number ranges in which one term dominates upon the other in its contribution to the overall area response.

To illustrate, consider the contributions of these processes to $F_{A,2}$. Figures 38-39 plot the fractional contribution, $f_{A,i}\big/\sum\limits_{i} f_{A,i}$, for each of the processes, $i = s_{L1}{}^3, s_{L1}s_{L2}, s_{L3}$.

Figure 39 : Fractional contributions of different nonlinearities, $f_{A,i}\big/\sum\limits_{i} f_{A,i}$, for each of the processes, $i = s_{L1}{}^3, s_{L1}s_{L2}, s_{L3}$, to $F_{A,2}$ for a lean, $\phi_o = 0.85$ flame with $\beta = 4$ for an axisymmetric (a) conical flame, (b) V-flame.

Prior to discussing these results, it is important to realize that these fractional contributions are amplitude independent. This however does not mean that these results are interpretable for any excitation amplitude, because, the higher order asymptotic analysis itself has a domain of validity as discussed in Figure 36. Furthermore, a part of the Strouhal number axis for each of these results will correspond to the region in $St - \varepsilon$ space where linear dynamics are prevalent, see Figure 37. These results have to be

interpreted by commencing from the Strouhal number where nonlinear processes begin to gain significance. Finally, these fractional contributions can have magnitudes exceeding unity, since the denominator of the fraction is a phasor sum of the three nonlinearity components.

Figure 39 plots the various nonlinearity contributions to the area transfer function for a lean conical and V-flame. Note that these are not contributions to the total transfer functions and, hence, have to be interpreted carefully. It can be seen that at low Strouhal numbers, for both the lean and the rich flames, both processes, i.e., exclusive $s_L - \phi$ nonlinearity and exclusive kinematic restoration effects, are equally important in contributing to burning area response. For conical flames, as Strouhal number increases, there is a range of Strouhal numbers over which $s_L - \phi$ nonlinearities possess larger gains than kinematic nonlinearities, but this range is small. This range seems to be absent for V-flames. As Strouhal number increases further, the smaller length scale of the wrinkles make it easier for kinematic restoration effects to destroy, and hence kinematic restoration almost exclusively controls high Strouhal number nonlinear flame response.

The phase characteristics of these various contributions are interesting to observe, especially in the low Strouhal number limit, where the exclusive contributions due to $s_L - \phi$ nonlinearity and kinematic restoration are out of phase. At higher Strouhal numbers, they tend to come in phase with each other though.
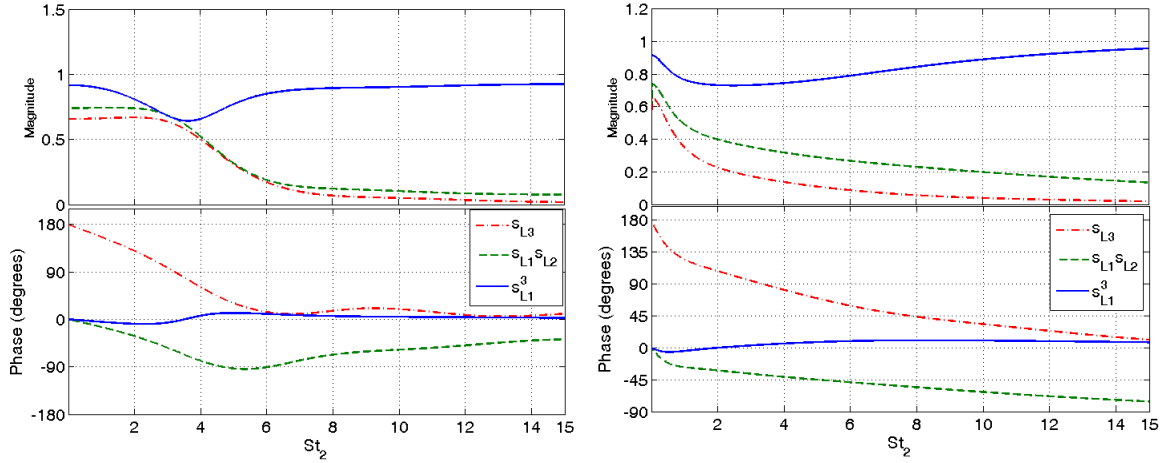
Figure 40 : Fractional contributions of different nonlinearities, $f_{A,i}i \big/ \sum_i f_{A,i}i$, **for each of the processes,** $i = s_{L1}^{\,3}, s_{L1}s_{L2}, s_{L3}$, **to** $F_{A,2}$ **for a rich,** $\phi_o = 1.277$ **flame with** $\beta = 4$ **for an axisymmetric (a) conical flame, (b) V-flame**

The discussion presented earlier for a lean flame is applicable even to the rich flame, owing to the fact that between the lean and rich flames, the major change to the total transfer function arises due to the absence of the heat of reaction contribution, while the area contribution continues to be a dominant mechanism for either case. It can be noted though, from Figure 40, that the fractional nonlinearity contributions to the area response for both the conical and V-flames for rich flames always have magnitudes lesser than unity. Interestingly, a node can be seen in the response exclusively due to kinematic nonlinearity, the s_{L3} term, in the rich response, which was apriori absent in the lean case.

The methodology used previously to understand the relative dominance of the two nonlinear processes to the burning area response can very well be extended to the total nonlinear response of the flame. In general, the total response of the flame may be written as:

$$F = F_o + \varepsilon^2 F_2 + O\left(\varepsilon^4\right) \tag{5.15}$$

Again, the lowest order nonlinear correction F_2, can itself be expressed as:

$$F_2 = \begin{cases} \left(f_{s_{L1}^3}\right)s_{L1}^3 + \left(f_{s_{L1}s_{L2}}\right)s_{L1}s_{L2} + \left(f_{s_{L3}}\right)s_{L3} \\ + \left(f_{h_{R1}s_{L1}^2}\right)h_{R1}s_{L1}^2 + \left(f_{h_{R1}s_{L2}}\right)h_{R1}s_{L2} \\ + \left(f_{h_{R2}s_{L1}}\right)h_{R2}s_{L1} + \left(f_{h_{R3}}\right)h_{R3} \end{cases} \tag{5.16}$$

These first row of contributions, $f_{(\ )}$, in the RHS of Eq.(5.16) arises due to $s_L - \phi$ nonlinearities and kinematic restoration, and affect the responses F_A and $F_{s_L - A}$. The second row of contributions arises again due to $s_L - \phi$ nonlinearities and kinematic restoration, and affect the responses $F_{h_R - A}$ and $F_{s_L - h_R - A}$. The third row of contributions arise exclusively due to $h_R - \phi$ nonlinearities. The first term affects the responses $F_{h_R - A}$ and $F_{s_L - h_R - A}$, while the second term affects only the $F_{h_R - A}$ term.

As an illustration, we next consider the contributions of $s_{L1}^3, s_{L1}s_{L2}, s_{L3}$ to total nonlinear flame response, F_2. Figures 40-42 plots the fractional contribution, $f_i i / F_2$, for each of the processes, $i = s_{L1}^3, s_{L1}s_{L2}, s_{L3}$. As observed earlier, these fractional contributions can exceed unity.
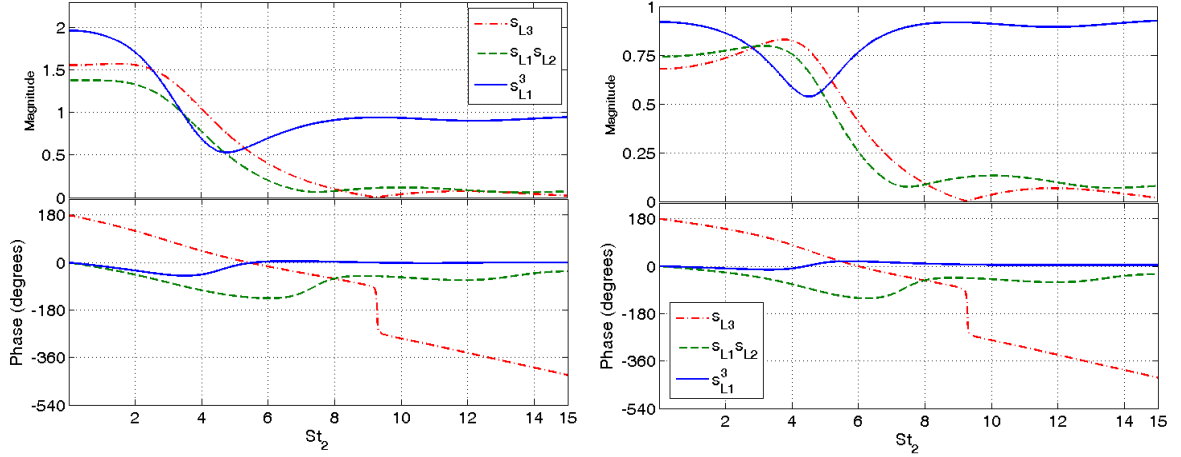
Figure 41 : Fractional contributions of different nonlinearities, $f_i i/F_2$, for each of the processes, $i = s_{L1}{}^3, s_{L1}s_{L2}, s_{L3}$, to F_2 , for an axisymmetric conical flame with $\beta = 4$. (a) $\phi_o = 0.85$ (b) $\phi_o = 1.277$

We first consider the relative contributions of the nonlinear terms that describe the exclusive $s_L - \phi$ and kinematic restoration processes for axisymmetric conical lean and rich flames, as shown in Figure 42. Unlike in the earlier case of contributions to the area response, there is now a distinct range of Strouhal numbers for which the $s_L - \phi$ nonlinearity dominates the kinematic restoration processes, which appears to be about the same for both the lean and rich cases, $St_2 \in (2.5,6)$ approximately. For about $St_2 > 6$, the kinematic restoration process seems to exclusively control overall flame response. This is again because of the ease with which normal propagation of the flame to itself can destroy small wavelength wrinkles that occur at large Strouhal numbers. It is also interesting to observe the occurrence of the node in the s_{L3} contribution – this actually occurs because of the interference of boundary and locally generated wave solutions.
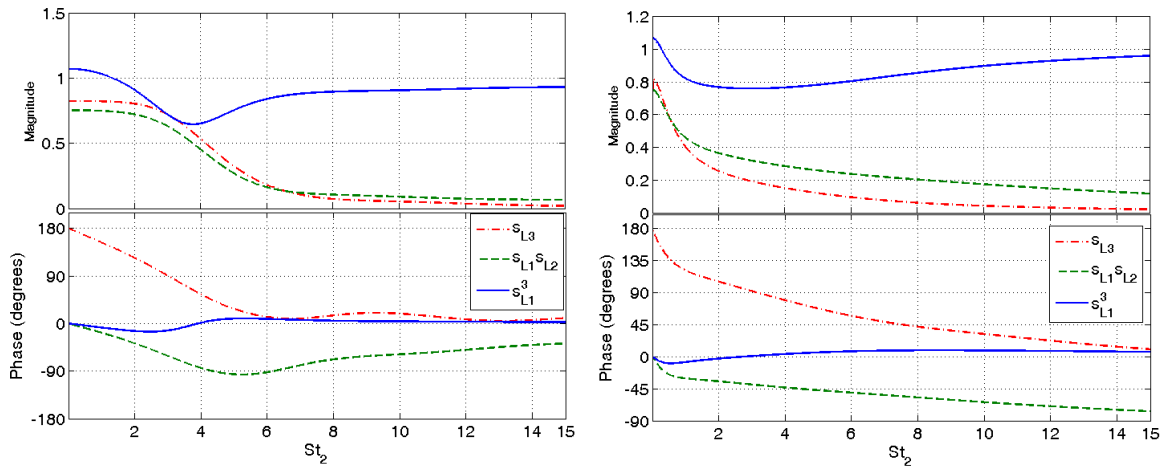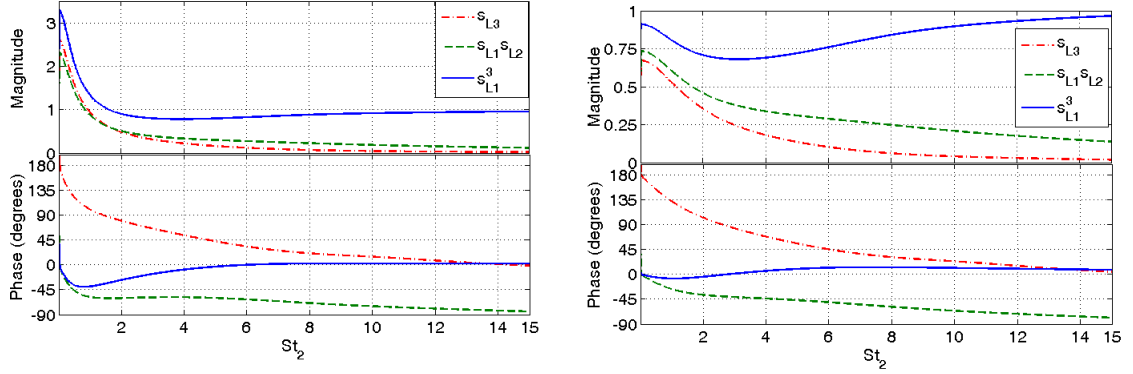
Figure 42 : Fractional contributions of different nonlinearities, $f_i i / F_2$, for each of the processes, $i = s_{L1}{}^3, s_{L1}s_{L2}, s_{L3}$, to F_2, for an axisymmetric V-flame with $\beta = 4$. (a) $\phi_o = 0.85$ (b) $\phi_o = 1.277$

The same exercise may be carried out for an axisymmetric V-flame. Interestingly, here, kinematic restoration dominates over all Strouhal numbers.

Though not presented here, a similar assessment may be performed for $h_R - \phi$ nonlinearities and that for nonlinearities arising from composite terms such as $h_{R1} s_{L1}{}^2$. This will enable in evaluating the relative roles of these various nonlinearity mechanisms to the overall flame response.

While the analysis presented hitherto is amplitude independent, the comparative contributions of various nonlinearity routes to the total transfer function (note - not total nonlinear correction, F_2, as considered earlier) is actually a three dimensional map with the excitation amplitude forming the third axis. With this, contours may be drawn for regions in the $St_2 - \varepsilon$ space, by specifying criteria which denote dominance of one nonlinearity mechanism over the other. This, in fact, leads to Figure 37.

We finally conclude this discussion by considering the behavior of the transfer function in the low St_2 limit for the cases where the asymptotic analyses detailed in the previous sections are always valid, irrespective of excitation amplitude (see Figure 37). We have the following results for the terms on the RHS of Eq.(5.8).

$$\lim_{St_2 \to 0} F_A = -\lim_{St_2 \to 0} F_{s_L - A} = -s_{L1} - \frac{3}{4}\varepsilon^2 \left(s_{L1}^{3} - 2s_{L1}s_{L2} + s_{L3} \right) \tag{5.17}$$

$$\lim_{St_2 \to 0} F_{s_L - h_R - A} = \frac{3}{4}\varepsilon^2 \left(h_{R2}s_{L1} - h_{R1}s_{L1}^{2} + h_{R1}s_{L2} \right) \tag{5.18}$$

$$\lim_{St_2 \to 0} F_{h_R - A} = h_{R1} + \frac{3}{4}\varepsilon^2 \left(h_{R3} - h_{R2}s_{L1} + h_{R1}s_{L1}^{2} - h_{R1}s_{L2} \right) \tag{5.19}$$

From Eq.(5.17), it can be seen that in the low St_2 limit, the contributions due to the burning area fluctuations and burning rate oscillations have the same absolute magnitude, but opposite signs. This means that the contributions in this limit are exactly out of phase and cancel each other. Physically, this may be reasoned as follows. Two lean flames with the same fuel flow rate but different air-flow rates will have the same steady heat release rate. Local variations in mass burning rate due to slow time scale perturbations in s_L must be balanced by the oscillations in the net burning area. As such, the low frequency limit for the transfer function is given by:

$$\lim_{St_2 \to 0} F = h_{R1} + \frac{3}{4}\varepsilon^2 h_{R3} \tag{5.20}$$

From this, it follows that in the limit of $St_2 \to 0$, the net flame response is purely dependent on the sensitivities of the heat of reaction, h_{Rj} (see Eq.(5.4)), and controlled by the $F_{h_R - A}$ term.

5.3.3. Numerical Results

With the preceding material as background, we next present results obtained from numerical computations. Figure 43(a) and Figure 43(b) plot the variation of the magnitude and phase of the total heat release transfer function with increasing excitation amplitudes for the lean and the rich flames, respectively.

(a)

(b)
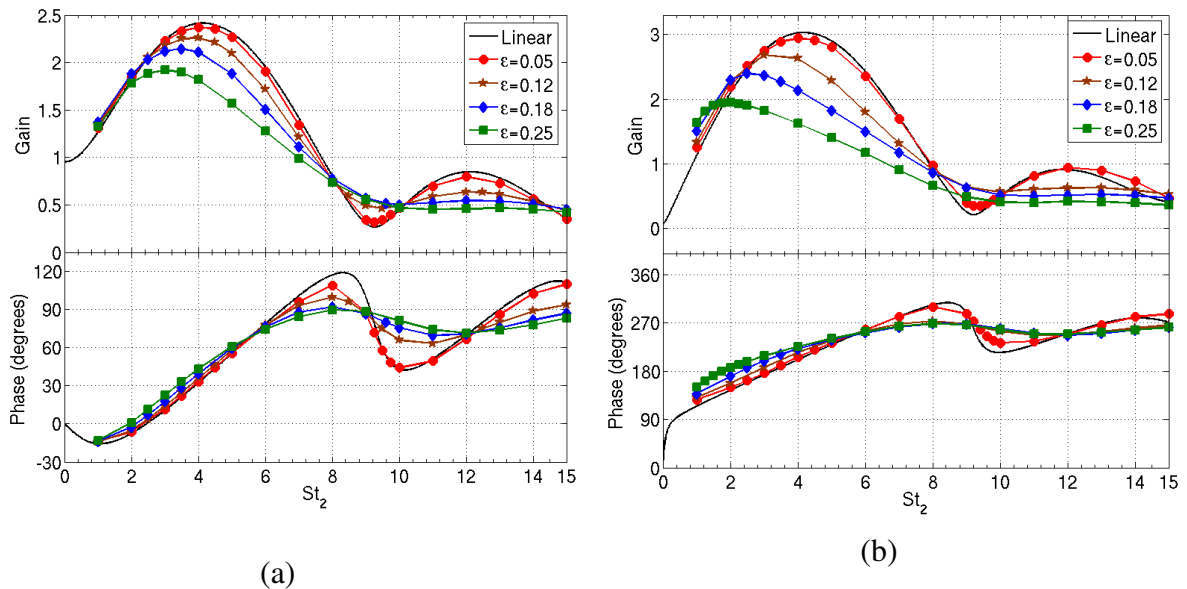
Figure 43 : Variation of the gain and phase of the non-linear transfer function, F, with Strouhal number, (a) $\phi_o = 0.85$ (lean) (b) $\phi_o = 1.28$ (rich), $\beta = 4$.
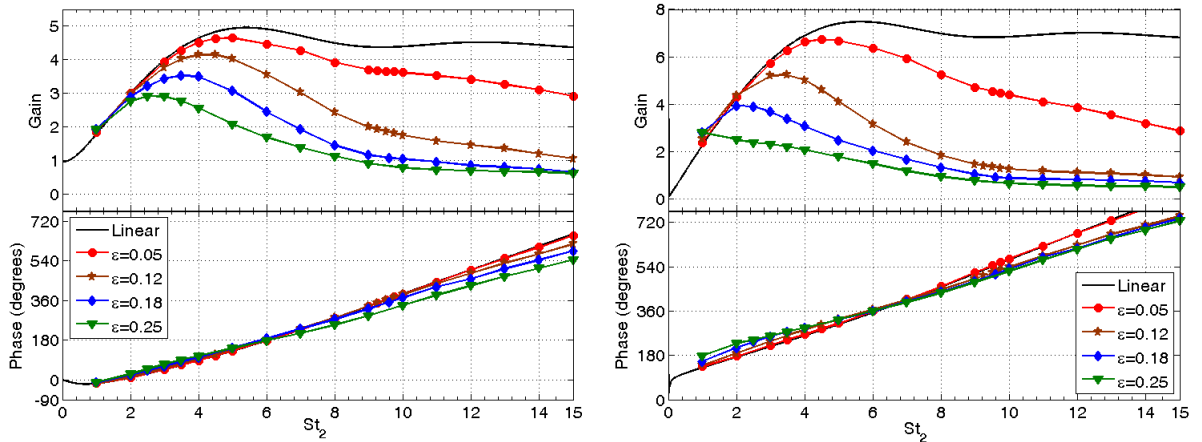
Figure 44 : Variation of the gain and phase of the nonlinear transfer function for an axisymmetric V-flame, *F*, with Strouhal number, (a) $\phi_o = 0.85$ (lean) (b) $\phi_o = 1.28$ (rich), $\beta = 4$.

Notice first that the transfer function response for all excitation amplitudes tends toward the linear value in both the lean and the rich flame cases as $St_2 \rightarrow 0$. This is due to the low frequency behavior of the transfer function explained in the previous section. With increasing St_2, the transfer function begins to deviate significantly from the linear value. As such the slight deviation from the linear value at low amplitudes with increasing St_2 can be ascribed to the manifestation of s_L-ϕ nonlinearities in both cases. For a chosen amplitude, with increasing St_2, the role of kinematic restoration as a means to destroy flame surface area and cause heat release saturation becomes increasingly significant. As the excitation amplitude is increased beyond $\varepsilon = 0.18$ in the lean case and $\varepsilon = 0.15$ in the rich case, the stoichiometric crossover mechanism becomes dominant.

It is also important to note the distinction in character of the transfer functions between conical flames and V-flames. For both lean and rich cases, it may be seen from Figure 44 that the total transfer function does not show any oscillatory behavior for low amplitudes. This is because of the exclusive contribution of burning area response to the overall V-flame response, due to the same reasons that have been discussed at length in

the context of linear V-flame response in Chapter 3. As the amplitude of excitation increases, in the case of V-flames, kinematic restoration effects (which dominate over s_L-ϕ nonlinearities) destroy flame surface area, leading to reduction in response magnitude. The stoichiometric crossover mechanism becomes dominant at the same amplitudes as in the conical case. Hence, at large amplitudes and large Strouhal numbers, kinematic restoration, along with stoichiometric crossover leads to flame transfer function saturation, for both lean and rich cases.

Next, it is also interesting to observe that the V-flame transfer function phases show a mostly monotonic linear variation with Strouhal number, as opposed to the non-monotonic trends seen for a conical flame. The exception occurs at very low Strouhal numbers where some non-monotonic behavior is seen. This is again an artifact of the response of the flame being controlled by only the burning area response mechanism over most of the Strouhal number range, but at very low Strouhal numbers, where the heat of reaction routes become important.

We now examine the converse scenario, i.e., the variation of heat release response with excitation amplitude at a fixed value of $St=2\pi$. Figure 45(a) and Figure 45(b) plot the variation of the magnitude of the heat release response (not its transfer function, as in Figure 43) with increasing excitation amplitude for the lean and rich cases respectively.
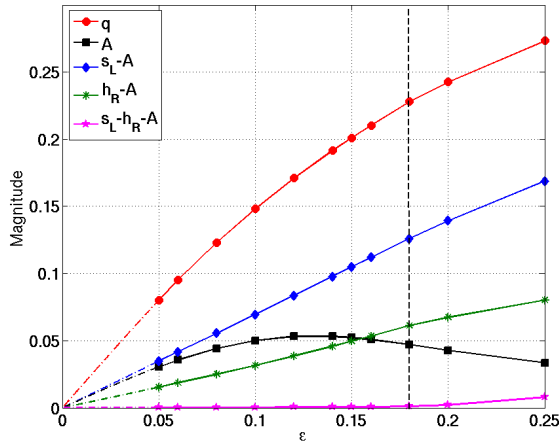
(a)
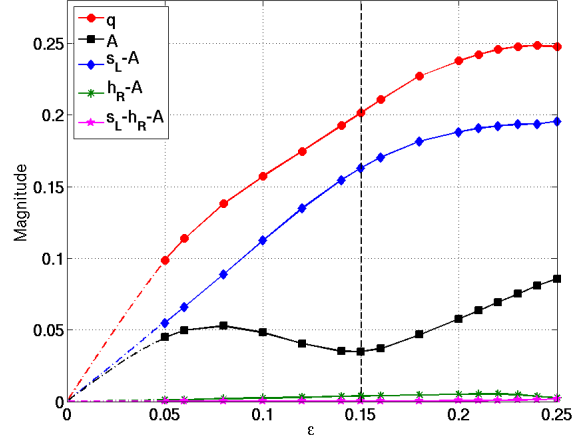
(b)

Figure 45: Magnitude of individual contributions to the total heat release of an axisymmetric conical flame, *q'*, (a) ϕ_o = 0.85 (lean) (b) ϕ_o = 1.28 (rich), β = 4, for *St₂=6.68 (St=2π)*. The vertical dashed black line marks the amplitude at which the instantaneous equivalence ratio begins to cross over into the rich/lean region over a part of the excitation cycle. The dash-dot interpolations to zero amplitude are obtained using corresponding expressions from asymptotic analysis .
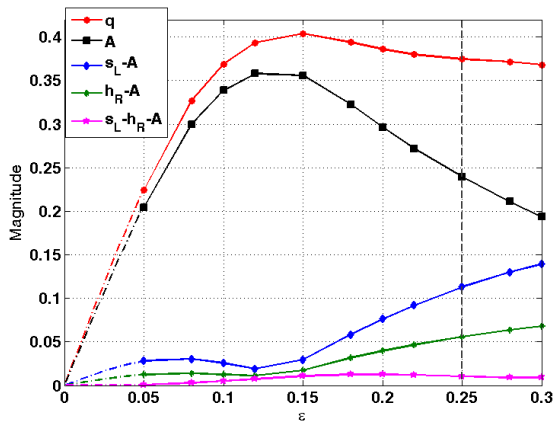
(a)
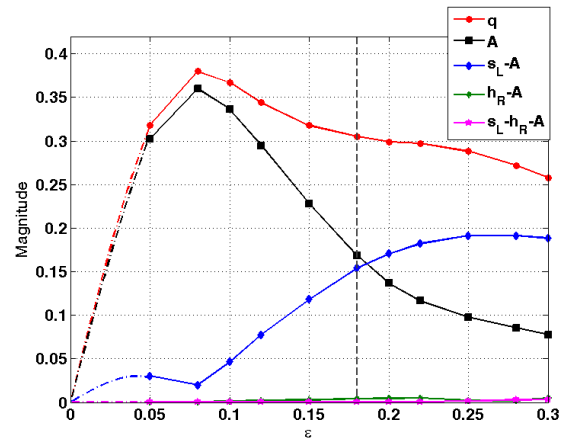
(b)

Figure 46: Magnitude of individual contributions to the total heat release, *q'*, for an axisymmetric V-flame. (a) ϕ_o = 0.85 (lean) (b) ϕ_o = 1.28 (rich), β = 4, for *St₂=6.68 (St=2π)*. The vertical dashed black line marks the amplitude at which the instantaneous equivalence ratio begins to cross over into the rich/lean region over a part of the excitation cycle. The dash-dot interpolations to zero amplitude are obtained using corresponding expressions from asymptotic analysis .

The dashed vertical lines on both show the amplitude where the stoichiometric cross-over mechanism is initiated. Overlaid are the magnitudes of the individual constituent components (see Eq.(5.7)) of the total heat release response at the excitation frequency in each case. We first attempt to understand the characteristics of the heat release magnitudes for a conical flame, and then extrapolate this understanding to that of a V-flame.

First, notice that the amplitude of the burning area oscillation, A, varies nonlinearly and non-monotonically, even with excitation amplitudes that are smaller than $\varepsilon_{crossover}$. This is a counterintuitive result as it shows that the absolute magnitude (i.e., not the relative rate of increase) of A fluctuations *decreases*, with increasing ε. This result is due to the spatially integrated character of the flame area.

(a)　　　　　　　　　　　　　　　　　(b)
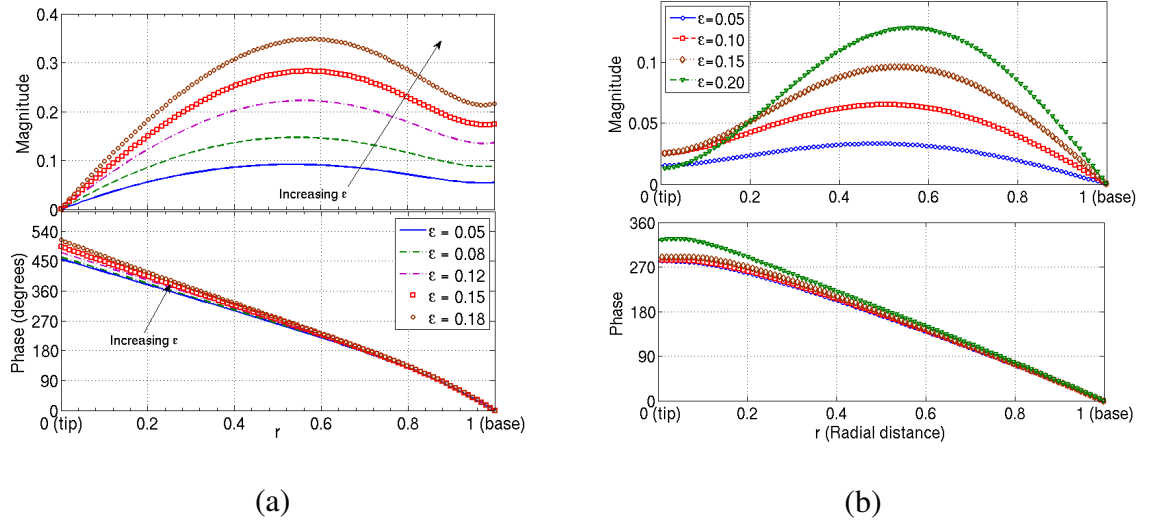
Figure 47 : Local burning area fluctuation magnitudes of a lean conical flame : $\phi_o = 0.85$ (lean), $\beta = 4$, $St_2 = 6.68$ ($St = 2\pi$). (a) Variation of normalized local burning area, $\partial\left(A\left(r,t\right)/A_o\right)/\partial r^*$ with radial location (b) Variation of integrated burning area, A, with radial location.

To better understand this, consider Figure 47(a), which plots the spatial dependence of the local flame area fluctuation magnitude (defined as $\partial\left(A\left(r^*,t^*\right)\big/A_o\right)/\partial r^*$).

It can be seen from Figure 47(a) that the local flame area fluctuation magnitude exhibits non-monotonic spatial dependence, but monotonically increases with ε at each position. Additionally, different spatial locations contribute differently in terms of phase relative to the flame base. The total magnitude of the area fluctuations is merely the magnitude of the integral of the local flame area fluctuations over the flame surface area. Mathematically, this amounts to a phasor addition. This phasor addition leads to a complex non-monotonic dependence in the burning area, with the flame locations closer to the tip acting to effectively reduce contributions from the parts of the flame closer to the base. This can be understood by considering Figure 47(b), which plots the spatially *integrated* area fluctuation magnitudes from the base of the flame to a given radial location. As such, the values at *r=0*, the flame tip, indicate the magnitudes of the burning area fluctuations integrated over the entire flame. At a given spatial location near the flame base, these curves monotonically increase with perturbation amplitude. They deviate from each other near the flame tip, however, due to cancellation associated with the amplitude dependent phase, leading to a net reduction in the total flame area fluctuation magnitude at higher amplitudes of excitation.

Next, the trends of the 's_L-A' contributions to the total heat release occur because of the various mechanisms that lead to area saturation. In the lean case, nonlinearities are dominated by kinematic restoration, as the crossover mechanism sets in at a larger amplitude than for rich flames, where kinematic restoration and crossover are both important at lower excitation amplitudes. Hence, the 's_L-A' contribution saturates for rich

flames. Although not reproduced here, a similar saturation is seen for lean flames at higher amplitudes at which cross-over occurs from the lean to the rich side. However, flammability cross-over mechanism might become a potential competitor at such high amplitudes.

Next, the 'h_R-A' and 's_L- h_R -A' contribution to the heat release magnitude is negligible for rich flames since h_R is fairly constant on the rich side and has negligible sensitivity to equivalence ratio fluctuations.

In the context of V-flames (Figure 46), at low amplitudes, most of the contribution to the total heat release arises out of burning area fluctuations, which are due to flame geometric reasons discussed in Chapter 3. As the amplitude increases, however, the 's_L-A' and 'h_R-A' routes become important. The competition between kinematic restoration effects and s_L-ϕ nonlinearity effects begins to reduce flame area and increase the contribution of the 's_L-A' route. As discussed previously, nonlinearities lead to 's_L-A' to saturate beyond the crossover amplitude; this is very clearly seen in the rich case. The overall heat release contribution also tends to saturate because of these competing nonlinearity mechanisms.

At even larger excitation amplitudes, there is a competition between three processes – crossover across the flame speed maximum, crossover across the flammability limits of the fuel mixture and kinematic restoration. The dynamics in such a situation needs detailed chemistry considerations and is not studied in this work.

5.4. Effect of Preheat and Pressure on Flame Response Characteristics

Consider next, the influence of reactant preheat temperature and pressure on flame response characteristics. This study provides an idea of how the understanding of flame response at atmospheric conditions as dealt with in the previous chapters can be extended to realistic gas turbine combustor operating conditions and flame configurations. For the purpose of this study, an axisymmetric V-flame at a mean equivalence ratio of 0.62 is considered. We first consider the effect of preheating reactants at constant pressure. Figure 48 plots the heat release transfer function characteristics for an axisymmetric, lean CH_4/air flame at atmospheric pressure and varying reactant temperature.
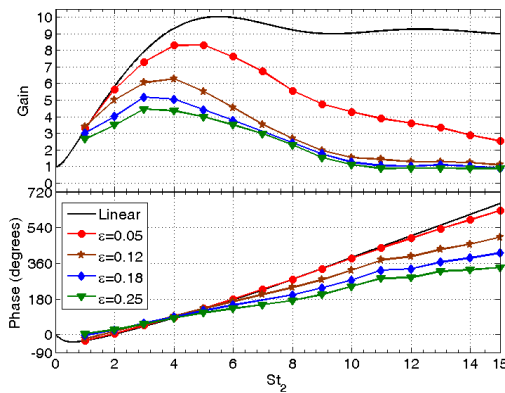
(a)
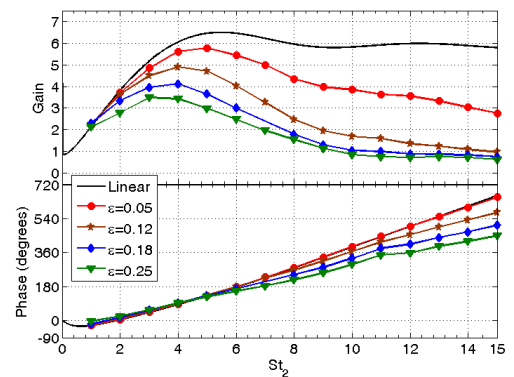
(b)
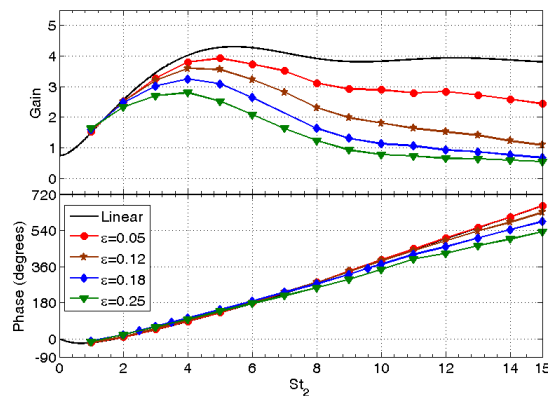
(c)

Figure 48 : Flame transfer function characteristics for an axisymmetric CH₄/Air V-flame ($\beta = 4$) at $\phi_o = 0.62$, with reactants at (a) 300 K, 1 atm, (b) 500 K, 1 atm, and (c) 700 K, 1 atm.

As may be seen from Figure 48, as the preheat temperature increases, the maximum value of the overall gain decreases. Also, the departure of the nonlinear gain from linear values occurs at higher Strouhal numbers with preheat, indicating a reduction in the nonlinear contribution with increasing preheat. This may also be seen from the phase plots, which although mostly invariant with reactant temperature for low Strouhal numbers, shows lesser departure from the linear phase variation with increasing preheat. These observations can be explained by the fact that at a given equivalence ratio, linear flame speed sensitivity decreases with increasing preheat temperature. Next, note that for a chosen high Strouhal number, say, $St_2 = 10$, flame transfer function saturation occurs at much higher amplitudes at higher preheat temperatures. This is again indicative of decreasing nonlinear character with increasing preheat.

We next consider the effect of reactant pressure on flame response as plotted in Figure 49 . It may be seen that as the reactant pressure increases at a fixed reactant pressure, the overall gain begins to attain higher values at a given Strouhal number. However, when the pressure changes by a factor of 15 (from 1 atm to 15 atm), the maximum gain changes by about a factor of 2.5 for $\varepsilon = 0.05$, and by about a factor of 1.3 for $\varepsilon = 0.25$. This shows that the influence of reactant pressure, although significant, reduces with increasing excitation amplitude.
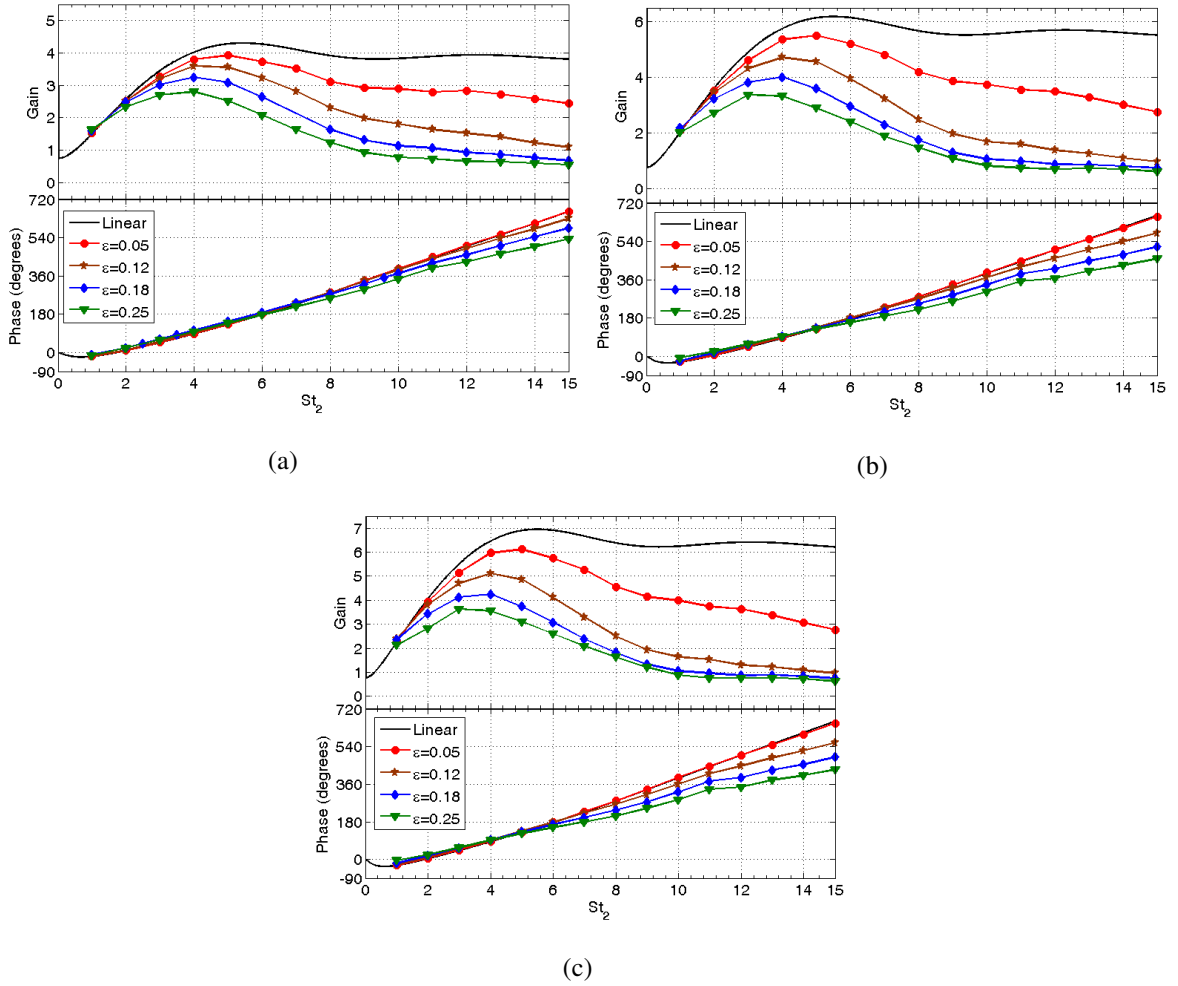
Figure 49 : Flame transfer function characteristics for an axisymmetric CH₄/Air V-flame ($\beta = 4$) at $\phi_o = 0.62$, with reactants at (a) 1 atm, 700 K (b) 5 atm, 700 K and (c) 15 atm, 700 K.

Furthermore, it can be seen that as pressure increases, flame response nonlinearity sets in at lower Strouhal numbers. This can be seen both from the fact that at higher Strouhal numbers, response saturation sets in at lesser excitation amplitudes as reactant pressure increases, and from the increasing disparity between linear and nonlinear phase characteristics at high Strouhal numbers as pressure increases. This is because flame speed sensitivity increases with reactant pressure.

Finally, consider a comparison of the difference in response characteristics between the 300 K, 1 atm case, Figure 48(a) and the 700 K, 15 atm case, Figure 49(c). It may be seen that while the general gain and phase trends remain similar, the overall transfer function gain magnitude reduces slightly while from 300 K, 1 atm to 700 K, 15 atm. The flame response character becomes less nonlinear for a given excitation amplitude. This also means that heat release saturation, either because of kinematic restoration effects, or flammability crossover, occurs at higher excitation amplitudes, providing a larger $St_2 - \varepsilon$ window to operate gas turbine combustors in before reaching the limit cycle.

5.5. Recent Progresses in Further Understanding

The flammability cross-over phenomenon could potentially become important in practical gas turbine which operate at nominal equivalence ratios close to the lean static flammability limit of the reactant mixture in a window in the ϕ-space, where both the NOx and CO emissions are at a joint minimum. As described previously, in such situations, even for an excitation amplitude, which under normal circumstances would have been considered to be in the 'linear' regime (See Figure 37), would now lead to nonlinearity because of local extinguishment.

This phenomenon has been recently studied by Wu and Hemchandra [137] as a continuation of the efforts to understand equivalence ratio coupled nonlinear flame response. They compute the response of a 2D slot CH_4/air flame in the presence of co-flowing products, by numerically solving the governing equations of reacting flow. They

find that, for cases where the co-flowing products are at the adiabatic flame temperature corresponding to the stoichiometric composition of the reactant mixture, flame holes are observed to occur due to local extinguishment of the flame because of regions of sub-flammable mixture composition. As hypothesized in the previous section, they confirm that this mechanism leads to heat release saturation.

The other case investigated by them is that of a co-flow hotter than the adiabatic flame temperature, where, in spite of the equivalence ratio dropping below the static flammability limit, combustion is sustained without the formation of holes. This indicates that the flammability crossover nonlinearity is not merely related to the static flammability limit of the mixture, as assumed in Figure 37, although static flammability is perhaps one of the parameters that determine this crossover amplitude.

This question has been answered by Im and co-authors [129, 138] in the context of opposed flow premixed flames submitted to composition fluctuations, and has been verified to hold true for flames with more complex geometry by Wu and Hemchandra [137]. Sankaran and Im [129] recognize that local extinction occurs at an equivalence ratio lower than the static flammability limit. They define a dynamic flammability limt, $\phi_{FL,D}$, as the lowest equivalence ratio in the excitation cycle at which a flame is sustained, i.e, without the formation of flame holes. Bansal and Im [138] then define a normalized dynamic flammability limit extension (NDFLE) as:

$$NDFLE = \frac{\phi_{FL,D} - \phi_{FL,S}}{\phi_o - \phi_{FL,S}} \tag{5.21}$$

and show that *NDFLE* is a decreasing function of the non-dimensional frequency, $\delta_T \left(\pi f / D_F \right)^{1/2}$, much along the lines of Stokes' second problem, as noted by Lauvergne and Egolfopolous [119]. Here, δ_T is the thermal thickness of the flame and D_F is the mass diffusivity of the fuel. Note also that since $NDFLE < 0$, its decrease with $\delta_T \left(\pi f / D_F \right)^{1/2}$ implies that sustained combustion can occur over a larger range of excitation amplitudes. Assuming $D_F = D_{Ox} = D$ and $\delta_T \sim D_T / s_{Lo}$, the non-dimensional frequency, $\delta_T \left(\pi f / D_F \right)^{1/2}$, reduces to $\left(Le\, St_\delta / 2 \right)^{1/2}$. This shows that the equivalence ratio amplitude at which flammability crossover occurs is dependent on the structural non quasi-steadiness Strouhal number.
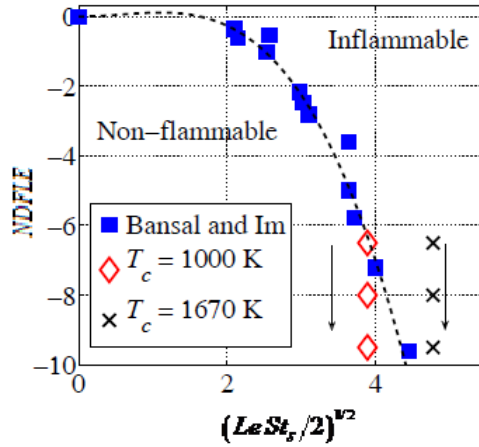
Figure 50 : Variation of NDFLE with excitation non-dimensional excitation frequency, $\left(Le\, St_\delta / 2 \right)^{1/2}$ **as computed by Bansal and Im [138] for CH₄/air flame. The diamond and crosses denote the computational cases of Wu and Hemchandra without and with heated co-flowing product gases, while the crosses denote different equivalence ratio excitation amplitudes increasing in the direction of the arrow, about a nominal equivalence ratio of** $\phi_o = 0.6$ **at an excitation corresponding to** $f = 200 Hz$, **for reactants flowing in at** $u_o = 85 cms^{-1}$. **Reproduced from Wu and Hemchandra [137] with permission.**

The computed plots of Bansal and Im [138] overlaid with the computational points of Wu and Hemchandra [137] is presented in Figure 50. Figure 50 shows that as the forcing Strouhal number is increased, the mixture remains inflammable over a larger range of excitation amplitudes. The differences between the occurrence of extinction events between the cold product co-flow and hot product co-flow cases computed by Wu and Hemchandra [137] are because they correspond to different regions of flammability of Figure 50. While, for the cold co-flow case, denoted by diamonds, increasing the excitation amplitude pushes NDFLE into the non-flammable region at the chosen excitation frequency, the NDFLE is still in the inflammable region for the hot co-flow case. Hence, flame holes occur in the former, while they are absent in the latter.

Notwithstanding the above, from Figure 37, it may be noted that the flammability crossover amplitude shows similar trend with Strouhal number as discussed above – i.e., the crossover amplitude becomes larger as the excitation frequency increases. Though our simplistic model predicts this trend correctly, quantitative information regarding the flammability crossover amplitude needs to be obtained from curves such as in Figure 50.

Chapter 6 : Comparison of Reduced Order Model with Experimental Data

6.1. Introduction

The advantages of using linear ROMs to predict flame response are many. First, they are simpler and less expensive than carrying out experimental or full-scale computational studies of the problem of interest. Second, it is easier to carry out parametric studies with ROMs. Third, ROMs can help in understanding physics more insightfully. For example, it is easier to see the $1/St$ variation of 2D V-flame velocity coupled flame transfer functions from the analytical expression and understand that the origin of that variation is in the phenomenon of wave interference. On the other hand, curve fitting a $1/St$ trend to experimental or computational data would not yield as much physical insight.

However, given the lack of complete physics into the G-equation based ROM, it is important to study how well the ROM can capture actual flame response physics, to develop confidence in using the ROM even as a supplementary tool to understand combustion dynamics in addition to experiments and full-scale CFD.

This question has been recently investigated into by Karimi et al. [59] who compare the velocity-coupled flame response transfer function obtained based on a level-set model [17, 60, 114] to experimental measurements of the transfer function over a range of low Strouhal numbers, $St = 2$ to 20. They encounter very encouraging results for

this case, suggesting that the usage of the kinematic equation without complete reacting fluid mechanics built into it is still very fair.

An analogous study carried out by Wangher et al. [104] aimed at comparing the pressure coupled flat flame response models Clavin et al. [101] and McIntosh [92] with their experiments. They concluded that more work was necessary to refine the model to be able to predict even flat flame response accurately.

However, no similar work seems to have been carried out in comparing experimentally measured equivalence ratio coupled flame transfer function with its theoretical counterpart. This is, at least in part, due to the difficulties associated with the generation of equivalence ratio fluctuations in a controlled manner. Furthermore, more fundamental issues exist, such as the equivalence of the flame transfer function as defined for experiments (for example, using chemiluminescence measurements) and for theory using heat release. In essence, this is an open area for further study. Nonetheless, a short summary of the efforts in this direction carried out as a part of this research work is presented.

6.1.1. Chemiluminescence Response of the Flame

We first start by considering the relationship between global heat release and chemiluminescence oscillations of premixed flames excited by fuel/air ratio oscillations. This comparison is important because chemiluminescence response measurements may not directly reflect the heat release response of flames when the fuel composition is oscillating.

The manner in which fuel/air ratio oscillations disturb the heat-release can be understood by considering the instantaneous global heat-release rate, given by the following integral of the heat release per unit flame area, q^L, over the flame surface area.

$$q(t) = \int\limits_{flame} q^L(\phi, p, T, \kappa, ...) dA = \int\limits_{flame} \rho s_L h_R dA \qquad (6.1)$$

We first discuss how equivalence ratio oscillations are manifested through oscillations in flame chemiluminescence. Measurements of naturally occurring flame chemiluminescence emissions from premixed flames have been used in numerous studies as an indicator of the local and global heat release rates [75, 79, 139-141]. Detailed chemical kinetic calculations of lean, premixed laminar CH_4-air flames show that CH*, OH* and CO_2* radicals occur within the reaction zone [139, 140]. While certainly not a perfect approach, as discussed further below, chemiluminescence is really the only practical method for inferring heat release rates at present.

There is significant experimental data [142-145] showing that at a fixed equivalence ratio, the quasi-steady chemiluminescence emission intensity from the flame exhibits a linear dependence on the reactant flow rate. For these reasons, unsteady chemiluminescence appears to be a good marker of unsteady heat release for flames responding to low frequency flow velocity oscillations. For example, the data below illustrate gain curves, defined as in Eq.(6.4), for global CH* and OH* chemiluminescence showing similar frequency sensitivities.
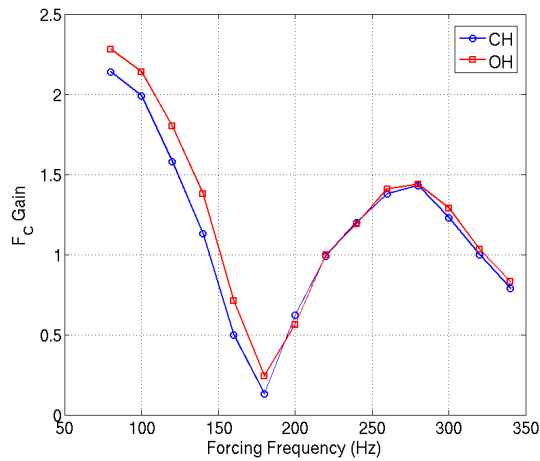
<center>(a)</center>
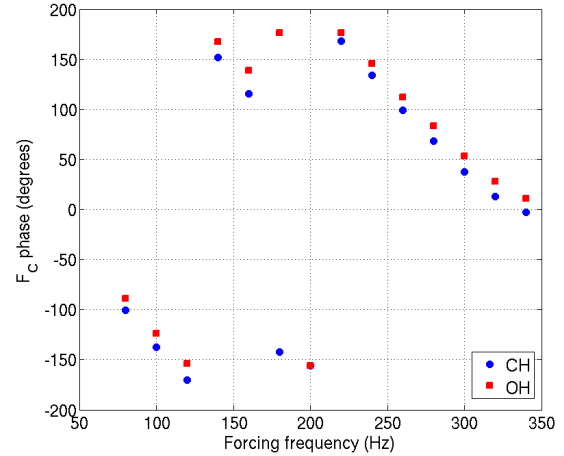
<center>(b)</center>

Figure 51 : Chemiluminescence transfer function (a) gain and (b) phase, with respect to velocity perturbations) for velocity-coupled flame response, for ϕ_o=0.75, u_o=25 m/s, 5% perturbation amplitude[14].

However, chemiluminescence emissions are not only a function of the instantaneous heat release rate, but other parameters as well, including fuel/air ratio, fuel type, strain rate, and unsteady effects. We start first with unsteady effects. Due to finite rate kinetics, one can expect there to be a certain phase lag between heat release and chemiluminescence in unsteady flames, even if they track each other perfectly in the quasi-steady limit. While we are not aware of studies explicitly considering this effect, data suggests that it may be negligible for a variety of frequencies of interest. This may be seen from the difference in phases of CH* and OH* chemiluminescence signals with respect to those of velocity perturbations at the flame base, as shown in Figure 51. Given the different chemical pathways (and presumably time scales) by which these species are formed, the fact that they give essentially similar phase (within 20 degrees) strongly suggests that they are

---

[14] B. Jones, J. G. Lee, D. A. Santavicca, Pennsylvania State University, University Park, PA - *Personal communication*

tracking the heat release in a quasi-steady manner. More data and analyses are needed, however, to further understand these effects.

We next consider other effects such as turbulence and strain rate and flame curvature. John and Summerfield [145], Hurle et al. [146] and, more recently, Lauer and Sattelmayer [147] have shown that turbulence reduces the global chemiluminescence emission intensity. Additionally, other studies [75, 140, 146] have systematically characterized the relationship between chemiluminescence and heat release fluctuations, showing that these are correlated as long as the strain rate and flame curvature are not "too large" (e.g., within a flame cusp). For highly strained flames, these studies indicate that the local chemiluminescence emission can go to zero, even without local extinction. The sensitivity to strain rate has also been discussed extensively [148]. It appears that the chemiluminescence sensitivity to strain rate is much less than its sensitivity to equivalence ratio.

Chemiluminescence sensitivities to fuel composition, including fuels such as methane, propane, ethylene, H_2/CO blends, and Jet A have been studied by researchers [143, 148]. Given the caveats already noted in this section, these studies show that chemiluminescence emissions tracked the unsteady heat release, although the specific sensitivities varied with the fuel.

Finally, we consider the fuel/air ratio sensitivity of chemiluminescence emissions, which forms the main focus of this study. The sensitivity of chemiluminescence to fuel/air ratio is well known from a number of experiments, showing that the variation of global chemiluminescence intensity with fuel-flow rate itself is an exponential function

of the equivalence ratio. This is demonstrated by global OH* and CH* measurements [75, 148, 149] and occurs due to the exponential dependence of the reaction rate upon the temperature [150].

To follow these ideas further, note first that the *local* instantaneous heat-release rate per unit flamelet surface area, q^L, is a function of ϕ, κ, p, T etc. Hence, we may expand q as

$$\frac{q^L}{q^L_o} = 1 + \frac{\partial\left(q^L/q^L_o\right)}{\partial\left(\phi/\phi_o\right)}\bigg|_o \frac{\phi'}{\phi_o} + \frac{\partial\left(q^L/q^L_o\right)}{\partial\left(p/p_o\right)}\bigg|_o \frac{p'}{p_o} + \frac{\partial\left(q^L/q^L_o\right)}{\partial\left(T/T_o\right)}\bigg|_o \frac{T'}{T_o} + \frac{\partial\left(q^L/q^L_o\right)}{\partial\left(\kappa/\kappa_o\right)}\bigg|_o \frac{\kappa'}{\kappa_o} + \ldots (6.2)$$

Further, note that the local chemiluminescence intensity per unit area, σ^L is an explicit function of equivalence ratio, strain rate, pressure etc., and is also implicitly dependent on them, by virtue of being a function of q^L, i.e., $\sigma^L = \sigma^L\left(q^L\left(\phi, \kappa, p, T, \ldots\right), \phi, \kappa, p, T \ldots\right)$. Hence, σ^L may simply be expanded as a function of ϕ, κ, p, T etc., accounting for both the implicit and explicit dependence, as follows.

$$\frac{\sigma^L}{\sigma^L_o} = 1 + \frac{\partial\left(\sigma^L/\sigma^L_o\right)}{\partial\left(\phi/\phi_o\right)}\bigg|_o \left(\frac{\phi'}{\phi_o}\right) + \frac{\partial\left(\sigma^L/\sigma^L_o\right)}{\partial\left(p/p_o\right)}\bigg|_o \left(\frac{p'}{p_o}\right) + \frac{\partial\left(\sigma^L/\sigma^L_o\right)}{\partial\left(T/T_o\right)}\bigg|_o \left(\frac{T'}{T_o}\right) + \frac{\partial\left(\sigma^L/\sigma^L_o\right)}{\partial\left(\kappa/\kappa_o\right)}\bigg|_o \left(\frac{\kappa'}{\kappa_o}\right) + \ldots$$

$$(6.3)$$

The partial derivatives on the RHS are the non-dimensional sensitivities of local chemiluminescence intensity which now account for both the explicit and implicit dependence. These are what are actually measured in experimental measurements of chemiluminescence emissions.

While all of these fluctuations are simultaneously present during an instability, σ^L has the highest sensitivity to fuel/air ratio disturbances. To illustrate, Nori's [148] results for CH$_4$/Air flames (at ϕ_o=0.7, p_o=1 atm, T_o=298K, κ_o=200s^{-1}) suggest dimensionless sensitivities of σ^L with respect to ϕ, κ, p and T (i.e., preheat temperature) that are on the order of 10, 1, 0.01 and 1 respectively.

Due to this exponential sensitivity of chemiluminescence to fuel/air ratio, there are problems associated with its interpretation if both the fuel/air ratio and heat release rate are oscillating. In particular, it can be anticipated that the relationship between the global (i.e., spatially integrated over the entire flame surface area) chemiluminescence intensity and the global heat release is not one-to-one when there is a spatial variation in equivalence ratio along the flame surface. This occurs because the chemiluminescence intensities of the local area elements are functions of the local equivalence ratio, which is now varying along the flame surface. Hence, the overall chemiluminescence emission intensity is a non-equally weighted sum of individual elements over the flame.

Thus, an important question must be addressed: How does the global chemiluminescence response, CH^G, of the flame compare with the global heat release response? The current work aims to address this question by analytically calculating and comparing transfer functions for the chemiluminescence and heat release responses, which are respectively defined as follows:

$$F_C = \frac{\widehat{CH'^G}/CH_o^G}{\widehat{\phi_{base}'}/\phi_o} \tag{6.4}$$

$$F_Q = \frac{\widehat{q'}/q_o}{\widehat{\phi_{base}'}/\phi_o}$$ (6.5)

Here, ϕ'_{base} denotes the fluctuations in equivalence ratio at the flame base and the hats (^) denote Fourier-transformed time domain variables. We will show that the comparison between F_C and F_Q depends upon the emitting species considered, area-averaged fuel/air ratio, and flame geometry.

6.2. Analytical Modeling

6.2.1. Global Chemiluminescence Response Modeling

The global chemiluminescence intensity can be calculated as an integral of the local chemiluminescence intensity per unit area. We write this local chemiluminescence intensity as a function of the local instantaneous heat release rate per unit flamelet surface area and local equivalence ratio. Mathematically, this may be expressed as follows:

$$CH^G(t) = \int_{flame} \sigma^L\left(q^L(\phi),\phi(z,t)\right)dA$$ (6.6)

Here, q is the heat release per unit area of the flame. By definition:

$$q(t) = \int_{flame} q^L(z,t)\,dA = \int_{flame} \rho s_L(\phi)h_R(\phi)\,dA$$ (6.7)

Further, note that the local heat release density may be estimated as the product of the local mass burning rate of the reactants and the heat of reaction of the reactants, both of which depend on the local equivalence ratio:

$$q^L(z,t) = \rho s_L(\phi(z,t)) h_R(\phi(z,t)) \tag{6.8}$$

We shall assume here that the fuel/air ratio oscillations occur at constant reactant density [23]. From Eq.(6.8), it follows that $q^L = q^L(\phi)$, so that we may write:

$$\sigma^L(q^L,\phi) = \sigma^L(q^L(\phi),\phi) = \sigma^L(\phi(z,t)) \tag{6.9}$$

With these considerations, the global chemiluminescence intensity CH^G, as expressed in Eq. (6.6), may be rewritten as follows:

$$CH^G(t) = \int_{flame} \sigma^L(\phi(z,t)) dA \tag{6.10}$$

For the sake of illustration, we will now assume that the mean equivalence ratio, ϕ_o, is spatially uniform, so that $\phi(z,t) = \phi_o + \phi'(z,t)$. Expanding $\sigma^L(\phi(z,t))$ about ϕ_o yields:

$$CH^G(t) = \int_{flame} \left(\sigma^L(\phi_o) + \frac{\partial \sigma^L}{\partial \phi}\bigg|_{(q_o,\phi_o)} \phi'(z,t) \right) dA \tag{6.11}$$

Note that $\sigma^L(\phi_o) = CH_o^G/A_o$ is the chemiluminescence intensity per unit flame surface area of the undisturbed flame, which is a constant.

Further, define a flame surface area averaged "effective" equivalence ratio fluctuation as:

$$\phi'_{eff}(t) = \int_{flame} \phi'(z,t) dA \tag{6.12}$$

The instantaneous global chemiluminescence intensity may be written in terms of $\phi'_{eff}(t)$ as

186

$$\frac{CH^G(t)}{CH_o^G} = \frac{A(t)}{A_o} + \left. \frac{\partial\left(\sigma^L(\phi)/\sigma^L(\phi_o)\right)}{\partial(\phi/\phi_o)} \right|_{\phi_o} \frac{\phi'_{eff}(t)}{\phi_o} \qquad (6.13)$$

On subtracting the mean quantities, this can be written as

$$\frac{CH'^G(t)}{CH_o^G} = \frac{A'(t)}{A_o} + m(\phi_o)\frac{\phi'_{eff}(t)}{\phi_o} \qquad (6.14)$$

where

$$m(\phi_o) = \left. \frac{\partial\left(\sigma^L(\phi)/\sigma^L(\phi_o)\right)}{\partial(\phi/\phi_o)} \right|_{\phi_o} \qquad (6.15)$$

The constant m is the sensitivity of the chemiluminescence intensity of the flame per unit area to fluctuations in equivalence ratio. This can be determined from kinetic calculations [148] or experimental data relating chemiluminescence intensity/flow rate to equivalence ratio [75].

6.2.2. Global Heat Release Response Modeling

The global heat release response modeling follows what has been described earlier in Chapter 2 and Chapter 3. To recapitulate, it was shown that:

$$\frac{q'(t)}{q_o} = \frac{A'(t)}{A_o} + \left[s_{L1,\phi}(\phi_o) + h_{R1,\phi}(\phi_o) \right]\frac{\phi'_{eff}(t)}{\phi_o} \qquad (6.16)$$

Note that, for a chosen fuel and fixed operating conditions, the sensitivities[15] s_{L1} and h_{R1} are functions of the mean equivalence ratio alone. However, these sensitivities change with preheat temperature, pressure, and other variables. Note from Eq.(6.14) and Eq.(6.16) that evaluation of the instantaneous global chemiluminescence intensity and global heat release of the flame requires us to estimate the fluctuations in burning surface area and the effective equivalence ratio.

6.2.3. Global Transfer Functions

With the framework presented in the previous subsections, we may evaluate transfer functions for the global chemiluminescence response, F_C and global heat release response, F_Q, by taking the Fourier transforms of Eq.(6.14) and Eq.(6.16) at the forcing Strouhal number, to yield:

$$F_C = F_A + mF_{\phi_{eff}} \tag{6.17}$$

$$F_Q = F_A + \left(s_{L1} + h_{R1} \right) F_{\phi_{eff}} \tag{6.18}$$

Here, F_A and $F_{\phi_{eff}}$ denote the transfer functions for the burning area and effective equivalence ratio fluctuation responses whose definitions are similar to those of F_C and F_Q, see Eq.(6.4) and Eq.(6.5).

---

[15] Hereafter, the subscript ϕ for the sensitivities is dropped, since sensitivities to ϕ are the only ones being considered in this chapter.

$$F_A = \frac{\widehat{A'}/A_o}{\widehat{\phi_{base}'}/\phi_o} \tag{6.19}$$

$$F_{\phi_{eff}} = \frac{\widehat{\phi_{eff}'}/\phi_o}{\widehat{\phi_{base}'}/\phi_o} \tag{6.20}$$

Equations (6.17) and (6.18) are very revealing for understanding the comparison between F_C and F_Q. First, both transfer functions have similar structures and the same two principal contributing terms – (i) fluctuating flame surface area and (ii) fluctuating effective equivalence ratio. Furthermore, Eq.(6.17) and Eq.(6.18) differ only in the coefficient which precedes the latter contribution, $F_{\phi_{eff}}$. The former contribution, F_A affects both F_C and F_Q in an <u>identical</u> manner. This has important implications. Specifically, it means that F_C and F_Q are the same only if either of the following two conditions is satisfied –

$$\begin{aligned} &(1) \ m \sim s_{L1} + h_{R1} \\ &(2) \ |F_A| \gg |F_{\phi,eff}| \end{aligned} \tag{6.21}$$

The first condition reflects the fact that F_C and F_Q are identical if the sum of the heat of reaction and flame speed sensitivities of the heat release identically equal the fuel/air ratio sensitivity of the local chemiluminescence intensity per unit area. The second condition states that even if there is a disparity between the two coefficients, their net effect on the total transfer function would be swamped out because of the heavy domination of the area response.

Equation (6.21) also isolates the two ways in which either response can change – viz., (a) by altering the burning area and effective equivalence ratio responses, or (b) by altering the chemiluminescence intensity sensitivity, flame speed sensitivity and heat of reaction sensitivity. The former can be achieved if the flame geometry and/or the mean flame shape changes. The latter occurs if the mean equivalence ratio, reactant pressure or reactant temperature changes. Hence, for fixed operating and geometric conditions, a change in fuel composition would affect flame response through affecting the sensitivities alone.

To understand these effects, we present results from illustrative calculations for these transfer functions in the next section that account for each of these effects. For these calculations we estimate the constant m from the slope of global chemiluminescence intensity/fuel flow rate versus equivalence ratio data from Lee and Santavicca [75] and Nori [148]. For example, a typical curve using CO_2^* as the chemiluminescing species is presented below. Similarly, the flame speed and heat of reaction sensitivities were calculated from the Premix module of CHEMKIN (using GRIMech 3.1) and GasEq, respectively.
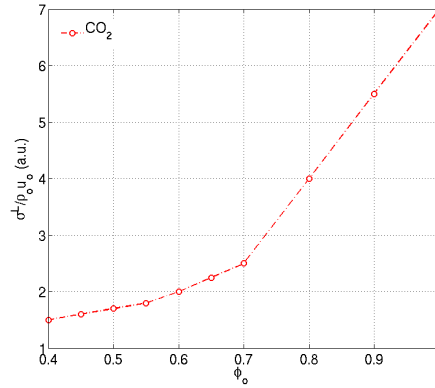
Figure 52 : Variation of CO_2* chemiluminescence intensity/fuel flow rate with mean equivalence ratio [75] .

6.3. Illustrative Results

This section presents illustrative results comparing F_C and F_Q. We intend to understand how factors such as different flame geometries, mean equivalence ratios, and thermodynamic conditions of the reactants affect F_C and F_Q. Additionally, different chemiluminescing species are considered to estimate F_C, in order to determine which of those compare best with F_Q. As noted in the earlier section, the relationship between global responses is influenced by the flame geometry or in the three sensitivity parameters. These two possibilities are discussed in the subsections that follow.

6.3.1. Flame Geometric Effects and Burning Area Response

We start by recapitulating expressions for the V-flame and conical flame transfer functions. For an axisymmetric V-flame, expressions for F_A and $F_{\phi_{eff}}$ are [39]:

$$F_A = -s_{L_1} \left\{ \frac{2\alpha}{1-\alpha} \left(\frac{1-\alpha+(iSt-1)\exp(iSt)-\alpha(iSt/\alpha-1)\exp(iSt/\alpha)}{St^2} \right) \right\} \tag{6.22}$$

$$F_{\phi_{eff}} = -\frac{2\left(1+iSte^{iSt}-e^{iSt}\right)}{St^2} \tag{6.23}$$

For a premixed conical flame, transfer function expressions may be obtained as follows [23].

$$F_A = s_{L_1} \left\{ \frac{2\alpha}{1-\alpha} \left(\frac{1-\alpha-\exp(iSt)+\alpha\exp(iSt/\alpha)}{St^2} \right) \right\} \tag{6.24}$$

$$F_{\phi_{eff}} = \frac{2\left(1+iSt-e^{iSt}\right)}{St^2} \tag{6.25}$$

Using the above, F_C and F_Q may be evaluated using Eq.(6.17) and Eq.(6.18). Further, the low Strouhal number limits of the above may be evaluated for either geometry as:

$$\lim_{St \to 0} F_A = -s_{L_1} \tag{6.26}$$

$$\lim_{St \to 0} F_{\phi_{eff}} = 1 \tag{6.27}$$

For the total responses, these limits hence become:

$$\lim_{St \to 0} F_C = m - s_{L1} \tag{6.28}$$

$$\lim_{St \to 0} F_Q = h_{R1} \tag{6.29}$$

Consider next the contribution of the area fluctuations and effective equivalence ratio fluctuations to the total transfer functions.

Figure 12 plots the contributions of response of flame surface area fluctuations and effective equivalence ratio fluctuations to F_C for a V-flame and conical flame. It can be clearly seen that the two processes contribute very differently to conical flames as compared to V-flames. In the case of V-flames, F_A dominates over $F_{\phi_{eff}}$ over most of the Strouhal number range.
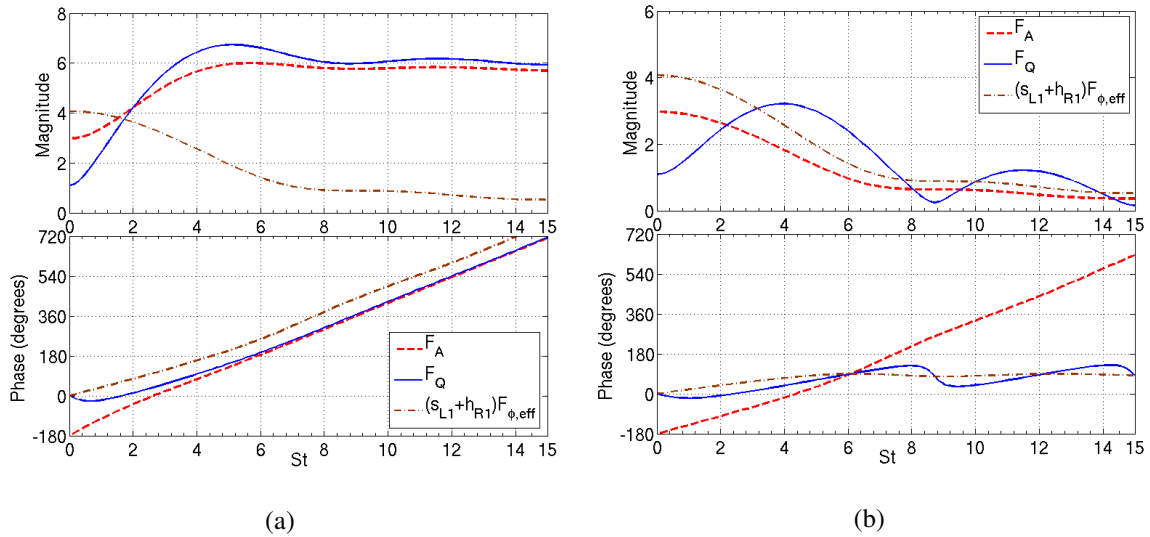
Figure 53 : Contributions to F_Q by area and effective equivalence ratio fluctuations for (a) V-flame (b) conical flame at 1 atm, 300 K, ϕ_o=0.6, β=4.

Hence, the heat release response of the flame is primarily due to F_A. However, at lower Strouhal numbers, these effects are comparable. This is seen in the phase too, where the heat release response phase and burning area response phase are noticeably different in the quasi-steady limit and are identical at larger Strouhal numbers.

However, in the case of conical flames, these two effects contribute comparably over the entire Strouhal number range. This noticeable difference in the response characteristics is merely because of the fact that a V-flame has maximum surface area at

the flame tip, while the conical flame has maximum surface area at the flame base. Hence, the maximum area in the V-flame is free to move and leads to higher response, while it is constrained at the flame attachment point for conical flames.

(a)   (b)

Figure 54 : Contributions to F_C by area and effective equivalence ratio fluctuations for (a) V-flame (b) conical flame at 1 atm, 300 K, ϕ_o=0.6, β=4.

The points raised in the above discussion can be directly applied to anticipate the relationship between F_C and F_Q. The V-flame is largely dominated by the area response at higher Strouhal numbers, while there is comparable contribution from the effective equivalence ratio response at lower Strouhal numbers. For the conical flame, these contributions are comparable over the entire range of Strouhal numbers considered. Based on the two conditions stated in Eq.(6.21), it can be seen that the V-flame F_C and F_Q reasonably agree over the range of Strouhal numbers where area response dominates.

However, in the case of conical flames, there may be some differences to the extent that the sensitivity coefficients differ.

To investigate further into this issue, we next consider the comparison between F_C and F_Q for reactants at 1 atm, 300 K, which is plotted in Figure 55.
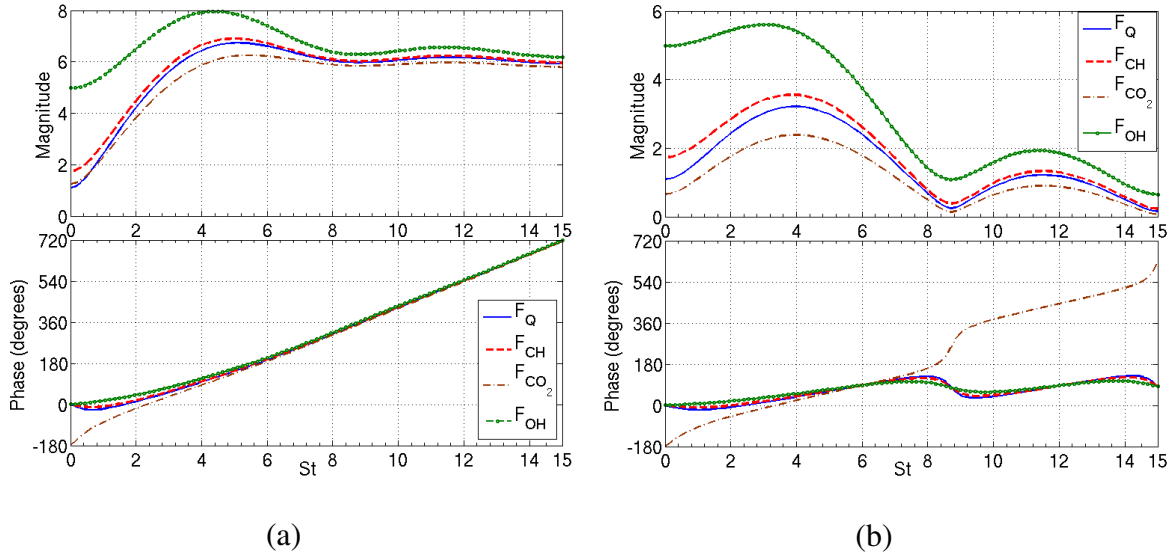
Figure 55 : Comparison between F_C and F_Q for (a) V-flame (b) Conical flame at 1 atm, 300 K. ϕ_o=0.6, β=4.

The following observations may be made from Figure 55. The F_C gain and phase for each of the three chemiluminescing species are qualitatively similar to F_C at all but very low Strouhal numbers. At very low Strouhal numbers, there is a disparity in gain as well as in phase. At these low Strouhal numbers, since F_A and $F_{\phi_{eff}}$ are comparable; condition (1) of Eq.(6.21) needs to be satisfied, which is not the case. For conical flames, there is a noticeable disparity in phase if CO_2* is used, while there is a disparity in gain if OH* is

used as the chemiluminescing species. These disparities are directly related to the degree to which the different sensitivities satisfy condition (1) of Eq.(6.21).

6.3.2. Effect of Variation of Sensitivities

We next consider the effect of chemiluminescence and local heat release sensitivity to fuel/air ratio. We shall start by considering the variation of the three sensitivities for reactants at 1 atm, 300 K, for different chemiluminescing species. This is plotted in Figure 56(a). At STP, CO_2*and OH* sensitivities, m_{CO_2} and m_{OH}, are reasonably close to the sum of the flame speed and heat of reaction sensitivities, $s_{L1} + h_{R1}$, for mean equivalence ratios between 0.7 and 0.9. Hence, these can be expected to yield F_C's that are close to F_Q. CH* might be preferable at lower equivalence ratios, while OH* seems to be preferable at near-stoichiometric fuel composition. Recall also that the value of m relative to s_{L1} is important in controlling the response at low Strouhal numbers; specifically, there is a 180 degrees phase difference between the quasi-steady F_C phase and F_Q phase if $m > s_{L1}$, see Eq.(6.28) and Eq.(6.29).

Next consider the effect of flame speed and heat of reaction sensitivities at 5 atm. It merely suffices to consider the variation of these sensitivities with equivalence ratio at 5 atm; conclusions regarding the comparison between F_C and F_Q can be drawn based upon the previous discussion and results. This is plotted in Figure 56(b), which suggests that at lower equivalence ratios, OH* seems to be preferable; also, $m < s_{L1}$ for all chemiluminescing species and hence, the quasi-steady phase difference between F_C and

196

F_Q would be 180 degrees. However, at higher equivalence ratios, say 0.9, CO_2* seems to yield closer agreement between F_C and F_Q, owing to its sensitivity, m_{CO_2} being closest to $s_{L1} + h_{R1}$. Also, it may be observed that at these equivalence ratios, because $m > s_{L1}$, irrespective of the chemiluminescing species, the phase predictions would be more accurate, even in the quasi-steady limit. Finally, it may be noted that, in general, one can expect very good agreement between F_C and F_Q if the mean equivalence ratio lies approximately between 0.7 and 0.85.

(a)

(b)
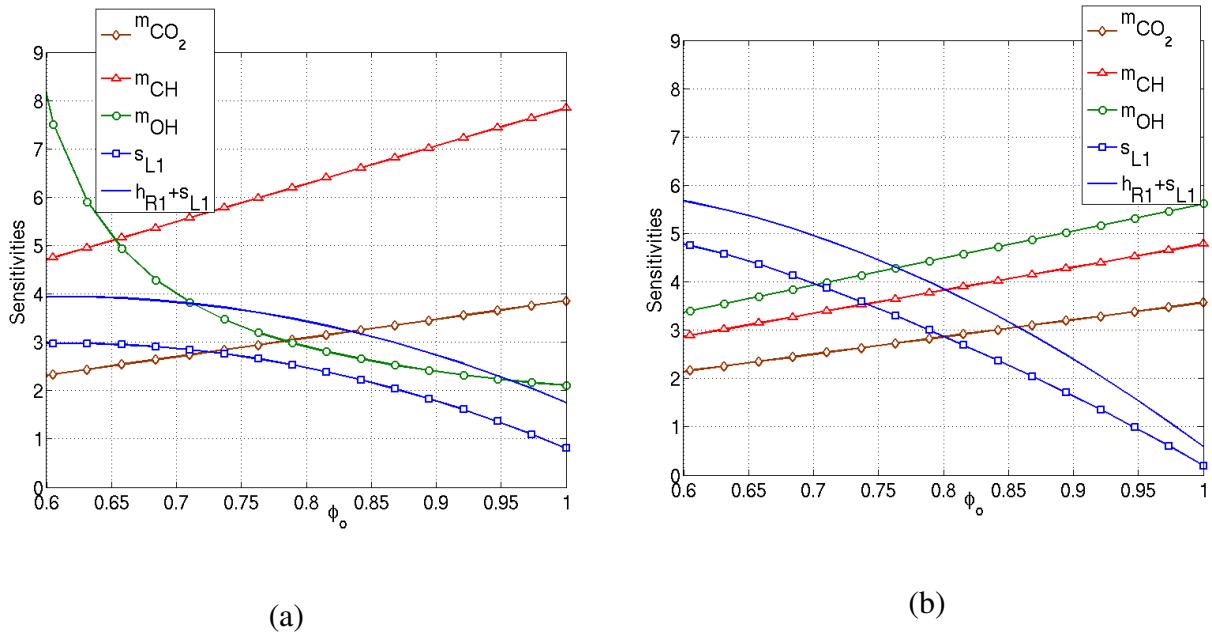
Figure 56 : Variation of various sensitivities with mean equivalence ratio at (a) 1 atm, 300 K (b) 5 atm, 300 K

Finally, we consider the effect of preheating the reactants to a higher temperature. The variation of various sensitivities versus equivalence ratio at 5 atm, 600 K is plotted in Figure 57.
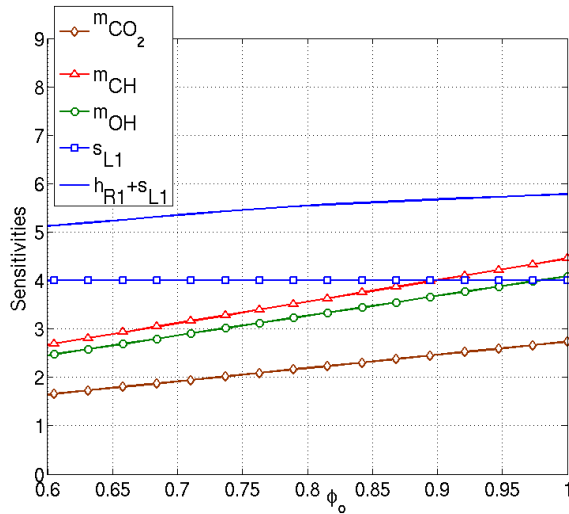
Figure 57 : Variation of various sensitivities with mean equivalence ratio at 5 atm, 600 K.

Using similar arguments as before, it may be seen from Figure 57 that at all equivalence ratios it may be expected that CH* and OH* F_C's would compare better with F_Q, while the low frequency phases would be off by 180 degrees for all of the chemiluminescing species, since $m < s_{L1}$ for all of them. At near-stoichiometric equivalence ratios (larger than 0.9, say), CH* appears to be capable of also yielding good comparison between the quasi-steady phase difference between F_C and F_Q.

Finally, it should be noted that this analysis is strictly valid for laminar flames. Clearly, the situation of most practical interest for performing these comparisons is in turbulent flames. There do not seem to be any factors which would lead to fundamentally different qualitative conclusions than drawn here, but further work on this specific problem is needed.

6.4. Comparison with Experimental Data

We next consider comparison between the linear reduced order model and the experimental data obtained at Pennsylvania State University. The experimental details may be found in Orawannukul et al. [151]. Some representative images are presented below.

(a)

(b)

(c)

(d)
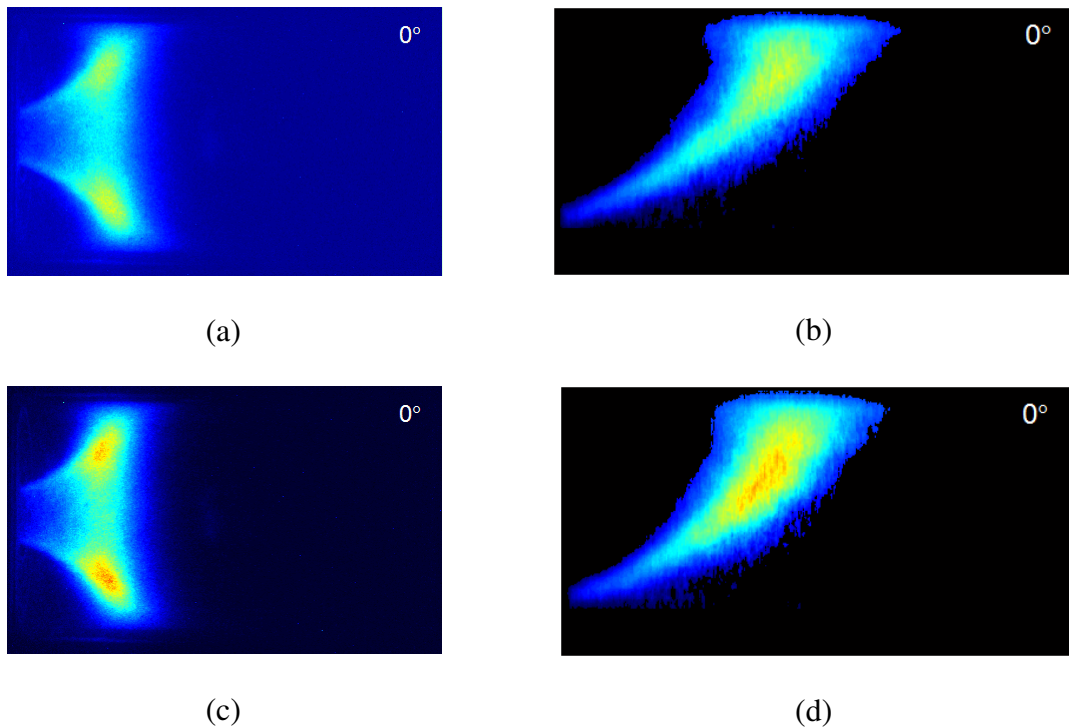
Figure 58 : Images of a swirl-stabilized CH$_4$/Air premixed flame with reactants at 1 atm, 548 K, $\phi_o = 0.6$. The left columns show line of sight images for (a) 260 Hz forcing and (c) 400 Hz forcing, while (b) and (d) are their respective deconvoluted counterparts used for chemiluminescence intensity calculations. Images reproduced from Orawannukul et al. [151].

Chemiluminescence intensity measurements are performed for a swirl-stabilized premixed CH$_4$/Air flame at $\phi_o = 0.6$. The reduced order model has been compared with experimental data for two conditions where the reactants are at (i) 1 atm, 473 K, and (ii) 1

atm, 548 K. Comparison of the ROM with experimental data involves the geometry of the mean flame, i.e., the length and width of the mean flame as the main parameters. The width of the flame was assumed to be the farthest radial location from the line of sight images, where the intensity value was non-zero. For example, with reference to Figure 58(a) or (c), the radial location corresponding to the upper tip of the green region of the flame was chosen to be the flame width. The length of the mean flame was determined using the axial heat release distribution, to be the axial extent of the flame that contributes 90% to the total integrated heat release. Note here that the determination of the mean flame geometry and model parameters is somewhat heuristic and influences how well the ROM compares with the data. This point is discussed a little later in this section.

Next, the flame speed and heat of reaction sensitivities were calculated from their respective variations with equivalence ratio at the operating conditions, using CHEMKIN and GasEq softwares respectively. The flame thickness, which is important to determine Markstein numbers, was determined to be the thermal thickness of the flame using CHEMKIN. The ROM included all the physics discussed earlier in this thesis, including interference effects, flame stretch, axial diffusion of equivalence ratio and vortical velocity disturbances and flame structural non quasi-steady response.

With this background, we now present actual comparison between ROM and experimental data in Figure 59. We first consider the magnitude plots for either condition.
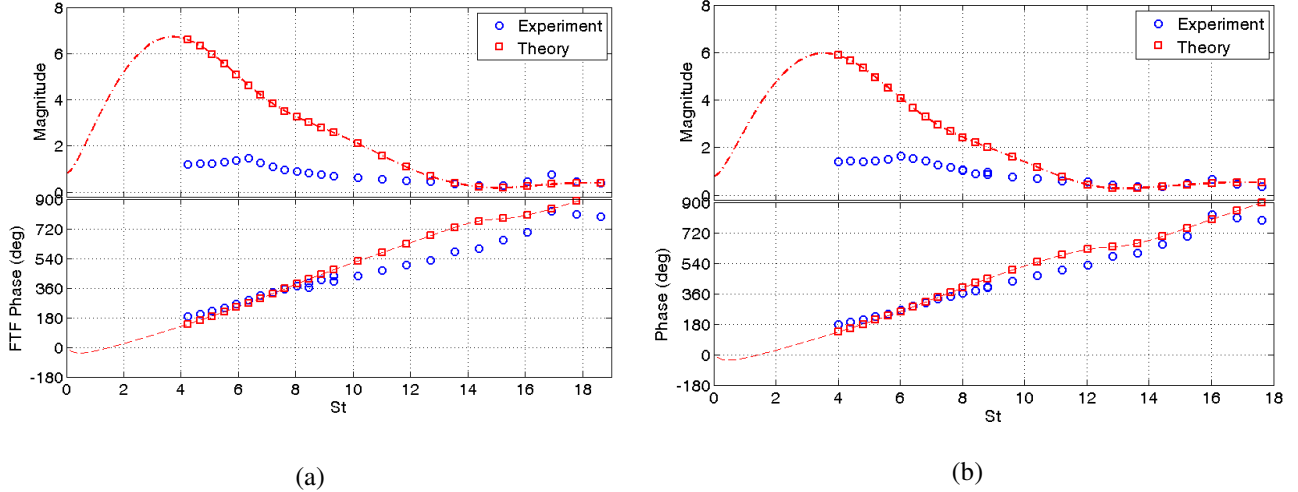
Figure 59: Comparison between linear heat release response model and experimental data for chemiluminescence response of an axisymmetric CH₄/Air flames with $\phi_o = 0.6$ **with reactants at (a) 1 atm, 473 K, and (b) 1 atm, 548 K.**

As may be seen clearly, for either reactant temperature, at low Strouhal numbers, there is significant disagreement between the experiment and the model gain. However, for higher Strouhal numbers, say $St > 12$ for case (a) and $St > 10$ for case (b), there is very good agreement between experimental data and the model. On the contrary, the phase comparison for either case, particularly for the case with higher preheat, is very encouraging, and hence the time lag associated with the flame heat release response is well modeled by the ROM.

The possible reasons in the disagreement in gain at low Strouhal numbers are next investigated into. As such, could potentially arise because of three reasons.

First, it needs to be noted that the comparison of the results is between the response of a swirl stabilized flame (experimental) and the response predicted by a model which absorbs all hydrodynamic effects into a stationary flame whose slope is constant. This model for a stationary flame, however, is important to make analytic progress.

Second, the experimental swirl flames are highly turbulent, which could augment the burning velocity of the flamelets, thereby leading to a more rapid destruction of flame wrinkles, which could lead to departures from the laminar theory.

Third, the comparison makes use of a stationary flame shape obtained from an Abel transform of the line of sight images in an axisymmetric model. This deconvolution of the line of sight images could lead to a flame angle that is not representative of the real flame angle.

Fourth, the oscillatory flame induces an oscillation in the velocity field just upstream of the flame, even though the initial approach flow had no velocity perturbations. This induced velocity perturbations has been studied by Birbaud et al. [87], who perform a DNS study of a conical flame perturbed by equivalence ratio perturbations. They estimate that velocity oscillations as strong as 15% of the mean flow velocity can be induced by the oscillating flame. More recently, Hemchandra [152] who performs a comparison of the reduced order model of Shreekrishna et al. [23] with DNS in the structurally quasi-steady limit, encounters similar disagreements at low Strouhal numbers, and conjectures those to arise out of the model not accounting for non-unity temperature ratio across the flame. To assess this disparity more critically, experimental data at higher preheat conditions need to be obtained. The temperature ratio across the flame decreases with preheat temperature, and it is possible that the model captures low Strouhal number physics better then. Furthermore, why these induced velocity effects do not affect the high Strouhal number comparison, can be understood from prior results in Chapter 4, which compare flame responses for different coupling processes, where it was

seen that equivalence ratio coupled flame response is usually more dominant than vortical velocity coupled flame response at higher Strouhal numbers.

Fifth, these induced velocity perturbations could generate acoustic waves which can also cause flame response. It will then not only necessitate for us to account for the magnitude effects due to acoustic velocity coupling, but also necessitate to account for the time lag associated with the backward travelling vortical wave to encounter a boundary or area change, where it can generate an acoustic wave. This complex phasing is not easy to account for through models, and is a potential area for exploration.

Finally, the determination of the flame geometric dimensions is somewhat heuristic, and hence the aspect ratio of the flame, which is a very important parameter for the reduced order model, is not precisely determined. In fact, approximating the mean flame shape to possess a constant slope, as assumed by the model, itself could be an assumption that needs refinement.

To appreciate this last point better, consider the effect of varying the cut-off parameter that describes the flame length, as plotted in Figure 60.

(a)   (b)
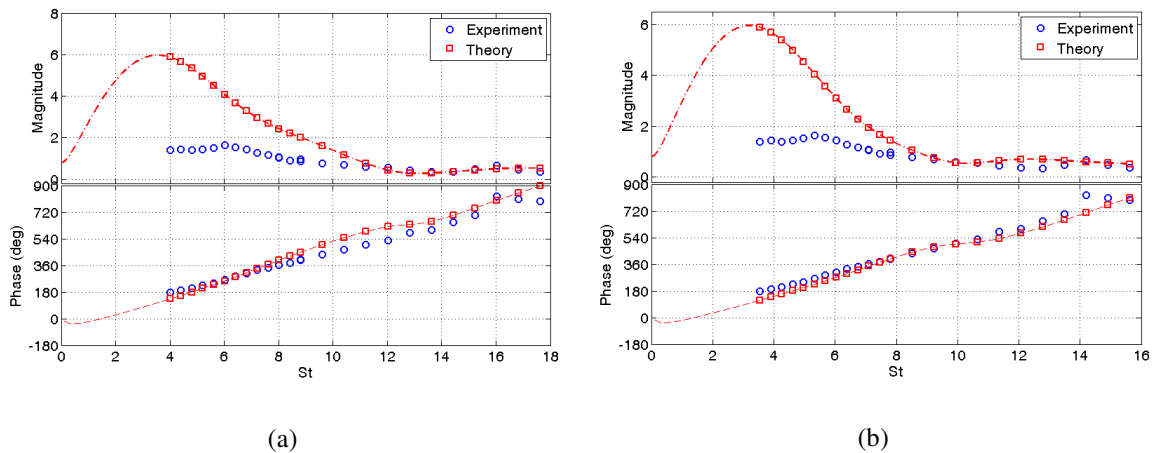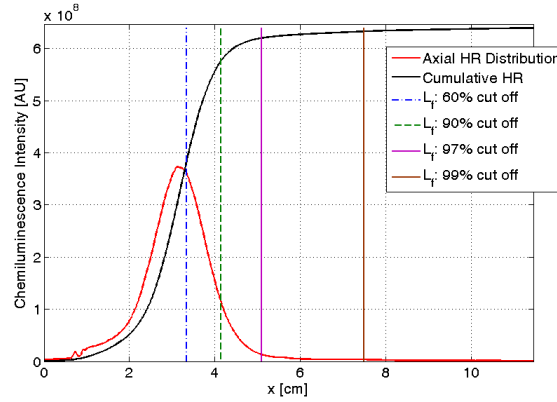
(c)

Figure 60: Study of the sensitivity of the comparative accuracy between experimental data and ROM to choice of flame length location based on percentage contribution to the total heat release. (a) 90% cut off, (b) 60% cut off, (c) Axial heat release distribution of the flame and where different cut off percentages correspond to in terms of flame length. A $\phi_o = 0.6$ axisymmetric CH$_4$/Air V-flame with reactants at 1 atm, 548 K is considered.

Figure 60 plots the comparison between experiment and model for the same flame image, but different choice of flame lengths based on the percentage contribution to the total heat release. Between the 90% cut off case, Figure 60(a), and the 60% cut off case, Figure 60(b), the variation of aspect ratio is about 25%, i.e., the aspect ratio for the 60% cut off case is 25% lesser than that for the 90% cut off case. The effect of this change in aspect ratio with regard to the magnitude of the flame response is that, in the latter case, the experimental data and model compare well with one another for $St \geq 7$, while in the latter case, good agreement is obtained for $St \geq 10$. This indicates that the choice of flame length is very crucial for this comparison. In fact, it can be seen from Figure 60(c), that choosing flame lengths based on 97% and 99% contributions lead to aspect ratios of the flame, which are 1.25 times and 1.8 times the aspect ratio based on 90% contribution to the total heat release. This shows that as the cut-off percentage increases, the aspect ratio begins to get more sensitive to the cut-off percentage. A similar analysis may be carried

out for the sensitivity of comparative accuracy to the choice of the radial location. Hence, it is important to envisage a standard, consistent way of determining the mean flame. This is certainly an area that deserves attention in future research.

Chapter 7 : Conclusions and Recommendations

7.1. Conclusions of this Research Work

Low emission combustion systems in land based gas turbines, which operate premixed or partially premixed, are prone to combustion instabilities, which destroy hardware and hamper performance, operability, reliability and emissions. Successful prediction of these dynamics in a combustor relies heavily on the heat release model which couples the acoustics of the system and the dynamics of the combustion process. This defines the principal objective of this research work which is to understand the heat release response of premixed flames to oscillations in reactant equivalence ratio, reactant velocity and pressure. The flame responses to these disturbances are studied in the linear (in excitation amplitude) regime; the equivalence ratio coupled flame response is studied in the nonlinear regime as well.

A thin, laminar, thermodiffusively stable, premixed flame whose thickness is smaller than all disturbance length in the flow, is assumed to be stabilized on a flame holder and attached to it at all times. The mean property fields (viz., reactant velocity, reactant equivalence ratio and pressure) are assumed to be homogeneous and disturbances in these quantities are assumed to be harmonic and to be occurring at the flame base. The flame front evolution and response to these disturbances is tracked by means of the G-equation, under the assumption that the flame does not affect the upstream flow. This is a commonly employed assumption in prior research efforts that have used the G-equation approach to understand flame response, and is understood to be

an important assumption to make analytic progress. Processes such as unsteady lift-off and local extinction are disregarded.

In the context of the above assumptions, this thesis addresses four outstanding issues in an attempt to contribute to the field in systematically understanding linear and nonlinear dynamics of laminar premixed flames.

First, this thesis studies the linear response of flames to equivalence ratio disturbances. The physics of equivalence ratio coupled flame response is very rich due to the existence of three independent routes that lead to flame heat release oscillations. Several physical phenomena associated with the flow and the flame influence the frequency response characteristics of the flame. The very low frequency, linear quasi-steady dynamics are completely controlled by flame heat release oscillations due to heat of reaction oscillations. At higher frequencies, flame stretch and axial decay smooth out the oscillations in the overall flame heat release response magnitude, while preheat zone non quasi-steadiness rescales the transfer function altogether. In fact, non quasi-steady phenomena associated with preheat zone diffusion scale all the three routes identically; flame stretch and disturbance diffusion, on the contrary, cause different routes to be affected differently.

Second, this research work also studies the quasi-steady, nonlinear flame response to equivalence ratio disturbances. These nonlinearities become significant as excitation amplitude and frequency are increased and are important in understanding limit cycle characteristics and saturation of the flame response. Two basic processes are identified as causing nonlinearities in flame response – (i) nonlinearities in burning area oscillation,

due to the nonlinearities in flame kinematics, and (ii) quasi-steady nonlinearities in the s_L-ϕ and h_R-ϕ relationships. A special case of the former is the crossover nonlinearity, which can occur at high excitation amplitudes while operating very close to either stoichiometry or the flammability limit of the reactant mixture. Both of these lead to heat release saturation. In the former case, saturation occurs because the flame speed and heat of reaction increase over a part of the excitation cycle, while decreasing over the other part of the cycle. In the latter case, the equivalence ratio can instantaneously assume values below the flammability limits of the mixture. This can lead to flame extinction and reignition phenomena over a part of the cycle, and lead to burning area saturation. Moreover, due to spatial variation in the equivalence ratio, "holes" in the flame advance or retreat with their own associated dynamics.

Third, in order to evaluate the equivalence ratio coupled flame response model developed as a part of this research work, comparisons between the chemiluminescence transfer function obtained experimentally and the heat release transfer functions obtained from the reduced order model (ROM) are performed for lean, CH_4/Air swirl-stabilized, axisymmetric V-flames. While the comparison between the experimental phase and ROM phase seem encouraging, the lower Strouhal number gains show disagreement; the determination of the sources of either trend requires further investigation.

Fourth, the physics of flame response at high frequencies is studied. In the course of this endeavor, flame response to pressure fluctuations is briefly discussed. The mass burning sensitivity to pressure disturbances increases roughly as the square root of the excitation frequency, leading to a weak $St_2^{-1/2}$ decay for the pressure coupled flame response. The equivalence ratio and velocity coupled flame responses decay more rapidly

due to disturbance diffusion and interference (phase cancellation) effects. These factors cause pressure coupling to be the most dominant coupling mechanism at high frequencies. In fact, pressure coupling is found to become important and dominant beyond frequencies of about ~1-3 kHz for laminar flames, and about ~10-15 kHz for turbulent flames at typical power generation and aero-engine operating conditions. These frequencies are in the vicinity of those that are typical of gas turbine combustor screech frequencies, thereby make pressure coupling an important mechanism to be understood in greater detail for a more complete understanding of thermoacoustic instabilities in gas turbines. The fact that a simple single-step chemistry model is used for the analyses needs to be revisited to be able to predict the crossover frequencies with greater accuracy. It must however be borne in mind that the above analyses do not capture high frequency transverse instabilities.

Such analyses provide valuable understanding regarding the importance of various physical phenomena, processes and mechanistic pathways that lead to flame heat release response, and where exactly in the frequency and amplitude spaces, each of these are important. This will serve as a means of streamlining focal areas for engineers and researchers both in the academia and in the industry, by down sampling the sample space of physical processes to consider while engaging in obtaining more physical insight and/or designing practical gas turbine for better performance and lower combustion dynamics.

7.2. Recommendations for Future Research

Further work is necessary in several key areas concerning linear response of premixed flames to upstream disturbances.

First, the ultra-high frequency limits of flame response, which include reaction zone non quasi-steadiness, diffusion zone non-compactness and reaction zone non-compactness cannot be understood using a flame front tracking approach, and the analysis employed in this work would fail to hold. It is necessary to solve the governing equations of fluid dynamics with suitable chemistry models to be able to understand flame response with complex geometries. An alternate approach would be to resort to a detailed analytical resolution of the flame structure employing the length scale separation that the assumption of high activation energy offers.

Second, as may be seen from Figure 35, geometric acoustic non-compactness of the flame is a critical consideration for high frequency response. When the flame is geometrically acoustically non-compact, the Rayleigh quotient is no longer merely proportional to the global spatially integrated heat release. The global heat release of the flame would then overlook the effect of pressure variations within the flame domain, and hence it is necessary to redefine the transfer function to be able to account for these variations.

Third, the current reduced order models do not incorporate the effects of gas expansion and flame-disturbance interaction. Accounting for these effects necessitate solving the G-equation together with the equations of fluid dynamics. More specifically, the hydrodynamics of the reactant and product sides can be solved simultaneously, with

suitable jump conditions at the flame interface. The interface as such, is determined dynamically by the G-equation, which needs information of the upstream flow, thereby making this an implicit procedure. The outcome of a simple closed form expression for the flame response accounting for this important piece of physics would well be worth the tediousness involved in their determination.

Fourth, the current nonlinear computations have been performed in the structurally quasi-steady limit, neglecting interesting high frequency phenomena. Work is needed to study the competition between flame nonlinearities, such as kinematic restoration and flammability crossover, and linear mechanisms, such as flame stretch and structural non quasi-steadiness, which have been seen to lead to flame response reduction. This will require performing a full scale reacting flow computational study with more detailed chemistry than a single-step mechanism.

Fifth, the current analysis does not consider the nonlinear interactions between flow and equivalence ratio perturbations. In most practical systems, equivalence ratio perturbations are caused by flow perturbations and, moreover, equivalence ratio oscillations will also induce flow perturbations because of the temperature jump across the flame. It has been shown by prior analyses that the flame response to flow perturbations can be highly nonlinear. However, it is not clear as to when the effect of one mechanism would dominate over the other. This would be a very physically insightful exercise to undertake and can be performed within the level-set framework used for this work.

Sixth, further work is necessary in understanding the disparities that exist in current comparisons between experimental data and theoretical ROMs with more certainty, either by performing more experiments or with the aid of DNS of the governing equations. Since most practical flames are swirl stabilized, more work is required to understand and model the hydrodynamics of the flow field that results in the mean flame, which will enable the model to migrate towards more fundamental origins than the mean flame shape itself as is the case in the modeling approach in this thesis. In addition to model refinement, there is also a need to determine the most physically meaningful methodology to extract input parameters for the ROMs from experimental data and images. Wrong inputs to a correct model would lead to wrong outputs and erroneous conclusions regarding the capability of the model to predict flame response.

Finally, the ROM developed as a part of this thesis work is strictly only valid for laminar flames. However, as long as a turbulent flame speed can be modeled to substitute the current laminar flame displacement speed that leads to wrinkle destruction, this model is still usable. In other words, for weakly turbulent flames, a model equation similar to the flame front evolution solved in this thesis can be written for the flame front location to study quantities of interest such as the flame brush thickness growth or even the turbulent correction to laminar flame response gain. This effort will enable the ROM to be useful in regimes beyond the laminar flamelet regime of the Borghi diagram.

Appendix A : Equivalence Ratio Disturbance Field

Consider a fuel/air mixture that is perturbed at the base of a flame. The species conservation equation may be written as:

$$\rho \frac{DY_i}{Dt} = w_i + \nabla \bullet \left(\rho \mathscr{D}_i \nabla Y_i \right), \; i = Ox, F \tag{G.1}$$

Assume $w_i = 0$ so that:

$$\rho \frac{DY_i}{Dt} = \nabla \bullet \left(\rho \mathscr{D}_i \nabla Y_i \right) = \rho \mathscr{D}_i \nabla^2 Y_i + \nabla \left(\rho \mathscr{D}_i \right) \bullet \nabla Y_i \tag{G.2}$$

Assume constant density and diffusivity, so that the mass fractions follow:

$$\frac{DY_i}{Dt} = \mathscr{D}_i \nabla^2 Y_i \tag{G.3}$$

Expanding in cylindrical coordinates, we get

$$\frac{\partial Y_i}{\partial t} + u \frac{\partial Y_i}{\partial z} = \mathscr{D}_i \left(\frac{1}{r} \frac{\partial Y_i}{\partial r} + \frac{\partial^2 Y_i}{\partial r^2} + \frac{\partial^2 Y_i}{\partial z^2} \right) \tag{G.4}$$

Now since the equivalence ratio is defined as

$$\phi = \frac{\left(Y_F / Y_{Ox} \right)}{\left(Y_F / Y_{Ox} \right)_s} \tag{G.5}$$

Eq.(G.4) may be cast into an advection equation for equivalence ratio as

$$\frac{D\phi}{Dt} - \mathscr{D}_F \nabla^2 \phi = \frac{1}{Y_{Ox}} \left(\mathscr{D}_F - \mathscr{D}_{Ox} \right) \nabla^2 Y_{Ox} + \frac{2\mathscr{D}_F}{Y_{Ox}} \left(\frac{\partial \phi}{\partial r} \frac{\partial Y_{Ox}}{\partial r} + \frac{\partial \phi}{\partial z} \frac{\partial Y_{Ox}}{\partial z} \right) \tag{G.6}$$

Both the mean and instantaneous equivalence ratio satisfy Eq.(G.6). We first write the mean equation as follows –

$$\bar{Y}_{Ox}\left(\frac{D\bar{\phi}}{Dt} - \mathscr{D}_F \nabla^2 \bar{\phi}\right) = \left(\mathscr{D}_F - \mathscr{D}_{Ox}\right)\nabla^2 \bar{Y}_{Ox} + 2\mathscr{D}_F\left(\frac{\partial \bar{\phi}}{\partial r}\frac{\partial \bar{Y}_{Ox}}{\partial r} + \frac{\partial \bar{\phi}}{\partial z}\frac{\partial \bar{Y}_{Ox}}{\partial z}\right) \quad (G.7)$$

Subtracting Eq.(G.7) from Eq.(G.6) yields equations for the equivalence ratio disturbance as follows –

$$Y_{Ox}'\left(\frac{D\bar{\phi}}{Dt} - \mathscr{D}_F \nabla^2 \bar{\phi}\right) + \bar{Y}_{Ox}\left(\frac{D\phi'}{Dt} - \mathscr{D}_F \nabla^2 \phi'\right) = \begin{cases} \left(\mathscr{D}_F - \mathscr{D}_o\right)\nabla^2 Y_{Ox}' \\ +2\mathscr{D}_F\left(\frac{\partial \phi'}{\partial r}\frac{\partial \bar{Y}_{Ox}}{\partial r} + \frac{\partial \bar{\phi}}{\partial r}\frac{\partial Y_{Ox}'}{\partial r} + \frac{\partial \bar{\phi}}{\partial z}\frac{\partial Y_{Ox}'}{\partial z} + \frac{\partial \phi'}{\partial z}\frac{\partial \bar{Y}_{Ox}}{\partial z}\right) \end{cases}$$

$$Y_{Ox}'\left(\frac{D\phi'}{Dt} - \mathscr{D}_F \nabla^2 \phi'\right) = 2\mathscr{D}_F\left(\frac{\partial \phi'}{\partial r}\frac{\partial Y_{Ox}'}{\partial r} + \frac{\partial \phi'}{\partial z}\frac{\partial Y_{Ox}'}{\partial z}\right)$$

$$(G.8)$$

Assuming that the mean fields are homogeneous and that the fuel and oxidizer mass diffusivities are equal to some average diffusivity, i.e., $\mathscr{D}_F \approx \mathscr{D}_{Ox} = \mathscr{D}$, to linear order, we get –

$$\frac{\partial(\phi'/\phi_o)}{\partial t} + u_o\frac{\partial(\phi'/\phi_o)}{\partial z} = \mathscr{D}\nabla^2(\phi'/\phi_o) \quad (G.9)$$

Expanding in cylindrical coordinates -

$$\frac{\partial(\phi'/\phi_o)}{\partial t} + u_o\frac{\partial(\phi'/\phi_o)}{\partial z} = \mathscr{D}\left(\frac{1}{r}\frac{\partial(\phi'/\phi_o)}{\partial r} + \frac{\partial^2(\phi'/\phi_o)}{\partial r^2}\right) + \mathscr{D}\frac{\partial^2(\phi'/\phi_o)}{\partial z^2} \quad (G.10)$$

We next assume that equivalence ratio disturbances occur at the base, harmonically at a frequency ω, and have a uniform radial profile at the burner exit plane, so that

214

$$\frac{\phi'_{base}}{\phi_o} = \frac{\phi'(r,0,t)}{\phi_o} = \varepsilon_\phi \cos \omega t \tag{G.11}$$

This enables us to neglect radial diffusion altogether in the region of our interest (flame zone). We then obtain from Eq.(G.11) that -

$$\frac{\partial (\phi'/\phi_o)}{\partial t} + u_o \frac{\partial (\phi'/\phi_o)}{\partial z} = \mathscr{D} \frac{\partial^2 (\phi'/\phi_o)}{\partial z^2} \tag{G.12}$$

Writing

$$\frac{\phi'}{\phi_o} = \Phi e^{-i\omega t} \tag{G.13}$$

The evolution equation reduces to

$$i\omega \Phi - u_o \frac{d\Phi}{dz} + \mathscr{D} \frac{d^2\Phi}{dz^2} = 0 \tag{G.14}$$

This has the characteristic equation -

$$i\omega - u_o \aleph + \mathscr{D} \aleph^2 = 0 \tag{G.15}$$

whose roots are -

$$\aleph_\pm = \frac{u_o}{2\mathscr{D}} \left(1 \pm (1-i\Gamma)^{1/2} \right); \quad \Gamma = \frac{4\omega \mathscr{D}}{u_o^2} \tag{G.16}$$

Note also, that,

$$\sqrt{1-i\Gamma} = \sqrt{\frac{\left(1+\Gamma^2\right)^{1/2}+1}{2}} - i\sqrt{\frac{\left(1+\Gamma^2\right)^{1/2}-1}{2}} \tag{G.17}$$

General solution for Φ is hence

$$\Phi(z) = d_1 \exp(\aleph_+ z) + d_2 \exp(\aleph_- z) \tag{G.18}$$

where

$$\aleph_{\pm} = \frac{u_o}{2\mathscr{D}}\left(1 \pm \left(\sqrt{\frac{\left(1+\Gamma^2\right)^{1/2}+1}{2}} - i\sqrt{\frac{\left(1+\Gamma^2\right)^{1/2}-1}{2}}\right)\right) \tag{G.19}$$

Further, diffusion attenuates disturbance amplitude and at infinity, we would have -

$$\phi'(z=\infty,t)=0 \tag{G.20}$$

Note from Eq.(G.19) that $\mathrm{Re}(\aleph_{+}) > 0$ so that the equivalence ratio disturbance amplitude becomes –

$$\Phi(z) = \varepsilon \exp(\aleph_{-}z) \tag{G.21}$$

Further, since $1 - \left(\left(\left(1+\Gamma^2\right)^{1/2}+1\right)\big/2\right)^{1/2} < 0 \ \forall\Gamma \in \mathbb{R}$, we have $\mathrm{Re}(\aleph_{-}) < 0$ so that the equivalence ratio amplitude decays downstream. This now yields an equivalence ratio perturbation field as -

$$\frac{\phi'(z,t)}{\phi_o} = \varepsilon_\phi \exp\left(-\frac{z}{\mathscr{L}_\phi(\omega)}\right)\cos\left(\omega\left(t - \frac{z}{u_{c,\phi}(\omega)}\right)\right) \tag{G.22}$$

where

$$\mathscr{L}_\phi(\omega) = \frac{2\mathscr{D}}{u_o}\left(\sqrt{\frac{\left(1+\Gamma^2\right)^{1/2}+1}{2}} - 1\right)^{-1}$$

$$k_{c,\phi} = \frac{u_o}{u_{c,\phi}} = \sqrt{2\left[\frac{\left(1+\Gamma^2\right)^{1/2}-1}{\Gamma^2}\right]} = k_{c,\phi}(\omega) \tag{G.23}$$

In non-dimensional form (non-dimensionalizing z by L_f, t by (L_f/u_o)) and retaining the same notation for dimensionless coordinates, the equivalence ratio field may be written as

$$\frac{\phi(z,t)}{\phi_o} = 1 + \varepsilon e^{-\aleph z} \cos\left(St\left(t - k_c z\right)\right) \tag{G.24}$$

where, it can be shown that:

$$\aleph = \frac{2St}{\Gamma}\left(\sqrt{\frac{\left(1+\Gamma^2\right)^{1/2}+1}{2}} - 1\right) \triangleq \frac{1}{\mathcal{L}} \tag{G.25}$$

is the inverse of the non-dimensional[16] characteristic diffusive decay length scale, $\mathcal{L}$. Note further, that Γ may be cast into the form:

$$\Gamma = \frac{4\omega\mathbb{D}}{u_o^2} = \frac{4}{Le}\frac{\omega\delta_f}{s_{Lo}}\left(\frac{s_{Lo}}{u_o}\right)^2 = \frac{4}{Le\left(1+\beta^2\right)}St_\delta \tag{G.26}$$

and hence is a measure of non-quasi steadiness of the flame preheat zone. Here, the Lewis number is defined as the ratio of thermal to mass diffusivity of the mixture, i.e., $Le = \mathscr{D}_T/\mathscr{D}$. Further, the thermal diffusivity is given by $\mathscr{D}_T = \delta_f s_{Lo}$. From Eq.(G.26), flame response is non-quasi steady when:

$$\Gamma \sim \frac{8\pi}{Le\left(1+\beta^2\right)} \tag{G.27}$$

Using Eq.(2.11), we get

---

[16] Non-dimensionalized by L_f

$$\frac{\Gamma}{St} = \frac{4\delta}{Le\beta\left(1+\beta^2\right)^{1/2}} \tag{G.28}$$

so that, we have

$$\mathcal{L} = \frac{1}{St}\frac{\Gamma}{2}\left(\sqrt{\frac{\left(1+\Gamma^2\right)^{1/2}+1}{2}}-1\right)^{-1} = \frac{2\delta}{Le\beta\left(1+\beta^2\right)^{1/2}}\left(\sqrt{\frac{\left(1+\Gamma^2\right)^{1/2}+1}{2}}-1\right)^{-1} \tag{G.29}$$

where Γ is given by Eq.(G.26).

In the local and global quasi-steady limit, we have $\Gamma \to 0$. From Eq.(G.25), we then get

$$\lim_{\Gamma \to 0} k_c = 1$$
$$\lim_{\Gamma \to 0} \mathcal{L} = \infty \tag{G.30}$$

Showing that in the quasi-steady limit, axial decay can be neglected and that the equivalence ratio disturbances propagate at the mean flow speed.

In the very high frequency limit, i.e. $\Gamma \gg 1$, from Eq.(G.29), we get

$$\mathcal{L} \sim \frac{2\left(\delta_f/R\right)}{Le\beta\left(1+\beta^2\right)^{1/2}}\sqrt{\frac{2}{\Gamma}} \sim \frac{1}{St_\delta^{1/2}} \tag{G.31}$$

$$K_c \sim \sqrt{\frac{2}{\Gamma}} \sim \frac{1}{St_\delta^{1/2}} \tag{G.32}$$

The following are observed from the variations of decay length and phase speed. Shorter flames face lesser diffusion and thinner flames (lesser diffusion) face lesser variation in phase speed of equivalence ratio disturbances. At higher Strouhal numbers, the phase speed is seen to vary and is no longer a constant. Further, the decay length varies

inversely as the mass diffusivity. This means that for highly diffusive mixtures, the decay length is very short.

Appendix B : Vortical Velocity Disturbance Field

We start with the vortical momentum equation, assuming a homogeneous mean flow velocity profile.

$$\frac{\partial u_{\Omega}'}{\partial t} + \left(u_o \cdot \nabla \right) u_{\Omega}' = \nu \nabla^2 u_{\Omega}'$$
(G.33)

Where, ν is the kinematic viscosity of the reactant mixture. Assuming, as in the case of equivalence ratio perturbations that the perturbations in vortical velocity occur uniformly at the burner exit plane, possessing the form:

$$\frac{u_{\Omega,base}'}{u_o} = \frac{u_{\Omega}'\left(r,0,t \right)}{u_o} = \varepsilon_u \cos \omega t$$
(G.34)

Equation (G.33) can be solved, much like its equivalence ratio counterpart, Eq.(G.12) to yield -

$$\frac{u_{\Omega}'\left(z,t \right)}{u_o} = \varepsilon_u \exp\left(-\frac{z}{\mathcal{L}_u\left(\omega \right)} \right) \cos\left(\omega\left(t - \frac{z}{u_{c,u}\left(\omega \right)} \right) \right)$$
(G.35)

where

$$\mathcal{L}_u\left(\omega \right) = \frac{2\nu}{u_o} \left(\sqrt{\frac{\left(1 + \Gamma_u^{\,2} \right)^{1/2} + 1}{2}} - 1 \right)^{-1}$$

$$k_{c,u} = \frac{u_o}{u_{c,u}} = \sqrt{2\left[\frac{\left(1 + \Gamma_u^{\,2} \right)^{1/2} - 1}{\Gamma_u^{\,2}} \right]} = k_{c,u}\left(\omega \right)$$
(G.36)

$$\Gamma_u = \frac{4\omega\nu}{u_o^{\,2}} = Sc \cdot \Gamma = \frac{4}{\Pr\left(1 + \beta^2 \right)} St_{\delta}$$

In non-dimensional form (non-dimensionalizing z by L_f, t by (L_f/u_o)) and retaining the same notation for dimensionless coordinates, the vortical velocity field may be written as

$$\frac{u_\Omega(z,t)}{u_o} = 1 + \varepsilon_u e^{-\aleph_u z} \cos\left(St\left(t - k_{c,u}z\right)\right) \tag{G.37}$$

where, it can be shown that -

$$\aleph_u = \frac{2St}{\Gamma_u}\left(\sqrt{\frac{\left(1+\Gamma_u^{\,2}\right)^{1/2}+1}{2}} - 1\right) \triangleq \frac{1}{\mathcal{L}_u} \tag{G.38}$$

is the inverse of the non-dimensional[17] characteristic diffusive decay length scale, $\mathcal{L}_u$. The quasi-steady and high Strouhal number tendencies of the phase speed and decay length scales of the velocity disturbances may be studied as for the equivalence ratio disturbances, and they yield the same results.

---

[17] Non-dimensionalized by L_f

Appendix C : Effect of Azimuthal Flame Stretch

This appendix discusses the relative roles of axial and azimuthal stretch on the flame dynamics. Retaining azimuthal stretch, the Fourier transform of the $O(\varepsilon)$ correction to the mean flame surface, at the forcing Strouhal number $\zeta_1(r^*, St) = \hat{\xi}_1$ is described by:

$$\sigma_c^* \frac{d^2 \zeta_1^*}{dr^{*2}} + \left(\frac{\sigma_c^*}{r^*} - 1 \right) \frac{d\zeta^*}{dr^*} - \frac{iSt}{\alpha} \zeta^* = \frac{e^{-i(1-r^*)St}}{\alpha} \tag{G.39}$$

A comparison of azimuthal to axial stretch effects yields

$$\frac{\kappa_{azi}^*}{\kappa_{ax}^*} \sim \frac{\sigma_c^* \left(1/r^* \right) \left(\partial \xi^* / \partial r^* \right)}{\sigma_c^* \left(\partial^2 \xi^* / \partial r^{*2} \right)} \sim \frac{\lambda_c^* \sin\psi}{r^*} \sim \frac{\alpha}{r^*} \cdot \frac{1}{St} \tag{G.40}$$

Here, λ_c^* is the convective wavelength and ψ is the flame half-angle, given by $\cot\psi = \alpha$. This equation shows that the influence of azimuthal stretch decreases as frequency increases, except for very small r values. A representative result, which was obtained by solving equation (G.39) numerically, along with the fixed-anchor and symmetry boundary conditions, Eq.(3.29) and Eq.(3.30) respectively, is provided for the case of $St=10$ in Figure 61.
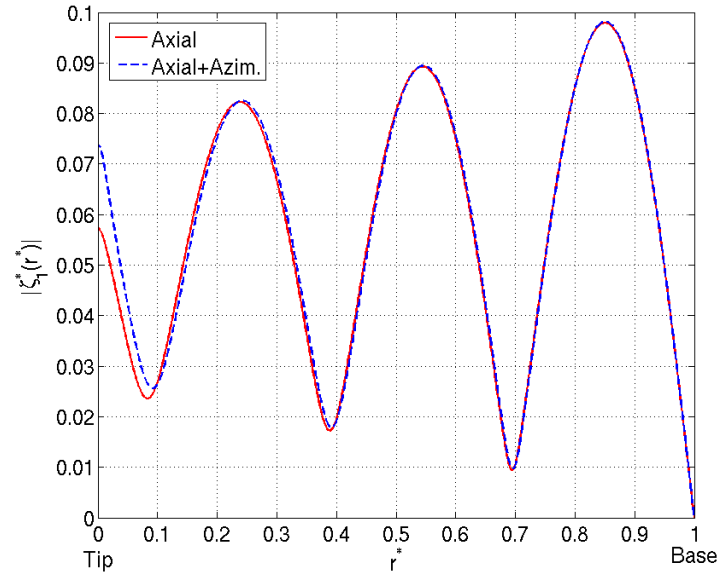
Figure 61 : Variation of the response amplitude of perturbation of the flame front about the mean flame for a conical flame with $\beta=4.0$, $Ma=1$, $\delta^*=0.1$ at a forcing Strouhal number of $St=10$.

This figure shows that the effect of azimuthal stretch is seen only at the flame tip and that over the rest of the flame, there is no significant influence.

Appendix D : Effect of Flame Stretch on the Mean Flame Shape

This appendix considers the stretch-effected solution for the mean flame shape, obtained from Eq.(3.4). The key objective of this section is to demonstrate that the stretch correction to the shape of the mean flame is exponentially small everywhere except near the flame tip, $r=0$. Assume the following relationship for flame speed [122]:

$$\frac{s_L}{s_{Lo}} = 1 - \delta_f \nabla \cdot \hat{n} + Ka(1 - Ma) \tag{G.41}$$

where $\hat{n}$ is the local normal to the flame surface and Ka is the Karlovitz number may be expressed in terms of the flame stretch rate k_{str} as

$$Ka = \frac{\delta_f}{s_{Lo}} k_{str} \tag{G.42}$$

Using Eq.(3.15) for the flame curvature, the dimensionless stationary flame equation is

$$\delta^* \beta \left(\frac{\partial^2 \xi^*}{\partial r^{*2}} + \frac{1}{r^*} \frac{\partial \xi^*}{\partial r^*} + \frac{\beta^2}{r^*} \left(\frac{\partial \xi^*}{\partial r^*} \right)^3 \right) = \left(1 + \beta^2 \left(\frac{\partial \xi^*}{\partial r^*} \right)^2 \right)^{3/2} \left(\frac{\left(1 + \beta^2 \left(\partial \xi^* / \partial r^* \right)^2 \right)^{1/2} - \left(1 + \beta^2 \right)^{1/2}}{\left(1 + \beta^2 \left(\partial \xi^* / \partial r^* \right)^2 \right)^{1/2} - Ma^o \left(1 + \beta^2 \right)^{1/2}} \right)$$

$$\tag{G.43}$$

Here, $Ma^o = 1 - Ma$ and $\delta^* = \delta/R$ is the dimensionless flame thickness. The boundary conditions for Eq.(G.43) are the anchor-fixed boundary condition at the base, Eq.(3.29) and the zero slope at the tip boundary condition, Eq.(3.30). Rewrite these equations as [153] :

$$\frac{d\left(\beta\xi^*\right)}{dr^*} = s$$

$$\delta^* \frac{ds}{dr^*} = V\left(s\right) - \delta^* \frac{f\left(s\right)}{r^*}$$

(G.44)

Here,

$$V\left(s\right) = \left(1+s^2\right)^{3/2} \left(\frac{\left(1+s^2\right)^{1/2} - \left(1+\beta^2\right)^{1/2}}{\left(1+s^2\right)^{1/2} - Ma^o \left(1+\beta^2\right)^{1/2}} \right)$$

$$f\left(s\right) = s + s^3$$

(G.45)

We now write the solution for the flame position as

$$\beta\xi\left(r^*,\delta^*\right) = X\left(r^*,\delta^*\right) + x\left(\rho,\delta^*\right) - x_{match}$$

$$s\left(r^*,\delta^*\right) = \Sigma\left(r^*,\delta^*\right) + \sigma\left(\rho,\delta^*\right)$$

(G.46)

where the stretched coordinate $\rho = r^*/\delta^*$ and x_{match} is a constant used to match the inner solutions (x, σ) and outer solutions (X, Σ). Following standard matched asymptotics procedures in singular perturbation theory [153-155], we note the outer solutions for the position and slope, which are the O(1) terms in the expansion of X and Σ in terms of δ^*, X_o and Σ_o are

$$\Sigma_o = -\beta; \quad X_o = \beta\left(1-r^*\right)$$

(G.47)

thereby satisfying the anchor-fixed boundary condition. Substituting Eq.(G.46) in Eq.(G.43) and substituting for the outer solution terms, we obtain equations for the corrections due to stretch as

$$\frac{dx}{d\rho} = \sigma$$

(G.48)

$$\frac{d\sigma}{d\rho} = V(\Sigma + \sigma) - V(\Sigma) - \frac{f(\Sigma + \sigma) - f(\Sigma)}{\rho} \tag{G.49}$$

Further expanding x, Σ and σ as a series in δ^*

$$\begin{aligned}
x(\rho) &= x_o(r^*) + \delta^* x_1(\rho) + O(\delta^{*2}) \\
\Sigma(r^*) &= \Sigma_o(r^*) + \delta^* \Sigma_1(r^*) + O(\delta^{*2}) \\
\sigma(\rho) &= \sigma_o(\rho) + \delta^* \sigma_1(\rho) + O(\delta^{*2})
\end{aligned} \tag{G.50}$$

and expanding Eqs. (G.48) and (G.49) to first order in δ^*, we obtain

$$\frac{dx_o}{d\rho} = \sigma_o \tag{G.51}$$

$$\frac{d\sigma_o}{d\rho} = V(-\beta + \sigma_o) - \frac{f(-\beta + \sigma_o) - f(-\beta)}{\rho} \tag{G.52}$$

The two boundary conditions on σ_o are:

$$\sigma_o(\rho = 0) = \beta \tag{G.53}$$

$$\sigma_o(\rho = \infty) = 0 \tag{G.54}$$

Using the Mean Value Theorem for f in Eq.(G.52), note that

$$f(-\beta + \sigma_o) - f(-\beta) = f'(\lambda_1)\sigma_o = (3\lambda_1^2 + 1)\sigma_o \geq \sigma_o \tag{G.55}$$

for some $\lambda_1 \in [-\beta, -\beta + \sigma_o] \subseteq [-\beta, 0]$. Hence, we have

$$\frac{d\sigma_o}{d\rho} \leq g(\rho, \sigma_o(\rho))\sigma_o \tag{G.56}$$

where

$$g(\rho) = \underbrace{\frac{V(-\beta + \sigma_o(\rho))}{\sigma_o(\rho)}}_{w(\sigma_o(\rho))} - \frac{1}{\rho} = w(\sigma_o(\rho)) - \frac{1}{\rho} \tag{G.57}$$

Note that

$$g(\rho) < w(\sigma_o(\rho)) \le \max_{\sigma_o \in [0,\beta]} w(\sigma_o(\rho)) \tag{G.58}$$

We will assume below that $Ma > 0$ to prevent the flame tip from opening. Further, given the approximate nature of Eq.(G.41), singularities in the solution can also develop for highly stretched flame tips, corresponding to points where the denominator of V (see Eq.(G.45)) is zero. To avoid such singularities, we require Ma to satisfy

$$Ma > 1 - \frac{1}{\left(1 + \beta^2\right)^{1/2}} \tag{G.59}$$

We split the interval of Markstein numbers given by Eq.(G.59) into two intervals, $Ma > 2$ and $Ma \in \left(1 - \left(1 + \beta^2\right)^{-1/2}, 2\right]$ for ease of further analysis.

Case (i) - $Ma > 2$:

For this case, it may be shown that

$$\max_{\sigma_o \in [0,\beta]} \frac{V(-\beta + \sigma_o)}{\sigma_o} = \frac{V(0)}{\beta} = -\frac{\beta}{\left(\left|Ma^o\right|\sqrt{1+\beta^2} + 1\right)\left(\sqrt{1+\beta^2} + 1\right)} < 0 \tag{G.60}$$

This gives

$$\frac{d\sigma_o}{d\rho} \le -\frac{\beta}{\left(\left|Ma^o\right|\sqrt{1+\beta^2} + 1\right)\left(\sqrt{1+\beta^2} + 1\right)} \sigma_o \tag{G.61}$$

which further yields that

$$\sigma_o = \beta\, O\left(e^{-\frac{\beta}{\left(|Ma^o|\sqrt{1+\beta^2}+1\right)\left(\sqrt{1+\beta^2}+1\right)^{\rho}}} \right) \tag{G.62}$$

<u>Case (ii) :</u> $Ma \in \left(1-\left(1+\beta^2\right)^{-1/2},2\right]$

We begin by noting that

$$w\left(\sigma_o\left(\rho\right)\right) = \frac{V\left(-\beta+\sigma_o\left(\rho\right)\right)}{\sigma_o\left(\rho\right)} < 0 \;\; \forall \rho \in \left(0,\infty\right) \tag{G.63}$$

Hence,

$$g\left(\rho\right) < w\left(\sigma_o\left(\rho\right)\right) < 0, \;\; \forall \rho \in \left[0,\infty\right) \tag{G.64}$$

We next show that w attains a maximum for $\rho \in \left[0,\infty\right)$. To see this, note that

$$w_o = w\left(\sigma_o\left(0\right)\right) = -\frac{\left(1+\beta^2\right)^{1/2}-1}{\beta\left(1-Ma^o\left(1+\beta^2\right)^{1/2}\right)} < 0 \tag{G.65}$$

$$w_\infty = w\left(\sigma_o\left(\infty\right)\right) = -\frac{\beta\left(1+\beta^2\right)^{1/2}}{1-Ma^o} = -\frac{\delta^*}{\sigma_c^{\;*}} < 0 \tag{G.66}$$

Further, w has no singularities in $\left[0,\infty\right)$ and is continuous and always lesser than zero.

This implies that there exists

$$\eta = \max_{\rho\in[0,\infty)} w\left(\sigma_o\left(\rho\right)\right) = \max\left\{w_o,w_\infty,w^*\right\} < 0 \tag{G.67}$$

for some $\rho *$ in $\left[0,\infty\right)$. Hence we have

$$\frac{d\sigma_o}{d\rho} \le -|\eta|\sigma_o \tag{G.68}$$

228

implying

$$\sigma_o \le \beta e^{-|\eta|\rho} \tag{G.69}$$

To conclude, we note that for $Ma^o < \left(1+\beta^2\right)^{-1/2}$ or equivalently, for $Ma > 1 - \left(1+\beta^2\right)^{-1/2}$

, irrespective of η, since

$$\lim_{\rho \to 0} \left| \frac{\sigma_o/\beta}{e^{-|\eta|\rho}} \right| = \lim_{\rho \to 0} \left| \frac{\sigma_o}{\beta} e^{\rho\delta^*/\sigma_c^*} \right| \le 1 \tag{G.70}$$

we can write

$$\sigma_o = \beta \, \mathrm{O}\left(e^{-\rho\delta^*/\sigma_c^*}\right) \tag{G.71}$$

Further,
$$x_o(\rho) = \int_0^\rho \sigma_o \, d\rho = \beta \left(1 - \frac{\sigma_c^*}{\delta^*} \mathrm{O}\left(e^{-\rho\delta^*/\sigma_c^*}\right) \right) \tag{G.72}$$

Hence, matching yields

$$\xi(r^*) = (1 - r^*) - \frac{Ma}{\beta\left(1+\beta^2\right)^{1/2}} \mathrm{O}\left(e^{-r^*/\sigma_c^*}\right) \tag{G.73}$$

Appendix E : Equivalence Ratio Coupled Linear Transfer Functions

Flame position solution:

$$\hat{\xi}_1\left(r^*\right) = \frac{s_{L1}e^{\Lambda_\phi\left(1-r^*\right)}}{H_c\left(G_1 + i\Lambda_\phi\right)\left(G_2 + i\Lambda_\phi\right)} + C_1 e^{G_1 r^*} + C_2 e^{G_2 r^*} \qquad \text{(G.74)}$$

This is the general solution, and the constants C_1 and C_2 will depend upon the boundary conditions. As can be seen, in the flame stretch affected case, the homogeneous solution (local solution) and the particular solution (the BC solution) are both affected by diffusion.

In the above,

$$G_{1,2} = \frac{-1 \pm \left(1 - 4i\sigma_c^* St_2\right)^{1/2}}{2\sigma_c^*}; \ H_c = \alpha\sigma_c^* \quad \text{(G.75)}$$

Axisymmetric V-flames:

$$C_1 = \left(-\frac{s_{L1}}{H_c}\right)\frac{\left(G_2^2 + \Lambda_\phi^2 e^{G_2 + i\Lambda_\phi}\right)}{\left(e^{G_2}G_1^2 - e^{G_1}G_2^2\right)\left(G_1 + i\Lambda_\phi\right)\left(G_2 + i\Lambda_\phi\right)}$$

$$C_2 = \left(-\frac{s_{L1}}{H_c}\right)\frac{\left(G_1^2 + \Lambda_\phi^2 e^{G_1 + i\Lambda_\phi}\right)}{\left(e^{G_2}G_1^2 - e^{G_1}G_2^2\right)\left(G_1 + i\Lambda_\phi\right)\left(G_2 + i\Lambda_\phi\right)} \qquad \text{(G.76)}$$

$$F_A = -2\alpha\left(C_1 f\left(G_1\right) + C_2 f\left(G_2\right) - \frac{s_{L1}}{H_c\left(G_1 + i\Lambda_\phi\right)\left(G_2 + i\Lambda_\phi\right)}ie^{i\Lambda_\phi}f\left(-i\Lambda_\phi\right)\right) \quad \text{(G.77)}$$

$$F_{s_L} = -2H_c \left(C_1 G_1 f(G_1) + C_2 G_2 f(G_2) + \left(\frac{s_{L1,\phi}}{H_c} \right) \left(\frac{G_1 G_2 + i\Lambda_\phi (G_1 + G_2)}{(G_1 + i\Lambda_\phi)(G_2 + i\Lambda_\phi)} \right) \frac{e^{i\Lambda_\phi}}{i\Lambda_\phi} f(-i\Lambda_\phi) \right) \quad \text{(G.78)}$$

$$F_{h_R} = -2h_{R1,\phi} \frac{e^{i\Lambda_\phi}}{i\Lambda_\phi} f(-i\Lambda_\phi) \quad \text{(G.79)}$$

where $f(x) = \dfrac{e^x - x - 1}{x}$.

Conical flames:

$$C_1 = -\left(\frac{s_{L1}}{H_c} \right) \frac{\left(G_2 + i\Lambda_\phi e^{G_2 + i\Lambda_\phi} \right)}{\left(e^{G_2} G_1 - e^{G_1} G_2 \right)(G_1 + i\Lambda_\phi)(G_2 + i\Lambda_\phi)}$$

$$\quad \text{(G.80)}$$

$$C_2 = -\left(\frac{s_{L1}}{H_c} \right) \frac{\left(G_1 + i\Lambda_\phi e^{G_1 + i\Lambda_\phi} \right)}{\left(e^{G_2} G_1 - e^{G_1} G_2 \right)(G_1 + i\Lambda_\phi)(G_2 + i\Lambda_\phi)}$$

$$F_A = 2\alpha \left(C_1 e^{G_1} f(-G_1) + C_2 e^{G_2} f(-G_2) + \left(\frac{s_{L1}}{H_c} \right) \frac{f(i\Lambda_\phi)}{(G_1 + i\Lambda_\phi)(G_2 + i\Lambda_\phi)} \right) \quad \text{(G.81)}$$

$$F_{s_L} = 2H_c \left(C_1 G_1 e^{G_1} f(-G_1) + C_2 G_2 e^{G_2} f(-G_2) + \left(\frac{s_{L1}}{H_c} \right) \left(1 + \frac{\Lambda_\phi^2}{(G_1 + i\Lambda_\phi)(G_2 + i\Lambda_\phi)} \right) \frac{f(i\Lambda_\phi)}{i\Lambda_\phi} \right)$$

$$\text{(G.82)}$$

$$F_{h_R} = 2h_{R1,\phi} \frac{f(i\Lambda_\phi)}{i\Lambda_\phi} \quad \text{(G.83)}$$

where $f(x) = \dfrac{e^x - x - 1}{x}$.

2D V-flames:

$$C_1 = \left(-\frac{s_{L1}}{H_c}\right)\frac{\left(G_2^{\;2} + \Lambda_\phi^{\;2} e^{G_2 + i\Lambda_\phi}\right)}{\left(e^{G_2}G_1^{\;2} - e^{G_1}G_2^{\;2}\right)\left(G_1 + i\Lambda_\phi\right)\left(G_2 + i\Lambda_\phi\right)}$$

$$(G.84)$$

$$C_2 = \left(-\frac{s_{L1}}{H_c}\right)\frac{\left(G_1^{\;2} + \Lambda_\phi^{\;2} e^{G_1 + i\Lambda_\phi}\right)}{\left(e^{G_2}G_1^{\;2} - e^{G_1}G_2^{\;2}\right)\left(G_1 + i\Lambda_\phi\right)\left(G_2 + i\Lambda_\phi\right)}$$

$$F_A = \alpha\left(-C_1 G_1 g\left(G_1\right) - C_2 G_2 g\left(G_2\right) + \frac{s_{L1,\phi}}{H_c\left(G_1 + i\Lambda_\phi\right)\left(G_2 + i\Lambda_\phi\right)} i\Lambda_\phi g\left(i\Lambda_\phi\right)\right) \quad (G.85)$$

$$F_{s_L} = H_c\left(-C_1 G_1^{\;2} g\left(G_1\right) - C_2 G_2^{\;2} g\left(G_2\right) + \frac{s_{L1,\phi}}{H_c} g\left(i\Lambda_\phi\right)\left(1 + \frac{\Lambda_\phi^{\;2}}{\left(G_2 + i\Lambda_\phi\right)\left(G_1 + i\Lambda_\phi\right)}\right)\right) (G.86)$$

$$F_{h_R} = h_{R1,\phi} g\left(i\Lambda_\phi\right) \quad\quad (G.87)$$

where $g\left(x\right) = \dfrac{e^x - 1}{x}$.

Appendix F : Velocity Coupled Transfer Functions

Flame position solution:

$$\hat{\xi}_1\left(r^*\right) = \frac{\left(1 - iH_s\Lambda_u\right)e^{\Lambda_u\left(1-r^*\right)}}{H_c\left(G_1 + i\Lambda_u\right)\left(G_2 + i\Lambda_u\right)} + C_1 e^{G_1 r^*} + C_2 e^{G_2 r^*} \; ; \; H_s = \sigma_s^* \qquad \text{(G.88)}$$

Axisymmetric V-flames:

$$C_1 = \left(\frac{-1 + iH_s\Lambda_u}{H_c}\right)\frac{\left(G_2^2 + \Lambda_u^2 e^{G_2 + i\Lambda_u}\right)}{\left(e^{G_2}G_1^2 - e^{G_1}G_2^2\right)\left(G_1 + i\Lambda_u\right)\left(G_2 + i\Lambda_u\right)}$$

$$\qquad\qquad \text{(G.89)}$$

$$C_2 = \left(\frac{-1 + iH_s\Lambda_u}{H_c}\right)\frac{\left(G_1^2 + \Lambda_u^2 e^{G_1 + i\Lambda_u}\right)}{\left(e^{G_2}G_1^2 - e^{G_1}G_2^2\right)\left(G_1 + i\Lambda_u\right)\left(G_2 + i\Lambda_u\right)}$$

$$F_A = -2\alpha\left(C_1 f\left(G_1\right) + C_2 f\left(G_2\right) + \frac{iH_s\Lambda_u - 1}{H_c\left(G_1 + i\Lambda_u\right)\left(G_2 + i\Lambda_u\right)} ie^{i\Lambda_u} f\left(-i\Lambda_u\right)\right) \quad \text{(G.90)}$$

$$F_{s_L} = -2H_c\left(C_1 G_1 f\left(G_1\right) + C_2 G_2 f\left(G_2\right) + \left(\frac{1 - iH_s\Lambda_u}{H_c}\right)\left(\frac{G_1 G_2 + i\Lambda_u\left(G_1 + G_2\right)}{\left(G_1 + i\Lambda_u\right)\left(G_2 + i\Lambda_u\right)}\right)\frac{e^{i\Lambda_u}}{i\Lambda_u} f\left(-i\Lambda_u\right)\right)$$

$$\text{(G.91)}$$

where $f\left(x\right) = \dfrac{e^x - x - 1}{x}$.

Conical flames:

$$C_1 = -\left(\frac{1-iH_s\Lambda_u}{H_c}\right)\frac{\left(G_2 + i\Lambda_u e^{G_2+i\Lambda_u}\right)}{\left(e^{G_2}G_1 - e^{G_1}G_2\right)\left(G_1 + i\Lambda_u\right)\left(G_2 + i\Lambda_u\right)}$$

$$C_2 = -\left(\frac{1-iH_s\Lambda_u}{H_c}\right)\frac{\left(G_1 + i\Lambda_u e^{G_1+i\Lambda_u}\right)}{\left(e^{G_2}G_1 - e^{G_1}G_2\right)\left(G_1 + i\Lambda_u\right)\left(G_2 + i\Lambda_u\right)}$$

(G.92)

$$F_A = 2\alpha\left(C_1 e^{G_1} f\left(-G_1\right) + C_2 e^{G_2} f\left(-G_2\right) + \left(\frac{s_{L1}}{H_c}\right)\frac{f\left(i\Lambda_u\right)}{\left(G_1 + i\Lambda_u\right)\left(G_2 + i\Lambda_u\right)}\right) \quad \text{(G.93)}$$

$$F_{s_L} = 2H_c\left(C_1 G_1 e^{G_1} f\left(-G_1\right) + C_2 G_2 e^{G_2} f\left(-G_2\right) + \left(\frac{s_{L1}}{H_c}\right)\left(1 + \frac{\Lambda_u^2}{\left(G_1 + i\Lambda_u\right)\left(G_2 + i\Lambda_u\right)}\right)\frac{f\left(i\Lambda_u\right)}{i\Lambda_u}\right)$$

(G.94)

where $f\left(x\right) = \dfrac{e^x - x - 1}{x}$.

2D V-flames:

$$C_1 = \left(\frac{-1+iH_s\Lambda_u}{H_c}\right)\frac{\left(G_2^2 + \Lambda_u^2 e^{G_2+i\Lambda_u}\right)}{\left(e^{G_2}G_1^2 - e^{G_1}G_2^2\right)\left(G_1 + i\Lambda_u\right)\left(G_2 + i\Lambda_u\right)}$$

$$C_2 = \left(\frac{-1+iH_s\Lambda_u}{H_c}\right)\frac{\left(G_1^2 + \Lambda_u^2 e^{G_1+i\Lambda_u}\right)}{\left(e^{G_2}G_1^2 - e^{G_1}G_2^2\right)\left(G_1 + i\Lambda_u\right)\left(G_2 + i\Lambda_u\right)}$$

(G.95)

$$F_A = \alpha\left(-C_1 G_1 g\left(G_1\right) - C_2 G_2 g\left(G_2\right) + \frac{1-iH_s\Lambda_u}{H_c\left(G_1 + i\Lambda_u\right)\left(G_2 + i\Lambda_u\right)}i\Lambda_u g\left(i\Lambda_u\right)\right) \quad \text{(G.96)}$$

$$F_{s_L} = H_c\left(-C_1 G_1^2 g\left(G_1\right) - C_2 G_2^2 g\left(G_2\right) + \left(\frac{1-iH_s\Lambda_u}{H_c}\right)\left(1 + \frac{\Lambda_u^2}{\left(G_2 + i\Lambda_u\right)\left(G_1 + i\Lambda_u\right)}\right)g\left(i\Lambda_u\right)\right) \quad \text{(G.97)}$$

where $g\left(x\right) = \dfrac{e^x - 1}{x}$.

$$\xi_2(r,t) = \frac{1}{8(1-\alpha)^2 \alpha^2 St} \left\{ \begin{array}{l} 2(1-\alpha)rSt\left(1+3\alpha^2\right)s_{L1}^{2} + 2a(1-\alpha)s_{L2} + s_{L1}^{2}\cos\left(2St_2\left(\alpha t-1+r\right)\right) \\[2mm] +\alpha^2 \left(\begin{array}{l} 8s_{L1}^{2}\sin\left(St_2(1-r)(1-\alpha)\right) \\[1mm] +\left(3\alpha s_{L1}^{2}+2(1-\alpha)s_{L2}\right)\sin\left(2St(1-r-t)\right) \\[1mm] -\left((3\alpha-8)s_{L1}^{2}+2(1-\alpha)s_{L2}\right)\sin\left(2St_2(1-r-\alpha t)\right) \\[1mm] -8s_{L1}^{2}\sin\left(St_2\left((1+\alpha)(1-r)-2\alpha t\right)\right) \end{array} \right) \end{array} \right\}$$

(G.98)

$$\xi_3(r,t) = \frac{1}{24(1-\alpha)^3 St_2} \left\{ \begin{array}{l} 12St_2 s_{L1}^{3}(1-\alpha)(1-r)\cos\left(St_2\left((2-\alpha)(1-r)-\alpha t\right)\right)+ \\[2mm] 3s_{L1}St_2\alpha^{-1}(1-\alpha)(1-r)\left\{ \begin{array}{l}\left(12\alpha^3-5\alpha^2+8\alpha-3\right)s_{L1}^{3} \\ -2\alpha(1-\alpha)(3-4\alpha)s_{L2}\end{array}\right\}\cos\left(St_2(1-r-\alpha t)\right)+ \\[2mm] 3s_{L1}St_2\alpha^{-1}(1-\alpha)(1-r)\left\{ \begin{array}{l}\left(3\alpha^2-8\alpha+1\right)s_{L1}^{2}+ \\ 2\alpha(1-\alpha)s_{L2}\end{array}\right\}\cos\left(3St_2(1-r-\alpha t)\right)- \\[2mm] 12s_{L1}^{3}St_2(1-\alpha)(1-r)\cos\left(St_2\left((a+2)(1-r)-3\alpha t\right)\right)- \\[2mm] 3\sin\left(St(1-r-t)\right)\left\{ \begin{array}{l}\left(2-4\alpha+9\alpha^2-12a^3\right)s_{L1}^{3}+ \\ 2\alpha(4-9\alpha)(1-\alpha)s_{L1}s_{L2}-6\alpha(1-\alpha)^2 s_{L3}\end{array}\right\}+ \\[2mm] \alpha\sin\left(3St(1-r-t)\right)\left\{\alpha s_{L1}^{3}(1+4\alpha)-6\alpha(1-\alpha)s_{L1}s_{L2}+2(1-\alpha)^2 s_{L3}\right\}+ \\[2mm] 3\sin\left(St_2\left((2-\alpha)(1-r)-\alpha t\right)\right)\left\{\left(6\alpha^2-18\alpha+1\right)s_{L1}^{3}+4\alpha(1-\alpha)s_{L1}s_{L2}\right\}- \\[2mm] 3\sin\left(St_2(1-r-t)\right)\left\{ \begin{array}{l}\left(12\alpha^3-6\alpha^2-11\alpha-1\right)s_{L1}^{3}+6\alpha(1-\alpha)(1-3\alpha)s_{L1}s_{L2}- \\ 6\alpha(1-\alpha)^2 s_{L3}+(1-\alpha)^2(1-r)^2 St_2^{2}s_{L1}^{3}\alpha^{-1}\end{array}\right\}- \\[2mm] \sin\left(3St_2(1-r-\alpha t)\right)\left\{ \begin{array}{l}\left(4\alpha^3-26\alpha^2+39\alpha-3\right)s_{L1}^{3}-6\alpha(1-\alpha)(3-\alpha)s_{L1}s_{L2}+ \\ 2\alpha(1-\alpha)^2 s_{L3}-3\alpha^{-1}(1-\alpha)^2(1-r)^2 St_2^{2}s_{L1}^{3}\end{array}\right\} \\[2mm] 3s_{L1}\sin\left(St_2\left((2+\alpha)(1-r)-3\alpha t\right)\right)\left\{\left(6\alpha^2-18\alpha+1\right)s_{L1}^{2}+4\alpha(1-\alpha)s_{L2}\right\}+ \\[2mm] 3\alpha(1-\alpha)\left\{s_{L1}\left(3s_{L1}^{2}-2s_{L2}\right)\right\}\sin\left(St_2\left((2\alpha-1)(1-r)-\alpha t\right)\right)- \\[2mm] 3\alpha s_{L1}\left((5+3\alpha)s_{L1}^{2}+2(1-\alpha)s_{L2}\right)\sin\left(St_2\left((1+2\alpha)(1-r)-3\alpha t\right)\right) \end{array} \right\}$$

(G.99)

Appendix H : Nonlinear Equivalence Ratio Coupled Flame Transfer Functions

The expressions for the constituents of the non-linear transfer function up to second order

in perturbation amplitude are presented below.

Burning area contribution

$$F_A = F_{A,o} + \varepsilon^2 F_{A,2} \qquad \text{(G.100)}$$

where ,

$$F_{A,o} = s_{L_1} \left\{ \frac{2\alpha}{1-\alpha} \left(\frac{1-\alpha - \exp(iSt) + \alpha\exp\left(iSt/\alpha\right)}{St^2} \right) \right\} \qquad \text{(G.101)}$$

$$F_{A,2} = \frac{1}{4\alpha^4 (2\alpha-1)^2 (1-\alpha)^3 (2-\alpha)^3 St_2^2} \sum_{j=1}^{27} A_j \qquad \text{(G.102)}$$

where,

$$A_1 = -\alpha(1-\alpha)^3\left(32\alpha^7 - 216\alpha^6 + 594\alpha^5 - 839\alpha^4 + 591\alpha^3 - 214\alpha^2 + 72\alpha - 16\right)$$

$$A_2 = -8\alpha\left(3\alpha^9 + 2\right)s_{L1}^{\ 3}\exp(i\alpha St_2)$$

$$A_3 = 336\alpha^{10}s_{L1}^{\ 3}\exp(iSt_2)$$

$$A_4 = \alpha^4(1-\alpha)(1+2\alpha)(2-\alpha)^3 s_{L1}^{\ 3}\exp\left(i(2\alpha-1)St_2\right)$$

$$A_5 = \alpha^3(2\alpha-1)^2\left(3\alpha^4 - 23\alpha^3 + 56\alpha^2 - 37\alpha - 10\right)s_{L1}^{\ 3}\exp\left(i(2-\alpha)St_2\right)$$

$$A_6 = -\alpha^3\left(32\alpha^8 + 1508\alpha^6 - 3748\alpha^5 + 5567\alpha^4 - 4963\alpha^3 + 2538\alpha^2 - 676\alpha + 72\right)s_{L1}^{\ 3}\exp(iSt_2)$$

$$A_7 = \alpha^2\left(156\alpha^7 - 330\alpha^6 + 113\alpha^5 + 552\alpha^4 - 948\alpha^3 + 778\alpha^2 - 396\alpha + 120\right)s_{L1}^{\ 3}\exp(i\alpha St_2)$$

$$A_8 = 2\alpha^2(2-\alpha)(1-\alpha)^3\left(12\alpha^5 - 24\alpha^4 - 44\alpha^3 + 103\alpha^2 - 52\alpha + 8\right)s_{L1}s_{L2}$$

$$A_9 = 48\alpha^{10}s_{L1}s_{L2}\exp(i\alpha St_2)$$

$$A_{10} = 120\alpha^{10}s_{L1}s_{L2}\exp(iSt_2)$$

$$A_{11} = -2\alpha^5(1-\alpha)(2-\alpha)^3 s_{L1}s_{L2}\exp\left(i(2\alpha-1)St_2\right)$$

$$A_{12} = 2\alpha^4(1-\alpha)(2-\alpha)(3-\alpha)(2\alpha-1)^2 s_{L1}s_{L2}\exp\left(i(2-\alpha)St_2\right)$$

$$A_{13} = -6\alpha^3\left(4\alpha^8 - 3\alpha^6 + 208\alpha^5 - 549\alpha^4 + 656\alpha^3 - 408\alpha^2 + 128\alpha - 16\right)s_{L1}s_{L2}\exp(iSt_2)$$

$$A_{14} = -2\alpha^2\left(188\alpha^7 - 566\alpha^6 + 789\alpha^5 - 419\alpha^4 - 136\alpha^3 + 264\alpha^2 - 112\alpha + 16\right)s_{L1}s_{L2}\exp(i\alpha St_2)$$

$$A_{15} = -6\alpha^3(2\alpha-1)^2(1-\alpha)^3(2-\alpha)^3 s_{L3}$$

$$A_{16} = -24\alpha^{10}s_{L3}\exp(i\alpha St_2)$$

$$A_{17} = -216\alpha^{10}s_{L3}\exp(iSt_2)$$

$$A_{18} = 6\alpha^4\left(4\alpha^7 + 133\alpha^5 - 260\alpha^4 + 289\alpha^3 - 182\alpha^2 + 60\alpha - 8\right)s_{L3}\exp(iSt_2)$$

$$A_{19} = 6\alpha^3\left(4\alpha^2 - 5\alpha + 2\right)\left(9\alpha^4 - 22\alpha^3 + 33\alpha^2 - 20\alpha + 4\right)s_{L3}\exp(i\alpha St_2)$$

$$A_{20} = -2i\alpha^2(2-\alpha)(2\alpha-1)(1-\alpha)^4\left(2\alpha^3 - 7\alpha^2 + 8\alpha + 2\right)s_{L1}^{\ 3}St_2$$

$$A_{21} = 48i\alpha^{11}s_{L1}^{\ 3}St_2\exp(iSt_2)$$

$$A_{22} = 2i\alpha^3(1-\alpha)(2-\alpha)(3-\alpha)(2\alpha-1)^2 s_{L1}^{\ 3}St_2\exp\left(i(2-\alpha)St_2\right)$$

$$A_{23} = -i\alpha^2\left(404\alpha^8 - 1388\alpha^7 + 2537\alpha^6 - 2727\alpha^5 + 1809\alpha^4 - 717\alpha^3 + 118\alpha^2 + 20\alpha - 8\right)s_{L1}^{\ 3}St_2\exp(iSt_2)$$

$$A_{24} = 4i\alpha^3(1+\alpha)(2\alpha-1)(2-\alpha)^2(1-\alpha)^4 s_{L1}s_{L2}St_2$$

$$A_{25} = -32i\alpha^{11}s_{L1}s_{L2}St_2\exp(iSt_2)$$

$$A_{26} = 2i\alpha^3\left(156\alpha^7 - 640\alpha^6 + 1439\alpha^5 - 1936\alpha^4 + 1595\alpha^3 - 786\alpha^2 + 212\alpha - 24\right)s_{L1}s_{L2}St_2\exp(iSt_2)$$

$$A_{27} = \alpha^2(1-\alpha)^2(2\alpha-1)^2(2-\alpha)^3 s_{L1}^{\ 3}St_2^2\exp(iSt_2)$$

$$(G.103)$$

Mass Burning Rate contribution

$$F_{s_L-A} = F_{o,s_L-A} + \varepsilon^2 F_{2,s_L-A} \qquad \text{(G.104)}$$

Where,

$$F_{o,s_L-A} = F_{o,s_L-A} = s_{L1} \left\{ \frac{2}{St^2}\left(1 + iSt - \exp(iSt)\right) \right\} \qquad \text{(G.105)}$$

and,

$$F_{2,s_L-A} = -\frac{1}{4\alpha^2 \left(1-2\alpha\right)^2 \left(1-\alpha\right)^2 \left(2-\alpha\right)^3 St_2^2} \sum_{j=1}^{16} S_j \qquad \text{(G.106)}$$

where,

$$S_1 = -2\alpha(1-\alpha)^2 \left(8\alpha^5 - 44\alpha^4 + 91\alpha^3 - 102\alpha^2 + 60\alpha - 10\right) s_{L1}^3$$

$$S_2 = 2\alpha^2 (1-\alpha)(2-\alpha)^3 s_{L1}^3 \exp\left(iSt_2 (2\alpha-1)\right)$$

$$S_3 = \alpha(2\alpha-1)^2 \left(3\alpha^3 - 14\alpha^2 + 12\alpha + 4\right) s_{L1}^3 \exp\left(i(2-\alpha)St_2\right)$$

$$S_4 = 4\alpha^2 \left(4\alpha^6 - 24\alpha^5 + 45\alpha^4 - 13\alpha^3 - 42\alpha^2 + 36\alpha + 8\right) s_{L1}^3 \exp\left(iSt_2\right)$$

$$S_5 = 3\alpha(2-\alpha)^3 (2\alpha-1)^3 s_{L1}^3 \exp\left(i\alpha St_2\right)$$

$$S_6 = 2(2-\alpha)(1-\alpha)^3 \left(8\alpha^4 - 48\alpha^3 + 95\alpha^2 - 48\alpha + 8\right) s_{L1} s_{L2}$$

$$S_7 = -2\alpha^2 (1-\alpha)(2-\alpha)^3 s_{L1} s_{L2} \exp\left(i(2\alpha-1)St_2\right)$$

$$S_8 = -2\alpha^2 (1-\alpha)(2-\alpha)(2\alpha-1)^2 s_{L1} s_{L2} \exp\left(i(2-\alpha)St_2\right)$$

$$S_9 = 4\alpha^2 (1-\alpha)(2\alpha-1)^3 (2-\alpha)^3 s_{L1} s_{L2} \exp\left(iSt_2\right)$$

$$S_{10} = 4(1-\alpha)(3\alpha-1)(2\alpha-1)^2 (2-\alpha)^3 s_{L1} s_{L2} \exp\left(i\alpha St_2\right)$$

$$S_{11} = -6(1-\alpha)^2 (2\alpha-1)^2 (2-\alpha)^3 s_{L3}$$

$$S_{12} = 6(1-\alpha)^2 (2\alpha-1)^2 (2-\alpha)^3 s_{L3} \exp\left(i\alpha St_2\right)$$

$$S_{13} = -2i\alpha(2-\alpha)(2\alpha-1)(1-\alpha)^2 \left(2\alpha^3 - 10\alpha^2 + 11\alpha - 1\right) s_{L1}^3 St_2$$

$$S_{14} = -2i\alpha(1-\alpha)(2-\alpha)(2\alpha-1)^2 s_{L1}^3 St_2 \exp\left(i(2-\alpha)St_2\right) \qquad \text{(G.107)}$$

$$S_{15} = -2i\alpha(2\alpha-1)(1-\alpha)^2 (2-\alpha)^2 s_{L1} s_{L2} St_2$$

$$S_{16} = -6i\alpha(1-\alpha)^2 (2\alpha-1)^2 (2-\alpha)^3 s_{L3} St_2$$

Heat of reaction contribution

$$F_{h_R - A} = F_{o, h_R - A} + \varepsilon^2 F_{2, h_R - A} \qquad \text{(G.108)}$$

$$F_{o, h_R - A} = h_{R1} \left\{ \frac{2}{St^2} \left(1 + iSt - \exp(iSt)\right) \right\} \qquad \text{(G.109)}$$

$$F_{2, h_R - A} = -\frac{1}{4\alpha^2 (1 - 2\alpha)^2 (1 - \alpha)^2 (2 - \alpha)^3 St_2^2} \sum_{j=1}^{19} H_j \quad \text{(G.110)}$$

$$H_1 = -6(1-\alpha)^2 (2\alpha-1)^2 (2-\alpha)^3 h_{R3}$$

$$H_2 = 6(1-\alpha)^2 (2\alpha-1)^2 (2-\alpha)^3 h_{R3} \exp(i\alpha St_2)$$

$$H_3 = -2\alpha(1-\alpha)^2 (8\alpha^2 - 12\alpha + 3)(2-\alpha)^3 h_{R2} s_{L1}$$

$$H_4 = -4\alpha^2 (1-\alpha)(1-2\alpha)^2 (2-\alpha)^3 h_{R2} s_{L1} \exp(iSt_2)$$

$$H_5 = 6\alpha(1-\alpha)(1-2\alpha)^2 (2-\alpha)^3 h_{R2} s_{L1} \exp(i\alpha St_2)$$

$$H_6 = -2\alpha^2 (1-\alpha)(2-\alpha)^3 h_{R2} s_{L1} \exp(i(2\alpha-1) St_2)$$

$$H_7 = -2\alpha(1-\alpha)^2 (8\alpha^5 - 44\alpha^4 + 91\alpha^3 - 102\alpha^2 + 60\alpha - 10) h_{R1} s_{L1}^2$$

$$H_8 = \alpha(1-2\alpha)^2 (3\alpha^3 - 14\alpha^2 + 12\alpha + 4) h_{R1} s_{L1}^2 \exp(i(2-\alpha) St_2)$$

$$H_9 = -4\alpha^2 (1+\alpha)(1-2\alpha)^2 (2-\alpha)^3 h_{R1} s_{L1}^2 \exp(iSt_2)$$

$$H_{10} = 3\alpha(2-\alpha)^3 (2\alpha-1)^3 h_{R1} s_{L1}^2 \exp(i\alpha St_2)$$

$$H_{11} = 2\alpha^2 (1-\alpha)(2-\alpha)^3 h_{R1} s_{L1}^2 \exp(iSt_2 (2\alpha-1))$$

$$H_{12} = 2(2-\alpha)(1-\alpha)^2 (2\alpha-1)^2 (3\alpha^2 - 12\alpha + 8) h_{R1} s_{L2}$$

$$H_{13} = -2\alpha^2 (1-\alpha)(2-\alpha)(2\alpha-1)^2 h_{R1} s_{L2} \exp(i(2-\alpha) St_2)$$

$$H_{14} = 2(1-\alpha)(3\alpha-2)(2\alpha-1)^2 (2-\alpha)^3 h_{R1} s_{L2} \exp(i\alpha St_2)$$

$$H_{15} = -6i\alpha(1-\alpha)^2 (2-\alpha)^3 (2\alpha-1)^2 h_{R3} St_2$$

$$H_{16} = 4i\alpha^2 (2\alpha-1)(1-\alpha)^2 (2-\alpha)^3 h_{R2} s_{L1} St_2$$

$$H_{17} = -2i\alpha(2\alpha-1)(2-\alpha)(1-\alpha)^2 (2\alpha^3 - 10\alpha^2 + 11\alpha - 1) h_{R1} s_{L1}^2 St_2$$

$$H_{18} = -2i\alpha(1-\alpha)(2-\alpha)(2\alpha-1)^2 h_{R1} s_{L1}^2 St_2 \exp(i(2-\alpha) St_2)$$

$$H_{19} = -2i\alpha(3\alpha-4)(1-\alpha)^2 (2-\alpha)^2 (2\alpha-1)^2 h_{R1} s_{L2} St_2$$

(G.111)

239

Nonlinear s_L-h_R interaction contribution

$$F_{s_L - h_R - A} = \varepsilon^2 F_{2, s_L - h_R - A} \quad \text{(G.112)}$$

$$F_{2, s_L - h_R - A} = -\frac{1}{2\alpha^2 (1-\alpha)(2\alpha-1)^2 St_2^2} \sum_{j=1}^{11} T_j \quad \text{(G.113)}$$

$$T_1 = 3(4\alpha^3 - 8\alpha^2 + 5\alpha + 1) h_{R2} s_{L1}$$

$$T_2 = 3(1-\alpha)(2\alpha-1)^2 h_{R2} s_{L1} \exp(i\alpha St_2)$$

$$T_3 = -\alpha(1-\alpha)(8\alpha^2 - 12\alpha + 3) h_{R1} s_{L1}^{\ 2}$$

$$T_4 = -2\alpha^2 (2\alpha-1)^2 h_{R1} s_{L1}^{\ 2} \exp(i St_2)$$

$$T_5 = -\alpha^2 h_{R1} s_{L1}^{\ 2} \exp(i(2\alpha-1) St_2)$$

$$T_6 = 3\alpha(2\alpha-1)^2 h_{R1} s_{L1}^{\ 2} \exp(i St_2) \qquad \text{(G.114)}$$

$$T_7 = -3(1-\alpha)(2\alpha-1)^2 h_{R1} s_{L2}$$

$$T_8 = 3(1-\alpha)(2\alpha-1)^2 h_{R1} s_{L2} \exp(i\alpha St_2)$$

$$T_9 = -3i\alpha(1-\alpha)(2\alpha-1)^2 h_{R2} s_{L1} St_2$$

$$T_{10} = 2i\alpha^2 (1-\alpha)(2\alpha-1) h_{R1} s_{L1}^{\ 2} St_2$$

$$T_{11} = -3i\alpha(1-\alpha)(2\alpha-1)^2 h_{R1} s_{L2} St_2$$

References

[1] Zinn B.T. and Powell E.A., *Nonlinear Combustion Instability in Liquid-Propellant Rocket Engines.* Proceedings of the Combustion Institute, 1970. Vol No.**13**(1): p. 491-503.

[2] Culick F.E.C., *Combustion Instabilities in Liquid-Fueled Propulsion Systems - an Overview.* AGARD Conference Proceedings, 1977. Vol No.**450**: p. 1-73.

[3] Culick F.E.C., Burnley V., and Sweson G., *Pulsed Instabilities in Solid-Propellant Rocket Engines.* Journal of Propulsion and Power, 1995. Vol No.**11**(4): p. 657-665.

[4] Wicker J.M., Greene W.D., Kim S.I., and Yang V., *Triggering of Longitudinal Combustion Instabilities in Rocket Motors : Nonlinear Combustion Response.* Journal of Propulsion and Power, 1996. Vol No.**12**(6): p. 1148-1158.

[5] Yang V. and Anderson W., eds. *Liquid Rocket Engine Combustion Instability.* Progress in Astronautics and Aeronautics. Vol. 169. 1995, AIAA.

[6] Harrje D.T. and Reardon F.H., *Liquid Propellant Rocket Combustion Instability*. 1972. p. 359.

[7] Lieuwen T. and Yang V., eds. *Combustion Instabilities in Gas Turbine Engines: Operational Experience, Fundamental Mechanisms, and Modeling*. Progress in Aeronautics and Astronautics, ed. F. Lu. Vol. 210. 2005, AIAA: Reston, VA.

[8] Yang V. and Culick F.E.C., *Analysis of Low Frequency Combustion Instabilities in a Laboratory Ramjet Combustor.* Combustion Science and Technology, 1986. Vol No.**45**(1-2): p. 1-25.

[9] Dowling A.P. and Stow S.R., *Acoustic Analysis of Gas Turbine Combustors.* Journal of propulsion and power, 2003. Vol No.**19**(5): p. 751-764.

[10] Candel S., *Combustion Dynamics and Control: Progress and Challenges.* Proceedings of the Combustion Institute, 2002. Vol No.**29**(1): p. 1-28.

[11] Ducruix S., Schuller T., Durox D., and Candel S., *Combustion Dynamics and Instabilities: Elementary Coupling and Driving Mechanisms.* Journal of propulsion and power, 2003. Vol No.**19**(5): p. 722-734.

[12] Paschereit C., Gutmark E.J., and Weisenstein W., *Structure and Control of Thermoacoustic Instabilities in a Gas-Turbine Combustor.* Combustion Science and Technology, 1998. Vol No.**138**(1-6): p. 213-232.

[13] Goy C.J., James S.R., and Rea S., *Monitoring Combustion Instabilities: E.On Uk's Experience*, in *Combustion Instabilities in Gas Turbine Engines: Operational Experience, Fundamental Mechanisms, and Modeling*, T. Lieuwen and V. Yang, Editors. 2005. p. 163-175.

[14] Rabovister J.K., Khinkhis M.J., Bannister R.L., and Miao F.Q., *Evaluation of Thermochemical Recuperation and Partial Oxidation Concepts for Natural Gas-Fired Advanced Turbine Systems*, ASME Turbo Expo, 1996, ASME#96-GT-290.

[15]   Dowling A.P. and Ffowcs-Williams J.E., *Sound and Sources of Sound*. Vol. 3. 1983, New York, NY: John Wiley & Sons Inc.

[16]   Rayleigh B.J.W.S., *The Theory of Sound*. Vol. 1. 1896: Macmillan.

[17]   Schuller T., Durox D., and Candel S., *A Unified Model for the Prediction of Laminar Flame Transfer Functions:: Comparisons between Conical and V-Flame Dynamics.* Combustion and flame, 2003. Vol No.**134**(1-2): p. 21-34.

[18] Schuller T., Durox D., and Candel S., *Dynamics of Noise Radiated by a Perturbed Impinging Premixed Jet Flame.* Combustion and Flame, 2002. Vol No.**128**(1-2): p. 88-110.

[19]   Dowling A.P. and Hubbard S., *Instability in Lean Premixed Combustors.* Proceedings of the Institution of Mechanical Engineers, Part A: Journal of Power and Energy, 2000. Vol No.**214**(4): p. 317-332.

[20]   Lieuwen T., Neumeier Y., and Zinn B.T., *The Role of Unmixedness and Chemical Kinetics in Driving Combustion Instabilities in Lean Premixed Combustors.* Combustion Science and Technology, 1998. Vol No.**135**(1-6): p. 193-211.

[21]   Lieuwen T., *Modeling Premixed Combustion-Acoustic Wave Interactions: A Review.* Journal of propulsion and power, 2003. Vol No.**19**(5): p. 765-781.

[22] Shanbhogue S., Shin D.H., Hemchandra S., Plaks D., and Lieuwen T., *Flame Sheet Dynamics of Bluff-Body Stabilized Flames During Longitudinal Acoustic Forcing.* Proceedings of the Combustion Institute, 2009. Vol No.**32**(2): p. 1787-1794.

[23]   Shreekrishna, Hemchandra S., and Lieuwen T., *Premixed Flame Response to Equivalence Ratio Perturbations.* Combustion Theory and Modelling, 2010. Vol No.**14**(5): p. 681-714.

[24]   Fleifil M., Annaswamy A.M., Ghoneim Z.A., and Ghoneim A.F., *Response of a Laminar Premixed Flame to Flow Oscillations: A Kinematic Model and Thermoacoustic Instability Results.* Combustion and Flame, 1996. Vol No.**106**(4): p. 487-510.

[25]   Ducruix S., Durox D., and Candel S., *Theoretical and Experimental Determination of the Transfer Function of a Laminar Premixed Flame.* Proceedings of the Combustion Institute, 2000. Vol No.**28**(1): p. 765-773.

[26]   Gutmark E.J., Parr T.P., Parr D.M., Crump J.E., and Schadow K.C., *On the Role of Large and Small Scale Structures in Combustion Control.* Combustion Science and Technology, 1989. Vol No.**66**(4): p. 167-186.

[27] Schadow K.C. and Gutmark E.J., *Combustion Instability Related to Vortex Shedding in Dump Combustors and Their Passive Control.* Progress in Energy and Combustion Science, 1992. Vol No.**18**(2): p. 117-132.

[28] Altay H.M., Speth R.L., Hudgins D.E., and Ghoneim A.F., *Flame–Vortex Interaction Driven Combustion Dynamics in a Backward-Facing Step Combustor.* Combustion and Flame, 2009. Vol No.**156**(5): p. 1111-1125.

[29] Broda J.C., Seo S., Santoro R.J., Shirhattikar G., and Yang V., *Experimental Study of Combustion Dynamics of a Premixed Swirl Injector.* Proceedings of the Combustion Institute, 1998. Vol No.**27**(2): p. 1849-1856.

[30] Menon S., *Acoustic-Vortex-Flame Interactions in Gas Turbines*, in *Combustion Instabilities in Gas Turbines : Operational Experience, Fundamental Mechanisms, and Modeling*, T. Lieuwen and V. Yang, Editors. 2005, American Institute of Aeronautics and Astronautics. p. 277-310.

[31] Dowling A., *Nonlinear Self-Excited Oscillations of a Ducted Flame.* Journal of fluid mechanics, 1997. Vol No.**346**(1): p. 271-290.

[32] Poinsot T. and Candel S.M., *A Nonlinear Model for Ducted Flame Combustion Instabilities.* Combustion science and technology, 1988. Vol No.**61**(4-6): p. 121-153.

[33] Lieuwen T. and Zinn B.T., *The Role of Equivalence Ratio Oscillations in Driving Combustion Instabilities in Low Nox Gas Turbines.* Proceedings of the Combustion Institute, 1998. Vol No.**27**(2): p. 1809-1816.

[34] Lieuwen T., Torres H., Johnson C., and Zinn B.T., *A Mechanism of Combustion Instability in Lean Premixed Gas Turbine Combustor.* Journal of Engineering in Gas Turbines and power, 1998. Vol No.**120**: p. 294-302.

[35] Kendrick D.W., Anderson T.J., Sowa W.A., and Snyder T.S., *Acoustic Sensitivities of Lean-Premixed Fuel Injector in a Single Nozzle Rig.* Journal of Engineering for Gas Turbines and Power, 1999. Vol No.**121**(3): p. 429-436.

[36] Straub D.L. and Richards G.A., *Effect of Fuel Nozzle Configuration on Premix Combustion Dynamics*, ASME Turbo Expo, 1998, ASME# 98-GT-492.

[37] Richards G.A. and Janus M.C., *Characterization of Oscillations During Premix Gas Turbine Combustion.* Journal of Engineering for Gas Turbines and Power, 1998. Vol No.**120**(2): p. 294-302.

[38] Blackshear P., *Driving Standing Waves by Heat Addition.* Proceedings of the Combustion Institute, 1953. Vol No.**4**(553-566).

[39] Shreekrishna and Lieuwen T., *High Frequency Premixed Flame Response to Acoustic Perturbations*, 15th AIAA/CEAS International Conference in Aeroacoustics, 2009, AIAA#2009-3261.

[40] Dowling A.P., *Thermoacoustic Instability.* 6th International Congress on Sound and Vibration, 1999. Vol: p. 3277-3292.

[41] Stow S.R. and Dowling A.P., *Low Order Modeling of Thermoacoustic Limit Cycles*, ASME Turbo Expo, 2004, ASME#GT2004-54245.

[42] Schuermans B., Bellucci V., Guethe F., Meili F., and Flohr P., *A Detailed Analysis of Thermoacoustic Interaction Mechanisms in a Turbulent Premixed Flame*, ASME Turbo Expo, 2004, ASME #GT2004-53831.

[43] Boyer L. and Quinard J., *On the Dynamics of Anchored Flames.* Combustion and Flame, 1990. Vol No.**82**(1): p. 51-65.

[44] Poinsot T.J., Trouve A.C., Veynante D.P., Candel S.M., and Esposito E.J., *Vortex-Driven Acoustically Coupled Combustion Instabilities.* Journal of Fluid Mechanics, 1987. Vol No.**177**(1): p. 265-292.

[45] Yu K.H., Trouvé A., and Daily J.W., *Low-Frequency Pressure Oscillations in a Model Ramjet Combustor.* Journal of Fluid Mechanics, 1991. Vol No.**232**(1): p. 47-72.

[46] Preetham, Sai Kumar T., and Lieuwen T., *Linear Response of Stretch-Affected Premixed Flames to Flow Oscillations : Unsteady Stretch Effects*, 45th AIAA Aerospace Sciences Meeting and Exhibit 2007, AIAA#2007-0176.

[47] Wang H.Y., Law C.K., and Lieuwen T., *Linear Response of Stretch-Affected Premixed Flames to Flow Oscillations.* Combustion and Flame, 2009. Vol: p. 889-895.

[48] Bloxsidge G., Dowling A., and Langhorne P., *Reheat Buzz: An Acoustically Coupled Combustion Instability. Part 2. Theory.* Journal of fluid mechanics, 1988. Vol No.**193**(-1): p. 445-473.

[49] Ohtsuka M., Yoshida S., Inage S., and Kobayashi N., *Combustion Oscillation Analysis of Premixed Flames at Elevated Pressures*, ASME Turbo Expo, 1998, ASME# 98-GT-581.

[50] Macquisten M. and Dowling A., *Low-Frequency Combustion Oscillations in a Model Afterburner.* Combustion and flame, 1993. Vol No.**94**(3): p. 253-264.

[51] Durox D., Schuller T., and Candel S., *Combustion Dynamics of Inverted Conical Flames.* Proceedings of the Combustion Institute, 2005. Vol No.**30**(2): p. 1717-1724.

[52] Bourehla A. and Baillot F., *Appearance and Stability of a Laminar Conical Premixed Flame Subjected to an Acoustic Perturbation.* Combustion and flame, 1998. Vol No.**114**(3-4): p. 303-318.

[53] Baillot F., Durox D., and Prud'Homme R., *Experimental and Theoretical Study of a Premixed Vibrating Flame.* Combustion and flame, 1992. Vol No.**88**(2): p. 149-168.

[54] Durox D., Baillot F., Searby G., and Boyer L., *On the Shape of Flames under Strong Acoustic Forcing: A Mean Flow Controlled by an Oscillating Flow.* Journal of fluid mechanics, 1997. Vol No.**350**(-1): p. 295-310.

[55] Preetham, *Modeling the Response of Premixed Flames to Flow Disturbances*, in *Aerospace Engineering*. 2007, Georgia Institute of Technology: Atlanta. p. 196.

[56] Preetham, Sai Kumar T., Santosh H., and Lieuwen T., *Linear Response of Laminar Premixed Flames to Flow Oscillations: Unsteady Stretch Effects.* Journal of propulsion and power, 2010. Vol No.**26**(3): p. 524-532.

[57] Baillot F., Bourehla A., and Durox D., *The Characteristics Method and Cusped Flame Fronts.* Combustion Science and Technology, 1996. Vol No.**112**(1): p. 327-350.

[58] Birbaud A., Durox D., and Candel S., *Upstream Flow Dynamics of a Laminar Premixed Conical Flame Submitted to Acoustic Modulations.* Combustion and flame, 2006. Vol No.**146**(3): p. 541-552.

[59] Karimi N., Brear M.J., Jin S.H., and Monty J.P., *Linear and Non-Linear Forced Response of a Conical, Ducted, Laminar Premixed Flame.* Combustion and flame, 2009. Vol No.**156**(11): p. 2201-2212.

[60] Preetham and Lieuwen T., *Nonlinear Flame-Flow Transfer Function Calculations: Flow Disturbance Celerity Effects*, AIAA Joint Propulsion Conference, 2004, AIAA#2004-4035.

[61] Dowling A., *A Kinematic Model of a Ducted Flame.* Journal of fluid mechanics, 1999. Vol No.**394**(-1): p. 51-72.

[62] Renard P.H., Thévenin D., Rolon J., and Candel S., *Dynamics of Flame/Vortex Interactions.* Progress in energy and combustion science, 2000. Vol No.**26**(3): p. 225-282.

[63] Schuller T., Ducruix S., Durox D., and Candel S., *Modeling Tools for the Prediction of Premixed Flame Transfer Functions.* Proceedings of the Combustion Institute, 2002. Vol No.**29**(1): p. 107-113.

[64] Lieuwen T., *Nonlinear Kinematic Response of Premixed Flames to Harmonic Velocity Disturbances.* Proceedings of the Combustion Institute, 2005. Vol No.**30**(2): p. 1725-1732.

[65] Preetham and Lieuwen T., *Nonlinear Flame-Flow Transfer Function Calculations: Flow Disturbance Celerity Effects, Part Ii*, 43rd AIAA Aerospace Sciences Meeting and Exhibit, 2005, AIAA 2005-0543.

[66] Putnam A., *Combustion Driven Oscillations in Industry*. 1971, New York: Elsevier.

[67] Krebs W., Flohr P., Prade B., and Hoffman S., *Thermoacoustic Instability Chart for High-Intensity Gast Turbine Combustion Systems.* Combustion Science and Technology, 2002. Vol No.**214**(7): p. 99-128.

[68] Dowling A.P. and Hubbard S., *Instability in Lean Premix Combustors.* Proceedings of the Institute of Mechanical Engineers, 2000. Vol No.**214**(A): p. 317-332.

[69] Prashant R.K., Annaswamy A.M., Hathout J.P., and Ghoneim A.F., *When Do Open-Loop Strategies for Combustion Control Work?* Journal of Propulsion and Power, 2002. Vol No.**18**(3): p. 658-668.

[70] Keller J.J., *Thermoacoustic Oscillations in Combustion Chambers of Gas Turbines.* AIAA Journal, 1995. Vol No.**33**(12): p. 2280-2287.

[71] Keller J.J., Egli W., and Hellat J., *Thermally Induced Low-Frequency Oscillations.* ZAMP, 1985. Vol No.**36**: p. 250-274.

[72] Cho J.H. and Lieuwen T., *Laminar Premixed Flame Response to Equivalence Ratio Oscillations.* Combustion and Flame, 2005. Vol No.**140**(1-2): p. 116-129.

[73] Mongia R., Dibble R., and Lovett J., *Measurement of Air-Fuel Ratio Fluctuations Caused by Combustor Driven Oscillations*, ASME Turbo Expo, 1998, ASME#98-GT-304.

[74] Lee D.S. and Anderson T.J., *Measurements of Fuel/Air-Acoustic Coupling in Lean Premixed Combustion System*, 37th AIAA Aerospace Sciences Meeting and Exhibit, 1999, AIAA#99-0450.

[75] Lee J.G. and Santavicca D.A., *Experimental Diagnostics for the Study of Combustion Instabilities in Lead Premixed Combustors.* Journal of Propulsion and Power, 2003. Vol No.**19**(5): p. 735-750.

[76] Peracchio A., A. and Proscia W.M., *Nonlinear Heat-Release/Acoustic Model for Thermoacoustic Instability in Lean Premixed Combustors.* Journal of Engineering for Gas Turbines and power, 1999. Vol No.**121**: p. 415-421.

[77] Stow S.R. and Dowling A.P., *Low Order Modeling of Thermoacoustic Limit Cycles.* ASME, 2004. Vol No.**ASME#GT2004-54245**.

[78] Schildmacher K., Koch R., and Bauer H., *Experimental Characterization of Premixed Flame Instabilities of a Model Gas Turbine Burner.* Flow, Turbulence and Combustion, 2006. Vol No.**76**(2): p. 177-197.

[79] Lee J.G., Kim K., and Santavicca D.A., *Measurement of Equivalence Ratio Fluctuation and Its Effect on Heat Release During Unstable Combustion.* Proceedings of the Combustion Institute, 2000. Vol No.**28**: p. 415-421.

[80] Venkataraman K.K., Preston L.H., Simons D.W., Lee B.J., Lee J.G., and Santavicca D.A., *Mechanism of Combustion Instability in a Lean Premixed Dump Combustor.* Journal of Propulsion and Power, 1999. Vol No.**15**(6): p. 909-918.

[81] Weigand P., Meier W., Duan X., and Aigner M., *Laser-Based Investigations of Thermoacoustic Instabilities in a Lean Premixed Gas Turbine Model Combustor.* Journal of Engineering for Gas Turbines and power, 2007. Vol No.**129**(3): p. 664-671.

[82] Ratner A., Pun W., Palm S.L., and Culick F.E.C., *Phase-Resolved No Planar Laser-Induced Flourescence of a Jet Flame in an Acoustic Chamber with Excitation at Frequencies < 60 Hz.* Proceedings of the Combustion Institute, 2002. Vol No.**29**(1): p. 85-90.

[83] Kang D.M., Culick F.E.C., and Ratner A., *Coupling between Combustor Pressure and Fuel/Oxidizer Mixing and the Consequences in Flame Behavior.* Combustion Science and Technology, 2008. Vol No.**180**(1): p. 127-142.

[84] Flohr P., Paschereit C., van Roon B., and Schuermans B., *Using Cfd for Time-Delay Modeling of Premixed Flames*, ASME Turbo Expo, 2001, ASME#2001-GT-376.

[85] Polifke W., Kopitz J., and Serbanovic A., *Impact of the Fuel Time Lag Distribution in Elliptical Premix Nozzles on Combustion Instability*, 7th AIAA/CEAS Aeroacoustics Conference, 2001, AIAA 2001-2104.

[86]   Angelberger C., Veynante D., and Egolfopoulos F.N., *Les of Chemical and Acoustic Forcing of a Premixed Dump Combustor.* Flow, Turbulence and Combustion, 2001. Vol No.**65**: p. 205-222.

[87] Birbaud A.L., Ducruix S., Durox D., and Candel S., *The Nonlinear Response of Inverted "V" Flames to Equivalence Ratio Nonuniformities.* Combustion and Flame, 2008. Vol No.**154**: p. 356-367.

[88] Schuermans B.B.H., Polifke W., and Paschereit C. *Modeling Transfer Matrices of Premixed Flames and Comparison with Experimental Results*. in *ASME International Gas Turbine and Aeroengine Congress and Exhibition*. 1999. Indianapolis, IN.

[89] Sattelmayer T., *Influence of the Combustor Aerodynamics on Combustion Instabilities from Equivalence Ratio Fluctuations.* Journal of Engineering for Gas Turbines and power, 2003. Vol No.**125**(1): p. 11-19.

[90]   Polifke W. and Lawn C.J., *On the Low-Frequency Limit of Flame Transfer Functions.* Combustion and Flame, 2007. Vol No.**151**: p. 437-451.

[91]   McIntosh A.C., *The Interaction of High Frequency, Low Amplitude Acoustic Waves with Premixed Flames*, in *Nonlinear Waves in Active Media*, J. Engelbrecht, Editor. 1989, Springer-Verlag: Heidelberg.

[92] McIntosh A.C., *Pressure Disturbances of Different Length Scales Interacting with Conventional Flames.* Combustion Science and Technology, 1991. Vol No.**75**(4): p. 287-309.

[93] McIntosh A.C., *The Linearized Response of the Mass Burning Rate of a Premixed Flame to Rapid Pressure Changes.* Combustion Science and Technology, 1993. Vol No.**91**(4): p. 329-346.

[94] McIntosh A.C., Batley G., and Brindley J., *Short Length Scale Pressure Pulse Interactions with Premixed Flames.* Combustion Science and Technology, 1993. Vol No.**91**: p. 1-13.

[95]   Ledder G. and Kapila A., *The Response of Premixed Flame to Pressure Perturbations.* Combustion Science and Technology, 1991. Vol No.**76**(1): p. 21-44.

[96] Keller D. and Peters N., *Transient Pressure Effects in the Evolution Equation for Premixed Flame Fronts.* Theoretical and Computational Fluid Dynamics, 1994. Vol No.**6**(2-3): p. 141-159.

[97] Peters N. and Ludford G.S.S., *The Effect of Pressure Variation on Premixed Flames.* Combustion Science and Technology, 1983. Vol No.**34**(1): p. 331-344.

[98] van Harten A., Kapila A., and Matkowsky B.J., *Acoustic Coupling of Flames.* SIAM Journal of Applied Mathematics, 1984. Vol No.**44**(5): p. 982-995.

[99] Buckmaster J.D. and Ludford G.S.S., *Theory of Laminar Flames*. 1982: Cambridge University Press.

[100] McIntosh A.C., *The Effect of Upstream Acoustic Forcing and Feedback on the Stability and Resonance Behaviour of Anchored Flames.* Combustion Science and Technology, 1986. Vol No.**49**(3-4): p. 143-167.

[101] Clavin P., Pelcé P., and He L., *One-Dimensional Vibratory Instability of Planar Flames Propagating in Tubes.* Journal of Fluid Mechanics, 1990. Vol No.**216**(1): p. 299-322.

[102] McIntosh A. and Wilce S., *High Frequency Pressure Wave Interaction with Premixed Flames.* Combustion Science and Technology, 1991. Vol No.**79**(1-3): p. 141-155.

[103] Johnson R., McIntosh A., and Brindley J., *Extinction of Premixed Flames by Pressure Drops.* Combustion and flame, 1995. Vol No.**102**(4): p. 493-500.

[104] Wangher A., Searby G., and Quinard J., *Experimental Investigation of the Unsteady Response of Premixed Flame Fronts to Acoustic Pressure Waves.* Combustion and Flame, 2008. Vol No.**154**(1-2): p. 310-318.

[105] Schmidt H. and Jimenez C., *Numerical Study of the Direct Pressure Effect of Acoustic Waves in Planar Premixed Flames.* Combustion and flame, 2010. Vol No.**157**(8): p. 1610-1619.

[106] Wu X. and Law C.K., *Flame-Acoustic Resonance Initiated by Vortical Disturbances.* Journal of fluid mechanics, 2009. Vol No.**634**(-1): p. 321-357.

[107] Wu X., Wang M., Moin P., and Peters N., *Combustion Instability Due to the Nonlinear Interaction between Sound and Flame.* Journal of fluid mechanics, 2003. Vol No.**497**(-1): p. 23-53.

[108] Wu X., *Asymptotic Approach to Combustion Instability.* Philosophical Transactions of the Royal Society A: Mathematical, Physical and Engineering Sciences, 2005. Vol No.**363**(1830): p. 1247.

[109] Wu X. and Moin P., *Large-Activation-Energy Theory for Premixed Combustion under the Influence of Enthalpy Fluctuations.* Journal of fluid mechanics, 2006. Vol No.**1**(-1): p. 1-35.

[110] Markstein G.H., *Non-Steady Flame Propagation.* 1964, New York: Pergamon.

[111] Marble F. and Candel S., *Acoustic Disturbance from Gas Non-Uniformities Convected through a Nozzle.* Journal of Sound and Vibration, 1977. Vol No.**55**(2): p. 225-243.

[112] Matalon M. and Matkowsky B., *Flames as Gasdynamic Discontinuities.* Journal of fluid mechanics, 1982. Vol No.**124**(1): p. 239-259.

[113] Kerstein A.R., Ashurst W.T., and Williams F.A., *Field Equation for Interface Propagation in an Unsteady Homogeneous Flow Field.* Physical Review, 1988. Vol No.**A27**: p. 2728-2731.

[114] Preetham, Hemchandra S., and Lieuwen T., *Dynamics of Laminar Premixed Flames Forced by Harmonic Velocity Disturbances.* Journal of Propulsion and Power, 2007. Vol No.**24**(6): p. 1390-1402.

[115] Preetham, Sai Kumar T., and Lieuwen T., *Response of Premixed Flames to Flow Oscillations : Unsteady Curvature Effects*, 44th AIAA Aerospace Sciences Meeting and Exhibit, 2006, AIAA#2006-0960.

[116] Clanet C., Searby G., and Clavin P., *Primary Acoustic Instability of Flames Propagating in Tubes : Cases of Spray and Premixed Combustion.* Journal of Fluid Mechanics, 1999. Vol No.**385**: p. 157-197.

[117] Michalke A., *Instability of a Compressible Circular Free Jet with Consideration of the Influence of the Jet Boundary Layer Thickness.* Z. fur Flugwissenschaften, 1971. Vol No.**19**(8): p. 319-328.

[118] Schuller T., Ducruix S., Durox D., and Candel S., *Modeling Tools for the Prediction of Premixed Flame Transfer Functions.* Proceedings of the Combustion Institute, 2005. Vol No.**30**: p. 107-113.

[119] Lauvergne R. and Egolfopoulos F.N., *Unsteady Response of C3h8/Air Laminar Premixed Flames Submitted to Mixture Composition Oscillations.* Proceedings of the Combustion Institute, 2000. Vol No.**28**: p. 1841-1850.

[120] Johnson R.G., McIntosh A.C., Batley G., and Brindley J., *Nonlinear Oscillation of Premixed Flames Caused by Sharp Pressure Changes.* Combustion Science and Technology, 1994. Vol No.**99**: p. 201-219.

[121] Oberlack M., Wenzel H., and Peters N., *On Symmetries and Averaging of the G-Equation for Premixed Combustion.* Combustion Theory and Modelling, 2001. Vol No.**5**(3): p. 363-383.

[122] Law C.K. and Sung C.J., *Structure, Aerodynamics and Geometry of Premixed Flamelets.* Progress in Energy and Combustion Science, 2000. Vol No.**26**(4-6): p. 459-505.

[123] Chu B.T. and Kovásznay L.S.G., *Non-Linear Interactions in a Viscous Heat-Conducting Compressible Gas.* Journal of Fluid Mechanics, 1958. Vol No.**3**(5): p. 494-514.

[124] Wen-Huei J. and Menon S., *Modes of Oscillation in a Non-Reacting Ramjet Combustor Flow.* Journal of Propulsion and Power, 1990. Vol No.**6**(5): p. 535-543.

[125] Huang Z., Bechtold J., and Matalon M., *Weakly Stretched Premixed Flames in Oscillating Flows.* Combustion Theory and Modeling, 1998. Vol No.**2**: p. 115-133.

[126] Joulin G., *On the Response of Premixed Flames to Time-Dependent Stretch and Curvature.* Combustion Science and Technology, 1994. Vol No.**97**: p. 219-229.

[127] Clavin P. and Joulin G., *High-Frequency Response of Premixed Flames to Weak Stretch and Curvature: A Variable-Density Analysis.* Combustion Theory and Modelling, 1997. Vol No.**1**(4): p. 429-446.

[128] Im H.G. and Chen J.H., *Effects of Flow Transients on the Burning Velocity of Laminar Hydrogen/Air Premixed Flames.* Proceedings of the Combustion Institute, 2000. Vol No.**28**: p. 1833-1840.

[129] Sankaran R. and Im H.G., *Dynamic Flammability Limits of Methane/Air Premixed Flames with Mixture Composition Fluctuations.* Proceedings of the Combustion Institute, 2002. Vol No.**29**(1): p. 77-84.

[130] McIntosh A.C., *Deflagration Fronts and Compressibility.* Philosophical Transactions of the Royal Society of London : A, 1999. Vol No.**357**: p. 3523-3538.

[131] Dupont T.F. and Liu Y., *Back and Forth Error Compensation and Correction Methods for Semi-Lagrangian Schemes with Application to Level Set Interface Computations.* Mathematics of Computation, 2007. Vol No.**76**: p. 647-668.

[132] Peng D., Merriman B., Osher S., Zhao H., and Kang M., *The Local Level-Set Method.* Journal of Computational Physics, 1996. Vol No.**155**: p. 410-438.

[133] Smereka P., *Numerical Approximations of a Delta Function.* Journal of Computational Physics, 2006. Vol No.**211**: p. 77-90.

[134] Peters N., *Turbulent Combustion*. 2000, Cambridge, UK: Cambridge University Press.

[135] Sung C.J. and Law C.K., *Analytic Description of the Evolution of Two-Dimensional Flame Surfaces.* Combustion and Flame, 1996. Vol No.**107**: p. 114-124.

[136] Buckmaster J.D., *Edge Flames.* Journal of Engineering Mathematics, 1997. Vol No.**31**: p. 269-284.

[137] Wu R. and Hemchandra S., *Premixed Flame Response to Equivalence Ratio Perturbations : Lean Flammability Cross-Over*, 7th US National Technical Meeting of the Combustion Institute, 2011,

[138] Bansal G. and Im H.G., *Time Scales in Unsteady Premixed Flame Extinction with Composition Fluctuations.* Combustion and flame, 2007. Vol No.**150**(4).

[139] Dandy D. and Vosen S., *Numerical and Experimental Studies of Hydroxyl Radical Chemiluminescence in Methane-Air Flames.* Combustion Science and Technology, 1992. Vol No.**82**(1): p. 131-150.

[140] Najm H.N., Paul P.H., Mueller C.J., and Wyckoff P.S., *On the Adequacy of Certain Observables as Measurements of Flame Burning Rate.* Combustion and Flame, 1998. Vol No.**113**(3): p. 312-332.

[141] Jones B., Lee J.G., Quay B.D., and Santavicca D.A., *Flame Response Mechanisms Due to Velocity Perturbations in a Lean Premixed Gas Turbine Combustor.* Journal of Engineering for Gas Turbines and Power, 2011. Vol No.**133**: p. 021503.

[142] Price R., Hurle I., and Sugden T., *Optical Studies of the Generation of Noise in Turbulent Flames.* Proceedings of the Combustion Institute, 1968. Vol No.**12**: p. 1093-1102.

[143] Clark T., *Studies of Oh, Co, Ch and C_2 Radiation from Laminar and Turbulent Propane-Air and Ethylene-Air Flames*, 1958, Vol No.**4**, NACA, TN 4266.

[144] Diederichsen J. and Gould R.D., *Combustion Instability: Radiation from Premixed Flames of Variable Burning Velocity.* Combustion and Flame, 1965. Vol No.**9**: p. 22-31.

[145] John R. and Summerfield M., *Effect of Turbulence on Radiation Intensity from Propane-Air Flames.* Jet Propulsion, 1957. Vol No.**27**: p. 169-178.

[146] Hurle I.R., Price R.B., Sugden T.M., Thomas R.R.S., and Thomas A., *Sound Emission from Open Turbulent Premixed Flames.* Proceedings of the Royal Society of London, Series A : Mathematical and Physical Sciences, 1968. Vol No.**303**: p. 409-427.

[147] Lauer M. and Sattelmayer T., *On the Adequacy of Chemiluminescence as a Measure for Heat Release in Turbulent Flames with Mixture Gradients*, ASME Turbo Expo, 2009, GT2009-59631.

[148] Nori V.N., *Modeling and Analysis of Chemiluminescence Sensing for Syngas, Methane and Jet-a Combustion*, in *Aerospace Engineering*. 2008, Georgia Institute of Technology: Atlanta.

[149] Miller S.A., *Development of Flame Chemiluminescence Probe for Determination of Primary Zone Equivalence Ratio in Gas Turbine Combustors*, in *Mechanical Engineering*. 1999, Pennsylvania State University: University Park.

[150] Samaniego J.M., Egolfopoulos F.N., and Bowman C.T., Co_2* *Chemiluminescence in Premixed Flames.* Combustion Science and Technology, 1995. Vol No.**109**(1): p. 183-203.

[151] Orawannukul P., Lee J.G., Quay B.D., and Santavicca D.A., *Fuel-Forced Flame Response of a Lean-Premixed Combustor*, ASME Turbo Expo, 2011, ASME# GT2011-46022.

[152] Hemchandra S., *Direct Numerical Simulation Study of Premixed Flame Response to Fuel-Air Ratio Oscillations*, ASME Turbo Expo 2011, 2011, ASME# GT2011-45590.

[153] O'Malley Jr. R.E., *Introduction to Singular Perturbations*. Applied Mathematics and Mechanics : An International Series of Monographs, ed. F. Frenkiel and G. Temple. Vol. 14. 1974, New York and London: Academic Press.

[154] Lagerstrom P.A., *Matched Asymptotic Expansions : Ideas and Techniques*. Applied Mathematical Sciences, ed. F. John, J.E. Marsden, and L. Sirovich. Vol. 76. 1988, New York: Springer-Verlag.

[155] Holmes M.H., *Introduction to Perturbation Methods*. Texts in Applied Mathematics. 1995, New York: Springer-Verlag. xiii, 337 p.

Curriculum Vitae

The author of this thesis, Shreekrishna Jayakumar Rao, was born in Bangalore, India in 1985, as the son of Jayakumar Krishna Rao and Dr. Radha Jayakumar. He did his initial schooling in The Home School, Bangalore and Vijaya High School, Bangalore. He completed his pre-university education (K-11 and K-12) from National College Jayanagar, Bangalore.

He earned his Bachelor's degree (Bachelor of Technology) in Aerospace Engineering from Indian Institute of Technology Madras, Chennai, India in July 2006, and his Master of Science degree in Aerospace Engineering from Georgia Institute of Technology, Atlanta, USA in December 2008.

He commenced his doctoral research in Aerospace Engineering in the Ben T Zinn Combustion Laboratory at Georgia Institute of Technology under the advisorship of Prof. Tim Lieuwen in August 2006. During the course of his Ph.D., he also worked at General Electric's Gas Turbine Technology Laboratory at GE Energy in Greenville, South Carolina, between May and August of 2010 as a summer intern in the Advanced Combustion Design and Combustion Dynamics team, as a part of the organization's Combustion and Emissions Technology unit.

His broad research interests lie in the area of Aerothermal Engineering and Fluid Mechanics, and more specifically, in the design and development of land-based and aero gas turbines, combustion dynamics modeling and prediction, turbulent reacting flows, acoustics and computational fluid dynamics. His other interests include Reliability, Risk Analysis and Mitigation. He is also interested in community outreach via innovative

teaching methodologies in basic mathematics and physics to students at the high school level.

Outside his professional and research interests, the author is a proficient vocalist specializing in the Carnatic genre of Indian classical music. He is also a passionate student of the various systems of Indian philosophy and their comparative study with Western philosophy. In his spare time, he enjoys solving problems from the Mathematical Olympiads, studying pure Mathematics, indulging in Sanskrit literature, learning new languages and listening to Western classical music.